Acta Universitatis Szegediensis

Acta Biologica Szegediensis

Volume 65,
Number 1,
2021

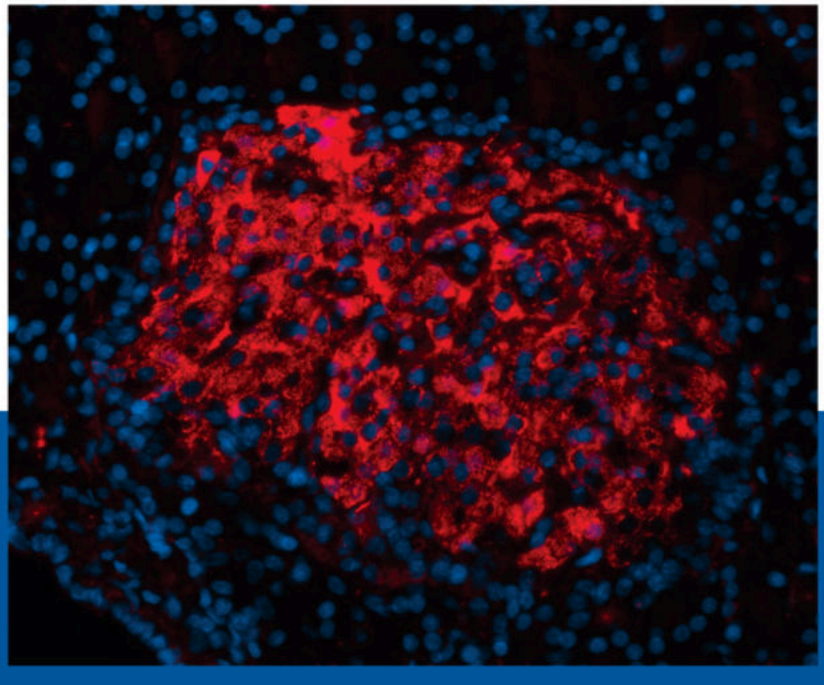

University of Szeged, Szeged, Hungary

http://abs.bibl.u-szeged.hu/index.php/abs

Acta Biologica Szegediensis

Volume 65(1):1-9, 2021
Acta Biologica Szegediensis
http://abs.bibl.u-szeged.hu/index.php/abs

DOI:10.14232/abs.2021.1.1-9

ARTICLE

The effect of nickel phytotoxicity on photosystem II activity and antioxidant enzymes in barley

Ali Doğru[1]*, Hüseyin Altundağ[2], Mustafa Şahin Dündar[2]

[1]Sakarya University Faculty of Arts and Science Department of Biology, Esentepe, 54187 Sakarya, Turkey
[2]Sakarya University Faculty of Arts and Science Department of Chemistry, Esentepe, 54187 Sakarya, Turkey

ABSTRACT In this study, the effect of mild (100 µM), moderate (300 µM) and severe (500 µM) nickel ($NiSO_4.7H_2O$) toxicity on the photosynthetic activity, photosynthetic pigment content and some antioxidant enzymes in the leaves of a barley cultivars (*Hordeum vulgare* L. cv. Tarm-92) was investigated. Moderate and severe nickel toxicity decreased root length while shoot length was not affected by nickel stress, probably due to over accumulation of nickel in roots. Similarly, biomass accumulation was declined by moderate and severe nickel toxicity as reflected by the lowered fresh and dry weight. Chlorophyll a, chlorophyll b and consequently total chlorophyll content decreased by all nickel applications, presumably because the reduced level of carotenoids. Chlorophyll a fluorescence measurements showed that nickel toxicity blocked electron movement in some specific points of the photosynthetic electron transport system. The constant Fo value indicated that PSII reaction centers was not damaged in the leaves of barley under nickel toxicity while the reduced Fm value showed that acceptor side of PSII was more sensitive to nickel toxicity as compared to donor side. Changes in JIP test parameters in the leaves of barley showed that primary photochemical reactions are reduced, and thermal dissipation of excess energy is increased. SOD and CAT activity is elevated in the leaves of barley under moderate and severe nickel toxicity which demonstrate an efficient superoxide dismutation. Severe nickel toxicity, however, did not affect SOD and CAT activity. The ascorbate-glutathione cycle was activated in the leaves of barley plants under nickel toxicity, probably indicating an efficient H_2O_2 detoxification. However, considerable H_2O_2 and MDA accumulation was observed in the leaves of barley under nickel stress. As a result, it may be concluded that the barley genotype Tarm-92 is moderately tolerant to nickel toxicity. **Acta Biol Szeged 65(1):1-9 (2021)**

KEY WORDS
antioxidant system
barley
chlorophyll a fluorescence
JIP test
nickel toxicity

ARTICLE INFORMATION
Submitted
27 February 2021
Accepted
08 March 2021
***Corresponding author**
E-mail: adogru@sakarya.edu.tr

Introduction

Any metal and metalloid that have a relatively higher density (above 5 g cm^{-3}) is known as heavy metal (Gautam et al. 2017). Natural processes such as weathering and volcanic eruption as well as anthropogenic activities such as mining, waste disposal and intensive utilization of fertilizers and pesticides has been known to result in heavy metal accumulation in agricultural areas (Khan et al. 2016). Both the quality of agricultural soils and crop yield may be decreased by heavy metal contamination (Rizwan et al. 2016). Human, animal and plant health, on the other hand, is under a threatening risk because of contamination of environment by excess heavy metals. The heavy metal toxicity in plants has drawn the attention of many environmental scientists during the last decade because plants form the major source of heavy metal entry into the food chain. Doğru (2020) has reported that some heavy metals such as Cu, Zn, Ni and Co are essential for plant growth and development, while some others (Cd, Cr, Pb and As) are not responsible for any physiological function. Plants require the essential heavy metals within physiological limits to fulfil their metabolic reactions because excess supply of heavy metals is known to be toxic for plants. Heavy metal toxicity affects various physiological pathways including water and mineral absorption from soil, photosynthesis, nitrogen metabolism and membrane functions all of which are result in the reduced crop yield and quality (Gopal and Rizvi 2008; Chen et al. 2009; Doğru 2020; Gajewska et al. 2009).

Ni forms about 0.008% of the earth's crust being 24th the most abundant element (Hedfi et al. 2007). Naturally, nickel is present in soils in the range of 3-100 ppm and in water 0-0.005 ppm, respectively (Sachan and Lal 2017). Ni, as the most recent element to be classified as essential, is required very small concentrations by plants for optimum growth and development. For example, Gajewska et al. (2006) have indicated that Ni at the concentration of 10 µM improved plant growth and increased biomass

accumulation. In the contaminated soils, on the other hand, Ni may exist in the range of 200 - 26 000 ppm which is 20-30-fold higher than the natural range (Izosimova 2005). Ahmad et al. (2009) and Ali et al. (2009) have reported that excessive nickel in the growth medium leads to the inhibition of germination and plant growth, degradation of chlorophyll pigments and reduction of photosynthetic activity. In addition, Ni toxicity also induces oxidative damage in some macromolecules such as lipids, proteins and nucleic acids as a result of the accelerated rate of reactive oxygen species (ROS) including hydrogen peroxide (H_2O_2), superoxide ($O_2^{\cdot-}$) and hydroxyl radical ($OH^{\cdot}$) (Gajewska and Sklodowska 2007). However, plants possess an efficient antioxidant system against oxidative stress which consist of enzymatic and non-enzymatic components (Bhaduri and Fulekar 2012).

Photosynthesis is an important metabolic process for plant growth and productivity. However, it has been well known that photosynthetic reactions are primary target for abiotic stress factors including Ni toxicity (Amari et al. 2017). Therefore, it is imperative to gain an improved understanding of the effect of Ni toxicity on photosynthetic processes to improve agricultural productivity. Today, chlorophyll a fluorescence has been reported to be the most modern and reliable technique for measuring photosynthetic activity (Maxwell and Johnson 2000; Doğru 2019; Doğru and Çakırlar 2020a and 2020b). The basic principle of chlorophyll a fluorescence kinetics is the redox state of quinone A (Q_A), which is the primary electron acceptor of photosystem II (PSII). Accordingly, the fluorescence yield is low when the Q_A is in the oxidised state, and the fluorescence yield is high when it is reduced. In this case, fluorescence yield is directly related to the net concentration of Q_A^- (Govindjee 2004). In addition, at the minimum fluorescence (Fo), that is, at the "O" point, all Q_A molecules are in oxidised state, the reaction centers of PSII are open and primary photochemical processes are at maximum level. However, at the maximum fluorescence (Fm), that is, at the "P" point, all Q_A molecules are reduced, the reaction centers of PSII are closed and primary photochemical processes are at minimum level (Govindjee 2004). If the chlorophyll a fluorescence signals are plotted versus to the logarithm of time, the "OJIP" curve is obtained. The basic principle of OJIP curve can be explained as follows: When light is applied to the surface of a leaf adapted to dark, the fluorescence of chlorophyll a increases from the minimum level ("O") to the "J" level (Fj) within 2 ms due to reduction of Q_A molecules. It then rises to the "I" point (Fı) in about 30 ms due to the reduction of the entire plastoquinone pool. In the last stage, chlorophyll a fluorescence increases form the "I" point to the maximum level ("P" or Fm) due to the higher electron density in the acceptor side of photosystem I (PSI) (Govindjee 2004). The technique that enables chlorophyll a fluorescence signals to examine the changes exhibited at "J", "I" and "P" points of the OJIP curve ant the interactions between these changes is called JIP test (Strasser et al. 2004). JIP test is used in the field of plant biology and agriculture in order to understand the reactions of the photosynthetic apparatus under many different environmental conditions (Yusuf et al. 2010). JIP test is based on energy flow theories in thylakoid membranes (Force et al. 2003). This test allows the investigation of the energy flow entering and leaving the PSII by means of parameters directly measured and calculated with the help of some equations.

As a result, the objective of this study is to investigate phytotoxic effects of mild, moderate and severe nickel toxicity in the leaves of barley plants through chlorophyll a fluorescence and some antioxidant enzymes.

Material and methods

Plant materials, growth conditions and experimental design

Barley genotype (*Hordeum vulgare* L. cv. Tarm-92) was grown in growth chamber in plastic pots containing Hoagland nutrient solution. The average temperature for day/night was 25/18 °C, respectively, relative humidity was 40-50%, the photoperiod for the day/night cycle was 16/8 h, respectively, and the maximum photosynthetically active radiation was about 200 µmol photon m^{-2} s^{-1}. After 10 days of growth, nickel treatments were initiated by applying half-strength Hoagland nutrient solution containing 100, 300 and 500 µM nickel sulphate ($NiSO_4 \cdot 7 H_2O$) to seedlings. Control plants (no nickel sulphate treatment) and nickel-treated plants were grown in the growth chamber under the same physical conditions for another 6 days. The leaf tissue of 16 days of plants was used for chlorophyll fluorescence measurements and biochemical analysis.

Determination of root and shoot length

Measurement of root and shoot length were done with a millimetric ruler. The longest root was taken into consideration for measurement. Root and shoot length were expressed as cm $plant^{-1}$. After harvesting, barley seedlings were weighed for fresh weight (FW) determination. Dry weight (DW) of plants was measured after drying in hot-air oven at 70 °C for 2 days.

Determination of nickel content

For measuring nickel content plants were carefully harvested and divided into roots and shoots. The leaves were washed with double-distilled water. The samples

were acid-digested and analysed by inductively coupled plasma emission spectroscopy (ICP-OES) after digestion with concentrated HNO_3.

Photosynthetic pigment analysis

Photosynthetic pigments were extracted from leaf segments in 3 ml 100% acetone. The absorbance of the extracts was measured at 644.8 and 661.6 nm using a Shimadzu mini 1240 UV visible spectrophotometer. The concentrations of chlorophyll a and chlorophyll b were calculated according to Lichtenthaler (1987).

Malondialdehyde (MDA) and hydrogen peroxide (H_2O_2) analysis

MDA and H_2O_2 content were determined by the method of Heath and Packer (1968) and Ohkawa et al. (1979), respectively. Fresh leaf material (0.1 g) was homogenized in 6 ml of 5% TCA (4 °C) and centrifuged at 10,000 rpm for 15 min and the supernatant was used in the subsequent determination. To 0.5 ml of the supernatant were added 0.5 ml of 0.1 M Tris-HCl (pH 7.6) and 1 ml of TCA-TBA reagent. The mixture was heated at 95 °C for 60 min and then quickly cooled in an ice bath. After centrifugation at 10 000 g for 5 min to remove suspended turbidity, the absorbance of supernatant at 532 nm was recorded. Non-specific absorbance at 600 nm was measured and subtracted from the readings recorded at 532 nm. Concentration of MDA was calculated using its extinction coefficient of 155 mM^{-1} cm^{-1}. For determination of hydrogen peroxide, 0.5 ml of 0.1 M Tris-HCl (pH 7.6) and 1 ml of 1 M KI were added to 0.5 ml of supernatant. After 90 min, the absorbance was read at 390 nm. A standard curve for hydrogen peroxide was prepared to determine hydrogen peroxide concentration in each sample.

Antioxidant enzyme activities

For determination of enzyme activities, 0.3 g fresh leaves material from non-acclimated and cold-acclimated leaves were powdered with liquid nitrogen and suspended in specific buffer with proper pH values for each enzyme. The homogenates were centrifuged at 14 000 rpm for 20 min at 4 °C and resulting supernatants were used for enzyme assay. The protein concentrations of leaf crude extracts were determined according to Bradford (1976), using BSA as a standard.

Superoxide dismutase (SOD; EC1.15.1.1) activity was determined by the method of Beyer and Fridovich (1987), based on the photo reduction of NBT (nitro blue tetrazolium). Extraction was performed in 1.5 ml homogenization buffer containing 10 mM K_2HPO_4 buffer (pH 7.0), 2% PVP and 1 mM Na_2EDTA. The reaction mixture consisted of 100 mM K_2HPO_4 buffer (pH 7.8), containing 9.9 x 10^{-3} M methionine, 5.7 x 10^{-5} M NBT, 1% Triton X-100 and enzyme extract. Reaction was started by the addition of 0.9 μM riboflavin and mixture was exposed to light with an intensity of 375 μmol m^{-2} s^{-1}. After 15 min, reaction was stopped by switching off the light and absorbance was read at 560 nm. SOD activity was calculated by a standard graphic and expressed as unit mg^{-1} protein.

Ascorbate peroxidase (APX; EC1.11.1.11) activity was determined according to Wang et al. (1991) by estimating the decreasing rate of ascorbate oxidation at 290 nm. APX extraction was performed in 50 mM Tris-HCl (pH 7.2), 2% PVP, 1 mM Na_2EDTA, and 2 mM ascorbate. The reaction mixture consisted of 50 mM KH_2PO_4 buffer (pH 6.6), 2.5 mM ascorbate, 10 mM H_2O_2 and enzyme, containing 100 μg proteins in a final volume of 1 ml. The enzyme activity was calculated from initial rate of the reaction using the extinction coefficient of ascorbate (E = 2.8 mM cm^{-1} at 290 nm).

Glutathione reductase (GR; EC 1. 6. 4. 2) activity was measured with the method of Sgherri et al. (1994). Extraction was performed in 1.5 ml of suspension solution, containing 100 mM KH_2PO_4 buffer (pH 7.0), 1 mM Na_2EDTA, and 2% PVP. The reaction mixture (total volume of 1 ml) contained 100 mM KH_2PO_4 buffer (pH 7.8), 2 mM Na_2EDTA, 0.5 mM oxidised glutathione (GSSG), 0.2 mM NADPH and enzyme extract containing 100 μg protein. Decrease in absorbance at 340 nm was recorded. Correction was made for the non-enzymatic oxidation of NADPH by recording the decrease at 340 nm without adding GSSG to assay mixture. The enzyme activity was calculated from the initial rate of the reaction after subtracting the non-enzymatic oxidation using the extinction coefficient of NADPH (E = 6.2 mM cm^{-1} at 340 nm).

Catalase activity was measured with the method of Aebi (1984). Extraction was performed in 1.5 ml of suspension solution, containing 100 mM KH_2PO_4 buffer (pH 7.5) and 1 mM Na_2EDTA. The homogenates were centrifuged at 14 000 rpm for 20 min at 4 °C and resulting supernatants were used for enzyme assay. The reaction mixture (total volume of 3 ml) contained 1.5 ml phosphate buffer (100 mM, pH 7), 0.95 ml distilled water, 0.5 ml H_2O_2 and 0.05 ml supernatant. Decrease in absorbance at 240 nm was recorded. The enzyme activity was calculated from the initial rate of the reaction using the extinction coefficient of H_2O_2 (E = 43.6 mM cm^{-1} at 240 nm).

Chlorophyll a fluorescence measurement

Barley seedlings were pre-darkened for 45-60 min at room temperature. Chlorophyll a fluorescence measurements were performed with the Handy PEA fluorimeter (Hansatech Instruments, King's Lynn, Norfolk, UK). Red actinic light (wavelength at peak 650 nm; spectral line half-width 22 nm) with the intensity of 3500 μmol photons m^{-2} s^{-1} was used for the induction of fluorescence and 1

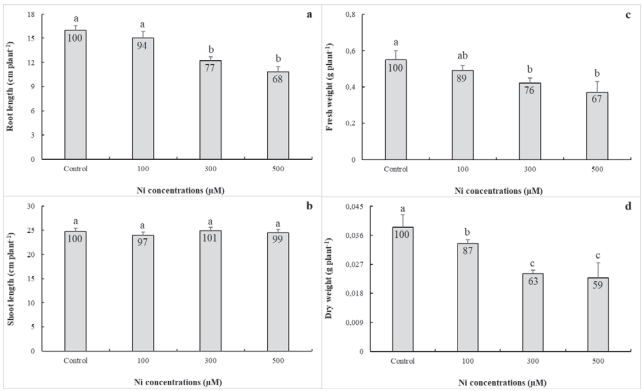

Figure 1. The effect of nickel toxicity on (a) root length, (b) shoot length, (c) fresh weight and (d) dry weight in barley seedlings. (Columns with different letters mean significant differences between the treatments according to Duncan's multiple range test (P<0.05) and numbers on the columns indicate % change relative to control, control = 100).

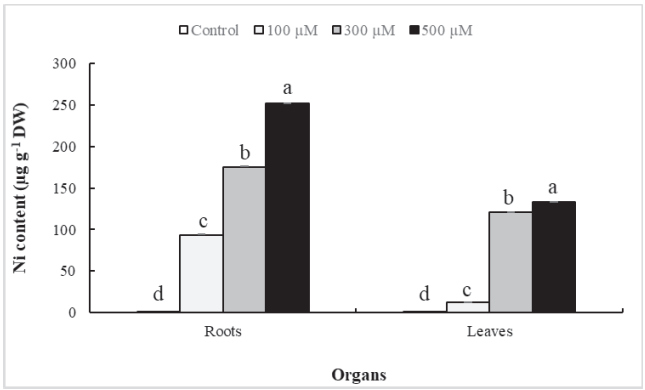

Figure 2. The effect of nickel toxicity on nickel content in the roots and leaves of barley seedlings.

s of transient fluorescence was recorded. The data were analysed, and the JIP test was conducted using Biolyzer software (Strasser et al. 2000). Measurements of chlorophyll fluorescence were done on 10 plants from each treatment and we had 3 replicates for each plant (n = 30).

Statistical analysis

Experiments were a randomised complete block design with three independent replicates. Analysis of variance (ANOVA) was performed using SPSS 20.0 statistical software for Windows. To separate significant differences between means, Duncan (least significant difference) test was used at P = 0.05.

Results

Mild nickel stress (100 µM) did not affect root growth in barley seedlings while moderate (300 µM) and severe nickel stress (500 µM) inhibited root growth to a certain extent (Fig. 1a) in comparison with control. Shoot growth, on the other hand, was not remarkably affected by nickel treatments (Fig. 1b). Like root growth, the fresh weight of barley seedlings under mild nickel toxicity were not affected, but moderate and severe nickel stress decreased the fresh weight considerably as compared to control (Fig.

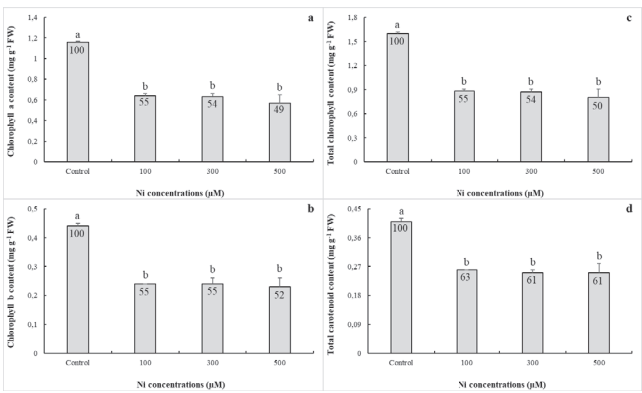

Figure 3. The effect of nickel toxicity on (a) chlorophyll a, (b) chlorophyll b, (c) total chlorophyll and (d) total carotenoid content in barley seedlings. (Columns with different letters mean significant differences between the treatments according to Duncan's multiple range test (P<0.05) and numbers on the columns indicate % change relative to control, control = 100).

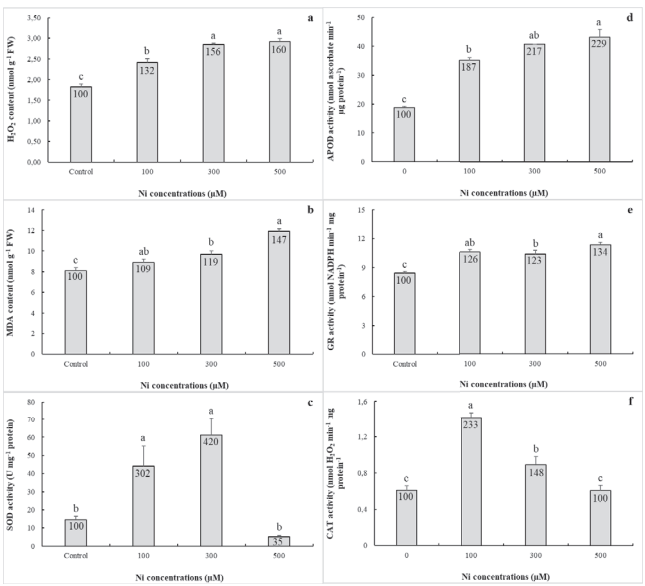

Figure 4. The effect of nickel toxicity on (a) H_2O_2 content, (b) MDA content, (c) SOD activity, (d) APOD activity, (e) GR activity and (f) CAT activity in barley seedlings. (Columns with different letters mean significant differences between the treatments according to Duncan's multiple range test (P<0.05) and numbers on the columns indicate % change relative to control, control = 100).

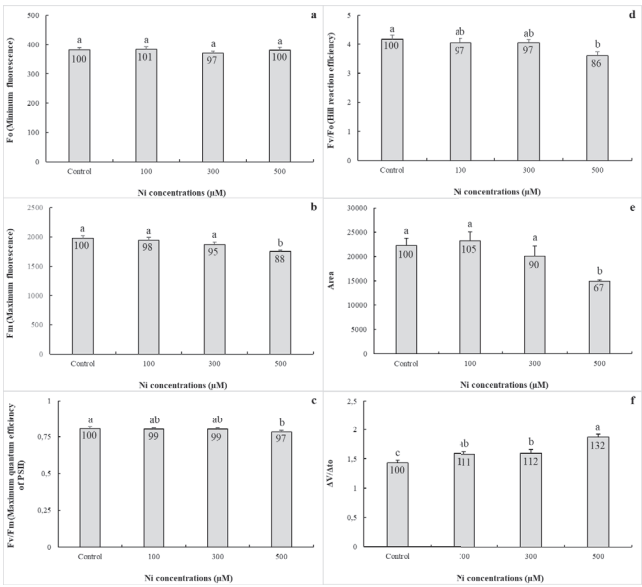

Figure 5. The effect of nickel toxicity on (a) Fo, (b) Fm, (c) Fv/Fm, (d) Fv/Fo, (e) Area and (f) ΔV/Δto in barley seedlings. (Columns with different letters mean significant differences between the treatments according to Duncan's multiple range test (P<0.05) and numbers on the columns indicate % change relative to control, control = 100).

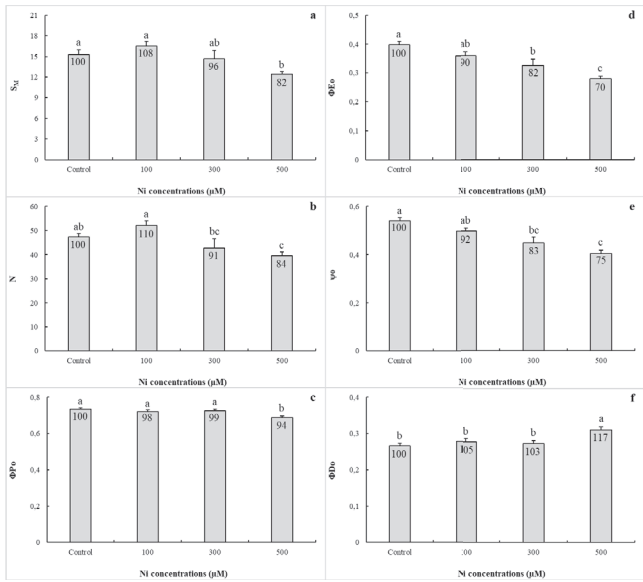

Figure 6. The effect of nickel toxicity on (a) SM, (b) N, (c) ΦPo, (d) ΦEo, (e) ψo and (f) ΦDo in barley seedlings. (Columns with different letters mean significant differences between the treatments according to Duncan's multiple range test (P<0.05) and numbers on the columns indicate % change relative to control, control = 100). Submitted: 15 November 2020.

1c). All nickel treatments led to the significantly reduced dry mass accumulation than control plants in barley seedlings (Fig. 1d). Nickel accumulation in the roots and leaves of barley seedlings represented a linear increase as the nickel concentration applied increased (Fig. 2). Chlorophyll a, chlorophyll b, total chlorophyll and total carotenoid content in the leaves of barley seedlings were significantly decreased by mild, moderate and severe nickel toxicity as compared to the respective controls (Fig. 3a, b, c and d). In the leaves of barley seedlings, mild, moderate and severe nickel stress led to the increased H_2O_2 and MDA content as compared to the controls (Fig. 4a and b). SOD and CAT activity in the leaves of barley seedlings was significantly elevated by mild and moderate nickel stress, but it was not affected by severe nickel stress as compared to control (Fig. 4c and f). APOD and GR activity in the leaves of barley seedlings was remarkably increased as a result of mild, moderate and severe nickel stress applications in comparison with the respective controls (Fig. 4d and e).

In comparison with control, all nickel treatments did not affect Fo (minimum fluorescence) in barley leaves (Fig. 5a). However, Fm (maximum fluorescence), Fv/Fm (maximum quantum efficiency of photosystem II), Fv/Fo (Hill reaction efficiency) and area (the area above the chlorophyll fluorescence curve between Fo and Fm) were remarkably decreased by only severe nickel stress as compared to controls (Fig. 5b, c, d and e). Mild, moderate and severe nickel stress led to the significant reduction in ΔV/Δto (the accumulation rate of the closed reaction centers) in the leaves of barley seedlings as compared to control (Fig. 5f). S_M (energy necessary for the closure of all reaction centers), N (the number indicating how many times quinone A is reduced while fluorescence reaches its maximum value) and ΦPo (maximum quantum yield of primary photochemistry) in the leaves of barley seedlings under severe nickel stress were significantly lower than the respective controls (Fig. 6a, b and c). Moderate and severe nickel stress led to the remarkably decreased ΦEo (quantum yield of electron transport from quinone A to plastoquinone) and ψo (efficiency of a trapped exiton that moves an electron from quinone A to the electron transport system) values in the leaves of barley seedlings as compared to controls (Fig 6. d and e). ΦDo (quantum yield of thermal dissipation) in the leaves of barley seedlings was significantly reduced by severe nickel stress as compared to control (Fig. 6f).

Discussion

The present study investigated the effect of mild (100 µM), moderate (300 µM) and severe nickel toxicity (500 µM) on some growth parameters, physiological and photochemical changes in a barley genotype, Tarm-92. The genotype Tarm-92, which is commonly grown in arid

and semi-arid parts of Central Anatolia and Transitional regions, is developed by Central Research Institute for Field Crops (Ankara) and registered in 1992. Tarm-92 (two-row feed barley) is known to be tolerant to drought, zinc and boron toxicity as well as moderately resistant to scald and barley leaf stripe. In addition, this barley genotype has facultative winter growth habit, high tillering capacity and good resistance to head loss, with the yield value of 350-450 kg da^{-1} under rainfed conditions.

Our results showed that root length of barley genotype is reduced by moderate and severe nickel toxicity which is correlated with higher level of nickel accumulation in roots as compared to leaves. Also, the decreased fresh and dry weights of barley plants were observed under nickel toxicity conditions. The nickel-induced reduction in plant growth has also been found in other plant species such as tomato, cotton, brassica and pea (Mosa et al. 2016; Khaliq et al. 2016; Ansari et al. 2015; Sirhindi et al. 2015). It has been reported that Ni toxicity led to the damage in the cell nucleus and nucleolus in root tips of tomato. Similarly, Shi and Cai (2009) have explored that excessive nickel treatments change the plasticity of cell wall, which consequently impair cell division and/or elongation. Thus, higher nickel accumulation in root cells may be responsible for the decreased root growth rate by interfering mitotic activity in our study (Gautam et al. 2017). Another possible explanation for the reduced growth rate of roots and biomass accumulation in barley plants under nickel toxicity may be the decreased uptake and translocation rate of some essential elements such as Mg, Ca, Fe, Cu and Zn which have similar chemical character to Ni (Amari et al. 2017). Kidd et al. (2009) have indicated that nickel could compete with these elements in uptake and utilization in plants and lead to mineral element deficiency. It has been reported that nickel can easily be translocated from roots to the upper parts of the plants by xylem and phloem vessels (Ishtiaq and Mahmood 2012). On the other hand, it has been manifested that plants keeping higher amount of heavy metal in their roots have been considered as more tolerant to heavy metal (Rao and Sresty 2000). Therefore, the genotype Tarm-92, may be accepted as relatively tolerant to nickel toxicity as reflected by lower nickel content in the leaves.

Our results showed that chlorophyll a, chlorophyll b, total chlorophyll and total carotenoid content decreased under nickel toxicity. It has been well documented that decreases in chlorophyll content and photosynthetic efficiency are used to monitor the heavy metal-induced damage in leaves (Asopa et al. 2016). Kamran et al. (2016) have indicated that nickel toxicity leads to chlorophyll loss as a result of Mg and Fe deficiency in the leaves of plant species. In addition, it has been claimed that the reduced chlorophyll content in plants under nickel toxicity may derive from either promotion of chlorophyllase activity or inhibition of chlorophyll-synthesizing enzymes (Abdel-Basset et al. 1995; Mysliwa-Kurdziel and Strzalka 2002). Carotenoids are responsible for the dissipation of excess excitation energy and protection of chlorophyll pigments from light-induced damages as well light absorption for photosynthetic electron transport (Trebst 2003; Hashimato et al. 2016). In this study, lower total carotenoid content observed in the leaves of barley plants may be associated with lower chlorophyll content due to photooxidation.

It has been stated that nickel toxicity interferes with photosynthetic electron transport reaction and some intermediates of cytochrome b6f and b559 in leaves (Shahzad et al. 2018). Several *in vitro* studies have showed that PSII is primary target for nickel toxicity in plants (Tripathy et al. 1981). Therefore, chlorophyll a fluorescence technique was used to investigate the performance of the photosynthetic apparatus in barley leaves under nickel toxicity. In our study, only severe nickel toxicity led to the decreased maximum quantum efficiency of PSII (as inferred Fv/Fm). This value is known to be close to 0.83 under optimum conditions and often proportional to photosynthetic efficiency (Kalaji et al. 2011). The lowered Fv/Fm values in the severe nickel-stressed leaves of barley plants clearly showed that large extent of photoinhibition has occurred in PSII units (Kalaji et al. 2011). On the other hand, relatively higher level of Fv/Fm ratio clearly demonstrated that electron transport reactions on PSII units remained almost intact under mild and moderate nickel toxicity. In the present study, Fo value was not affected by nickel toxicity treatments. It has been reported that several stress factors may result in the increase in Fo (Maxwell and Johnson 2000). Meravi and Prajapati (2018), for example, claimed that higher level of Fo may be associated with the accumulation of inactive PSII reaction centers. Kalaji et al. (2011) have shown that the reason for the higher Fo values is the slowing down of the transport of electrons from Q_A to Q_B and/or the decrease in the efficiency of PSII to capture light energy. Thus, it may be concluded that nickel stress did not lead to structural damage in PSII reaction centers in barley leaves. The lowered level of Fm value in the leaves of barley suggested that restrictive effect of severe nickel stress on the photosynthetic electron transport reactions in PSII acceptor side appeared, as indicated by Doğru and Çakirlar (2020a, 2020b). In addition, the results of this study clearly indicated that decline in Fv/Fm ratio in the severe nickel-stressed leaves of barley plants was mostly due to decrease in Fm. It has been well documented that water-splitting complex on the donor side of PSII is the most sensitive component in the photosynthetic electron transport system (Kalaji et al. 2011). Pereira et al. (2000)

have indicated that the decrease in Fv/Fo may the result from the impairment in photosynthetic electron transport reactions. The efficiency of Hill reaction or water splitting complex on the donor side of PSII (as indicated by Fv/Fo) was declined in the leaves of barley under severe nickel stress. The reduced Fv/Fo in the leaves of barley plants may be the assumption that a lower number of electrons were transported from the oxygen-evolving complex (OEC) to the plastoquinone pool, which could be a result of severe nickel toxicity-induced damages in OEC. It has been revealed by previous studies that nickel can competitively replace calcium ion in the binding site of OEC (Kidd et al. 2009). In this study, the decreased value of the parameter area in the leaves of barley clearly confirmed that electron transport rate into PQ pool is reduced by severe nickel stress (Oukarroum et al. 2015). In addition, mild, moderate and severe nickel toxicity led to the increased level of the accumulation of the closed reaction centers, as confirmed by higher $\Delta V/\Delta$ to and lower S_M and N values in the leaves of barley (Gupta 2020). Under these conditions, it is clear that PSII reaction centers are already in the closed state (reduced) and small amount of Q_A molecules are reduced until Fm value is reached under severe nickel toxicity. ΦEo and ψo, on the other hand, was declined by moderate and severe nickel toxicity in the leaves of barley seedlings, indicating that electron transport from Q_A to PQ is inhibited to a certain extent. As a result, severe nickel toxicity reduced ΦPo while ΦDo increased. This situation may be manifested that severe nickel toxicity led to thermal dissipation of absorbed light energy and primary photochemistry is reduced.

It has been well known that chloroplasts are the main site of ROS accumulation in plant cells because of the impairment of the photosynthetic electron transport reactions under stressful conditions (Doğru and Çakırlar 2020a, 2020b). Chloroplasts also possess enzymatic and non-enzymatic antioxidants to detoxify ROS. SOD, for example, is a metalloenzyme and responsible for the dismutation of superoxide radicals to H_2O_2. Assche and Clijsters (1990) have reported that SOD is a key antioxidant enzyme to protect plants from heavy metal-induced oxidative stress. Induction of SOD is very important for plants to overcome oxidative stress (Alscher et al. 2002). In our study, SOD activity was increased by mild and moderate nickel toxicity, probably indicating an efficient superoxide dismutation and H_2O_2 production. In barley leaves under severe nickel toxicity, however, SOD activity remained unchanged. Hao et al. (2006) have stated that nickel toxicity interferes indirectly with several antioxidant enzymes by replacing the essential elements such as Fe, Zn, and Mg. It is also probable an interaction between nickel ions and ligand groups of SOD, resulting in the inhibition of enzyme activity (Amari et al. 2017). APOD and GR, which are the most important enzymes of ascorbate-glutathione cycle, are in charge of detoxification of H_2O_2 (Doğru and Çakırlar 2020a). In the present study, APOD and GR activity is almost increased by mild, moderate and severe nickel toxicity in a dose-dependent manner. This result clearly showed that ascorbate-glutathione cycle is active in the leaves of barley plants under nickel toxicity and detoxification of H_2O_2 occurs efficiently. However, our results indicated considerable H_2O_2 accumulation in the leaves of barley under mild, moderate and severe nickel stress. This result may be explained by negative correlation between nickel concentration applied and CAT activity, and a possible overproduction of H_2O_2. Like H_2O_2 accumulation, MDA content in the leaves of barley was escalated with increasing nickel concentrations, indicating membrane damage. This results also explain the decreased level of chlorophyll pigments and photosynthetic activity in the leaves of barley under nickel toxicity.

In conclusion, severe nickel stress was more effective in photochemical, growth and physiological parameters in barley plants. Root growth, biomass accumulation and photosynthetic pigment content in barley plants was decreased by mild, moderate and severe nickel toxicity. Chlorophyll a fluorescence measurements clearly showed that acceptor side of PSII was more sensitive to nickel toxicity as compared to donor side. Nickel toxicity did not damage PSII reaction centers but inhibited electron transport between intermediates of PSII units. Therefore, primary photochemistry was declined, and thermal energy dissipation is increased by nickel stress in the leaves of barley. In addition, it is obvious that nickel toxicity led to the oxidative stress in the leaves of barley, as reflected by higher H_2O_2 and MDA content. Higher APOD and GR activity confirmed higher efficiency of ascorbate-glutathione cycle in the leaves of barley plants under nickel toxicity. SOD and CAT activity, however, remained unchanged under severe nickel toxicity. As a result, it may be concluded that Tarm-92 is moderately tolerant to nickel toxicity.

Acknowledgement

This study is supported by Sakarya University Scientific Research Projects Coordination Unit. Project Number: 2012-02-04-014.

References

Abdel-Basset R, Issa AA, Adam MS (1995) Chlorophyllase activity: effects of heavy metals and calcium. Photosynth

31:421-425.
Aebi H (1984) Catalase *in vitro*. Meth Enzymol 105:121-126.
Ahmad MSA, Hussain M, Ashraf M, Ahmad R, Ashraf MY (2009) Effect of nickel on seed germinability of some elite sunflower (*Helianthus annuus* L.). Pak J Bot 41:1871-1882.
Ali MA, Ashraf M, Athar HR (2009) Influence of nickel stress on growth and some important physiological/biochemical attributes in some diverse canola (*Brassica napus* L.) cultivars. J Hazard Mat 172:964-969.
Alscher RG, Ertürk N, Heath LS (2002) Role of superoxide dismutases (SODs) in controlling oxidative stress. J Exp Bot 53:1331-1341.
Amari T, Ghnaya T, Abdelly C (2017) Nickel, cadmium and lead phytotoxicity and potential of halophytic plants in heavy metal extraction. South Afr J Bot 111:99-110.
Ansari MKA, Ahmad A, Umar S, Zia MH, Iqbal M, Owens G (2015) Genotypic variation in phytoremediation potential of Indian mustard exposed to nickel stress: a hydroponic study. Int J Phytorem 17:135-144.
Asopa PP, Bhatt R, Sihag S, Kothari S, Kachhwaha S (2016) Effect of cadmium on physiological parameters of cereal and millet plants-a comparative study. Int J Phytorem 19:225-230.
Assche FV, Clijsters H (1990) Effects of metals on enzyme activity in plants. Plant Cell Environ 13:195-206.
Beyer WF, Fridovich I (1987) Assaying for superoxide dismutase activity: Some large consequences of minor changes in conditions. Anal Biochem 161:559-566.
Bhaduri AM, Fulekar M (2012) Antioxidant enzyme responses of plants to heavy metal stress. Rev Environ Sci Biotechnol 11:55-69.
Bradford MM (1976) A rapid and sensitive method for the quantitation of microgram quantities of protein utilizing the principle of protein-dye binding. Anal Biochem 72:248-254.
Chen C, Huang D, Liu J (2009) Functions and toxicity of nickel in plants: recent advances and future prospects. Clean: Soil, Air, Water 37:304-313.
Doğru A (2019) Evaluation of lead tolerance in some barley genotypes by means of chlorophyll a fluorescence. Bartin Uni Int J Nat App Sci 2:228-238.
Doğru A (2020) Antioxidant responses of barley (*Hordeum vulgare* L.) genotypes to lead toxicity. Biologia 75:1265-1272.
Doğru A, Çakirlar H (2020a) Effects of leaf age on chlorophyll fluorescence and antioxidant enzymes activity in winter rapeseed leaves under cold acclimation conditions. Braz J Bot 43:11-20.
Doğru A, Çakirlar H (2020b) Is leaf age a predictor for cold tolerance in winter oilseed rape plants? Func Plant Biol 47(3):250-262.
Force L, Critchley C, van Rensen JJS (2003) New fluorescence parameters for monitoring photosynthesis in plants. 1. The effect of illumination on the fluorescence parameters of the JIP test. Photosynt Res 78:17-33.
Gajewska E, Skł odowska M, Słaba M, Mazur J (2006) Effect of nickel on antioxidative enzyme activities, proline and chlorophyll contents in wheat shoots. Biol Plant 50:653-659.
Gajewska E, Skłodowska M (2007) Effect of nickel on ROS content and antioxidative enzyme activity in wheat leaves. Biometals 20:27-36.
Gajewska E, Wielanek M, Bergier K, Skłodowska M (2009) Nickel induced depression of nitrogen assimilation in wheat roots. Acta Physiol Plant 31:1291-1300.
Gautam S, Rathoure AK, Chhabra A, Pandey SN (2017) Effects of nickel and zinc on biochemical parameters in plants-A review. Octa J Environ Res 5(1):14-21.
Gopal R, Rizvi AH (2008) Excess lead alters growth, metabolism and translocation of certain nutrients in radish. Chemosphere 70:1539-1544.
Govindjee (2004) Chlorophyll a fluorescence: a bit of basics and history. In Papageorgiou G, Govindjee, Eds., Chlorophyll a Fluorescence A Signature of Photosynthesis. Springer, Dordrecht, pp 1-42.
Gupta R (2020) Manganese repairs the oxygen-evolving complex (OEC) in maize (*Zea mays* L.) damage during seawater vulnerability. J Soil Sci Plant Nutr 20:1387-1396.
Hao F, Wang X, Chen J (2006) Involvement of plasma-membrane NADPH oxidase in nickel-induced oxidative stress in roots of wheat seedlings. Plant Sci 170:151-158.
Hashimoto H, Uragami C, Cogdell RJ (2016) Carotenoids and Photosynthesis. In Stange C, Ed., Carotenoids in Nature. Subcellular Biochemistry. Cham, Springer, pp 111-139.
Heath RL, Packer L (1968) Photoperoxidation in isolated chloroplasts I. Kinetic and stoichiometry of fatty acid peroxidation. Arch Biochem Biophys 125:189-198.
Hedfi A, Mahmoudi E, Boufahja F, Beyrem H, Aissa P (2007) Effects of increasing levels of nickel contamination on structure of offshore nematode communities in experimental microcosms. Bull Environ Contam Toxicol 79:345-349.
Ishtiaq S, Mahmood S (2012) Phytotoxicity of nickel and its accumulation in tissues of three Vigna species at their early growth stages. J Appl Bot Food Qual 84:223-228.
Izosimova A (2005) Modelling the interactions between calcium and nickel in the soil-plant system. FAL Agr Res 288:99.
Kalaji MH, Govindjee, Bosa K, Kościelniak J, Gołaszewska KZ (2011) Effects of salt stress on photosystem II efficiency and CO_2 assimilation of two Syrian barley landraces. Env Exp Bot 73:64-72.
Khaliq A, Ali S, Hameed, A, Farooq MA, Farid M, Shakoor MB, Mohmood K, Ishaque W, Rizwan M (2016) Silicon alleviates nickel toxicity in cotton seedlings through enhancing growth, photosynthesis and suppressing

Ni uptake and oxidative stress. Arch Agron Soil Sci 62:633-647.

Khan MU, Shahbaz N, Waheed S, Mahmood A, Shinwari ZK, Malik RN (2016) Comparative health risk surveillance of heavy metals via dietary foodstuff consumption in different land-use types of Pakistan. Hum Ecol Risk Assess Int J 22:168-186.

Kidd P, Barcelo J, Bernal MP, Navari-Izzo F, Poschenrieder C, Shilev S, Clemente R, Monterroso C (2009) Trace element behaviour at the root-soil interface: implications in phytoremediation. Environ Exp Bot 67:243-259.

Lichtenthaler HK (1987) Chlorophylls and carotenoids: pigments of photosynthetic membranes. Meth Enzymol 148:350-382.

Maxwell K, Johnson NG (2000) Chlorophyll fluorescence-a practical guide. J Exp Bot 51:659-668.

Mosa A, El-Banna MF, Gao B (2016) Biochar filters reduced the toxic effects of nickel on tomato (*Lycopersicon esculentum* L.) grown in nutrient film technique hydroponic system. Chemosphere 149:254-262.

Mysliwa-Kurdziel B, Strzalka K (2002) Influence of metals on biosynthesis of photosynthetic pigments. In: Prasad, M. N. V., Strzalka, K. (Eds.) Physiology and Biochemistry of Metal Toxicity and Tolerance in Plants. Kluwer Academic Publishers, Netherlands, pp.201-227.

Ohkawa H, Ohishi N, Yagi NY (1979) Assay of lipid peroxides in animal tissue by thiobarbituric acid reaction. Anal Biochem 95:351-358.

Oukarroum A, Bussotti F, Goltsev V, Hazem MH (2015) Correlation between reactive oxygen species production and photochemistry of photosystems I and II in *Lemna minor* L. plants under salt stress. Env Exp Bot 109:80-88.

Pereira WE, de Siqueira DL, Martinez CA, Puiatti M (2000) Gas exchange and chlorophyll fluorescence in four citrus rootstocks under aluminium stress. J Plant Physiol 157:513-520.

Rao KM, Sresty T (2000) Antioxidative parameters in the seedlings of pigeonpea (*Cajanus cajan* (L.) Millspaugh) in response to Zn and Ni stresses. Plant Sci 157:113-128.

Rizwan M, Ali S, Qayyum MF, Ibrahim M, Rehman MZ, Abbas T, Ok YS (2016) Mechanisms of biochar-mediated alleviation of toxicity of trace elements in plants: a critical review. Environ Sci Pollut Res 23:2230-2248.

Sachan P, Lal N (2017) An overview of nickel (Ni^{2+}) essentiality, toxicity and tolerance strategies in plants. Asian J Biol 2:1-15.

Sgherri CLM, Loggini B, Puliga S, Navari-Izzo F (1994) Antioxidant system in *Sporobolus stapfianus*: changes in response to desiccation and rehydration. Phytochem 35:561-565.

Shahzad B, Tanveer M, Rehman A, Cheema SA, Fahad S, Rehman S, Sharma A (2018) Nickel; whether toxic or essential for plants and environment: a review. Plant Physiol Biochem 132:641-651.

Sirhindi G, Mir MA, Sharma P, Gill SS, Kaur H, Mushtag R (2015) Modulatory role of jasmonic acid on photosynthetic pigments, antioxidants and stress markers of *Glycine max* L. under nickel stress. Physiol Mol Biol Plants 21:559-565.

Strasser RJ, Srivastava A, Tsimilli-Michael M (2000) The fluorescence as a tool to characterize and screen photosynthetic samples. In: Yunus, M., Pathre, U., Mohanty, P. (Eds.), Probing Photosynthesis: Mechanisms, Regulation and Adaptation. Taylor & Francis, London, pp.445-483.

Strasser RJ, Tsimilli-Mitchael M, Srivastava A (2004) Analysis of chlorophyll fluorescence transient. (AIPH) Chlorophyll a Fluorescence 19:321-362.

Trebst A (2003) Function of β-carotene and tocopherol in photosystem II. Z Natur 58:609-620.

Tripathy BC, Bhatia B, Mohanty P (1981) Inactivation of chloroplast photosynthetic electron-transport activity by Ni^{2+}. Biochim Biophys Acta Bioenerg 638:217-224.

Wang SY, Jiao H, Faust M (1991) Changes in ascorbate, glutathione and related enzyme activity during thidiazuron-induced bud break of apple. Plant Physiol 82:231-236.

Yusuf MA, Kumar D, Rajwanshi R, Strasser RJ, Tsimilli-Michael M, Govindjee, Sarin VB (2010) Overexpression of γ-tocopherol methyl transferase gene in transgenic *Brassica juncea* plants alleviates abiotic stress: physiological and chlorophyll fluorescence measurements. Biochim Biophys Acta 1797:1428-1438.

Acta Biologica Szegediensis

Volume 65(1):11-16, 2021
Acta Biologica Szegediensis
http://abs.bibl.u-szeged.hu/index.php/abs

DOI:10.14232/abs.2021.1.11-16

ARTICLE

TU-DAMD employment for molecular characterization of *Salvia judaica* and *Salvia palaestina* species

Basel Saleh

Department of Molecular Biology and Biotechnology, Atomic Energy Commission of Syria, Damascus, Syria.

ABSTRACT Genetic diversity in perennial *Salvia judaica* Boiss (Judean sage) and *Salvia palaestina* Benth (Palestinian sage) species using touch-up directed amplification of minisatellite region DNA (TU-DAMD) has been performed in two separated sets; in the first set (set A) the initial annealing temperature was increased from 50 °C to 55 °C, whereas, in the second one (set B), it increased from 55 °C to 60 °C by 0.5 °C/cycle during the first 10 PCR amplification cycles. Fifteen DAMD primers have been tested for each set. Set (A) produced 89.39% polymorphism level (P%) with polymorphic information content (PIC) average of 0.33 and marker index (MI) average of 3.96. Whereas, in set (B) these values were recorded to be 94.02%, 0.34 and 3.98 for P%, PIC and MI, respectively. Data showed that the two mentioned sets successfully highlighted high polymorphism level between the two studied *Salvia* sp. This work studies genetic diversity of *S. judaica* and *S. palaestina* species using TU-DAMD test as a novel molecular marker.

Acta Biol Szeged 65(1):11-16 (2021)

KEY WORDS

genetic diversity
Salvia judaica
Salvia palaestina
TU-DAMD

ARTICLE INFORMATION

Submitted
02 February 2021.
Accepted
22 February 2021.
***Corresponding author**
E-mail: ascientific3@aec.org.sy

Introduction

Salvia genus belongs to Lamiaceae family, includes approximately 1000 species, and was considered as one of the largest plant genera (Walker et al. 2004). This genus commonly known as sage and it is considered as the largest genus within the family (Hu et al. 2018). According to Mouterde (1983), 28 *Salvia* species were grown along the Syrian coastline at different sea altitudes up to 900 m.

Salvia judaica Boiss (Judean sage) is a perennial plant native to Mediterranean woodlands and shrublands (https://web.archive.org) and distributed in Turkey, Syria, Lebanon, and Palestine (Mouterde 1983). Whereas, *Salvia palaestina* Benth (Palestinian sage) is a perennial plant native to Palestine, Turkey, Syria, Iraq, Iran and the Sinai Peninsula and north-eastern Egypt (Loutfy 2002; Betsy 2003). It grows at wide range of habitats from 300 to 1220 m altitude.

Molecular markers have been widely and successfully used in plants genetic studies at genotypes, species and genera levels. Of which, directed amplification of minisatellite region DNA (DAMD) marker has been successfully employed in studies genetic variability of many plant species (Heath et al. 1993; Saleh 2019a).

More recently, Saleh (2019b) reported *S. tomentosa* species genetic diversity using touch-down directed amplification of minisatellite DNA (TD-DAMD) marker. The previous study reported various molecular markers that have been employed for genetic diversity of different *Salvia* species, *e.g.*, random amplified polymorphic DNA (RAPD) marker in *S. hispanica* L. (Cahill 2004), inter simple sequence repeat (ISSR) marker in *S. lachnostachys* (Erbano et al. 2015), RAPD, amplified fragment length polymorphism (AFLP) (Wen et al. 2007), sequence-related amplified polymorphism (SRAP) and ISSR (Song et al. 2010) in *S. miltiorrhiza* Bge, nuclear ribosomal DNA and plastid DNA sequences in *S. lutescens* var. *intermedia* (Takano 2017), chloroplast simple sequence repeats (cpSSR's) in *S. divinorum* (Casselman 2016), chloroplast and nuclear ribosomal DNA sequences and allozyme polymorphisms in *S. japonica* (Sudarmono and Okada 2008) and directed amplification of minisatellite region DNA (DAMD) in *Salvia* sp. (Karaca et al. 2008).

DAMD maker has been developed for the first time in common bean landraces by Ince and Karaca (2011) to touch-down directed amplification of minisatellite DNA (TD-DAMD) marker. Then this maker has been used for molecular characterization of other plant species *e.g.* for *Salvia* species (Ince and Karaca 2012); *Allium* sp. (Deniz et al. 2013); carnation cultivars (Ince and Karaca 2015), commercial cotton (Gocer and Karaca 2016) and *S. tomentosa* (Saleh 2019b).

On the basis of TD-DAMD marker, an attempt has been carried out based on increasing annealing temperature by 0.5 °C/cycle during the first 10 PCR amplification cycles in place to reducing it in TD-DAMD and thereby named as touch-up directed amplification of minisatellite DNA

Table 1. Descriptive sites of collected studied samples in the current study.

Species	Code	City province	Altitude (m)	Annual rainfall (mm)
Salvia judiaca	SJ1	Lattakia	80	750
Salvia judiaca	SJ2	Lattakia	600	750
Salvia judiaca	SJ3	Lattakia	680	1250
Salvia palaestina	SP4	Damascus	920	260
Salvia palaestina	SP5	Damascus	950	260
Salvia palaestina	SP6	Damascus	1200	150
Ballota damascena	BD7	Damascus	970	260

(TU-DAMD) in nouvelle test. Thereby, the current study highlights genetic diversity of *S. judaica* and *S. palaestina* species through TU-DAMD marker as a new assay for their molecular characterization.

Materials and Methods

Plants materials

Leaves samples (5-10 plants/genotype) were collected from *Salvia judaica* (rural Lattakia) (SJ) and *Salvia palaestina* (rural Damascus) (SP) species with *Ballota damascena* Boiss (Lamiaceae) (rural Damascus) (BD) as outside far reference, during blooming stage (Table 1). Samples were frozen in liquid nitrogen and kept at -80 °C until use.

DNA isolation

Total genomic DNA was extracted from frozen leaves samples (3 samples of *S. judaica*, 3 samples of *S. palaestina* and 1 sample of *B. damascena*) using CTAB (cetyltrimethylammonium bromide) method as described by Doyle and Doyle (1987).

Touch-Up Directed Amplification of Minisatellite region DNA (TU-DAMD) test

TU-DAMD test has been performed in two separated tests; in the first test (set A) the initial annealing temperature was increased from 50 °C to 55 °C by 0.5 °C/cycle during the first 10 PCR amplification cycles. Whereas, in the second one (set B), it increased from 55 °C to 60 °C by 0.5 °C/cycle during the first 10 PCR amplification cycles. Then, similar PCR amplification program was performed at annealing Tm of 55 °C for the both tests during the remaining 30 PCR amplification cycles as described by Seyedimoradi et al. (2012) for DAMD marker.

PCR products were separated on a 2% ethidium bromide-stained agarose (Bio-Rad) in 0.5 × Tris-borate-EDTA (TBE) buffer, by electrophoresis at 85 V for 2.5 h, and visualized with a UV transilluminator. PCR amplification products size was estimated with a 1 kb DNA ladder standard. Fifteen DAMD primers have been tested for each set to investigate genetic diversity in *S. judaica* and *S. palaestina* species (Table 2).

TU-DAMD data analysis

PCR products were photographed under UV, and each size class was scored as 0 or 1 for the absence or presence class, respectively. Unweighted pair group method using arithmetic averages (UPGMA) was constructed based on the estimated percent disagreement values (PDVs) using Statistica 6 (Statsoft 2003) program. Moreover, genetic similarity (GS) among examined samples was estimated according to Nei and Li (1979) index. Whereas, polymorphic information content (PIC) values were estimated for each tested primer according to the formula:

$$PIC = 1 - \Sigma(Pij)^2$$

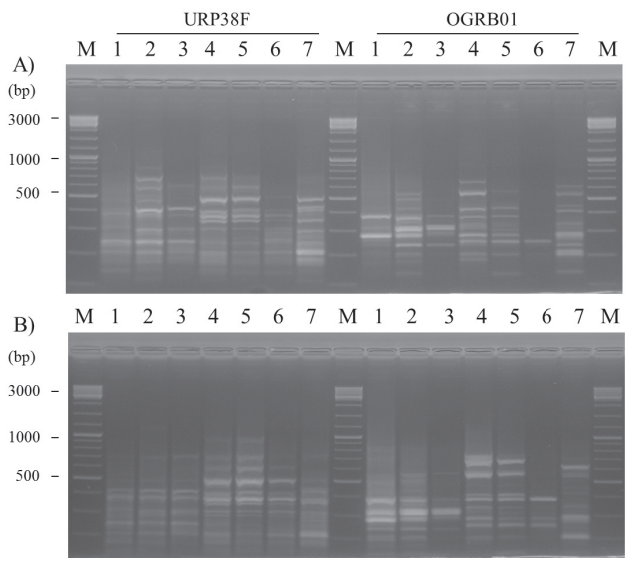

Figure 1. TU-DAMD polymorphism profile yielded by set (A): Tm increased from 50 °C to 55 °C and set (B): Tm increased from 55 °C to 60 °C by 0.5 °C/cycle during the first 10 PCR amplification cycles using URP38F and OGRB01 DAMD primers for *S. judaica* (lines 1-3); *S. palaestina* (lines 4-6) and *B. damascena* (line 7). M: VC100bp Plus DNA Ladder (Vivantis) size standard.

Table 2. DAMD primers used in the current study.

Primer number	Primer name	Primer sequence 5'-3'
1	URP1F	ATCCAAGGTCCGAGACAACC
2	URP2R	CCCAGCAACTGATCGCACAC
3	URP4R	AGGACTCGATAACAGGCTCC
4	URP9F	ATGTGTGCGATCAGTTGCTG
5	URP25F	GATGTGTTCTTGGAGCCTGT
6	URP38F	AAGAGGCATTCTACCACCAC
7	OGRB01	AGGGCTGGAGGAGGGC
8	FVIIex8C	CCTGTGTGTGTGCAT
9	FVIIex8	ATGCACACACACAGG
10	HBV5	GGTGTAGAGAGGGGT
11	33.6	GGAGGTGGGCA
12	HVRc	CCTCCTCCCTCCT
13	URP2F	GTGTGCGATCAGTTGCTGGG
14	URP6R	GGCAAGCTGGTGGGAGGTAC
15	URP17R	AATGTGGGCAAGCTGGTGGT

Where Pij is the frequency of the i^{th} pattern revealed by the j^{th} primer combination, summed across all patterns revealed by the primers (Botstein et al. 1980). Indeed, marker index (MI), a universal metric to represent the amount of information obtained per experiment for a given kind of marker was also estimated for each tested primer as described by Powell et al. (1996) according to the formula:

$$MI = PIC \times \eta\beta$$

Where PIC is the mean PIC value, η the number of bands, and β the proportion of polymorphism.

In the current study, statistical comparison based on Mantel test has been performed among TU- DAMD, A (set A), B (set B) and C (set A + B) data.

Results

TU-DAMD test has been employed to investigate genetic diversity of *S. judaica* and *S. palaestina* species. Polymorphism pattern including set (A) and (B) as yielded by URP38F and OGRB01 DAMD primers was presented in Fig. 1. Data showed that for set (A), total bands number ranged between 8 (FVIIex8C)-18 (OGRB01) bands with a mean average of 13.20 bands/primer. Whereas, polymorphic bands number ranged between 8 (FVIIex8C) -18 (OGRB01) polymorphic bands with a mean average of 11.80 polymorphic bands/primer. Indeed, set (A) produced 198 bands of which 177 (89.39%) were polymorphic. Whereas, PIC value ranged between 0.23 (HBV5) - 0.41 (URP25F) with a mean average of 0.33 (Table 3). As for set (B), total bands number ranged between 7 (FVIIex8) - 18 (URP38F & OGRB01) bands with a mean average of 12.27 bands/primer. Whereas, polymorphic bands number ranged between 6 (FVIIex8) - 18 (OGRB01) polymorphic bands with a mean average of 11.53 polymorphic bands/primer. Indeed, set (B) produced 184 bands of which 173 (94.02%) were polymorphic. Whereas, PIC value ranged between 0.23 (FVIIex8) - 0.40 (URP25F) with a mean

Table 3. Banding pattern of TU-DAMD amplified fragments scored.

Set (A)					
Primer name	TB	PB	P%	PIC	MI
URP1F	13	12	92.31	0.38	4.56
URP2R	11	11	100.00	0.39	4.29
URP4R	14	11	78.57	0.24	2.64
URP9F	16	14	87.50	0.35	4.90
URP25F	13	13	100.00	0.41	5.33
URP38F	17	16	94.12	0.29	4.64
OGRB01	18	18	100.00	0.38	6.84
FVIIex8C	8	8	100.00	0.39	3.12
FVIIex8	10	9	90.00	0.27	2.43
HBV5	15	11	73.33	0.23	2.53
33.6	11	11	100.00	0.37	4.07
HVRc	13	8	61.54	0.28	2.24
URP2F	14	13	92.86	0.34	4.42
URP6R	14	13	92.86	0.36	4.68
URP17R	11	9	81.82	0.3	2.70
Total	198	177			
Average	13.20	11.80	89.66	0.33	3.96
Set (B)					
Primer name	TB	PB	P%	PIC	MI
URP1F	14	14	100.00	0.34	4.76
URP2R	8	8	100.00	0.33	2.64
URP4R	16	14	87.50	0.34	4.76
URP9F	14	14	100.00	0.32	4.48
URP25F	8	8	100.00	0.4	3.20
URP38F	18	14	77.78	0.31	4.34
OGRB01	18	18	100.00	0.39	7.02
FVIIex8C	12	12	100.00	0.4	4.80
FVIIex8	7	6	85.71	0.23	1.38
HBV5	9	8	88.89	0.27	2.16
33.6	16	16	100.00	0.34	5.44
HVRc	11	10	90.91	0.32	3.20
URP2F	8	7	87.50	0.35	2.45
URP6R	15	14	93.33	0.37	5.18
URP17R	10	10	100.00	0.39	3.90
Total	184	173			
Average	12.27	11.53	94.11	0.34	3.98

TB: total bands; PB: polymorphic bands; P%: polymorphic %; PIC: polymorphic information content; MI: marker index.

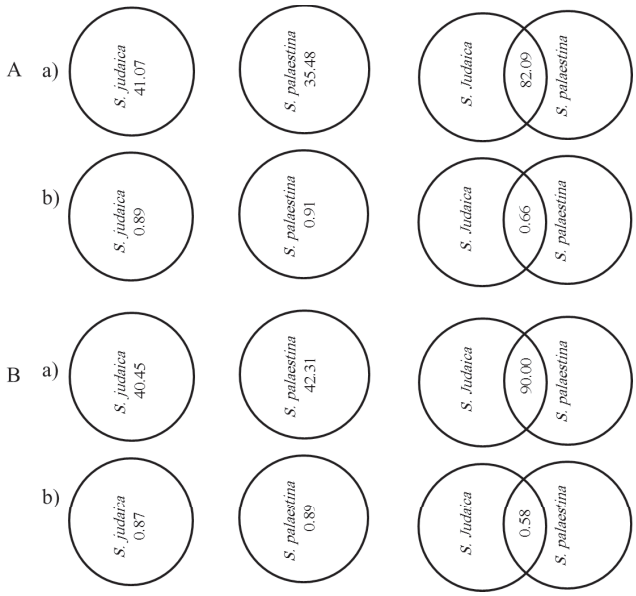

Figure 2. Polymorphism level (P%) (a) and genetic similarity (GS) (b) values in *S. judaica* and *S. palaestina* species through TU-DAMD A (set A) and B (set B) data.

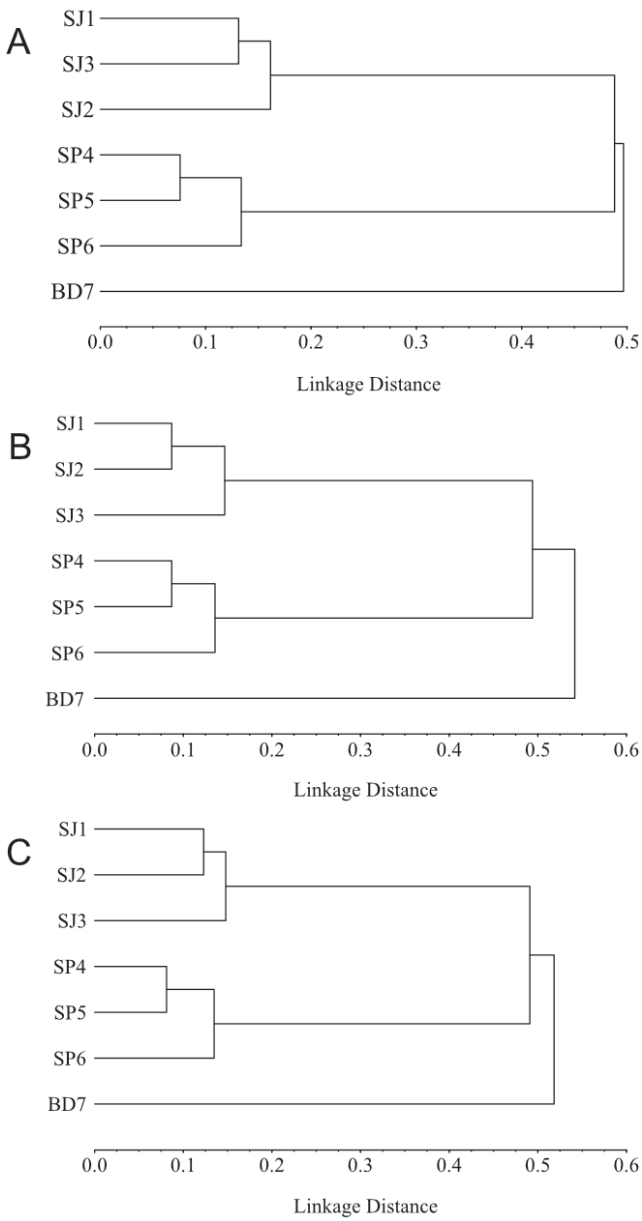

Figure 3. UPGMA Cluster analysis revealing relationships between *S. judaica* and *S. palaestina* through TU-DAMD A (set A), B (set B) and C (set A+B) data.

average of 0.34 (Table 3).

Genetic diversity was separately detected in the two studied *Salvia* sp. (Fig. 2). In this regards, for set (A), P% was recorded to be 41.07, 35.48 and 82.09% with genetic similarity (GS) of 0.89, 0.91 and 0.66 for *S. judaica*, *S. palaestina* and *S. judaica* + *S. palaestina* together, respectively. As for set (B), these values were recorded to be 40.45, 42.31 and 90.00% for P% with GS of 0.87, 0.89 and 0.58 for *S. judaica*, *S. palaestina* and *S. judaica* + *S. palaestina* together, respectively.

UPGMA cluster analysis constructed (Fig. 3) based on PDV (Table 4), revealed that *B. damascena* was genetically so far from the two studied *Salvia* sp. Whereas, the two studied *Salvia* sp. were grouped into two main groups. The first group involved SJ samples ; whereas, the second one involved SP samples (Fig. 3) for set (A), set (B) and set (A) + set (B) together.

Cluster analysis revealed that SJ1 and SJ3 and also SP4 and SP6 samples were the most closed samples by showing the lowest PDV value of 0.13 for set (A) (Table 4). As for set (B), SP5 and SP6 samples were the most closed samples by showing the lowest PDV value of 0.13 (Table 4).

Whereas, in set (A) and set (B) combination, SJ1 and SJ2 samples were the most closed samples by showing the lowest PDV value of 0.12 (Table 4).

Mantel test revealed a highly significant correlation among the possible combination. In this regards, very good fit (r=0.994) has been recorded between A+C and B+C data and also between A+B data (r=0.977).

Discussion

Genetic diversity of *S. judaica* and *S. palaestina* species through TU-DAMD marker has been highlighted based on two (A) and (B) TU-DAMD sets.

The current study revealed that P% for set (A), was recorded to be 41.07, 35.48 and 82.09%; whereas, for set (B), these values were recorded to be 40.45, 42.31 and 90.00% for *S. judaica*, *S. palaestina* and *S. judaica* + *S.*

Table 4. Percent disagreement values (PDV) yielded by TU-DAMD data based on UPGMA routine in statistical program.

Set (A)							
Genotype	SJ1*	SJ2	SJ3	SP4	SP5	SP6	BD7
SJ1	0.00						
SJ2	0.16	0.00					
SJ3	0.13	0.17	0.00				
SP4	0.53	0.52	0.47	0.00			
SP5	0.51	0.48	0.44	0.08	0.00		
SP6	0.49	0.53	0.42	0.13	0.14	0.00	
BD7	0.49	0.54	0.44	0.52	0.49	0.48	0.00
Set (B)							
Genotype	SJ1	SJ2	SJ3	SP4	SP5	SP6	BD7
SJ1	0.00						
SJ2	0.09	0.00					
SJ3	0.15	0.14	0.00				
SP4	0.54	0.48	0.47	0.00			
SP5	0.52	0.47	0.47	0.09	0.00		
SP6	0.54	0.48	0.48	0.14	0.13	0.00	
BD7	0.59	0.53	0.53	0.54	0.53	0.52	0.00
Set (A)+(B)							
Genotype	SJ1	SJ2	SJ3	SP4	SP5	SP6	BD7
SJ1	0.00						
SJ2	0.12	0.00					
SJ3	0.14	0.15	0.00				
SP4	0.54	0.50	0.47	0.00			
SP5	0.51	0.47	0.46	0.08	0.00		
SP6	0.52	0.51	0.45	0.13	0.14	0.00	
BD7	0.54	0.54	0.49	0.53	0.51	0.50	0.00

Set A: The initial annealing temperature (Tm) was increased from 50 °C to 55 °C and set B - Tm increased from 55 °C to 60 °C by 0.5 °C/cycle during the first 10 PCR amplification cycles.
**S. judaica* (SJ1-SJ3), *S. palaestina* (SP4-SP6) and *B. damascena* (BD7).

palaestina together, respectively.

This observation could suggest low genetic diversity in *S. judaica* and *S. palaestina*. Our data were coherent with Safaei et al. (2016), who reported that P% was recorded to be 38.46, 47.25, 57.14, 49.45, 42.86 and 28.57% for *S. hypoleuca, S. nemorosa, S. limbata, S. xanthocheila, S. spinosa* and *S. reuterana,* respectively, using 10 ISSR primers. Similarly, Altindal (2019) reported P% of 32.03% in *S. officinalis* using 16 ISSR primers. Similar observation has been also noted by Tonk et al. (2010) in other Lamiaceae family members, who reported that GS values ranged between 0.49 - 0.73 indicated low genetic variability in Turkish oregano (*Origanum onites* L.) species using RAPD marker. Moreover, Gocer and Karaca (2016) reported 120 total bands, of which 42 (35%) were polymorphic among 26 cotton samples using 10 DAMD primers.

However, high genetic diversity has been recorded in other Lamiaceae family members. In this regards; Swamy and Anuradha (2011) reported 96 total bands of which 80 (83.3%) were polymorphic in patchouli cultivars (*Pogostemon cablin* Benth.) using RAPD marker. Moreover, Talebi et al. (2015) reported 240 total bands of which 198 (82.5%) were polymorphic with a mean average PIC of 0.248 in *Thymus daenensis* subsp. *daenensis* using SRAP marker. Indeed, Tapeh et al. (2018) reported 198 total bands of which 184 (92.9%) were polymorphic with a mean PIC average of 0.39 in Iranian *Teucrium* (*Teucrium polium* L.) populations using ISSR marker.

More recently, Saleh (2019b) reported 158 total bands of which 131 (82.911%) were polymorphic with a mean PIC and MI values of 0.264 and 2.269, respectively, in *S. tomentosa* based on Td-DAMD marker.

Since the molecular marker efficacy depend on the produced polymorphism degree; the current study could suggest that the two sets similarly and successfully highlighted genetic diversity between the two studied *Salvia* spices by showing similar PIC and MI values of 0.33 and 3.96 and 0.34 and 3.98 between *S. judaica* and *S. palaestina* species for set (A) and set (B), respectively.

Conclusion

Genetic diversity in *S. judaica* and *S. palaestina* species has been highlighted based on two TU-DAMD (A) and (B) sets. This work revealed that the two employed sets gave similar highly genetic diversity between the two studied *Salvia* sp. Whereas, low genetic diversity within each species has been recorded using the two employed sets. Based on data presented herein, it worth noting to use and validate this novel assay for molecular characterization of other plant species.

Acknowledgements

I thank Dr. I. Othman (Director General of AECS) and Dr. N. Mirali (Head of Molecular Biology and Biotechnology Department in AECS) for their support, and the Plant Biotechnology group for technical assistance.

References

Altindal D (2019) Determination of genetic diversity of natural sage populations in Muğla region of Turkey. Int J Environ Sci Technol 16(2):1-6.

Betsy C (2003) The New Book of *Salvias*: Sages for Every Garden. Timber Press.

Botstein D, White RL, Skolinck M, Davis RW (1980) Construction of a genetic linkage map in man using restriction fragment length polymorphisms. Am J Hum Gene 32:314-331.

Cahill JP (2004) Genetic diversity among varieties of Chia (*Salvia hispanica* L.). Gen Res Crop Evol 51(7):773-781.

Casselman I (2016) Genetics and phytochemistry of *Salvia divinorum*. PhD Thesis, Southern Cross University, Lismore, NSW.

Deniz I, Genc I, Ince AG, Aykurt C, Elmasulu S, Sümbül H, Sönmez S, Çitak S (2013) Taxonomic data supporting differences between *Allium elmaliense* and *Allium cyrilli*. Biologia 68(3):373-383.

Doyle JJ, Doyle JL (1987) A rapid DNA isolation procedure for small quantities of fresh leaf tissue. Phytochem Bull 19:11-15.

Erbano M, Schühli SG, dos Santos ÉP (2015) Genetic variability and population structure of *Salvia lachnostachys*: Implications for breeding and conservation programs. Int J Mol Sci 16:7839-7850.

Gocer EU, Karaca M (2016) Genetic characterization of some commercial cotton varieties using Td-DAMD-PCR markers. J Sci Engin Res 3(4):487-494.

Heath DD, Iwama GK, Devlin RH (1993) PCR primed with VNTR core sequence yields species specific patterns and hypervariable probes. Nucl Acid Res 21:5782-5785.

Hu G-X, Takano A, Drew BT, Liu E-D, Soltis DE, Soltis PS, Peng H, Xiang C-L (2018) Phylogeny and staminal evolution of *Salvia* (Lamiaceae, Nepetoideae) in East Asia. Ann Bot 122:649-668.

Ince AG, Karaca M (2011) Genetic variation in common bean landraces efficiently revealed by Td-DAMD-PCR markers. Plant Omics 4(4):220-227.

Ince AG, Karaca M (2012) Species-specific touch-down DAMD-PCR markers for *Salvia* species. J Med Plant Res 6(9):1590-1595.

Ince AG, Karaca M (2015) Td-DAMD-PCR assays for fingerprinting of commercial carnations. Turk J Biol 39:290-298.

Loutfy B (2002) Flora of Egypt, Volume 3: Verbenaceae-Compositae. Al Hadara Pub.

Mouterde PSJ (1983) Nouvelle Flore du Liban et de la Syria. Part 3. pp.159-170.

Nei M, Li W (1979) Mathematical model for studying genetic variation in terms of restriction endonucleases. Proc Natl Acad Sci USA 76:5269-5273.

Powell W, Morgante M, Andre C, Hanafey M, Vogel J, Tingey S, Rafalski A (1996) The comparison of RFLP, RAPD, AFLP and SSR (microsatellite) markers for germplasm analysis. Mol Breed 2:225-238.

Safaei M, Sheidai M, Alijanpoor B, Noormohammadi Z (2016) Species delimitation and genetic diversity analysis in *Salvia* with the use of ISSR molecular markers. Acta Bot Croat 75(1):45-52.

Saleh B (2019a) Molecular characterization using directed amplification of minisatellite-region DNA (DAMD) marker in *Ficus sycomorus* L. (Moraceae). Open Agric J 13:74-81.

Saleh B (2019b) Genetic diversity of *Salvia tomentosa* Miller (Lamiaceae) species assessment using Td-DAMD molecular marker. Acta Biol Szeged 63(2):135-141.

Seyedimoradi H, Talebi R, Hassani D, Karami F (2012) Comparative genetic diversity analysis in Iranian local grapevine cultivars using ISSR and DAMD molecular markers. Environ Exp Biol 10:125-132.

Song Z, Li X, Wang H, Wang J (2010) Genetic diversity and population structure of *Salvia miltiorrhiza* Bge in China revealed by ISSR and SRAP. Genetica 138:241-249.

Statsoft Statistica (2003) (Data analysis software system), Version 6, Statsoft Inc., www.statsoft.com

Sudarmono S, Okada H (2008) Genetic differentiations among the populations of *Salvia japonica* (Lamiaceae) and its related species. HAYATI J Biosci 15(1):18-26.

Swamy KM, Anuradha (2011) Analysis of genetic variability in patchouli cultivars (*Pogostemon cablin* Benth.) by using RAPD markers. Res Biotechnol 2(6):64-71.

Takano A (2017) Taxonomic study on Japanese *Salvia* (Lamiaceae): Phylogenetic position of *S. akiensis*, and polyphyletic nature of *S. lutescens* var. *intermedia*. Phyto Keys 80:87-104.

Talebi M, Rahimmalek M, Norouzi M (2015) Genetic diversity of *Thymus daenensis* subsp. *daenensis* using SRAP markers. Biologia 70(4):453-459.

Tapeh RNG, Bernousi I, Moghadam AF, Mandoulakani BA (2018) Genetic diversity and structure of Iranian *Teucrium* (*Teucrium polium* L.) populations assessed by ISSR markers. J Agr Sci Tech 20:333-345.

Tonk FA, Yüce S, Bayram E, Giachino RRA, Sönmez Ç, Telci İ, Furan MA (2010) Chemical and genetic variability of selected Turkish oregano (*Origanum onites* L.) clones. Plant Syst Evol 288(3-4):157-165.

Walker JB, Sytsma KJ, Treutlein J, Wink M (2004) *Salvia* (Lamiacae) is not monophyletic: Implications for the systematics, radiation, and ecological specializations of *Salvia* and tribe Mentheae. Am J Bot 91:1115-1125.

Wen C, Wu Z, Tian W, Liu M, Zhou Q, Xie X (2007) AFLP analysis of genetic diversity of *Salvia miltiorrhiza* Bge. Acta Agric Bor-Sin 22(S2):122-125.

Acta Biologica Szegediensis

Volume 65(1):17-27, 2021
Acta Biologica Szegediensis
http://abs.bibl.u-szeged.hu/index.php/abs

DOI:10.14232/abs.2021.1.17-27

ARTICLE

Using of GGE biplot in determination of genetic structure and heterotic groups in wheat (*Triticum aestivum* L.)

Ensieh Es'haghi Shamsabadi[1], Hossein Sabouri[1]*, Habibollah Soughi[2], Seyed Javad Sajadi[1], Ahmad Reza Dadras[3]

[1]Department of Plant Production, Collage of Agriculture Science and Natural Resources, Gonbad Kavous University, Gonbad, Golestan, Iran.
[2]Crop and Horticultural Science Research Department, Golestan Agricultural and Natural Resources Research and Education Center, AREEO, Gorgan, Iran.
[3]Crop and Horticultural Science Research Department, Zanjan Agricultural and Natural Resources Research and Education Center, AREEO, Zanjan, Iran.

ABSTRACT The present study was undertaken to analyze diallel data using GGE biplot model to gather information about genetic interrelationships among parents and identification of heterotic combinations for yield and yield components in bread wheat varieties. For this purpose, 8 bread wheat genotypes tested across in half-diallel crosses design, GGE biplot technique was used. Parents included the genotypes of Kouhdasht, Karim, Ehsan, Mehregan, N-92-9, Line 17, N80-19 and Atrak. The hybrids obtained from the one-way cross (28 hybrids) in agricultural years of 2016-17 were evaluated as randomized complete block design in two replications on the research farm of Gonbad Kavous University. The evaluated traits included the grain yield, weight of spike grains, number of grains in spike and number of spikes. Additive main effects and genotype × environment interaction (GGE) were employed in the evaluation of genotypes; analyses showed significant (P< 0.01) G × E, (genotype × environment interaction) with respect to plant seed yield. GGE biplot analysis showed that Karim was as the best general combiners for grain yield, number grain per spike and grain weight per spike, whereas Ehsan had the highest GCA effects for number of spikes. Ehsan and Karim had higher specific combining ability than other genotypes. The studied genotypes for this trait were divided into two heterotic groups where the first group included the genotypes of Kouhdasht, N-92-9, N80-19 and Atrak and the second group contained the genotypes of Line 17, Mehregan and Karim. Mehregan line had a weak combining ability with all testers and N-92-9 had also more power than others. Based on the biplot, the Karim genotype with high general adaptation was introduced as the ideal genotype in terms of grain yield, spike number, grain number per spike and grain weight, so the Karim genotype can be adapted to obtain high yield hybrids.

KEY WORDS
GGE biplot
general combining ability
heterotic group
hybrid
specific combining ability
Triticum aestivum L

ABBREVIATIONS

GGE: Genotype, Genotype by Environment interactions
SCA: Specific Combining Ability
GCA: General Combining Ability
GNP: Number of grains in plant
GNS: Number of grains in spike
WSG: Weight of spike grains
YLD: grain yield

ARTICLE INFORMATION
Submitted
02 February 2021.
Accepted
08 March 2021.
***Corresponding author**
E-mail: hossein.sabouri@gonbad.ac.ir

Introduction

Grain yield is a complex trait outcome from several genes and their interaction with environment. Due to self-pollination nature of wheat and homozygosity of many loci, it is necessary to introduce different genes, which are known to be yield contributor (Ullah et al. 2010).

To breed the agricultural high-yielding genotypes like wheat, the comprehensive information on the confluence parents' genetic structure as well as the inheritance and desired combining ability of their traits. This is realized by using the quantitative genetic techniques including the diallel crosses (Biriyay et al. 2017).

Heritability is among the most important properties of a quantitative trait because phenotype in quantitative traits is the result of inheri0tance and environment. Importance of heritability of a trait lies behind the determination of techniques selected for population breeding, inbreeding and other aspects of selection; the heritability, hence, is among the primary goals of genetic study of a quantitative trait. Identifying the effective factors in heritability allows the breeders to design a breeding plan in such a way that the genetic improvement is maximized using the existing resources. Heritability is of two general and specific types. The latter is the ratio of total genotype variance to the phenotype variance and the former is defined as the ration of additive genetic variance to the phenotype variance. The specific heritability measures the relative importance which is transferred to the next generation of

progenies; therefore, it is a more appropriate criterion for predicting the expected efficiency from selection. Mass selection for the traits with higher specific heritability is more effective (Sabouri and Mohammadi-Nejad 2009).

Diallel crosses are used in genetic studies for determining the heritance of trait among a set of genotypes and for identifying the better parents in order to produce the hybrid genotypes or agricultural varieties. The findings of this breeding method help to breeders for generating superior hybrids (Dehghani et al. 2013). Common analysis of diallel data is limited to the division of changes in all crosses, general combining ability (GCA) of each parent and specific combining ability (SCA) of each cross. Specific effects are belonging to the crosses and do not give much information about the parents. Diallel crosses data can be analyzed by principal component (PC) biplot techniques following Yan and Hunt (2002). Biplot approach to diallel data analysis provides a much better understanding from the parents. For a set of definite data, they provide information such as GCA impact of each parent, SCA impact of each parent (not every cross), the best testers, heterotic groups and parents' genetic structure regarding the studied trait (Moghaddam et al. 2012).

Biplot technique was firstly proposed by Gabriel (1971) and a proper graphic method was introduced to analyze data by other scientists (Crossa et al. 2002; Gauch 2006). Biplot technique is usually designed for regional experiments, but it is also possible to use it based on reciprocal data of genotype-tester. This method is based on the values of main components corrected using the mean tester. This new approach provides a graphical demonstration of the data using principle components (PC1 and PC2) which are obtained through principle component analysis (Yan and Hunt 2002). Different investigators on different plants, investigated the results of diallel crosses by Biplot technique and determined the heterotic groups and then reported a good consistency between the results of Griffing method and Biplot graphic method (Khalil and Raziuddin 2017; Ali et al. 2017; Dogan 2016; Kendal et al. 2019; Adie et al. 2014; Khalil et al. 2010; Biriyay et al. 2017; Sharifi and Safari Motlagh 2011; Sharifi 2013; Golkar et al. 2017; Ghotbi et al. 2018; Vanda and Houshmand 2011).

Tulu and Wondimu (2019) used biplot to investigate Ethiopian bread wheat varieties for stability of yield and identification of suitable genotypes compatible with South-western Ethiopia environment. According to the GGE biplot analysis of the two main components PC1 and PC2, 63.88 and 15.71% of the total GGE sum of squares were justified, and two growth environments were identified for wheat and ideal genotypes.

Sharifi et al. (2019) using GGE biplot approach indicated high narrow and broad sense heritabilities and heterosis of crosses for yield and some of morphological traits in wheat.

Pagliosa et al. (2017) indicated GGE biplot as an effective method for visual comparisons of GCA and SCA effects and identifying superior spring wheat genotypes.

Sadeghzadeh-Ahari et al. (2014) also used biplot analysis for evaluation of diallel crosses of six varied-ties of durum wheat for yield and identified the ideal general combiner, the best crosses and heterosis patterns for seed yield and yield components.

Dehghani et al. (2013) evaluated the diallel data obtained from the crosses of 5 wheat genotypes and its 10 hybrids in the greenhouse with three pathotype namely 7E18A-, 38E0A+ and 134E134A+. Results showed that two main components of biplot are responsible for 95%, 94% and 85% of variation for pathotypes.

Rastogi et al. (2013) followed the GGE biplot model using the 5×5 diallel data to identify the specific alkaloids in (*Papaver somniferum* L.). For further investigation and approval of GGE biplot model accuracy, results obtained from the diallel analysis were compared with Griffing results. Three parents A (papline), B (NB5KR40-7/2-3) and E (58/1) were detected as the good general compounds.

Mostafavi et al. (2012) evaluated the analysis of 14 corn inbreed genotypes using the diallel method. GGE biplot model was used to extract the interaction among the genotypes and hybrids. Results showed that the specific combining ability of grain yield was higher than the general combining ability that indicting the significant impact of dominant genes in genetic controlling of grain yield. Results of biplot diagrams were mostly consistent with the Griffing's results.

Alam et al. (2017) evaluated eight wheat genotypes under the thermal stress conditions. Results of diallel analysis showed a significant difference for grain yield in probability level of 1% and determined some dominant genotypes. GGE biplot results showed a good consistency between the Griffing technique results and biplot graphic method.

To study the yield in terms of genetics and some agricultural traits in six genotypes of bread wheat, (Mostafavi and Zabet 2013) used the biplot of diallel data. To evaluate the genotypes' potential, GGE biplot graphic technique was used. The studied traits included the grain yield, spike weight, hundred grain weight, number of fertile tillers, spike length, awn length, peduncle length and plant height. The general and specific combining ability for all traits was significant in 1% probability level. For grain yield of Gascogne genotype was the best general combination; Gascogne, Gaspard, Ghods and Pishtaz hybrids has the highest specific combination. These results were confirmed by biplot graphic method.

Ruswandi et al. (2015) evaluated 138 F1 hybrids, 46 parents and 3 tester genotypes in Indonesia to analyze

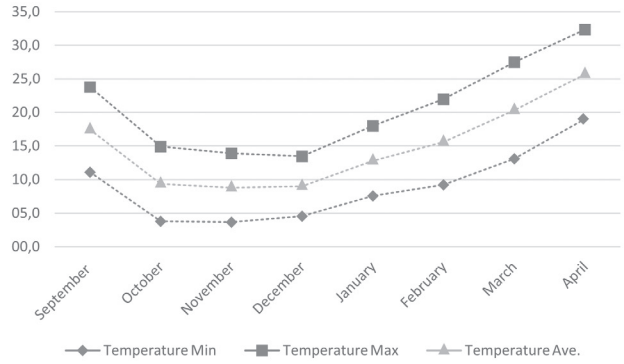

Figure 1. Temperature changes in the 2016-2017 crop season.

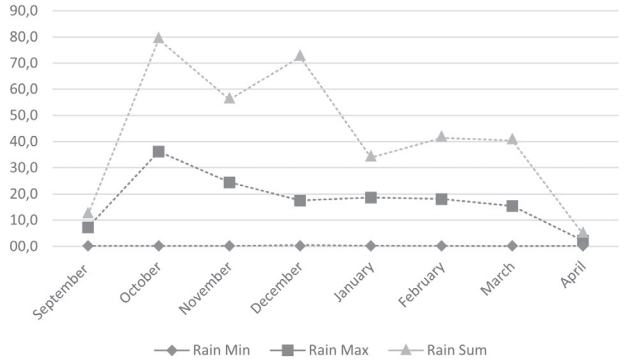

Figure 2. Raining changes in the 2016-2017 crop season.

the line × tester data and maturity time as well as grain yield using the GGE method to identify the genetic relations among the parents and the best combination in corn hybrid. High GCA effect was determined for maturity time and grain yield based on the average GGE biplot.

Graphic analysis of biplot shows the best input through the tester patterns and provides information such as GCA, SCA for each genotype, parents' heterotic groups, dominant hybrids and assumptions related to the genetics of genotypes; this is very important in terms of yield in increasing the products.

This study aims at the graphic determination of wheat diallel data to obtain the dominant hybrids using the biplot analysis for future research.

Material and Methods

Plant material

The present study was conducted in the research farm of Agricultural University of Gonbad Kavous (37° 15′ N and 45° 46′ E) during the 2017-18 within as the randomized complete block design in desired irrigation conditions in two replications. Parents and F_1 seeds were sown on 5 December 2017 as four rows with the spacing of 20 cm between rows and 5 cm between plants on rows. Plots were separated from each other by 1 m. A 1.5 m alley was kept between blocks. The studied parents included 8 genotypes as: Atrak, Ehsan, Karim, Kouhdasht, Line 17, N-80-19 and N-92-9, taken from the Agriculture and Natural Resources Research and Training Center of Golestan Province (Table 1). The local climate is temperate; summers are hot and dry and winters are mild and rainy. Climatically, the region has warm and semi-arid climate. The rainfall and temperature within 2017-18 changes represented in Figure 1 and 2. To determine the physicochemical characteristics of the experimental site before conducting the experiment, soil samples were taken from the depth of 0-30 cm. The testing soil was of loam silty with acidity of 7.8 and electric conductivity of 1 dS/m with 1.5% organic materials and 18-19% of lime. The optimum nitrogen levels determined as 150 kg/ha N fertilizer. Half of N was added at planting time and rest was added during seed filling stage. Weed control was done manually during the growing season. Tebuconazole 25% EW 25 was used to control the rusts. Also, tebuconazole 2% was used to control common bunt, loose smut and

Table 1. Characteristics and pedigree of parents.

Cultivar	Characteristics	Pedigree
N-80-19	Late-stage, spring, high yield, susceptible to drought	SW89.3064.STAR...
KOHDASHT	Early-stage, spring, drought resistant	TR8010200
ATRAK	Spring, short, high tillers	Kauz˝s˝
EHSAN	Late-stage, spring, high yield, susceptible to drought	SABUF.7.ALTAR...
N-92-9	Spring, drought resistant	KLCQ.ER2000..WBLL1
MEHREGAN	Spring, high yield	OASIS.SKAUZ..4*BCN.3.2*PASTOR
KARIM	Spring, suitable for rainy season	Hamam-4
LINE17	Early-stage, short	Jup.alds..att"s".vee"s".3....

powdery mildew. TILT 25% EC was applied for bacterial leaf streak and chaff black control. The studied cultivars were harvested on May 26, 2018.

Evaluated traits

Fifty plants were selected randomly and the number of spikes (GNP), number of grains in spike (GNS), weight of spike grains (WSG), and grain yield (YLD) were evaluated.

Data analysis

Genotype main effect plus genotype-by-environment interaction (GGE) biplots are used to analyze two-way data, where rows and columns represent different experimental units (Yan and Hunt 2002). After obtaining the first two principal components of the adjusted data matrix, the biplot model can be written as:

$$\gamma ij - \beta j = \lambda 1 \xi i1 \eta j1 + \lambda 2 \xi i2 \eta j2 + \varepsilon ij$$

where γij is the genotypic value of the cross between entry i and tester j for traits; βj is the average of all combinations consisting tester j; $\lambda 1$ and $\lambda 2$ are the singular values for the first and second principal components (PC1 and PC2, respectively); $\xi i1$ and $\xi i2$ are the PC1 and PC2 eigenvectors, respectively, for entry i; $\eta j1$ and $\eta j2$ are the PC1 and PC2 eigenvectors, respectively, for tester j; and εij is the residual of the model associated with the combination of entry i and tester j. Each genotype in diallel cross data is an entry and a tester, So, i and j can represent to the same or different genotypes. When $i \neq j$, the genotype is a population hybrid and when $i = j$, the genotype is a pure line.

All of the biplots were developed using the GGE biplot software (Yan 2001).

Results and Discussion

Grain yield

GGE biplot analysis has been importance for the plant breeders because it will present the relationship between traits as visually (Oral 2018). In biplot analysis of diallel data, every genotype was taken both as the line and tester. In these diagrams, genotypes and testers are shown in italic and capital letters. To determine the parents' general combining ability in biplot analysis, the smaller circle shows the average tester obtained from averaging the PC1 and PC2 values of all testers. The line crossing the biplot origin and average tester with an arrow to the average tester is called the average tester axis or ATC horizontal axis and the line passing the biplot origin and orthogonal to the average tester axis is called the vertical axis of average tester or ATC vertical axis (Yan and Hunt 2002; Moghaddam et al. 2012).

GGE biplot is responsible for 63% percent of data variation for the grain yield (42% and 21% by PC1 and PC2 from the total variation). The total variation in common analyses of diallel are divided into parents' GCA effects and crosses' SCA effects (Fig. 3a, b, c, d).

Ehsan and Karim have minimum and maximum general combining abilities, respectively (Fig. 1a). The distance of each genotype from the vector of average testers estimates the specific combining ability and shows each genotype's tendency to generate dominant hybrids with some testers, not all of them; therefore, the Karim and Atrak genotypes on the bottom of ATC horizontal genotypes have the biggest SCA impacts on the ATC vertical axis. N-92-9 on top of horizontal line followed by line 17 had larger SCA effects than the Mehregan line. Since the N80-19 and Kouhdasht genotypes have the smallest image on the ATC vertical axis, they have the least specific combining ability impact.

In order to group the testers into heterotic categories, graph (1-b) was used. In this figure, two groups of testers including Ehsan, Kouhdasht and Atrak testers were on top of the dotted line PC2 and N80-19, Mehregan, Line 17, N-92-9 and Karim testers was on below the line PC2. Upper testers have positive interaction with N-92-9, Mehregan and Line 17. Similarly, testers of N80-19, Mehregan, Line 17, N-92-9 and Karim have positive interaction with Ehsan, Atrak, Kouhdasht and N80-19. This interaction pattern shows clearly the heterosis in crosses (Atrak, Ehsan and Kouhdasht) × (Karim, Line 17, Mehregan, N80-19 and N-92-9). Therefore, we will have two different heterotic groups. Based on a study, it was found that genotypes and environments included in the same sector had a positive relationship and genotypes emerging in different sectors had a negative relationship (Islam et al. 2014).

An ideal tester should have two criteria: firstly, it should discriminate the genotypes better, secondly, it should have good yield. Based on this definition, an ideal tester should be located on ATC axis of which the vector should be higher than other testers so that it is considered as the most discriminating tester; such tester is observed in concentric circles and the more it is close to the center, the more it would be desired. N-92-9 is known as the best tester (Fig. 3c). In contrast, Karim tester is the most undesired tester and has the lowest value in terms of representativeness. The best testers are N-92-9, Line 17, Mehregan, N80-19, Ehsan, Kouhdasht, Atrak and Karim, respectively.

Polygon scheme of biplot helps the identification of best crosses between the genotypes and testers. Polygon includes straight genotypes which connect the farthest lies from biplot origin such that other genotypes are located

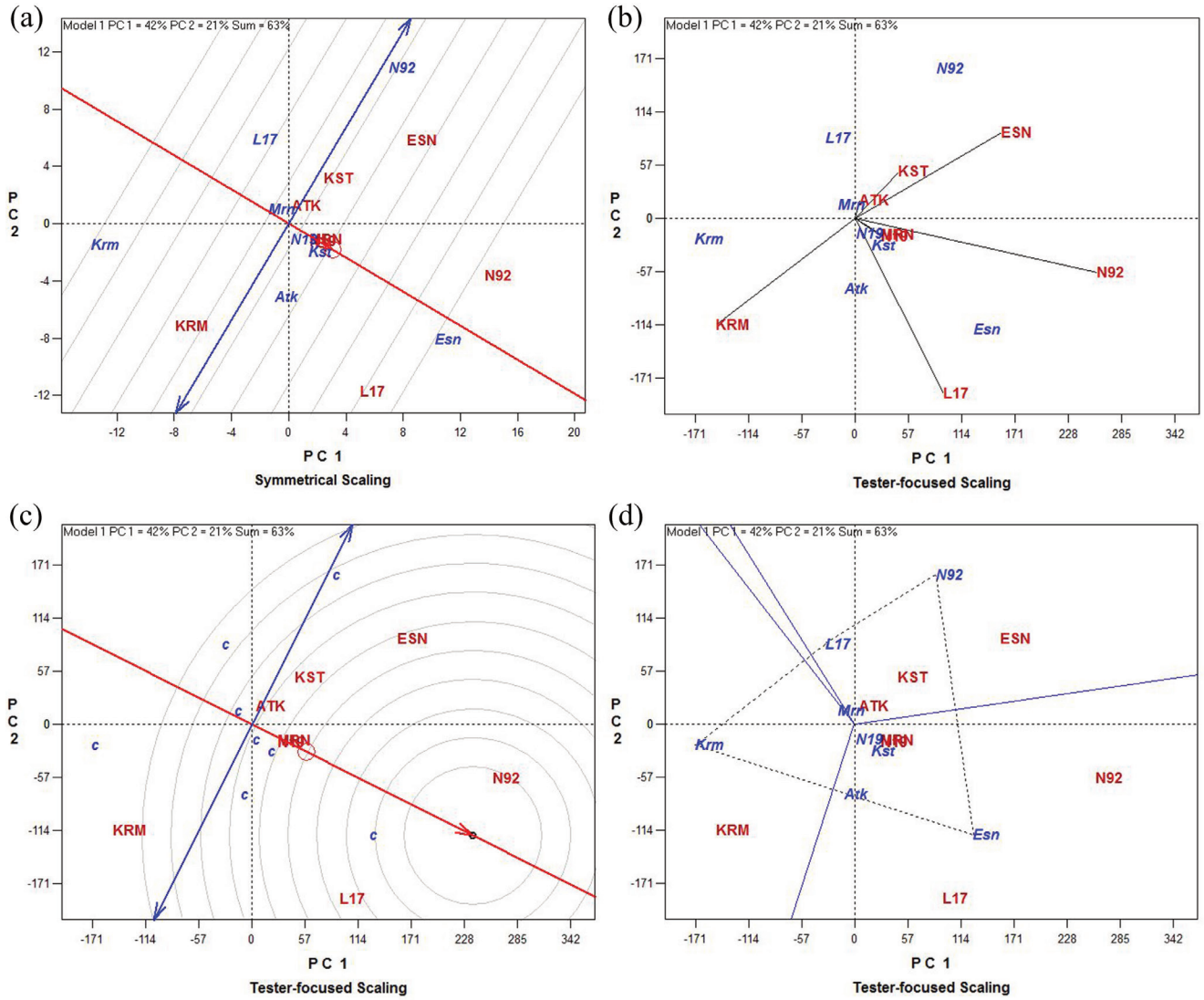

Figure 3. 2D diagram of diallel data for grain yield per m2 for 8 genotypes of bread wheat. (a) position of genotypes, testers and average testers; (b) axis of average genotypes to determine the relationships among them, (c) rating the testers based on the best tester, (d) polygon display and genotypes and testers positions. Small letters determine the relationships among them, (c) rating the testers based on the best tester, (d) polygon display and genotypes and testers positions. The lowercase letters indicate the genotypes and the capital letter indicate the testers. Circle shows the position of average testers.

inside the polygon. Vertical genotypes on each polygon drawn from the biplot origin and expanding out of the polygon divide the biplot into several sections. Therefore, definition of (Fig. 3d) was divided into three sections in which the Karim, Ehsan and N-92-9 genotypes are on the vertex. N-92-9 line and Ehsan tester are on one angle and Ehsan line and N-92-9 tester on the other angle. This means that there are many combining abilities between genotypes of N-92-9 and Ehsan and their hybrid is so heterotic. Karim tester was besides the Karim line indicating this pure genotype should be better than all crosses related to Karim and as a result, heterosis between Karim and any other parent would not be possible. Kouhdasht and Atrak testers, on one side, and Kouhdasht and Atrak genotypes, on the other side, are observable indicating the low combining ability of these genotypes together. Other researchers have confirmed the effectiveness of the biplot method in interpreting diallel data in wheat (Mostafavi and Zabet 2013; Motamedi and Safari 2017).

Weight of spike grain

The biplot diagram related to the spike grain weight was responsible for 82% of data variations. Therefore, by locating the genotypes in the positive and negative

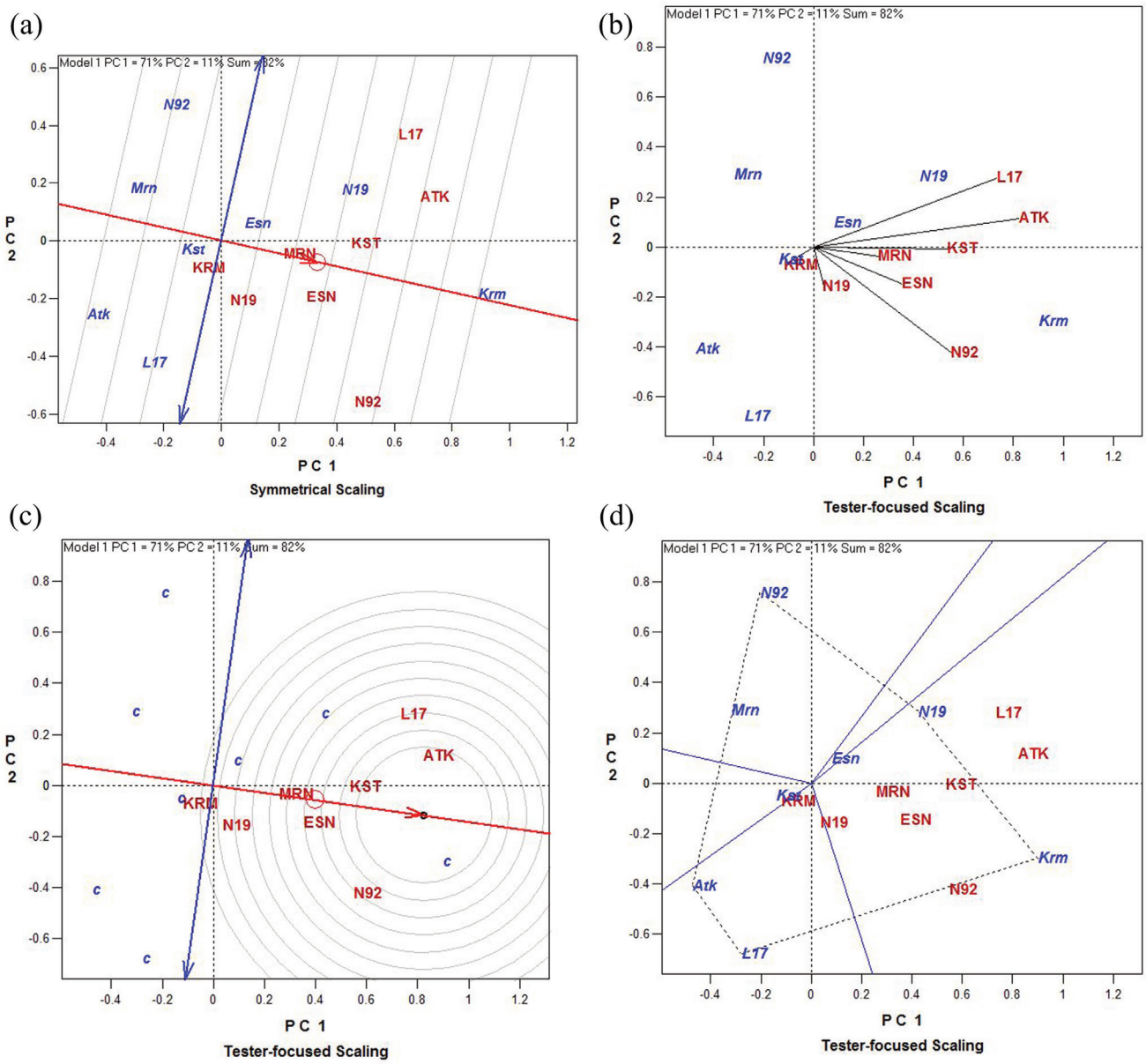

Figure 4. 2D diagram of diallel data for grain yield per m2 for 8 genotypes of bread wheat. (a) position of genotypes, testers and average testers; (b) axis of average genotypes to determine the relationships among them, (c) rating the testers based on the best tester, (d) polygon display and genotypes and testers positions. Small letters determine the relationships among them, (c) rating the testers based on the best tester, (d) polygon display and genotypes and testers positions. The lowercase letters indicate the genotypes and the capital letter indicate the testers. Circle shows the position of average testers.

ends of testers average vector, maximum and minimum general combining abilities of genotypes would be Karim and Atrak, respectively. Concerning the distance of each line to the vector of average testers, genotypes of Line 17 and Atrak on the lower part of ATC horizontal axis and N-92-9 Line on top of horizontal line followed by N80-19 have larger SCA impact than others. Since the Karim has the smallest image on the ATC vertical axis, they have the lowest specific combining ability (Fig. 4a).

Concerning the testers of Line 17 and Atrak on top of dotted lone PC2 and testers of N80-19, Mehregan, Ehsan and Karim below the PC2 line, it seems that the despite locating on the line, Kouhdasht tester does not belong to these two heterotic groups (Fig. 4b). Upper testers have positive interaction with N-92-9, Mehregan, Ehsan and N80-19. Similarly, N80-19, Mehregan, N-92-9, Ehsan

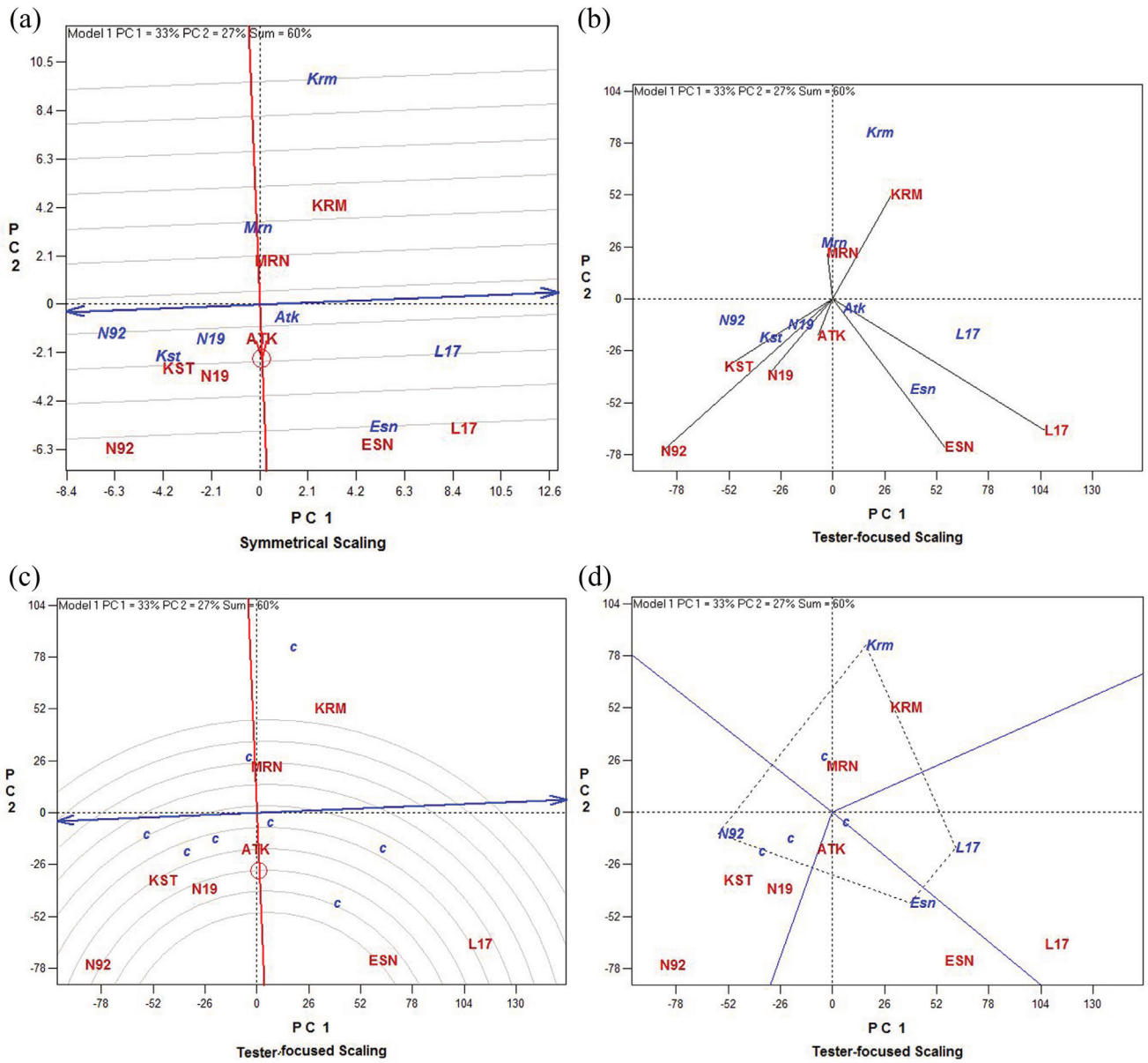

Figure 5. 2D diagram of diallel data for grain yield per m2 for 8 genotypes of bread wheat. (a) position of genotypes, testers and average testers; (b) axis of average genotypes to determine the relationships among them, (c) rating the testers based on the best tester, (d) polygon display and genotypes and testers positions. Small letters determine the relationships among them, (c) rating the testers based on the best tester, (d) polygon display and genotypes and testers positions. The lowercase letters indicate the genotypes and the capital letter indicate the testers. Circle shows the position of average testers.

and Karim testers have also positive interactions with Karim, Kouhdasht, Atrak and Line 17. This interaction line clearly shows the heterosis in crosses (Atrak & Line 17) × (N-92-9, Ehsan, Karim, N80-19 and Mehregan). Therefore, we have two different heterotic groups.

Atrak tester is known as the best tester (Fig. 4c). In contrast, Karim tester is the most undesired tester and has the lowest value in terms of representativeness. The testers are ranked as: Atrak, Kouhdasht, Line 17, N-92-9, Ehsan, Mehregan, N80-19 and Karim, respectively.

Karim, Atrak, Line 17, N-92-9 genotypes were located on the vertex (Fig. 4d). Hence, we have 4 groups of genotypes. No tester was seen in Line 17, Atrak and N-92-9. Consequently, these genotypes are not the best cross pairs with no genotypes and generate the worst hybrids by some testers or all of them. One N-92-9 tester was besides the

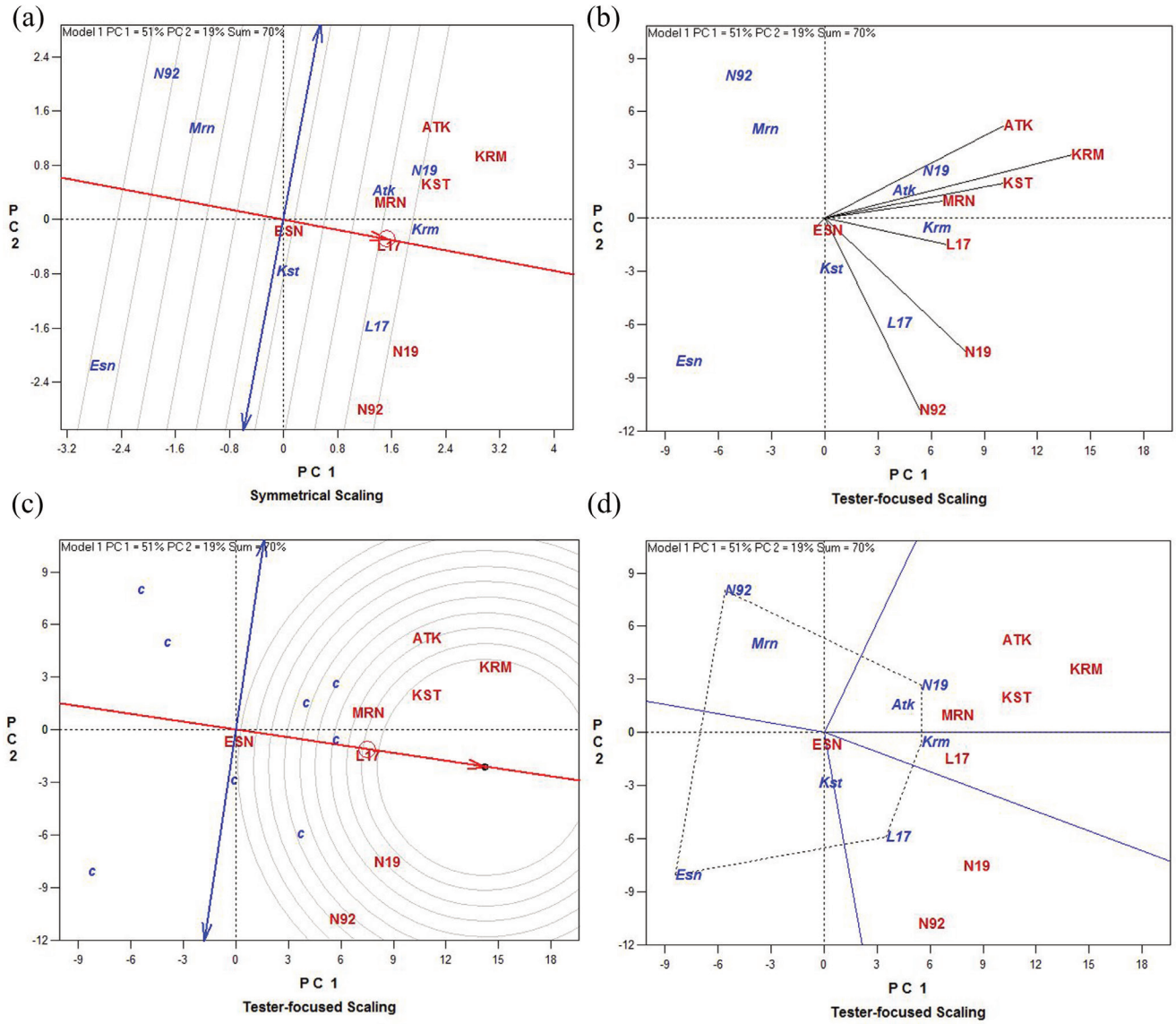

Figure 6. 2D diagram of diallel data for grain yield per m2 for 8 genotypes of bread wheat. (a) position of genotypes, testers and average testers; (b) axis of average genotypes to determine the relationships among them, (c) rating the testers based on the best tester, (d) polygon display and genotypes and testers positions. Small letters determine the relationships among them, (c) rating the testers based on the best tester, (d) polygon display and genotypes and testers positions. The lowercase letters indicate the genotypes and the capital letter indicate the testers. Circle shows the position of average testers.

Karim indicating this genotype is the best cross pair with this tester; i.e. Karim × N-92-9 cross means the prediction of best cross among the ones related to the N-92-9 tester. Since the Karim parent was not on the similar section as a tester, Karim × N-92-9 cross should be heterotic; i.e. it should be better than its both parents (Karim × Karim and N-92-9 × N-92-9). Kouhdasht, Mehregan, Ehsan and N80-19 testers are seen in one section, i.e. besides the Karim indicating the Karim would be the best cross pair for these testers. Since the Karim tester was not on this section, all Karim crosses with these testers are heterotopic. Kouhdasht and Mehregan testers are approximately on the same line separating the sections of Karim and N80-19. Therefore, N80-19 should be a good pair for cross with Mehregan and Kouhdasht. The Line 17 and Atrak testers are on the N80-19 section, hence this line is an appropriate pair for cross with the aforementioned testers and since the inverse does not occur in another section, this cross, Line 17 × N80-19 and N80-19 ×Atrak, is heterotic.

Number of spikes

Biplot diagram related to the number of spikes is responsible for 60% of data variations. The maximum and minimum general combining abilities were for Ehsan and Karim, respectively. N-92-9, Kouhdasht, Line 17 and Ehsan have higher specific combining ability than others (Fig. 5a). For number of spikes, two heterotic groups were observed where the first group included Mehregan and Karim testers and the second included N80-19, Kouhdasht, N-92-9, Ehsan, Karim and Line 17 testers (Fig. 5b). Ehsan and Karim testers were the best and worst tester for number of spike (Fig. 5c). Biplot was divided into four sections in which Karim, Line 17, Ehsan and N-92-9 were on the vertex (Fig. 5d). Concerning the figure, the testers related to each figure were besides them; i.e. combination of Ehsan tester × Ehsan genotype, Line 17 tester × Line 17 genotype, Karim tester × Karim genotype, and N-92-9 tester × N-92-9 genotype indicated that these genotypes should be better than all their related crosses, as a result, heterosis between these genotypes and each parent would not possible. Because faster and easier interpretation is one of the advantages of the biplot method, its use was recommended for researchers to show the differences between the genotypes selected (Pržulj and Momčilović 2012; Motamedi and Safari 2017; Karaman 2020).

Number of grains in spike

In connection to the trait of number of grains in spike, 70% of data variance were justified and Karim and Ehsan genotypes showed the maximum and minimum general combining abilities (Fig. 6a). Genotypes of N-92-9 and Atrak had the highest specific combining ability. Order of testers for this trait based on the most valuable and least valuable was Karim and Ehsan (Fig. 4c). The heterotic groups include Atrak, Karim, Kouhdasht and Mehregan testers in the first group and Line 17, N80-19, genotype N-92-9 and Ehsan testers on the second group (Fig. 6b). N80-19 genotype showed a high combining ability with Mehregan, Kouhdasht, Atrak and Karim testers. On the other hand, on the other part of Karim genotype with Line 17 tester and Kouhdasht genotype with Ehsan tester were appropriate pairs for cross. As the N80-19 and genotype N-92-9 testers were on the Line 17 part, this genotype was introduced as the best cross pairs with these testers. In general, hybrids N80-19 × Mehregan, N80-19 × Kouhdasht, N80-19 × Karim, N80-19 × Atrak, Karim × Line 17, Ehsan × Kouhdasht, Line 17 × N-92-9 and Line 17 × N80-19 were highly heterotic. On the vertexes of genotype N-92-9 and Ehsan, no tester was found. As a result, these lines are not the best cross pairs with none of genotypes and they generate the worst hybrids with some or all testers (Fig. 6d).

According to the above results, Karim genotype for grain yield, weight of spike grains and number of grains in spike and Ehsan genotype for the number of spikes by being located at the positive end of the average vector line of testers with high general combining ability and increasing gene action, can be used as a general parent in breeding programs or in the preparation of artificial or hybrid varieties and conversely, genotype N-92-9 for all four traits studied, including grain yield, weight of spike grains, number of spikes and number of grains in spike and genotype Line 17 for grain yield traits, weight of spike grains and number of spikes and Atrak genotype for grain yield traits, spike weight and number of grains in spike, which have a high degree of combining ability due to the non-additive effects of gene action on inheritance of these traits, should be used as hybrid parents.

Also, the best genotypes obtained based on high GCA and low SCA as the best testers include N-92-9 for grain yield, Atrak for weight of spike grains, Ehsan genotype fro number of spikes and Kouhdasht for number of grains in spike compared to other testers, in order for distinction of the lines, were introduced.

Therefore, the graphs provided by biplot analysis can double their validity by simultaneously examining GCA and SCA hybrids.

Conclusion

Based on graphic results, Karim was the best general combining abilities for grain yield, number of grains in spike and weight of spike grains as well as Ehsan for number of spikes. The maximum value of heterosis was in (Atrak, Ehsan and Kouhdasht) × (Karim, Line 17, Mehregan, N80-19, N-92-9) crosses for grain yield; (Atrak and Line 17) × (Mehregan, Karim, Ehsan, N-92-9 and N80-19) crosses for weight of spike grains; (Mehregan and Karim) × (Kouhdasht, Mehregan, Ehsan, Karim, Line 17, N-92-9 and N80-19) crosses for number of spike and (Atrak, Karim, Kouhdasht, Mehregan) × (Line 17, Ehsan, N-92-9 and N80-19) crosses for number of grain in spike which is highly suitable in breeding plans to obtain the hybrids with high yield at the same weather conditions. Concerning the dominance of graphic techniques in easier and faster interpretation of results and consistency of results of numerical analyses with graphic results, these analytical techniques can be described for convenience in studies. Based on the results of present study, GGE biplot indicated good potential for identifying suitable parents and heterotic crosses and the best hybrids according to diallel mating design.

Acknowledgment

The authors acknowledge the Research Deputy of Gonbad Kavous University for providing funding to complete this work.

References

Adie MM, Krisnawati A, Gatut-Wahyu AS (2014) Assessment of genotype × environment interactions for black soybean yield using AMMI and GGE biplot. Inter J Agric Inn Res 2:673-678.

Alam MA, Farhad M, Hakim MA, Barma NC, Malaker PK, Reza MM, Hossain MA, Li M (2017) AMMI and GGE biplot analysis for yield stability of promising bread wheat genotypes in Bangladesh. Pak J Bot 49:1049-56.

Ali S, Khan NU, Khalil IH, Iqbal M, Gul S, Ahmed S, Ali N, Sajjad M, Afridi K, Ali I, Khan SM (2017) Environment effects for earliness and grain yield traits in F1 diallel populations of maize (*Zea mays* L.). J Sci Food Agric 97:4408-4418.

Biriyay G, Mostafavi K, Khodarahmi M (2017) Investigation of diallel results in bread wheat under drought stress conditions using GGE-biplot method. Environ Stress Crop Sci 9:363-374.

Crossa J, Cornelius PL, Yan W (2002) Biplots of linear-bilinear models for studying crossover genotype× environment interaction. Crop Sci 42:619-33.

Dehghani H, Moghaddam M, Bihamta MR, Sabaghnia N, Mohammadi R (2013) Biplot analysis of diallel data in strip rust of wheat. Aust Plant Pathol 42:601-608.

Dogan Y, Kendal E, Oral E (2016) Identifying of relationship between traits and grain yield in spring barley by GGE Biplot analysis. Agric Forest/Poljoprivreda i Sumarstvo 62:239-252.

Gabriel KR (1971) The biplot graphic display of matrices with application to principal component analysis. Biometrika 58:453-67.

Gauch HG (2006) Statistical analysis of yield trials by AMMI and GGE. Crop Sci 46:1488-1500.

Ghotbi V, Azizi F, Zamani MJ, Rozbehani A (2018) Biplot and heterosis analysis in half-diallel crosses from second selfing generation of alfalfa. J Crop Breed 10:104-114.

Golkar P, Shahbazi E, Nouraein M (2017) Combining ability × environment interaction and genetic analysis for agronomic traits in safflower (*Carthamus tinctorius* L.): biplot as a tool for diallel data. Acta Agric Sloven 109:229-240.

Islam MR, M Anisuzzaman, H Khatun, N Sharma, Z Islam, A Akter, PS Biswas (2014) AMMI analysis of yield performance and stability of rice genotypes across different haor areas. Eco-friendly Agril 7:20-24.

Karaman M (2020) Evaluation of the physiological and agricultural properties of some of bread wheat (*Triticum aestivum* L.) genotypes registered in Turkey using biplot analysis. Pak J Bot 52:1989-1997.

Kendal E, Karaman M, Tekdal S, Dogan S (2019) Analysis of promising barley (*Hordeum vulgare* L.) lines performance by AMMI and GGE biplot in multiple traits and environment. Appl Eco Env Res 17:5219-5233.

Khalil IA, Rahman H, Saeed N, Khan NU, Durrishawar NI, Ali F, Sajjad M, Saeed M (2010) Combining ability in maize single cross hybrids for grain yield: a graphical analysis. Sarhad J Agric 26:373-379.

Khalil IA, Raziuddin (2017) Combining ability for seed yield in indigenous and exotic (*Brassica napus*) genotypes. Sarhad J Agric 33:177-182.

Moghaddam M, Safari P, Daniali SF (2012) GGE Biplot: A Graphical Tool for Plant Breeders, Geneticists and Crop Sciences. 1th ed., Parivar Publishing, Tabriz, Iran. pp. 267-278.

Mostafavi K, Zabet M (2013) Genetic study of yield and some agronomic traits in bread wheat using biplot of diallel data. Seed Plant Improv J 29:503-518.

Mostafavi M, Choukan RA, Taeb MO, Heravan EM, Bihamta M (2012) Heterotic grouping of Iranian maize inbred lines based on yield-specific combining ability in diallel crosses and GGE biplot. J Res Agric Sci 8:113-125.

Motamedi M, Safari P (2017) Biplot analysis of diallel data for water deficit stress tolerance in wheat. Plant Genet Res 4:61-74.

Oral E (2018) Effect of nitrogen fertilization levels on grain yield and yield components in triticale based on AMMI and GGE biplot analysis. Appl Ecol Environ Res 16:4865-4878.

Pagliosa ES, Benin G, Beche E, da Silva CL, Milioli AS, Tonatto M (2017) Identifying superior spring wheat genotypes through diallel approaches. Austral J Crop Sci 11:112.

Pržulj N, Momčilović V (2012) Spring barley performances in the Pannonian zone. Genetika 44:499-512.

Rastogi A, Mishra BK, Siddiqui A, Srivastava M, Shukla S (2013) GGE biplot analysis based on diallel for exploitation of hybrid vigour in opium poppy (*Papaver somniferum* L.). J Agric Sci Tech 15:151-162.

Ruswandi D, Supriatna J, Waluyo B, Makkulawu AT, Suryadi E, Chindy ZU, Ruswandi S (2015) GGE biplot analysis for combining ability of grain yield and early maturity in maize mutant in Indonesia. Asian J Crop Sci 7:160-173.

Sabouri H, Mohammadi-nejad GH (2009) Biometrical Genetics, 1th Ed., Gorgan Publishing, Gorgan, Iran.

Sadeghzadeh-Ahari D, Sharifi P, Karimizadeh R, Mohammadi M (2014) Biplot analysis of diallel crosses for yield and some morphological traits in durum wheat. Iran J Genet Plant Breed 3:28-40.

Sharifi P (2013) Genotype plus genotype by environment

interaction (GGE) biplot analysis of nutrient quality traits in rice (*Oryza sativa* L.). Philipp J Crop Sci 38:9-20.
Sharifi P, Mohammadi M, Karimizadeh R (2019) Biplot analysis of diallel crosses for yield and some of morphological traits in wheat. Vegetos 32:420-430.
Sharifi P, Safari Motlagh MR (2011) Biplot analysis of diallel crosses for cold tolerance in rice at the germination stage. Crop Pasture Sci 62:169-176.
Tulu L, Wondimu A (2019) Adaptability and yield stability of bread wheat (*Triticum aestivum*) varieties studied using GGE-biplot analysis in the highland environments of South-western Ethiopia. Afric J Plant Sci 13:153-162.
Ullah S, Khan AS, Raza A, Sadique S (2010) Gene action analysis of yield and yield related traits in spring wheat (*Triticum aestivum*). Inter J Agric Bio 12:125-128.
Vanda M, Houshmand S (2011) Estimation of genetic structure of grain yield and related traits in durum wheat using diallel crossing. Iranian J Crop Sci 13:206-218.
Wynne JC, Enery DA, Rice PH (1970) Combining ability estimation in *Arachis hypogaea*. L. II. Field performance of F1 hybrids. Crop Sci 10:713-715.
Yan W (2001) GGE biplot - a Windows application for graphical analysis of multienvironment trial data and other types of two-way data. Agron J 93:1111-1118.
Yan W, Hunt LA (2002) Biplot analysis of diallel data. Crop Sci 42:21-30.

Acta Biologica Szegediensis

Volume 65(1):29-34, 2021
Acta Biologica Szegediensis
http://abs.bibl.u-szeged.hu/index.php/abs
DOI:10.14232/abs.2021.1.29-34

ARTICLE

A comparative study on *Acorus calamus* (Acoraceae) micropropagation and selection of suitable population for cultivation in Iran

Abbas Gholipour[1]*, Seyed Kamal Kazemitabar[2], Hamed Ramzanpour[1]

[1]Department of Biology, Faculty of Sciences, Payame Noor University (PNU), Tehran, Iran;
[2]Department of Plant Breeding, Sari Agricultural and Natural Resources University (SANRU), Sari, Iran

ABSTRACT In addition to various medicinal properties, *Acorus calamus* (sweet flag) is used in health, food, and perfume industries. Since this species is a rare plant in Iran, its propagation and cultivation are of the great importance. The aim of this study was to investigate the effects of different plant growth regulators on micropropagation of this plant and to select the appropriate population. The root, the rhizome and the leaf explants of three populations (Arzefon, Pelesk, and Alandan) were cultured on MS medium supplemented with different concentrations of α-naphthalene acetic acid (NAA) and 6-benzylaminopurine (BAP) for callus induction and plant regeneration. The results showed that only rhizome explant resulted in direct plant regeneration. Among different treatments, the 1 mg/l treatment of BAP and NAA - with the highest mean number of regenerated plants (3.75 ± 0.85), the highest percentage of grown explants (91.6%) and maximum average length of regenerated plants (12.06 ± 0.32 cm) - was the best treatment for regeneration of sweet flag. The highest mean number of root (6.6 ± 0.1) was observed in Alandan population in 1 mg/l treatment of indole-3-butyric acid (IBA). According to the present study, Alandan population is suitable for cultivation purposes in Iran.

KEY WORDS
Acorus calamus
medicinal plants
micropropagation
sweet flag
tissue culture

ARTICLE INFORMATION
Submitted
15 November 2020.
Accepted
03 February 2021.
***Corresponding author**
E-mail: a.gholipour@pnu.ac.ir

Introduction

Medicinal plants, as valuable natural resources, play an important role in the health and economy of any country. There are many reports about medicinal properties of *Acorus calamus* L. (sweet flag) in the traditional medicine of India, China and Iran. These medicinal properties include the treatment of appetite, digestive disorders, colic pain, fever, speech stammering, toothache, kidney and liver troubles, rheumatism, gout and rejuvenator of the brain and nervous system (Motley 1994; Imam et al. 2013; Mozaffarian 2013; Kumar et al. 2014). On the other hand, this plant is used in perfumery, health, and food industries (Motley 1994; Kumar et al. 2014).

A. calamus has recently been rediscovered in Iran after about 50 years from Mazandaran province (Gholipour and Sonboli 2013). It is a rhizomatous perennial semi-aquatic plant from the family Acoraceae which mainly grows around the ponds in Iran. According to the available information, sweet flag has been distributed in three localities with very restricted distribution in Mazandaran (North of Iran) and is considered as a rare plant in Iran (Gholipour and Sonboli 2013). At present, the raw materials of sweet flag for medicinal and other uses are provided from natural habitats. For this reason, harvesting this plant will probably lead to the extinction of the species in Iran. Due to the many usages of *A. calamus* and high demand, domestication and cultivation of this plant in Iran is necessary. Sweet flag often has vegetative reproduction through rhizome, and no seed is produced in the wild population of Iran. On the other hand, since this plant does not produce seed, the preparation of seedlings is one of the main problems in the cultivation of this plant. At present, in countries where this plant is cultivated, the rhizomes of the previous year's plant are kept under soil until the growing season and then used to prepare seedlings (Lokesh 2004; Imam et al. 2013). Keeping the living rhizome underground for about 4 months is one of the major problems in cultivating of this plant.

Plant tissue culture is a suitable technique for solving problems in the field of cultivation, exploitation and conservation of medicinal and ornamental plants (Mohamed et al. 2007; Bhagat 2011; Imam et al. 2013; Chandana et al. 2018; Fallah et al. 2019). Some studies have successfully propagated *A. calamus* through tissue culture technique, but there is some difference between them in the proper combination of the plant growth regulators

Table 1. Localities and vouchers information of the studied populations of *A. calamus*.

No.	Locality/Time/Height/Collector	Voucher number
1	Iran, Mazandaran, Sari, Arzefon village, Malepeshte Ab-bandan / 03. 11. 2017 / 331 m / Gholipour A	SPNH-5919
2	Iran, Mazandaran, Sari, Shahid Rajaii dam road, Pelesk village, Ab-bandane Pelesk / 05. 07. 2018 / 660 m / Gholipour A	SPNH-5991
3	Iran, Mazandaran, Sari to Kiasar road, before Kiasar, Alandan, Ab-bandane Alandan / 09. 06. 2018 / 1350 m / Gholipour A	SPNH-5997

(Hettiarachchi et al. 1997; Rani et al. 2000; Anu et al. 2001; Ahmed et al. 2007; Altaf et al. 2010; Sandhyarani et al. 2011; Devi et al. 2012; Verma and Singh 2012; Dixit et al. 2014; Babar et al. 2020). It seems that one of the reasons for these differences is due to the geographical distribution of the studied populations. Based on a review of scientific literature, no information is available on the micropropagation of *A. calamus* using native plants of Iran. This study was conducted to prepare a suitable protocol for micropropagation of this plant using tissue culture technique on plant samples of three populations and, selecting the appropriate population for large-scale cultivation and conservation purposes in Iran.

Materials and Methods

Plant materials and sterilization

Fresh plant materials (rhizomes, roots, and leaves) of three populations of *A. calamus* were collected from Arzefon, Pelesk, and Alandan (Sari- Mazandaran- North of Iran) ponds (Table 1). Herbarium vouchers are deposited in Sari Payame Noor University Herbarium (SPNH). The samples were cleaned and thoroughly washed in running tap water. The 0.5-1.5 cm segments of root, rhizome, and leaf were cut. All samples were washed in liquid detergent for 5 min. The explants were then washed several times in tap water, followed by washing with distilled water to remove detergent traces. Samples were sterilized with ethanol 70% for 3 min. Due to the fungal infection of rhizomes of this plant, we treated the rhizome explants in mercuric chloride solution ($HgCl_2$) 0.1% (w/v) for 15 min. Again, the explants were thoroughly washed several times in autoclaved distilled water.

Establishment of culture

In callus induction experiment, root, leaf and rhizome explants were cultured in MS medium supplemented with 0.5, 1 and 2 mg/l α-naphthalene acetic acid (NAA). In direct plant regeneration experiment, the explants were incubated on MS medium supplemented with four combined treatments of 1-2 mg/l 6-benzylaminopurine (BAP) and 0.5-1 mg/l α-naphthalene acetic acid (NAA) (Table 2). In both experiments; callus induction and direct plant regeneration, control samples were incubated on MS medium without any plant growth regulator. The experiments were performed in a completely randomized block design with 3 replications, and 3-4 explants were incubated in each replication. The cultures were incubated in a growth chamber at 25 ± 2 °C temperature, 16 hours' photoperiod, and 75-85% humidity for 15 days. The time it takes for bud break of each explant, the num-

Table 2. The effect of different plant growth regulators treatments on plant regeneration of rhizome explants in three Iranian populations of *A. calamus* (15 days after cultures). Values are mean ± standard error; all values are averaged except growing explant percentage.

	Mean days for bud break			Grown explants percentage (%)			Mean number of regenerated plantlets			Average length of plantlets (cm)		
Populations	Arzefon	Pelesk	Alandan	Arzefon	Pelesk	Alandan	Arzefon	Pelesk	Alandan	Arzefon	Pelesk	Alandan
Treatments												
Control	15 ± 0.35	7 ± 0.175	13	16.6	16.6	8.3	0.5	0.5	0.25	1 ± 0.062	2.5 ± 0.125	1.5
BAP 1 mg/l + NAA 0.5 mg/l	2.5 ± 0.01	2.87 ± 0.01	4.25 ± 0.04	58.3	66.6	66.6	1.75 ± 0.25	2	3 ± 0.57	3.62 ± 0.31	4.81 ± 0.18	6.64 ± 1
BAP 1 mg/l + NAA 1 mg/l	3.5 ± 0.016	3 ± 0.02	3.06 ± 0.01	75	58.3	91.6	2.25 ± 0.25	1.75 ± 0.25	3.75 ± 0.85	4.95 ± 0.21	3.87 ± 0.23	12.06 ± 0.32
BAP 2 mg/l + NAA 0.5 mg/l	3.25 ± 0.02	5 ± 0.026	7.6 ± 0.44	66.6	83.3	25	2 ± 0.40	2.5 ± 0.28	1.5 ± 0.95	0.56 ± 0.15	3.12 ± 0.46	11.5 ± 0.03
BAP 2 mg/l + NAA 1 mg/l	2.75 ± 0.007	3.5 ± 0.036	4 ± 0.023	66.6	75	83.3	2 ± 0.40	2.25 ± 0.25	3.5 ± 0.28	0.31 ± 0.06	3.31 ± 0.23	8.25 ± 0.32

Table 3. The effects of IBA at different concentrations on the plantlets root production of three Iranian populations of *A. calamus* (21 days after cultures). Values are mean ± standard error.

	Mean number of roots			Root formation (%)			Average length of roots (cm)		
Populations	Arzefon	Pelesk	Alandan	Arzefon	Pelesk	Alandan	Arzefon	Pelesk	Alandan
Treatments									
IBA 0.5 mg/l	1.6 ± 0.26	3 ± 0.09	5 ± 0.09	33.3	100	100	1.25 ± 0.02	3 ± 0.06	2.5 ± 0.06
IBA 1 mg/l	2 ± 0.15	2.3 ± 0.05	6.6 ± 0.1	66.6	100	100	0.5 ± 0.01	1.75 ± 0.06	3.75 ± 0.04

ber of grown explants, the number of plants regenerated per culture, and the length of regenerated plantlets were recorded after 15 days of culture.

Root induction

The regenerated plantlets (about 5-7 cm) were aseptically transferred to rooting medium containing MS medium supplemented with 0.5 and 1 mg/l indole-3-butyric acid (IBA). The cultures were incubated in the growth chamber under the same conditions as the plant regeneration experiment. After 21 days, the number and the length of the initiated roots were measured per culture.

Evaluation of Biomass performance

The weight of 12 well-developed rooted plantlets from each population were measured, then planted in pots containing an autoclaved mixture of soil and sand (3:1). The pots, after being acclimatized were transferred to the greenhouse, and maintained in the same condition. After 30 days, all plantlets were removed from the pots, washed thoroughly with tap water and the weight of each plantlet in each population was measured. Finally, all plantlets were planted in the field of Sari Payame Noor University.

Data analysis

In direct plant regeneration experiment, mean time of bud break, the percentage of grown explants, mean number and mean length of regenerated plantlets in each treatment were calculated in cultures of each population. In rooting induction culture, mean number of initiated roots, the percentage of root formation and mean length of root in each treatment were calculated for plant samples of each population. The plantlets survival rate and mean total final plantlets weight per population were calculated for viability and biomass yield evaluation. Analysis of variance (ANOVA) and Duncan multiple range test were performed at the 5% level of significance using SPSS ver. 19 software (IBM 2010) for data analysis of plant regeneration, root induction and biomass performance.

RESULTS

Callus induction and plant regeneration

Callus induction and indirect plant regeneration of sweet flag were not successful in leaf and root explants. Plant regeneration occurred only in the rhizome explants, while no callus was produced in its different treatments. The results of direct plant regeneration treatments of three Iranian populations of *A. calamus* samples are presented in Table 2. Regeneration of plantlets occurred in all treatments, but various responses to different concentrations of plant growth regulators were observed in explants of three populations. The lowest mean time of explant bud break (2.5 ± 0.01 days) was found in 1 mg/l BAP in combination with 0.5 mg/l NAA treatment of Arzefon population, while the highest one (15 ± 0.35 days) was observed in control treatment of this population. Based on the analysis of variance (ANOVA), there was no significant difference (Sig = 0.439) between the mean time of explant bud break in different treatments of three studied populations. As a result, different combinations of plant growth regulators have relatively similar effects on explant bud breaking time for plant regeneration. In all treatments, except control treatments and 2 mg/l BAP in combination with 0.5 mg/l NAA treatment of Alandan population, the first explant began to grow after 2 days.

The maximum percentage of grown explant (91.6%) was observed in 1 mg/l BAP combined with 1 mgl^{-1} NAA treatment of Alandan population and the least one (8.3%) was observed in control treatment of this population. Analysis of variance showed that there was a significant difference at 5% level in the grown explant percentage between populations (Sig = 0.011). Duncan's multiple range tests showed that there was a significant difference (Sig = 0.012) between Alandan and Pelesk populations plant samples in terms of grown explants percentage in 1 mg/l BAP in combination with 1 mg/l NAA treatment and 2 mg/l BAP combined with 0.5 mg/l NAA treatment.

The highest mean number of the regenerated plantlet (3.75 ± 0.85) was found in 1 mg/l BAP in combination with 1 mg/l NAA treatment of Alandan population plant samples and the least one (0.5) was observed in control treatment of this population (Fig. 1A). In this investiga-

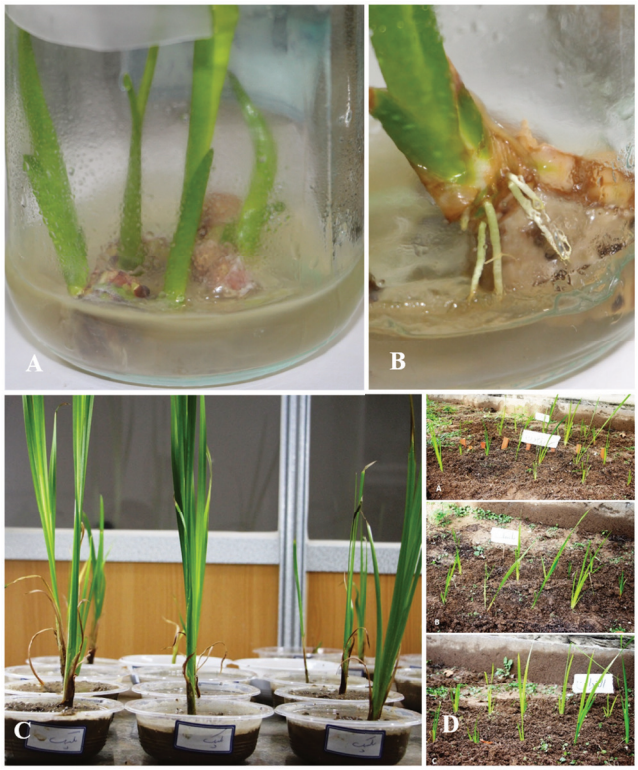

Figure 1. Micropropagation of plant samples of Iranian populations of *A. calamus* from rhizome explants. **A**: Regenerated plantlets of Alandan population from 1 mg/l BAP + 1 mg/l NAA treatment. **B**: Root induction in 1 mg/l IBA treatment of Alandan population plantlet. **C**: Plantlets of Pelesk population in greenhouse. **D**: Developed regenerated plantlets of Arzefon, Pelesk and Alandan populations planted in the field.

tion, the maximum number of regenerated plantlets (15) was found in 1 mg/l BAP and NAA treatment of Alandan population culture, and the maximum number of plantlets per explant (4 plantlets) was produced in an explant of Alandan population. Analysis of variance indicated that there was a significant difference at 5% level for the mean number of the regenerated plantlets between different populations (Sig = 0.016). Duncan multiple range test showed that there was a significant difference (Sig = 0.017) between Alandan and Pelesk, and Alandan and Arzefon populations cultures (Sig = 0.020) in terms of mean number of regenerated plantlets.

The highest average length of regenerated plantlets (12.06 ± 0.32 cm) was found in 1 mg/l BAP in combination with 1 mg/l NAA treatment of Alandan population after 15 days. There was a significant difference in the mean length of the regenerated plantlets between Alandan with Arzefon and Pelesk populations (Sig = 0.001). In contrast, no significant difference was observed between Arzefon and Pelesk populations plant samples (Sig = 0.40) in 1 mg/l BAP in combination with 1 mg/l NAA and 1 mg/l BAP combined with 0.5 mg/l NAA treatments.

Rooting of regenerated plants

The effects of different concentrations of IBA on root induction of the studied populations were presented in Table 3. In the control medium, no roots were developed. The percentage of root formation was recorded 100% in two treatments of Alandan and Pelesk population plantlets, while the lowest one (33.3%) was observed in 0.5 mg/l IBA treatment of Arzefon population plantlets. The maximum mean number of the developed root (6.6 ± 0.1) and the highest mean length of root (3.75 ± 0.04 cm) were observed in 1 mg/l IBA treatment of Alandan population plantlets (Fig. 1B). Based on the analysis of variance, there was a significant difference in terms of the mean number of produced roots (Sig = 0.005) and the mean length of roots (Sig = 0.01) between three populations plantlets. As a result, different growth regulator treatments had different effects on root production in regenerated plantlets of different populations.

Viability rate and biomass performance

All rooted plantlets of Arzefon and Pelesk populations grew in the greenhouse, while the survival rate was 83% in Alandan population plantlets (Table 4). Analysis of variance on biomass yield of the three studied populations showed a significant difference between the populations (Sig = 0.000). Duncan's multiple range tests showed that there was a significant difference (Sig = 0.017) between Pelesk with Alandan and Arzefon populations, and there was no significant difference between Arzefon and Alandan populations (Sig = 0.061). As a result, the plantlets of Pelesk population, with about 400% increase in biomass after 30 days, showed better performance compared to other populations plantlets (Fig. 1C).

Table 4. Variation of viability and biomass production of plantlets in three Iranian populations of *A. calamus* (after 30 days).

Populations	Viability (%)	Primary total weight (g)	Final total weight (g)	Average final total weight (g)
Arzefon	100	22.35	55.25	4.6 ± 0.01a
Pelesk	100	22.5	102.3	8.5 ± 0.13b
Alandan	83.3	22.30	52.5	4.37 ± 0.19a

Discussion

To achieve an effective micropropagation protocol and determine the appropriate population, the tissue culture of plant samples of three populations of *A. calamus* was performed for the first time in Iran. As other studies have reported (Rani et al. 2000; Ahmed et al. 2007; Sandhyarani et al. 2011; Verma and Singh 2012; Dixit et al. 2014), fungal contamination of the culture medium was the most important problem in this study. In accordance with some studies, callus formation and indirect plant regeneration using rhizome, leaf and root explants at different concentrations of plant growth regulators were not successful (Rani et al. 2000; Ahmed et al. 2007; Sandhyarani et al. 2011; Verma and Singh 2012). Dixit et al. (2014) reported regeneration of this plant using leaf explant in combined treatment of BA and NAA (2.5 mg/l + 1 mg/l). According to this study, only the lowest basal part of the leaf was effective in plant regeneration and the rest part of leaf was not useful. It seems that the small buds at the base of the leaf were probably effective in regenerating the plant.

The results of the present research, like previous studies, showed that rhizome is suitable organ for micropropagation of sweet flag (Hettiarachchi et al. 1997; Rani et al. 2000; Ahmed et al. 2007; Sandhyarani et al. 2011; Verma and Singh, 2012; Dixit et al. 2014). Various plant growth regulators, including cytokinins (Kin and BAP) and auxins (IBA, IAA, and NAA), have been used alone or in combination for callus induction, plant regeneration, and root formation in this plant. The results of the present study, as in other studies, showed that BAP (among the cytokinins) and IBA and NAA (among the auxins) are the most suitable plant growth regulators for *A. calamus* micropropagation (Rani et al. 2000; Ahmed et al. 2007; Sandhyarani et al. 2011; Verma and Singh, 2012; Dixit et al. 2014).

1 mg/l BAP and NAA treatment is the most suitable treatment in comparison with other treatments, in direct plant regeneration of Iranian populations of sweet flag. In the study of Hettiarachchi et al. (1997), the combined treatment of 0.5 mg/l BAP with 0.2 mg/l NAA showed the best performance in plant regeneration. On the other hand, the highest number of regenerated plants was found in combined treatment of BAP and NAA (Anu et al. 2001). The maximum number of regenerated plants was observed in combined treatment of BAP and NAA (2 mg/l and 0.5 mg/l) (Ahmed et al. 2007; Verma and Singh 2012). The maximum number of proliferated shoots was observed in MS medium supplemented with 4 mg/l BAP and 0.5 mg/l IAA (Rani et al. 2000). The results of the present study are in accordance with other studies in terms of the type of plant growth regulators (BAP and NAA), but there are differences in the concentration of plant growth regulators (Hettiarachchi et al. 1997; Anu et al. 2001; Ahmed et al. 2007; Verma and Singh, 2012). Since most of the mentioned studies have been done on plant samples of Indian populations, one of the possible reasons for this discrepancy is related to the geographical distribution differences of the studied populations.

The regenerated plantlets of Arzefon, Pelesk, and Alandan populations showed different responses in rooting treatments. The plantlets of Alandan population, with the highest mean number (6.6 ± 0.1) and average length of root (3.75 ± 0.04 cm) in 1 mg/l IBA treatment, showed the best performance among root induction treatments. The results of this study are completely in accordance with the studies of Ahmed et al. (2007), Altaf et al. (2010) and Verma and Singh (2012) in terms of type and concentration of plant growth regulators. The maximum number of the roots was observed in 9.8 μM concentration of IBA (Anu et al. 2001), and 2 mg/l IBA (Sandhyarani et al. 2011). Based on the results of this study, Alandan population plantlets showed better response in root induction experiment than other populations.

The regenerated plantlets of Iranian populations showed significant viability in the greenhouse. Plants of Arzefon and Pelesk populations had 100% viability, whereas plant samples of Alandan showed 83% viability. On the other hand, all the plantlets transferred to the field also survived until the end of growing season (Fig. 1D). The rooted plants showed about 90-95% viability in the greenhouse (Rani et al. 2000; Anu et al. 2001; Altaf et al. 2010), while Verma and Singh (2012) reported that about 75% of the plants survived in the field. In terms of survival rate of the regenerated plantlets in greenhouse and field, the results of this study are in accordance with some of the findings. According to the results of this study, plants of Alandan population of *A. calamus* are recommended for micpropagation and cultivation in Iran.

Conclusion

Due to the increasing demand for *A. calamus* products, it is necessary that this rare plant be propagated and cultivated in Iran. Because of vegetative reproduction, and no seed production in the Iranian wild populations of the species, the providing of plantlets for planting in suitable season is a great problem in the cultivation of this plant. This study presented an efficient protocol for sweet flag micropropagation to providing large-scale plantlets without any time limitation, and suggested plants of Alandan population of *A. calamus* as suitable accession for cultivation in Iran. This protocol can also be used for the conservation purposes of this plant.

Acknowledgments

The authors are thankful to Azam Ebrahimi, Maryam Ramrodi, and Maryam Nikzad for their cooperation in laboratory works. The authors would like to thank Ms. Zahra Sadeghi for English language editing of the manuscript. This study was funded by Iran National Science Foundation (INSF) and Payame Noor University (grant number 96003519).

REFERENCES

Ahmed MB, Ahmed S, Salahin M, Sultana M, Khatun M, Razvy MA, Hannan MM, Islam R, Hossain MM (2007) Standardization of a suitable protocol for *in vitro* clonal propagation of *Acorus calamus* L. an important medicinal plant in Bangladesh. Am-Euras J Sci Res 2(2):136-140.

Altaf A, Shashidhara S, Rajshekharan PE, Harees KV, Honnesh NH (2010) *In vitro* regeneration of *Acorus calamus* - an important medicinal plant. J Curr Pharma Res 2(1):36-39.

Anu A, Babu KN, John CZ, Peter KV (2001) *In vitro* clonal multiplication of *Acorus calamus*. J Plant Biochem Biotechnol 10:53-55.

Babar PS, Deshmukh AV, Salunkhe SS, Chavan JJ (2020) Micropropagation, polyphenol content and biological properties of Sweet Flag (*Acorus calamus*): a potent medicinal and aromatic herb. Vegetos 33:296-303.

Bhagat N (2011) Conservation of endangered medicinal plant (*Acorus calamus*) through plant tissue culture. J Pharmacogn 2(1):21-24.

Chandana BC, Kumari Nagaveni HC, Lakshmana D, Shashikala SK, Heena MS (2018) Role of plant tissue culture in micropropagation, secondary metabolites production and conservation of some endangered medicinal crops. J Pharmacogn Phytochem 7(3S):246-251.

Devi NS, Kishor R, Sharma GJ (2012) Microrhizome induction in *Acorus calamus* Linn. - An important medicinal and aromatic plant. Hortic Environ Biotechnol 53:410-414.

Dixit V, Purshottam DK, Agnihotri P, Husain T, Misra P (2014) A highly efficient shoot organogenesis system of *Acorus calamus* - a threatened medicinal plant of Indian Himalaya. Experiment J 21(1):1453-1461.

Fallah M, Farzaneh M, Yousefzadi M, Ghorbanpour M, Mirjalili MH (2019) *In vitro* mass propagation and conservation of a rare medicinal plant, *Zhumeria majdae* Rech. f & Wendelbo (Lamiaceae). Biocatal Agric Biotechnol 17:318-325.

Gholipour A, Sonboli A (2013) Rediscovery of *Acorus calamus* (Acoraceae) in Iran. Taxonomy and Biosystematics 5(15):113-116. [In Persian]

Hettiarachchi A, Fernando KKS, Jayasuriya AHM (1997) *In vitro* propagation of Wakada (*Acorus calamus*). J Natn Sci Coun Sri Lanka 25(3):151-157.

IBM (2010) IBM SPSS Statistics for Windows, Version 19.0. IBM, New York, USA.

Imam H, Riaz Z, Azhar M, Sofi G, Hussain A (2013) Sweet flag (*Acorus calamus* Linn.): An incredible medicinal herb. Int J Green Pharm 7:288-296.

Kumar A, Kumar P, Kumar V, Kumar M (2014) Traditional uses of wetland medicinal plant *Acorus calamus*: review and perspectives. Int J Referred Online Res 2(5):37-67.

Lokesh GB (2004) Sweet flag (*Acorus calamus*) cultivation and economics aspects. Nat Prod Rad 3(1):19-20.

Mohammed E-S E-M, Dewir YH, Singh N (2007) Indirect shoot organogenesis and plantlets regeneration from stem of ornamental *Dieffenbachia maculata* cv. Marianna. Acta Biol Szeged 51(2):113-116.

Motley TJ (1994) The ethnobotany of sweet flag, *Acorus calamus* (Araceae). Econ Bot 48:397-412.

Mozaffarian V (2013) Identification of Medicinal and Aromatic Plants of Iran. Farhange-Moaser Publication, Tehran. p.42-43. [In Persian]

Rani AS, Subhadra VV, Reddy VD (2000) *In vitro* propagation of *Acorus calamus* Linn. – a medicinal plant. Indian J Exp Biol 38:730-732.

Sandhyarani N, Kishor R, Sharma GJ (2011) Clonal propagation of triploid *Acorus calamus* Linn. using dual-phase culture system. J Crop Sci Biotechnol 14(3):213-217.

Verma S, Singh N (2012) *In vitro* Mass multiplication of *Acorus calamus* L. - an endangered medicinal plant. Am Eurasian J Agric Environ Sci 12(11):1514-1521.

Acta Biologica Szegediensis

Volume 65(1):35-45, 2021
Acta Biologica Szegediensis
http://abs.bibl.u-szeged.hu/index.php/abs
DOI:10.14232/abs.2021.1.35-45

ARTICLE

Epidermal micromorphology of floret parts in *Aeluropus* (Poaceae)

Samaneh Mosaferi* and Maryam Keshavarzi

Department of Plant Sciences, Faculty of Biological Sciences, Alzahra University, Tehran, Iran

ABSTRACT *Aeluropus* from Poaceae comprises 5 species in the world and 3 species in Iran. This halophytic perennial is distributed in salty and dry soils of Asia, Europe, and Africa. In addition to being used as fodder, it can stabilize the soil by its rhizome or stolon. These features make *Aeluropus* a valuable plant. In this study, lemma and palea of 10 populations of *Aeluropus* were studied micromorphologically by scanning electron microscope (SEM) to determine diagnostic features among species studied. Eight characters as micro-prickle, macro-hair, long cell outline, cork and silica cells, papilla, salt gland, and epicuticular wax were studied. The occurrence of salt glands and silica cells in populations/taxa studied showed the ability of *Aeluropus* to tolerate harsh habitats. Our result showed the taxonomic value of floret micromorphological features to separate *Aeluropus* species.
Acta Biol Szeged 65(1):35-45 (2021)

KEY WORDS
Aeluropus
Aeluropodinae
Chloridoideae
lemma
palea

ARTICLE INFORMATION
Submitted
26 January 2021.
Accepted
18 May 2021.
***Corresponding author**
E-mail: s.mosaferi@alzahra.ac.ir

Introduction

Aeluropus Trin. (Poaceae, Chloridoideae) is one of the two genera of subtribe Aeluropodinae with 5 species in the world (The Plant List 2013). Previously it comprised 4 species in Iran (Bor 1970). As *A. pungens* (M. Bieb.) K. Koch was synonymized to *A. littoralis* (Gouan) Parl., its species reduced to three taxa (The Plant List 2013). Some infra-specific taxa were recorded for this genus in Iran (Khodashenas 2009).

Members of this halophytic weed are distributed in tropical regions of Asia, Europe, and Africa (Zhang et al. 2006). This genus contains rhizomatous or stoloniferous perennials that help the soil stabilization. It has dense capitate, spike like or panicle inflorescence with compressed spikletes, chartaceous unequal glumes which are shorter than lemma, keeled lemma which is glabrous or hairy on margins, palea with ciliate on keel and oblong-elliptic or oblong-obovate caryopsis (Bor 1970; Zhang et al. 2006).

Aeluropus is distributed in saline soils, sandy shores and dry regions (Zhang et al. 2006). Members of Poaceae family grown in saline soils, have unicellular or bicellular salt glands as a common adaptive feature (Wahit 2003; Kobayashi 2008; Céccoli et al. 2015). All Poaceae subfamilies have micro-hairs except Pooideae (Amarasinghe and Watson 1988, 1989; Kobayashi 2008) but functional salt glands are only observed in Chloridoideae (Bell and Ó Leary 2003; Kobayashi et al. 2007; Hameed et al. 2013). This subfamily is adapted to harsh and saline environments by having salt gland (Taleisnik and Anton 1988; Columbus et al. 2007; Peterson et al. 2010).

The importance of micromorphological characters in Poaceae has been established by different authors. Different vegetative and reproductive parts as leaf (Mavi et al. 2011; Ortúñez and Cano-Ruiz 2013), glume (Klimko and Wysakowska 2015), lemma (Acedo and Llamas 2001; Li et al. 2010, Ortúñez and Cano-Ruiz 2013; Harms and Mendenhall 2015), palea (Klimko et al. 2009; Ortúñez and De La Fuente 2010), and caryopsis (Terrell and Peterson 1993; Gandhi et al. 2013, Zhang et al. 2014; Liu et al. 2015) have been studied micromorphologically to solve taxonomic problems at different levels in Poaceae.

Lemma and palea epidermal characters are of taxonomic value in identifying and studying relationship between genera and species in Chloridoideae (Liu et al. 2010). There are limited studies on the micromorphology of *Aeluropus* species. Liu et al. (2010) studied lemma and palea characters in *A. littoralis*. Features as long cell outline, cork cell, micro-hair, macro-hair, papillae, micro-prickle and silica body have been used to characterize this taxon from other members of Chloridoideae.

This study aims to describe micromorphological characters of lemma and palea in *Aeluropus* species in Iran and to discuss taxonomic value of these features at interspecific level.

Table 1. Voucher details of population studied.

Species	No.	Locality	Longitude	Latitude	Altitude (m)	Voucher No.
A. littoralis (Gouan) Parl.	1	Kerman, Kahnooj	28º 01' 15''	57º 43' 33''	531	99 a ALUH
	2	Sistan and Baluchestan, Hirmand, Bar-Ahuyi	31º 06' 46''	61º 47' 01''	481	ha-169 ALUH
	3	East Azerbaijan, Tabriz to Ahar, Talkheh Rud	38˚ 01' 55''	46 º 56' 58''	1635	8511 ALUH
	4	Tehran, Saveh	35º 01' 17''	50º 21' 24''	998	8512 ALUH
A. lagopoides (L.) Thwaites	5	Semnan, Garmsar	35º 13' 06''	52º 20' 27''	850	8513 ALUH
	6	Kerman, Jazmourian, Zeh-e-kalut	27º 48' 15''	58º 36' 11''	392	99 b ALUH
	7	Sistan and Baluchestan, Hirmand, Bar-Ahuyi	31º 06' 46''	61º 47' 01''	481	ha-168 ALUH
	8	Fars, Maharlu lake	29º 26' 05''	52º 46' 38''	1461	66947 ALUH
A. macrostachyus Hack.	9	Kerman, Kahnooj	28º 01' 15''	57º 43' 33''	531	851 ALUH
	10	Sistan and Baluchestan, 20 km of Mirjaveh to Jaleq	27º 35' 33''	62º 41' 28''	849	49878 IRAN

Materials and Methods

To study the micromorphological features, 10 accessions of 3 species of *Aeluropus* were considered. Samples were obtained from specimens at Alzahra University Herbarium (ALUH) and Herbarium of Iranian Research Institute of Plant Protection, Department of Botany (IRAN). They were identified using taxonomic literatures such as Flora Iranica (Bor 1970), Flora of Iraq (Bor 1968) and Flora of Turkey (Davis 1985). Voucher specimens and localities are mentioned in Table 1.

For lemma and palea studies, mature florets of spikelets, were chosen and complete lemmas and paleas were separated. Middle part of abaxial surfaces were examined without any treatment. At first, each part was examined by Olympus stereomicroscope and Dino Lite digital microscope. Then samples were mounted on metallic stubs, coated with gold in a sputter coater with 100 Å layer of gold and examined and photographed with Hitachi SU3500 scanning electron microscope (SEM). Eight diagnostic characters of lemma and palea were evaluated (Tables 2 and 3). Terminology was adapted from Snow (1996), Acedo and Llamas (2001), Mejía-Saules and Bisby (2003) and Liu et al. (2010) for lemma and palea characters. Barthlott et al. (1998) terminology was used for epicuticular wax variation.

Table 2. Micro-morphological characters of lemma surfaces in populations/taxa studied.

Species	Pop. no.	Characters							
		Micro-prickle	Macro-hair	Long cell out line	Cork cell	Silica cell	Papillae	Bicellular micro-hair	Epicuticular wax
A. littoralis	1	a-type	absent	wide U-shaped	absent	dumbbell-shaped	on long cell	long base-cell	granule, platelet
	2	a-type, b-type	papilla-base	wide U-shaped	oblong	dumbbell-shaped	on long and short cells	long base-cell	platelet, granule
	3	absent	absent	straight	oblong	cross-shaped	on long and short cells	long base-cell	platelet, granule
	4	a-type	absent	straight	absent	dumbbell-shaped	on long and short cells	short base-cell	granule, platelet
A. lagopoides	5	absent	geniculate, papilla-base	wide U-shaped	absent	dumbbell-shaped	on long cell	long and short base-cell	granule
	6	a-type, b-type	absent	wide U-shaped	squared	dumbbell-shaped	on long and short cells	long and short base-cell	cube, granule
	7	absent	geniculate	straight	absent	dumbbell-shaped	on long and short cells	long and short base-cell	granule, platelet
	8	absent	papilla-base	wide U-shaped	absent	dumbbell-shaped	on long and short cells	long base-cell	platelet
A. macro-stachyus	9	absent	geniculate	Ω-shaped	oblong	dumbbell-shaped	on long and short cells	long base-cell	granule
	10	a-type	geniculate	Ω-shaped	absent	dumbbell-shaped	on long and short cells	long base-cell	granule, platelet

Table 3. Micro-morphological characters of palea surfaces in populations/taxa studied.

Species	Pop. no.	Characters							
		Micro-prickle	Macro-hair	Long cell out line	Cork cell	Silica cell	Papillae	Bicellular micro-hair	Epicuticular wax
A. littoralis	1	b-type	absent	Ω-shaped	absent	cross- shaped	on long cell	absent	cube, granule
	2	a-type, b-type	geniculate	Ω-shaped	absent	cross- shaped	absent	absent	platelet, granule
	3	a-type, b-type	absent	Ω-shaped	oblong	absent	absent	short base-cell	granule, platelet
	4	absent	absent	Ω-shaped	crescent-shaped	cross- shaped	on long cell	absent	platelet, granule
A. lagopoides	5	absent	absent	wide U-shaped	crescent-shaped	absent	absent	absent	granule
	6	a-type	absent	Ω-shaped	scalariform, oblong	absent	on long cell	short base-cell	granule
	7	absent	absent	wide U-shaped	oblong	absent	absent	absent	platelet, granule
	8	c- type	absent	wide U-shaped	oblong, crescent-shaped	absent	absent	absent	platelet
A. macrostachyus	9	b-type, c-type	absent	Ω-shaped	absent	saddle-shaped	absent	absent	cube, granule
	10	a-type	absent	Ω-shaped	absent	cross- shaped	on long cell	absent	granule

Results

Lemma micromorphology

Lemma micromorphological details of each population are summarized in Table 2. Outline of long cell in intercostal areas were straight to wide U-shaped in *A. littoralis* and *A. lagopoides* and Ω-shaped in *A. macrostachyus* (Figs. 1-3). Short cells were found in species studied. Cork cells were absent in most populations studied. Cork cells were only observed in Bar-Ahuyi and Talkheh Rud population of *A. littoralis* (Figs. 1B-C). Zeh-e-kalut population of *A. lagopoides* showed square cork cells (Fig. 2b). Three other populations did not have cork cells.

In *A. macrostachyus*, Kahnooj population had small oblong cork cell. They were frequent in costal zones with dense distribution (Fig. 3a).

Dumbbell-shaped silica cells were found in all taxa. In Talkheh Rud population of *A. littoralis*, cross-shaped silica cells were determined. This population had the densest distribution of silica cells among other populations of *A. littoralis* (Fig. 1c). The density of silica cells in *A. macrostachyus* was the highest among species studied (Fig. 3).

Papillae occurred on long and short cells of lemma surface in populations/taxa studied. They were only observed on long cells in Kahnooj population of *A. littoralis* (Fig. 1A) and Garmsar population of *A. lagopoides* (Fig. 2A).

Macro-hairs showed variation in length and density. These unicellular structures were densely covered the lemma surface of *A. lagopoides* (especially in Garmsar population) (Fig. 2A) while in *A. macrostachyus* they were sparse. In *A. macrostachyus*, geniculate macro-hairs were seen (Fig. 3) while in *A. lagopoides*, two types of macro-hairs, geniculate and papilla- base, were seen (Fig. 2). Except Bar-Ahuyi population, there was no macro-hair in *A. littoralis* populations (Fig. 1).

In lemma and palea, three types of micro-prickles were observed: barbs developed from the apex of the base with direct point (a- type), barbs with direct point not developed from the base (b-type) and barbs with recurved point not developed from the apex of the base (c-type) (adapted from Ellis 1979). Micro-prickles were commonly found in *A. littoralis* lemma surface (Fig. 1) but in two other taxa, these features were sparse.

Salt glands were observed in all taxa studied. These bicellular excretory organs were commonly found in coastal areas of lemma epidermis. Taxa studied showed chloridoid type of bicellular micro-hairs. This type of micro-hair was classified to two sub-types: short-base cell and long-cell base. *A. macrostachyus* had long-cell base type (Fig. 3) but *A. littoralis* and *A. lagopoides* had both types (Figs. 1-2).

Epicuticular wax showed differences in type and distribution among taxa/population studied. In *A. littoralis*, platelet and granule waxes were seen in populations. These waxes were densely covered the lemma surface of Saveh population (Fig. 1D-d). Among populations of *A. lagopoides*, Garmsar population showed the densest cover of granular wax (Fig. 2a). Zeh-e-kalut population showed sparse distribution of cube and granule wax. Other populations showed medium coverage of platelet and granule

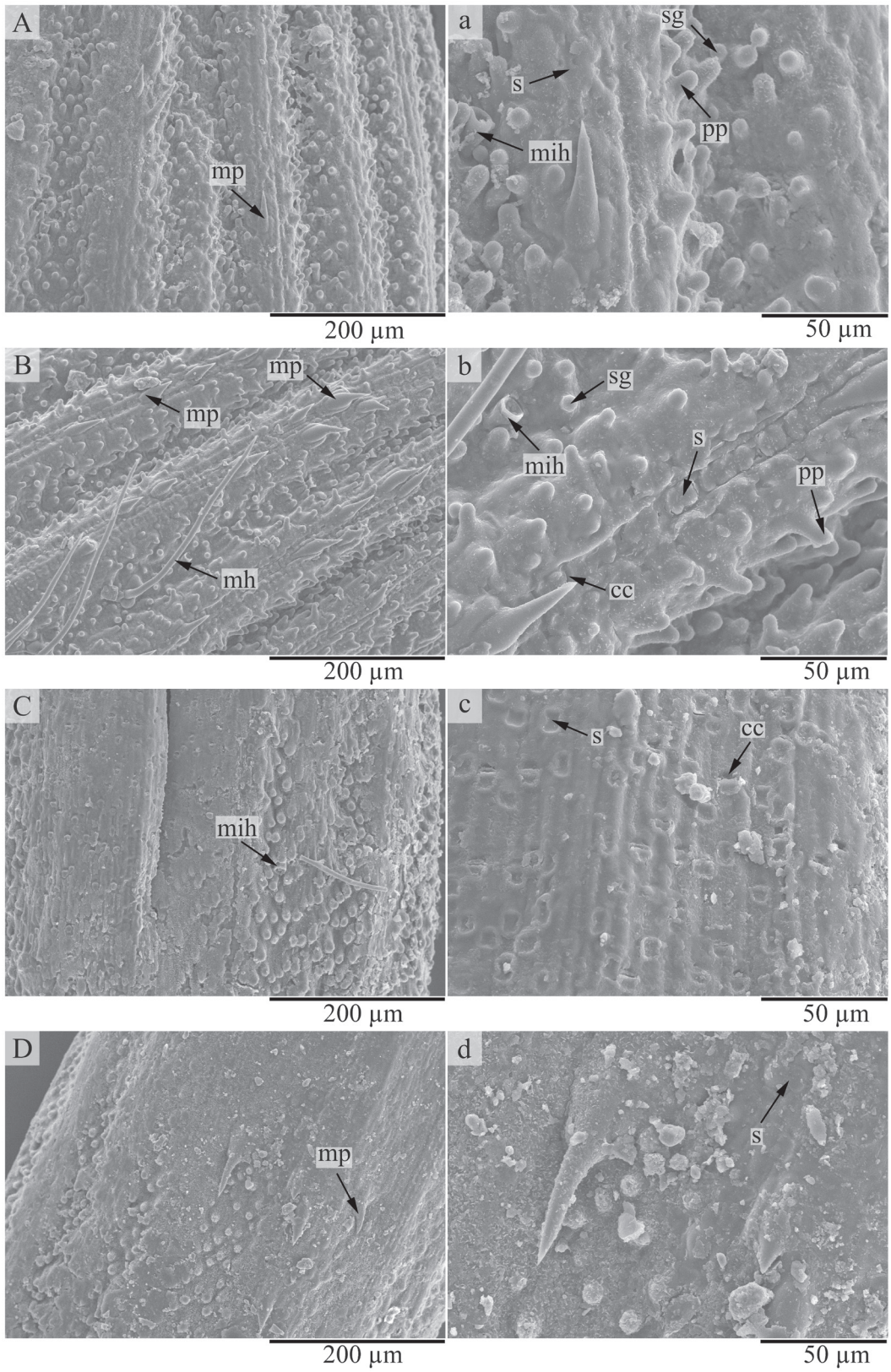

Figure 1. SEM micrographs of lemma surfaces in *A. littoralis*. A-a: Kahnooj; B-b: Bar-Ahuyi; C-c: Talkheh Rud; D-d: Saveh. cc: cork cell; s: silica cell; mh: macro-hair; mih: micro-hair; mp: micro-pickle; pp: papillae; sg: salt gland.

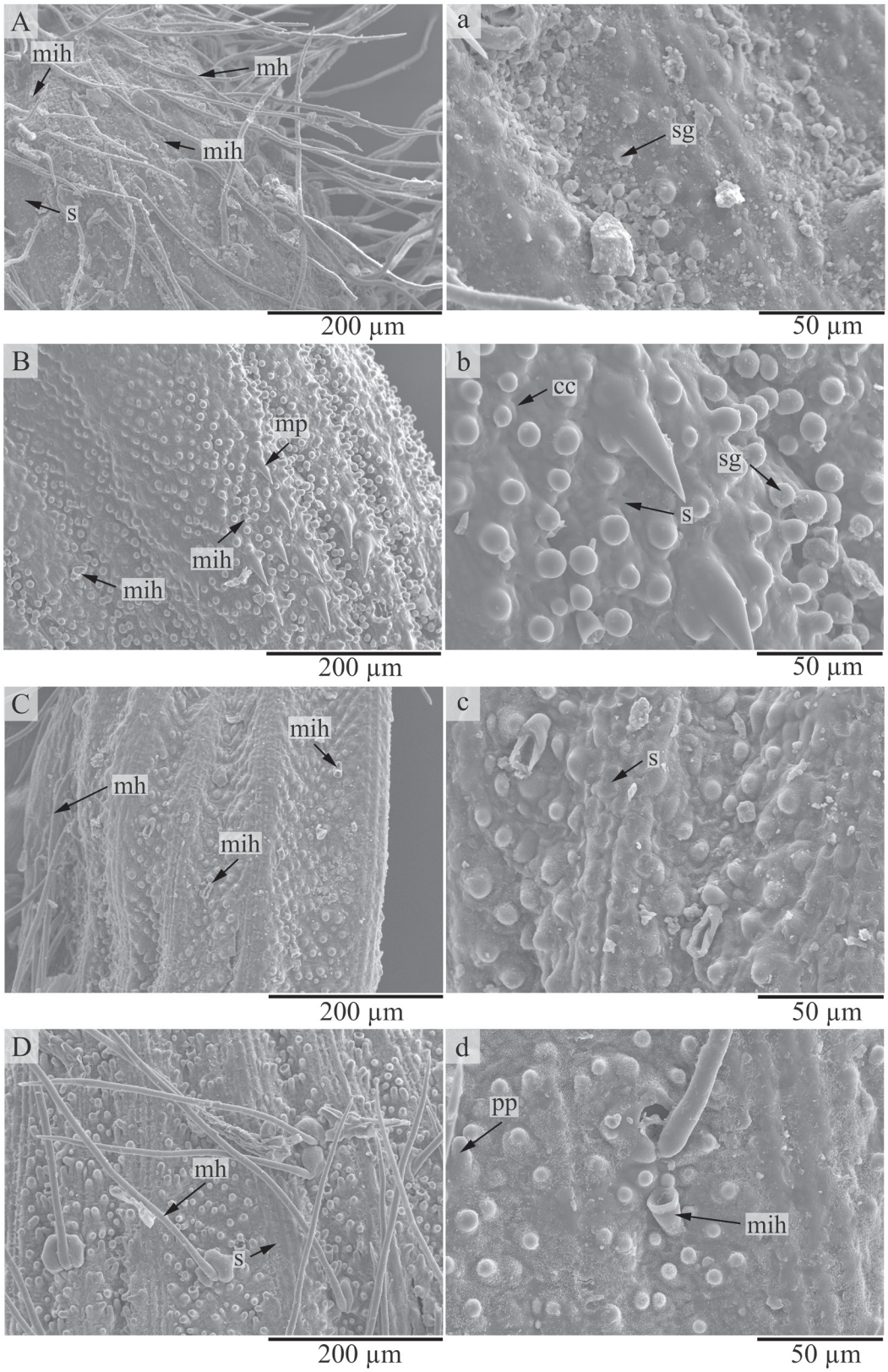

Figure 2. SEM micrographs of lemma surfaces in *A. lagopoides.* A-a: Garmsar; B-b: Zeh-e-kalut; C-c: Bar-Ahuyi; D-d: Maharlu lake. cc: cork cell; s: silica cell; mh: macro-hair; mih: micro-hair; mp: micro-pickle; pp: papillae; sg: salt gland.

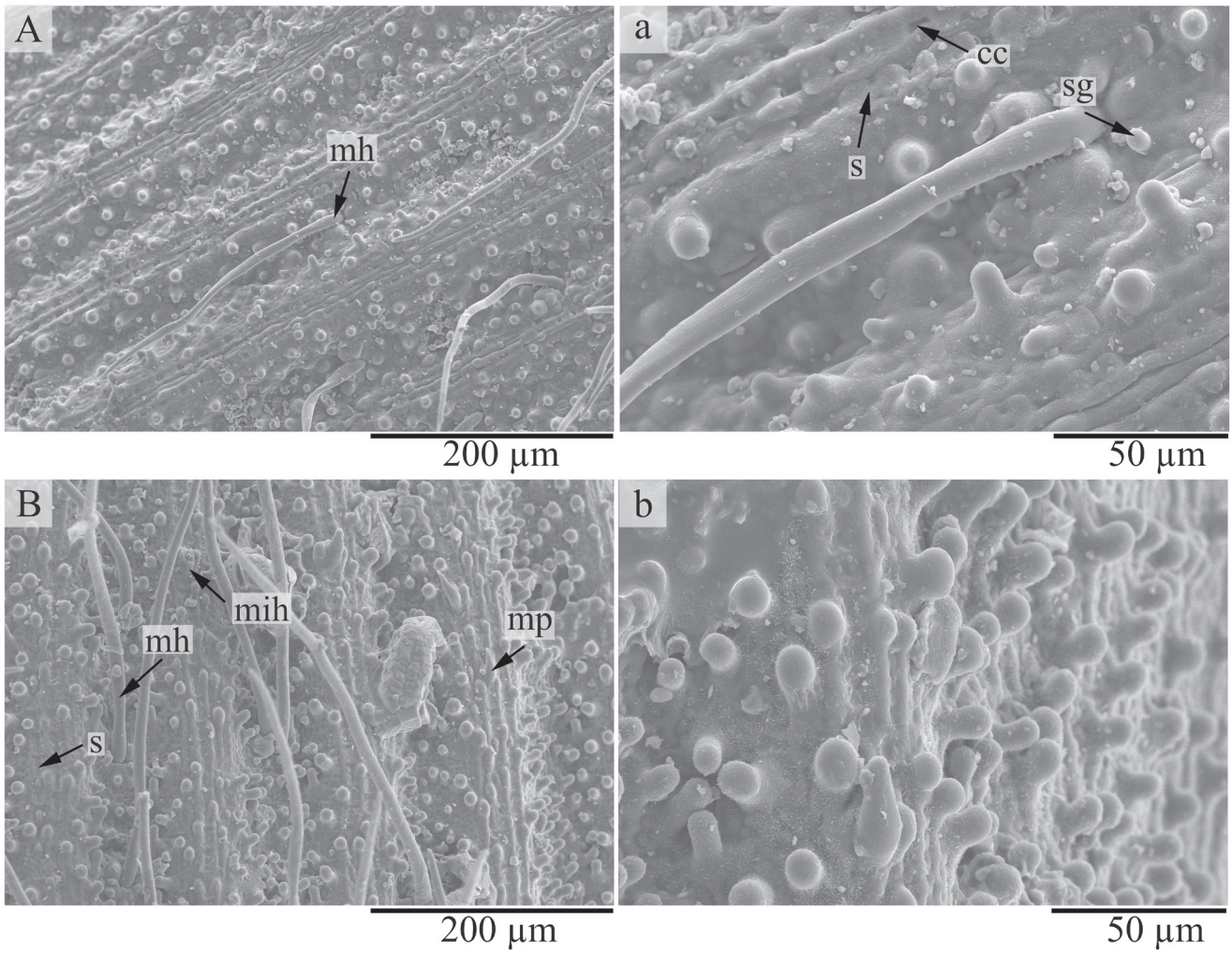

Figure 3. SEM micrographs of lemma surfaces in *A. macrostachyus*. A-a: Kahnooj; B-b: Mirjaveh to Jaleq. cc: cork cell; s: silica cell; mh: macro-hair; mih: micro-hair; mp: micro-pickle; sg: salt gland.

wax types (Fig. 2). Lemma surface of *A. macrostachyus* was sparsely covered with granule and platelet waxes (Fig. 3).

Palea micromorphology

A. littoralis and *A. macrostachyus* showed Ω-shaped outline in long cells (Figs. 4, 5E-F) while *A. lagopoides* showed wide U-shaped in long cells outline except Zeh-e-kalut population (Fig. 5A-D) (Table 3). *A. littoralis* and *A. lagopoides* showed cork cells in some populations. *A. littoralis* had oblong and crescent- shaped cork cells (Fig. 4D) but populations of *A. lagopoides* showed modifications in shape of cork cells (Fig. 5A-D). Cork cells were not observed in *A. macrostachyus* (Fig. 5E-F). Silica cells were only observed in *A. littoralis* and *A. macrostachyus*. Two populations of *A. macrostachyus* had saddle- shaped and cross- shaped silica cells (Fig. 5E-F) while in *A. littoralis* only cross-shaped ones were found (Fig. 4). Bar-Ahuyi population of *A. littoralis* had the densest distribution of silica cells and Kahnooj population of *A. macrostachyus* had the sparest.

Papillae were found on long cells of four populations studied. Macro-hairs were lacking in species studied except Bar-Ahuyi population of *A. littoralis* (not shown). In *A. littoralis*, all populations had micro-prickles except Saveh population. In *A. lagopoides*, only Maharlu lake and Zeh-e-kalut populations had micro-prickles. Bar-Ahuyi population of *A. littoralis* and Maharlu lake population of *A. lagopoides* showed more micro-prickles among other populations mostly distributed in the margin (not shown).

Chloridoid type of bicellular micro-hairs were only present in Talkheh Rud population of *A. littoralis* (Fig. 4C) and Zeh-e-kalut population of *A. lagopoides* (not shown). These two populations showed short-base cell chloridoid type.

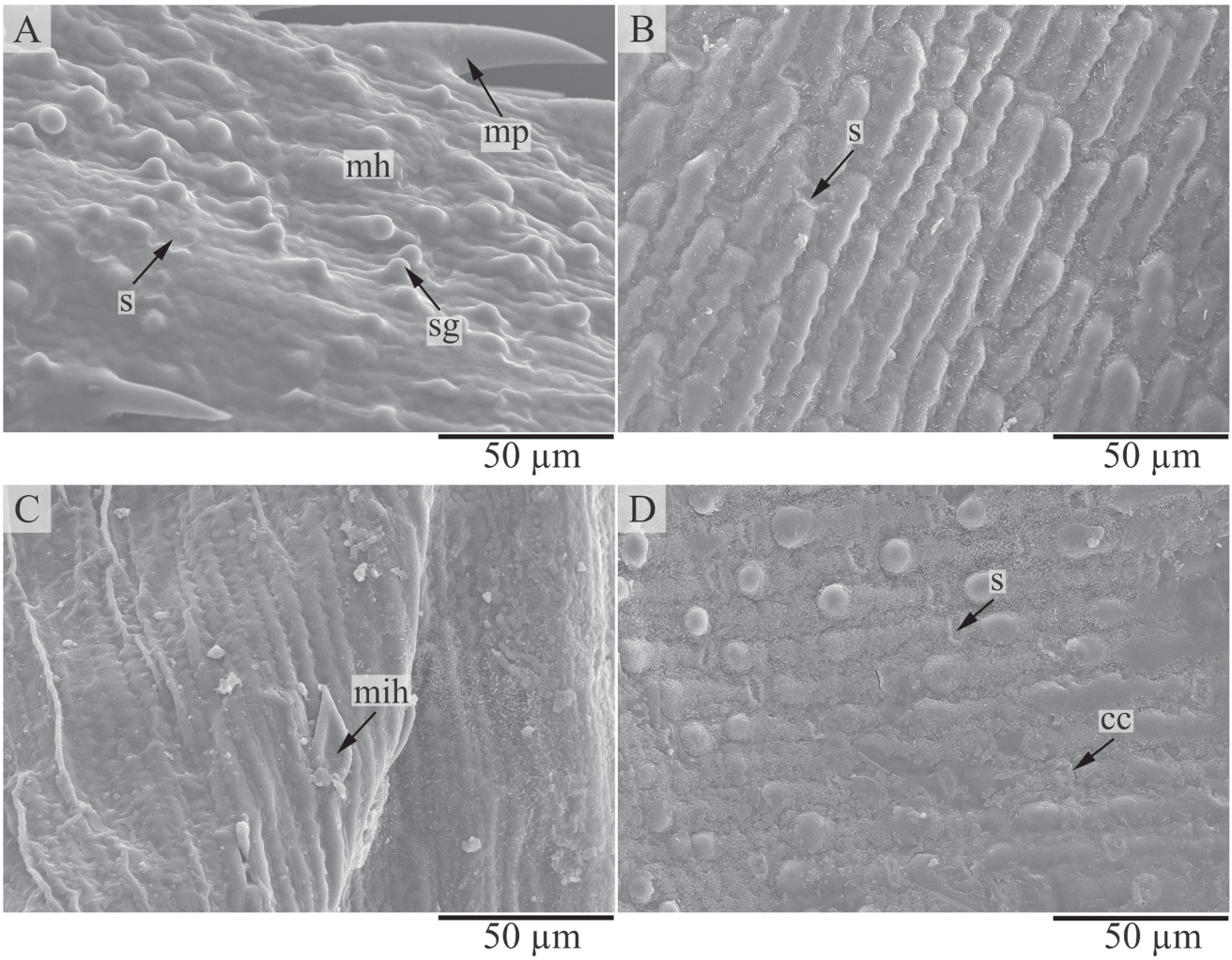

Figure 4. SEM micrographs of palea surfaces in *A. littoralis*. A: Kahnooj, B: Bar-Ahuyi, C: Talkheh Rud, D: Saveh. cc: cork cell, s: silica cell, mih: micro-hair; mp: micro-pickle, sg: salt gland.

Dense platelet waxes covered palea surface of Saveh population in *A. littoralis*. A little number of granules were also seen in this population (Fig. 4D). Platelet and granular waxes were irregularly distributed in palea surfaces of Bar-Ahyui and Talkheh Rud populations (Fig. 4B-C). Wax was scarce in Kahnooj population. In populations of *A. lagopoides*, granule and platelet waxes were seen with dense distribution except Zeh-e-kalut population (Fig. 5A-D). In *A. macrostachyus* wax was rare (Fig. 5E-F).

Discussion

Aeluropus is a halophyte plant distributed in dry and saline regions of different parts of Iran (Bor 1970). This grass showed dumbbell-shaped, cross-shaped and saddle-shaped silica cells in lemma and palea surfaces of nearly all populations studied. These features enable *Aeluropus* to live in water deficiency (Santi et al. 2018). In addition, Chloridoid type of salt glands in the form of long base-cells and short base-cells microhairs were scattered in the different parts of *Aeluropus* accessions that enable them to tolerate high salinity (Kobayashi 2008; Céccoli et al. 2015). We found epicuticular wax in shapes of cube, granule, and platelet with different density on the lemma and palea surfaces showing adaptation in different conditions.

The natural occurrence of this plant in saline habitats makes it a useful candidate for stabilizing the soil. Moreover, this plant can be used as forage especially in salty and dry soils where little fodders can grow (Zhang et al. 2006; Barzegargolchini et al. 2017).

In this study, the highest level of silica body occurred in lemma surface of *A. macrostachyus*. Presence of more silica cells cause less grazing (Quigley and Anderson

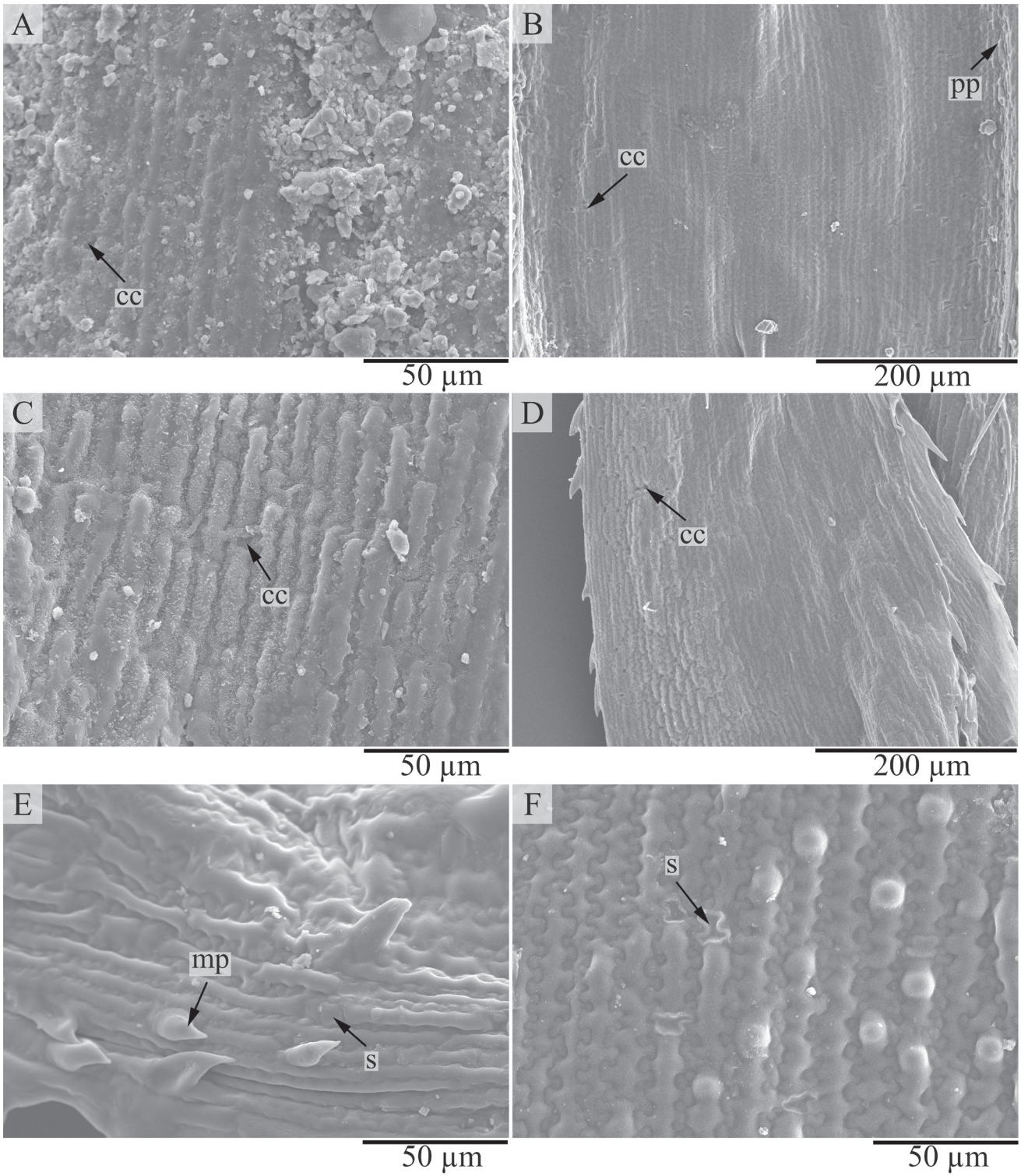

Figure 5. SEM micrographs of palea surfaces in *A. lagopoides*. A: Garmsar, B: Zeh-e-kalut, C: Bar-Ahuyi, D: Maharlu lake; E-F: *A. macrostachyus*; E: Kahnooj; F: Mirjaveh to Jaleq. cc: cork cell; s: silica cell; mp: micro-pickle; pp: papillae.

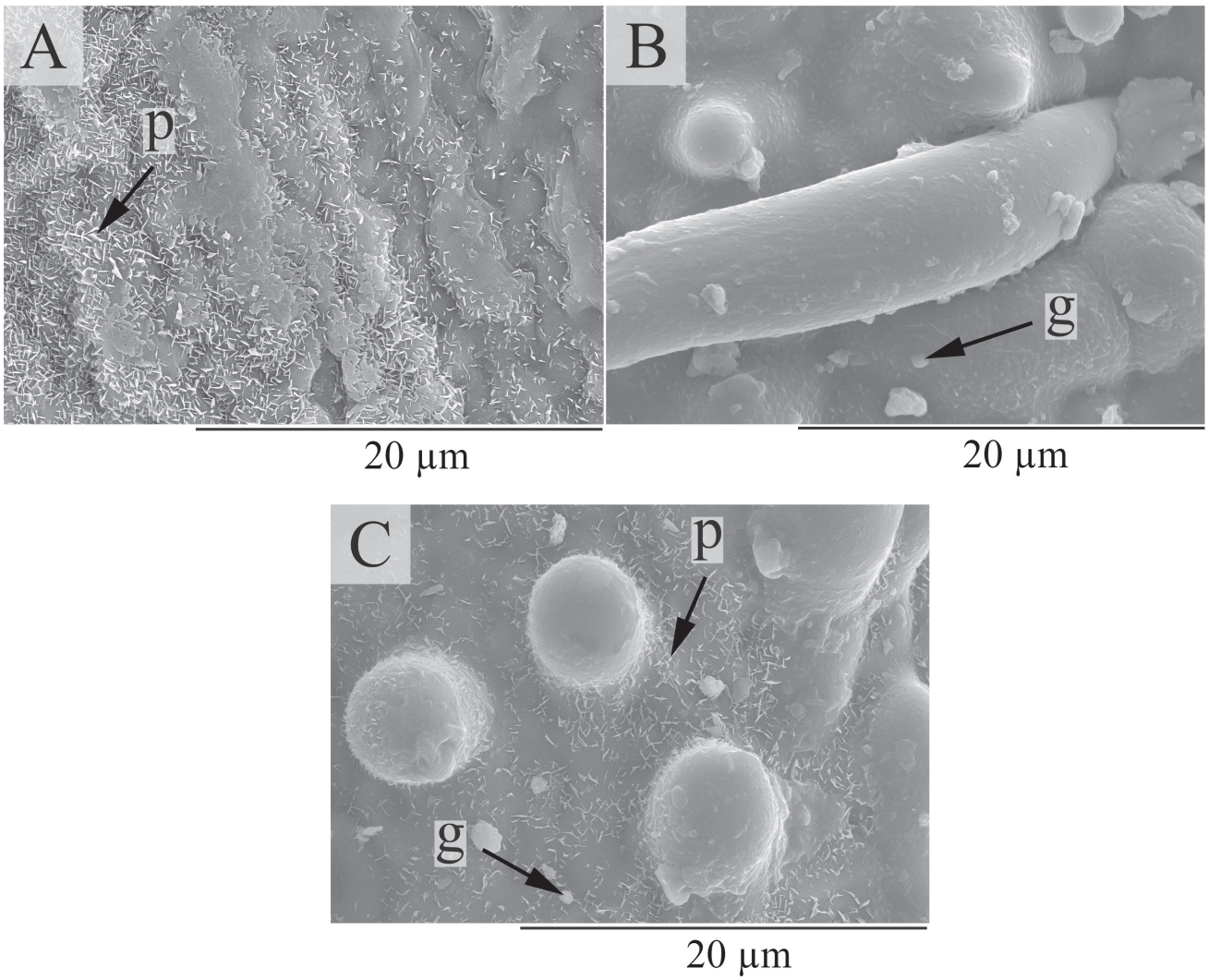

Figure 6. SEM micrographs of lemma and palea surfaces. A: platelet waxes in lemma surface of *A. lagopoides* (Maharlu lake population); B: granule waxes in lemma surface of *A. macrostachyus* (Mirjaveh to Jaleq population); C: platelet and granule waxes in palea surface of *A. littoralis* (Saveh population). p: platelet wax; g: granule wax.

2014). It maybe because of this, foraging quality of two palatable taxa, *A. littoralis* and *A. lagopoides* were studied more by different authors (Abbasi et al. 2002; Sharifi Rad et al. 2013).

All species possessed papillae, silica cells and salt glands on lemma surfaces. Except four populations (no. 2, 3, 6, 9), we did not find cork cells on lemma surfaces. Despite palea, papilla-base and geniculate macro-hairs occurred in lemma surface of most populations.

The results of our study suggest that lemma and palea micromorphology may be useful to distinguish *Aeluropus* species. Although some characters as shape of silica cells in lemma and absence of macro-hairs in palea were uniform among taxa studied, some others differed among species. For example, *A. macrostachyus* was the only species with Ω-shaped outline in long cells of lemma and with no salt gland on palea surface. Our results confirmed its distinct position based on morphological characters as Abivardi et al. (2010) mentioned before. Liu et al. (2010) noted to U-shaped outline for long cells and dumbbell shape for silica cells in lemma of *A. littoralis*. Our results were in agreement with them. Despite some overlapping features, generally our micro-morphological results separate the three species studied.

Acknowledgement

We are grateful to the curator of Herbarium of Iranian Research Institute of Plant Protection, Department of

Botany (Iran) for permission to access *Aeluropus* specimens.

References

Abbasi F, Khavarinethad RA, Kouchaki A, Fahimi H (2002) Effect of salinity on growth and physiological aspects of *Aeluropus littoralis*. Desert 7:101-110.

Abivardi F, Keshavarzi M, Assadi M, Seifali M (2010) Numerical taxonomy of *Aeluropus* Trin. species (Poaceae) in Iran. TBJ 2:85-102.

Acedo C, Llamas F (2001) Variation of micromorphological characters of lemma and palea in the genus *Bromus* (Poaceae). Ann Bot Fenn 38:1-14.

Amarasinghe V, Watson L (1988) Comparative ultrastructure of microhairs in grasses. Bot J Linn Soc 98:303-319.

Amarasinghe V, Watson L (1989) Variation in salt secretory activity of microhairs in grasses. Aust J Plant Physiol 16:219-229.

Barthlott W, Neinhuis Ch, Cutler D, Ditsch F, Meusel I, Theisen I, Wilhelmi H (1998) Classification and terminology of plant epicuticular waxes. Bot J Linn Soc 126:237-260.

Barzegargolchini B, Movafeghi A, Dehestani A, Mehrabanjoubani P (2017) Morphological and anatomical changes in stems of *Aeluropus littoralis* under salt stress. JPMB 5:40-48.

Bell HL, Ó Leary JW (2003) Effects of salinity on growth and cation accumulation of *Sporobolus virginicus*. Am J Bot 90:1416-1424.

Bor NL (1968) *Aeluropus* Trin. In Townsend CE, Guest ER, Al-Rawi A, Eds., Flora of Iraq, Vol. 9. Iraq Ministry of Agriculture, Baghdad, 420-425.

Bor NL (1970) *Aeluropus* Trin. In Rechinger KH, Ed., Flora Iranica, Vol. 70. Akad. Druck- und Verlagsanstalt, Graz, 419-423.

Céccoli G, Ramos J, Pilatti V, Dellaferrera I, Tivano JC, Taleisnik E, Vegetti AC (2015) Salt glands in the Poaceae family and their relationship to salinity tolerance. Bot Rev 81:162-178.

Columbus JT, Cerros-Tlatilpa R, Kinney MS, Siqueiros-Delgado ME, Bell HL, Griffith MP, Refulio-Rodriguez NF (2007) Phylogenetics of Chloridoideae (Gramineae): a preliminary study based on nuclear ribosomal internal transcribed spacer and chloroplast trnL-F sequences. Aliso 23:565-579.

Davis PH (1985) *Aeluropus* Trin. In Davis PH, Guner A, Eds., Flora of Turkey and the east Aegean Islands, Vol. 9. Edinburgh University Press, Edinburgh, 569-572.

Ellis RP (1979) A procedure for standardizing comparative leaf anatomy in the Poaceae. II. The epidermis as seen in surface view. Bothalia 12:641-671.

Gandhi D, Alberts S, Pandya N (2013) Morphometric analysis of caryopsis in some species of *Eragrostis* (Poaceae). Telopea 15:87-97.

Hameed M, Ashraf M, Naz N, Nawaz T, Batool R, Ahmad MS, Ahamd F, Hussain M (2013) Anatomical adaptations of *Cynodon dactylon* (L.) Pers. from the salt range (Pakistan) to salinity stress. II. leaf anatomy. Pak J Bot 43:133-142.

Harms RT, Mendenhall J (2015) Taxonomic utility of lemma micromorphological characters in the *Sporobolus compositus* and *Sporobolus vaginiflorus* complexes (Poaceae). Lundellia 18:1-9.

Khodashenas M (2009) Two new records and a new combination of the genus *Aeluropus* (Poaceae) for the flora of Iran. IJB 15:61-62.

Klimko M, Pudelska H, Wojciechowska B, Klimko W (2009) Variation of micromorphological characters of lemma and palea in *Aegilops kotschyi* and *Aegilops biuncialis* × *Secale cereal* hybrids, amphiploids and parental forms. Steciana 13:167-176.

Klimko M, Wysakowska I (2015) Epidermal features of glumes and florets in *Aegilops geniculata* Roth and *Aegilops peregrina* (Hack.) Maire et Weiller × *Secale cereal* L. hybrids, amphiploids and parental forms. Steciana 19:13-24.

Kobayashi H (2008) Ion secretion via salt glands in Poaceae. JJPS 2:1-8.

Kobayashi H, Masaoka Y, Takahashi Y, Ide Y, Sato S (2007) Ability of salt glands in Rhodes grass (*Chloris gayana* Kunth) to secrete Na^+ and K^+. Soil Sci Plant Nutr 53:764-771.

Liu H, Hu XY, Liu YX, Liu Q (2015) Caryopsis micromorphological survey of *Sorghum* (Poaceae) - Taxonomic implications. S Afr J Bot 99:1-11.

Liu Q, Zhang DX, Peterson PM (2010) Lemma micromorphological characters in the Chloridoideae (Poaceae) optimized on a molecular phylogeny. S Afr J Bot 76:196-209.

Mavi DÖ, Doğan M, Cabi E (2011) Comparative leaf anatomy of the genus *Hordeum* L. (Poaceae). Turk J Bot 35:357-368.

Mejía-Saules F, Bisby FA (2003) Silica bodies and hooked papillae in lemmas *Melica* species (Gramineae: Pooideae). Bot J Linn Soc 141:447-463.

Ortúñez E, Cano-Ruiz J (2013) Epidermal micromorphology of the genus *Festuca* L. subgenus *Festuca* (Poaceae). Plant Syst Evol 299:1471-1483.

Ortúñez E, De La Fuente V (2010) Epidermal micromorphology of the genus *Festuca* L. (Poaceae) in the Iberian Peninsula. Plant Syst Evol 284:201-218.

Peterson PM, Romaschenko K, Johnson G (2010) A classification of the Chloridoideae (Poaceae) based on multi-gene phylogenetic trees. Mol Phylogenet Evol 55:580-598.

Quigley KM, Anderson TM (2014) Leaf silica concentration in Serengeti grasses increases with watering but not clipping. insights from a common garden study and

literature review. Front Plant Sci 5:1-10.
Santi LP, Haris N, Mulyanto D (2018) Effect of bio-silica on drought tolerance in plants. 2018. IOP conference series: Earth and Environmental Science 183(012014):1-8.
Sharifi Rad M, Sharifi Rad J, Teixeira Da Silva JA, Mohsenzadeh S (2013) Forage quality of two halophytic species, *Aeluropus lagopoides* and *Aeluropus littoralis*, in two phenological stages. IJAPP 4:998-1005.
Snow N (1996) The phylogenetic utility of lemmatal micromorphology in *Leptochloa* s.l. and related genera in subtribe Eleusininae (Poaceae, Chloridoideae, Eragrostideae). Ann Missouri Bot Gard 83:504-529.
Taleisnik EL, Anton AM (1988) Salt glands in *Pappophorum* (Poaceae). Ann Bot 62:383-388.
Terrell EE, Peterson PM (1993) Caryopsis morphology and classification in the Triticeae (Pooideae: Poaceae). Smithson Contrib Bot 83:1-25.
The Plant List (2013) Version 1.1. http://www.theplantlist.org/ (Accessed 01.01.2013).
Wahit A (2003) Physiological significance of morpho-anatomical features of halophytes with particular reference to Cholistan Flora. Int J Agric Biol 5:207-212.
Zhang MSH, Chen SH, Philips SM (2006) *Aeluropus* Trin. In Zhengyi W, Raven PH, Deyuan H, Eds., Flora of China, Vol. 22. 458-459. http://www.efloras.org/flora_page.aspx?flora_id=2. (Accessed 22.02.2008).
Zhang Y, Hu X, Liu Y, Liu Q (2014) Caryopsis micromorphological survey of the genus *Themeda* (Poaceae) and allied spathaceous genera in the Andropogoneae. Turk J Bot 38:665-676.

Acta Biologica Szegediensis

Volume 65(1):47-57, 2021
Acta Biologica Szegediensis
http://abs.bibl.u-szeged.hu/index.php/abs
DOI:10.14232/abs.2021.1.47-57

ARTICLE

Action of *Ganoderma lucidum* mycelial growth filtrates on *Erysiphe diffusa* and embryotoxicity assessment in a chicken embryo model

Mycheli P. da Cruz[1#*], Lucas T. Larentis[2#], Edgar de S. Vismara[2], Lilian de S. Vismara[2], Patricia F. de Freitas[2], Sérgio M. Mazaro[2]

[1]Graduate Program in Plant Genetic Resources, Federal University of Santa Catarina, Florianópolis, Brazil.
[2]Biological Control Laboratory, Federal University of Technology – Paraná, Dois Vizinhos, Brazil.

ABSTRACT This work aimed to evaluate the antimicrobial effect of *Ganoderma lucidum* mycelial growth filtrates (MGF) on the phytopathogen *Erysiphe diffusa* and their potential effects on the embryonic development of *Gallus gallus*. The antimicrobial activity was evaluated on *E. diffusa* spores by the microdilution broth method. To evaluate embryotoxic and teratogenic effects, fertile eggs of *G. gallus* received injections of solutions containing the filtrates of *G. lucidum* through the air chamber. After three days of incubation, we opened the eggs and evaluated egg viability, embryo survival, malformation occurrence, embryonic staging and heart rate. Live embryos were prepared using whole mount technique and the morphological analysis was performed. We used the generalized linear model to fit embryotoxicity and teratogenicity data. We verified that *G. lucidum* MGF showed inhibitory activity in vitro against *E. diffusa* and the minimum inhibitory concentrations ranged from 5 to 10 mg/mL. We could also observe that the filtrates did not present embryotoxic or teratogenic effects on the early embryonic development of *G. gallus,* but induced significant differences in the embryonic mean heart rate and on the stage of embryonic development.
Acta Biol Szeged 65(1):47-57 (2021)

KEY WORDS
antimicrobial activity
chicken embryo
medicinal mushroom
mycelial growth filtrate
powdery mildew

ARTICLE INFORMATION
Submitted
19 April 2021.
Accepted
21 July 2021.
***Corresponding author**
E-mail: mychelipreuss@outlook.com

Introduction

Ganoderma lucidum is one of the best-known medicinal mushrooms and has been used by traditional medicine in Asian countries for thousands of years (Lu et al. 2020), mainly because of its therapeutic properties (Ahmad 2020). It has been reported that *G. lucidum* contains over 400 bioactive compounds, produced by spores, mycelia and fruiting bodies (Batra et al. 2013), like triterpenoids, polysaccharides, amino acids, enzymes and dietary fibers (Lakhanpal and Rana 2005; Yang et al. 2019). Although its therapeutic properties are widely studied, there are few works exploring its action over pathogenic species of agricultural interest. However, some studies have shown antimicrobial activity of *G. lucidum* against phytopathogens like *Pseudomonas syringae*, *Erwinia amylovora* and *Mycosphaerella fijiensis* (Ofodile et al. 2005; Perez-Holguin et al. 2017; Arias-Londoño et al. 2019).

Soybean powdery mildew, caused by the parasitic fungus *Erysiphe diffusa*, occurs in countries such as Brazil, United States, Paraguay and Bolivia (Dunn and Gaynor 2020). Initial symptoms are evidenced by the growth of a thin whitish layer on the leaves surface that can reduce productivity and lead to economic losses (Igarashi et al. 2010). Transmission of the disease can occur through the dispersion of spores and by infected seeds and plant remains, for example, which makes it difficult to control (Pérez-Vega et al. 2013). Application of fungicides is the most used control method (Perina et al. 2013); though, it can cause problems, such as the selection of resistant pathogenic strains and environmental contamination (Resende et al. 2009). Hence, the identification of antimicrobial compounds with unique and versatile aspects, such as low toxicity and antimicrobial potency is crucial (Jogaiah et al. 2019).

Despite the benefits of using alternatives to commercial synthetic phytosanitary products, certain substances present in so-called biopesticides, considered natural, can be harmful to non-target organisms, invertebrates or vertebrates (Yim et al. 2014; Machado et al. 2017). Because of that, several regulatory agencies recommend safety tests to assess possible harmful effects of these products on model organisms (Environmental Protection Agency 1996; Ministério da Agricultura, Pecuária e Abastecimento 2012; Organisation for Economic Co-operation and De-

#These authors contributed equally to this work.

velopment 2012). Among the species most used as a model for vertebrates is the domestic chicken (*Gallus gallus*), since its manipulation in laboratory is quite common in tests for assessing the toxicity of biological and alternative pest control agents (Lim et al. 2012; Haas et al. 2017).

G. gallus embryo is considered one of the first model organisms used in the study of vertebrate embryonic development (Rallis 2007). Studies with similar methods to those used in this work have been carried out since the end of the 19th century, and *in ovo* testing of chemicals has expanded since the 1960s (McLaughlin et al. 1963). Many factors contribute to its use in research; among them are the molecular and cellular similarities with human embryos (Vergara and Canto-Soler 2012), its rapid and well-documented development, and low costs of acquisition (Schoenwolf 1999; Smith et al. 2012).

This study aimed to evaluate whether the mycelial growth filtrate of *G. lucidum* has an inhibitory effect *in vitro* on *E. diffusa* and the possible effects on the non-target organism *G. gallus* development.

Materials and Methods

Organisms

Federal University of Technology – Paraná Institutional Animal Care and Use Committee approved all the experimental procedures in this study (protocol n. 2018-10).

Ganoderma lucidum (Curtis) P. Karst., isolate CC339ST, was obtained from Brazilian Agricultural Research Corporation (Embrapa) – Genetic Resources and Biotechnology (Brasília, DF, Brazil). Inoculated Petri dishes with potato-dextrose-agar (PDA; Kasvi, Brazil) were incubated at 28 °C for seven days and stored at 4 °C. Mycelium was activated in PDA for 10 days following the same procedure and then used for inoculation in liquid medium. The isolate of *Erysiphe diffusa* (Cooke & Peck) U. Braun & S.Takam. was maintained in young soybean plants, *Glycine max* (L.) Merr, cultivar NA 5909.

For the embryotoxicity and teratogenicity tests, fertile eggs of layer chickens (*Gallus gallus* subsp. *domesticus* L., 1758), aged from 36 to 40 weeks, were purchased from a commercial hatchery located in Dois Vizinhos, PR, Brazil.

Submerged fermentation of Ganoderma lucidum

This process was performed according to Cruz et al. (2019). To obtain the filtrates, ten mycelial agar discs (5 mm in diameter) were transferred to Erlenmeyer flasks containing 200 mL of potato-dextrose (PD; Kasvi, Brazil) liquid culture medium, pH 5.1. For 15 days, the flasks were shaken on a rotary shaker, at 120 rpm, in the dark, at 28 ± 2 °C. After this period, the elicitors 2 mM salicylic acid (AS) and 5% lignin were dissolved in water, sterilized and subsequently added to the flasks containing *G. lucidum*. Elicitors are biotic or abiotic compounds capable of stimulating an organism's defense and they are used in liquid medium to increase the intensity of cellular responses and subsequent influence on the production of secondary metabolites (Murthy et al. 2014).

We performed three repetitions for each treatment, using nine Erlenmeyer flasks in total. The flasks containing the treatments with the elicitors were kept in an orbital shaker at 120 rpm, in the dark, at 28 ± 2 °C, for 50 days. In order to obtain *G. lucidum* mycelial growth filtrates (MGF), the media then were filtered through Whatman filter paper n. 41, to separate the mycelium. As a result, we obtained MGF of *G. lucidum* (i) without elicitation; (ii) elicited with lignin; and (iii) elicited with AS.

Determination of minimum inhibitory concentration (MIC)

In vitro antimicrobial activity on *E. diffusa* was evaluated using the microdilution broth method, following the M38-A standard, with some modifications, standardized by the Clinical and Laboratory Standards Institute (2002).

Following the Folin-Ciocalteu method described by Singleton and Rossi (1965), we determined the total phenolic content of *G. lucidum* samples. Gallic acid was used to obtain the standard curve (0.0094-0.15 mg/mL), and the results were expressed as mg of gallic acid equivalents (GAE) per mL of filtrate. In 96-well microdilution plates, 100 µL of PD culture medium and 200 µL of *G. lucidum* MGF were added and the initial concentration was based on values of phenolic compounds found in the filtrates, starting with 80 mg of GAE/mL. Each solution was pipetted only in the first well of the column and therefrom a serial dilution was performed, with the final concentrations obtained: 40, 20, 10, 5, 2.5, 1.25, 0.625, and 0.312 mg/mL. Then, 10 µL of a microbial suspension of *E. diffusa* prepared in saline solution with turbidity equivalent to 0.5 on the McFarland scale (1.0×10^6 CFU/mL) was added to each well. Distilled water was used as negative control and a commercial copper oxychloride-based fungicide (50 ppm) as positive control.

The microplates were kept in a growth chamber at 25 °C ± 1 °C, for 24 h. In order to reveal the results, 3 h before the end of the incubation, 10 µL of 0.01% 2,3,5-triphenyltetrazolium chloride (Sigma-Aldrich, USA) was added to each well. In the presence of microorganisms (live cells) a reduction reaction occurs, resulting in the formation of a red, stable and non-diffusible compound, known as triphenylformazan (Summanen et al. 1992). The minimum inhibitory concentration was considered as being the lowest concentration capable of inhibiting the visible growth of the fungus.

Analysis of the effects on the early embryonic development of G. gallus

After a disinfecting process with 70% ethyl alcohol and ultraviolet light (for 15 minutes), fertile eggs were then divided in five experimental groups: CF – non-injected eggs; CV – eggs injected with PD culture medium; F01 – eggs injected with *G. lucidum* MGF without elicitation; F02 – eggs injected with lignin-elicited *G. lucidum* MGF; and F03 – eggs injected with AS-elicited *G. lucidum* MGF. Each group had 40 eggs, totaling 200 incubated eggs. Each egg received 100 μL of the respective solution (at 20%) through the air chamber, using disposable syringes of 1 mL. After the injection, the eggshell orifice was sealed with adhesive tape and the eggs were kept in an incubator for three days, under a controlled temperature of 37.5 °C, relative humidity between 50% and 60% and constant forced ventilation.

After the incubation period, the eggs were opened to check the heart rate (HR), according to Kmecick (2017). Only embryos who presented heartbeats were used in other analyses. Eggs with no evidence of embryonic development were considered inviable and discarded. Taking into account that the chicken embryo's ability to feel pain begins to develop only from the seventh day of incubation (Rosenbruch 1997), there was no anesthetic protocol for euthanasia. Anyway, after the HR check, embryos were kept in a freezer, providing minimal stress to the animals (American Veterinary Medical Association 2020).

After euthanasia, the embryos were prepared using the whole mount technique as described by Ortolani-Machado et al. (2012). The morphological analysis occurred according to the descriptions of the stages of normal embryonic development for the species by Hamburger and Hamilton (1951) using a Stemi 305 stereoscopic microscope (Zeiss, Germany), equipped with an AxioCam ERc5s camera (Zeiss, Germany).

Statistical analysis

Embryotoxicity and teratogenicity test data were analyzed statistically using R, version 4.0.3 (R Core Team 2020) and RStudio, 1.3.1073 (Rstudio Team 2020), with the statistical packages *agricolae*, version 1.3-3 (Mendiburu 2020) and *lmtest*, version 0.9-38 (Zeileis and Hothorn 2002).

We used the generalized linear model, proposed by Nelder and Wedderburn (1972), to analyze data related to viability, survival, malformation occurrence and heart rate. Poisson distribution was applied to heart rate data and we used a logit-link binomial distribution to data concerning viability, survival and malformations rates. As a way to assess the goodness of fit, we used the Hosmer-Lemeshow test (Hosmer and Lemeshow 2000).

To compare the treatments, Wald test (Wald 1943) was performed for nested models and, when the result was significant ($p \leq 0.05$), Tukey's test (Tukey 1949) was applied at 5% of error probability. As so to analyze data referring to the embryonic stages of development, we used Kruskal and Wallis (1952) statistical approach, which is an extension of Wilcoxon-Mann-Whitney test for more than two groups (Neuhäuser 2011).

Results and discussion

Determination of minimum inhibitory concentration (MIC)

G. lucidum filtrates showed direct *in vitro* antimicrobial action on *E. diffusa* spores. Minimum inhibitory concentrations verified were 5 mg/mL for the *G. lucidum* MGF without elicitation and 10 mg/mL for elicited filtrates (Table 1). In contrast to what was expected, the addition of the elicitors in the submerged culture of *G. lucidum* did not result in a greater accumulation of antimicrobial compounds. In a previous study, we observed that *G. lucidum* filtrates could activate soybean defense mechanisms through a process called systemic acquired resistance, helping to control powdery mildew (Cruz et al. 2019).

Nonetheless, these results suggest the *G. lucidum* MGF potential in the control of plant disease, since most of the research related to fungi fruiting bodies and mycelium extracts only report the activity of isolated polysaccharides and manly just their antibacterial potential. Results on mycelial growth filtrates over phytopathogenic fungi are still limited, most of them *in vitro* studies. *G. lucidum* extracts have already shown bactericidal action, principally on *Bacillus cereus*, *Enterobacter aerogenes*, *Staphylococcus aureus*, *Escherichia coli* and *Pseudomonas aeruginosa* and the diverse extraction methods (hexane, dichloromethane, ethyl acetate and methanol) offer different antimicrobial spectra against microorganisms strains (Kamra and Bhatt 2012).

Heleno *et al*. (2013) reported that *G. lucidum* methanolic extract showed greater activity against *S. aureus* and *B. cereus* than antibiotics ampicillin and streptomycin. Minimum inhibitory concentration were in the range

Table 1. *In vitro* minimum inhibitory concentration of *G. lucidum* MGF on *E. diffusa* spores by the microdilution broth method.

Treatments	MIC (mg/mL)
Distilled water	-
AS (2 mM)	-
Lignin (5%)	-
G. lucidum MGF (20%)	5
G. lucidum MGF + lignin (20%)	10
G. lucidum MGF + AS (20%)	10

Table 2. Number of embryos used for each analysis according to the amount of incubated eggs (IE), inviable eggs (IN) and dead embryos (DE) per experimental group.

Experimental group	Parameters analyzed						
	IE	IN	DE	S**	HR	M***	ES
Negative control (CF)	40	0	15	40	25	20	20
PD culture medium (CV)	40	4	8	36	28	23	20****
G. lucidum MGF (F01)	40	10	15	30	15	12	12
Lignin-elicited *G. lucidum* MGF (F02)	40	7	11	32*	21	17	17
AS-elicited *G. lucidum* MGF (F03)	40	8	10	31*	21	16	16

S: survival rate; HR: embryonic mean heart rate; M: morphological analysis; ES: embryonic staging.
* One embryo from each group was not considered for any of the analyses due to a manipulation error and consequent samples loss.
** Inviable eggs were disregarded for survival analysis.
*** Some embryos were not used in this analysis because they were not in good condition; CF, CV and F03 - 5 embryos; F02 - 4 embryos; and F01 - 3 embryos.
**** It was not possible to determine the stage of development of three embryos; two of them with severe malformations.

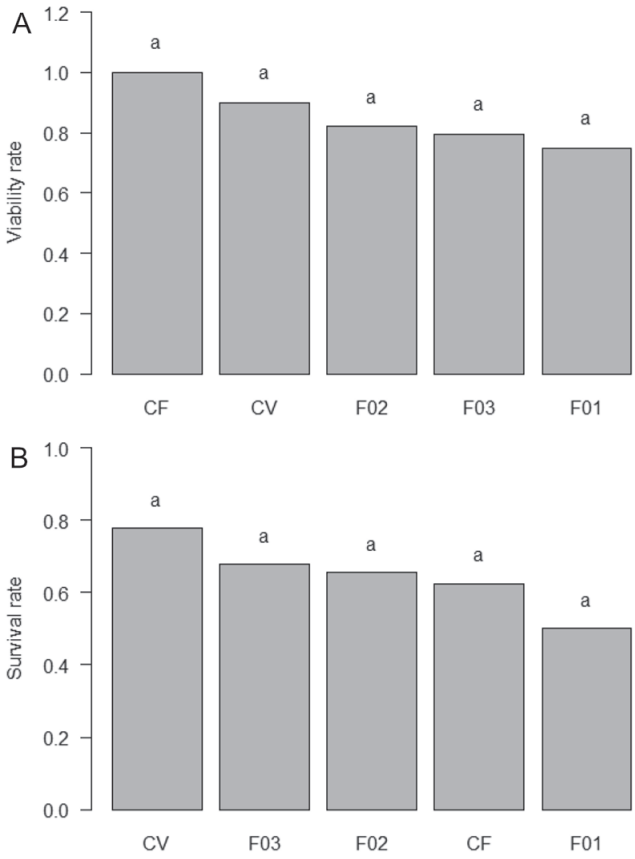

Figure 1. Egg viability (A) and survival rate (B) of *G. gallus* embryos exposed to *G. lucidum* mycelial growth filtrates (MGF) through the air chamber.

CF: negative control; CV: PD culture medium; F01: *G. lucidum* MGF; F02: lignin-elicited *G. lucidum* MGF; F03: AS-elicited *G. lucidum* MGF.
Means followed by the same letter do not differ statistically by Tukey's test, at 5% significance level.

of 0.0125 to 0.75 mg/mL and bactericidal concentrations from 0.035 to 1.5 mg/mL. Keypour et al. (2008) reported that the chloroform extract isolated from *G. lucidum* fruiting body inhibited *S. aureus* (8 mg/mL) and *Bacillus subtillis* (16 mg/mL). The study also found that a variety of lipid derivatives, like sterols and triterpenoid acids, were present in the extract.

Ćilerdžić et al. (2016a) were some of the few researchers who studied the antimicrobial and antioxidant activity of fermentation broth filtrates of *G. lucidum*. These authors report that the filtrates showed great antibacterial potential, inhibiting the growth of *S. aureus* and *E. coli* at concentrations of 6.25% and 12.5%, respectively, and against *Aspergillus niger*, *Penicillium cyclopium* and *P. aeruginosa* only at maximum concentration (100%). In this way, filtrates are potent antimicrobial agents and can be obtained more quickly and cheaply, when compared to *G. lucidum* fruiting bodies extracts (Ćilerdžić et al. 2016b).

Works with the isolation of proteins and polysaccharides have also been mentioned in the literature. An antifungal protein called ganodermin, isolated from *G. lucidum* fruiting body inhibited the growth of *Botrytis cinerea*, *Fusarium oxysporum* and *Physalospora piricola*, with an average inhibitory concentration value of 15.2 mM, 12.4 mM and 18.1 mM, respectively (Wang and Ng 2006). Two hydroquinones, ganomycins A and B, isolated from *Ganoderma pfeifferi* were effective for bacterial inhibition. MIC values of the compounds were 25 μg/mL against *S. aureus* and 2.5 μg/mL against *Micrococcus flavus* (Mothana et al. 2000).

The results of this work demonstrate that the filtrates of *G. lucidum* have the potential to be used as an agent of biological control against plant diseases. It is suggested that future studies focus on *in vivo* tests with plants, against other pathogenic microorganisms, and on the extraction of compounds that present antimicrobial properties. A better understanding of these compounds is crucial to identify

Table 3. Number of embryos considered to be normal (N) and malformed (MF) during the morphological analysis per experimental group.

Experimental group	N	MF
Negative control (CF)	20	-
PD culture medium (CV)	21	2
G. lucidum MGF (F01)	10	2
Lignin-elicited *G. lucidum* MGF (F02)	14	3
AS-elicited *G. lucidum* MGF (F03)	16	-

Malformation occurrence among the groups did not differ statistically by Tukey's test, at 5% significance level.

the potential effects on various diseases in the field.

Analysis of the effects on the early embryonic development of G. gallus

Table 2 shows the number of embryos used in each analysis according to the amount of eggs incubated, inviable eggs and dead embryos per experimental group. Both viability and survival parameters did not show significant differences when comparing data from treatments and control groups. Thus, it can be said that the *G. lucidum* MGF did not significantly affect egg viability and were not toxic to the development of the embryos of *G. gallus* (Fig. 1).

Since eggs did not complete total period of incubation, we are considering the viability parameter as the ratio between the number of eggs with embryos that resumed development out of the total number of incubated fertile eggs. Therefore, when opened, eggs both with alive and dead embryos were considered viable. Fig. 1A shows that *G. lucidum* MGF exposure did not significantly alter this variable. Viability rates among groups ranged from 75% in the F01 group to 100% in the CF group. In embryotoxicity studies, this parameter can indicate whether the tested substance has the potential to interfere with the resumption of normal embryo development, which ceases almost completely after laying, at temperatures below 25 ºC (Bellairs and Osmond 2014). In the event of interference, the treated groups are likely to have very high unviability rates when compared to a control group. This type of analysis is uncommon and often disregarded in embryotoxicity studies, which preferentially report just mortality/survival rates among the groups. In this situation, the discussion is focused just on the number of dead/alive embryos out of the total eggs incubated, disregarding possible effects over development restart.

Fig. 1B shows the survival rate of *G. gallus* embryos exposed to the *G. lucidum* filtrates. Even though there is a numerical difference among the groups, the filtrates cannot be considered toxic or lethal to chicken embryos. Lee et al. (2003), when administering aqueous extract of *G. lucidum* intraperitoneally or orally, observed a significant increase in the survival of mice implanted with different tumors. Çelik and Özparlak (2019) investigated the possible genotoxic effects of the aqueous extract of wild *G. lucidum* using a type of micronucleus test on chicken embryo cells. Their results showed that the extract had no genotoxic action and, in addition, they have observed antigenotoxic properties. Similar works involving *G. lucidum* and avian embryos are scarce. Dulay et al. (2012) carried out perhaps the most significant study analyzing the direct effects of *G. lucidum* extracts on embryos. They observed significantly higher mortality rates, 72 hours after exposure, in groups of *Danio rerio* embryos treated with *G. lucidum* extract at 5%, 10% and 20%, and the lethal effect was dependent on dose and time of exposure.

Some authors report toxicity test results involving *G. lucidum* and other animals, adults in general. Atoji-Henrique (2015), using the same *G. lucidum* strain of our study, demonstrated that the supply of mycelium included in rabbit food did not interfere with the ingestive behavior, nor with the performance and other parameters of animal carcass. In the lowest of the concentrations (0.5%), intestinal segments related to the absorption of nutrients were favored. Nascimento et al. (2015) performed an acute test on Swiss mice and concluded that the administration of *G. lucidum* hydroethanolic extract (1 mL/kg) did not present significant toxicity.

As well as viability and survival rates, malformations occurrence did not vary significantly among groups (Table 3), which means that *G. lucidum* filtrates cannot be considered teratogenic to *G. gallus* embryos. These results are similar to those found by Özparlak et al. (2018), who, when analyzing the effects of wild and cultivated forms of *G. lucidum* on embryos of domestic chicken did not find embryotoxic or teratogenic effects, nor any interference in the bone development of embryos at macroscopic level. In the study by Dulay et al. (2012), performed with *D. rerio* embryos, it was possible to observe caudal malformations and growth retardation. Tail malformations were observed in 55.56% of embryos treated with 1% *G. lucidum* extract and in all embryos treated with the same extract at 5%. In the same way it was possible to verify a delay in the growth of embryos exposed to 5%, 10% and 20% extracts (Dulay et al. 2012).

During the morphological analysis, aspects of encephalic, optical and auditory vesicles, of limbs, neural tube and body curvature of the embryos were observed. The main malformations observed in the embryos, regardless of the experimental group, are shown in Fig. 2. Among the most representative are (i) gastroschisis (Fig. 2B and 2C); (ii) caudal atrophy (Fig. 2D); (iii) failure in telencephalon development (Fig. 2F); (iv) total malformation (Fig. 2E) – Fig. 2A shows a normal embryo. It is noteworthy that

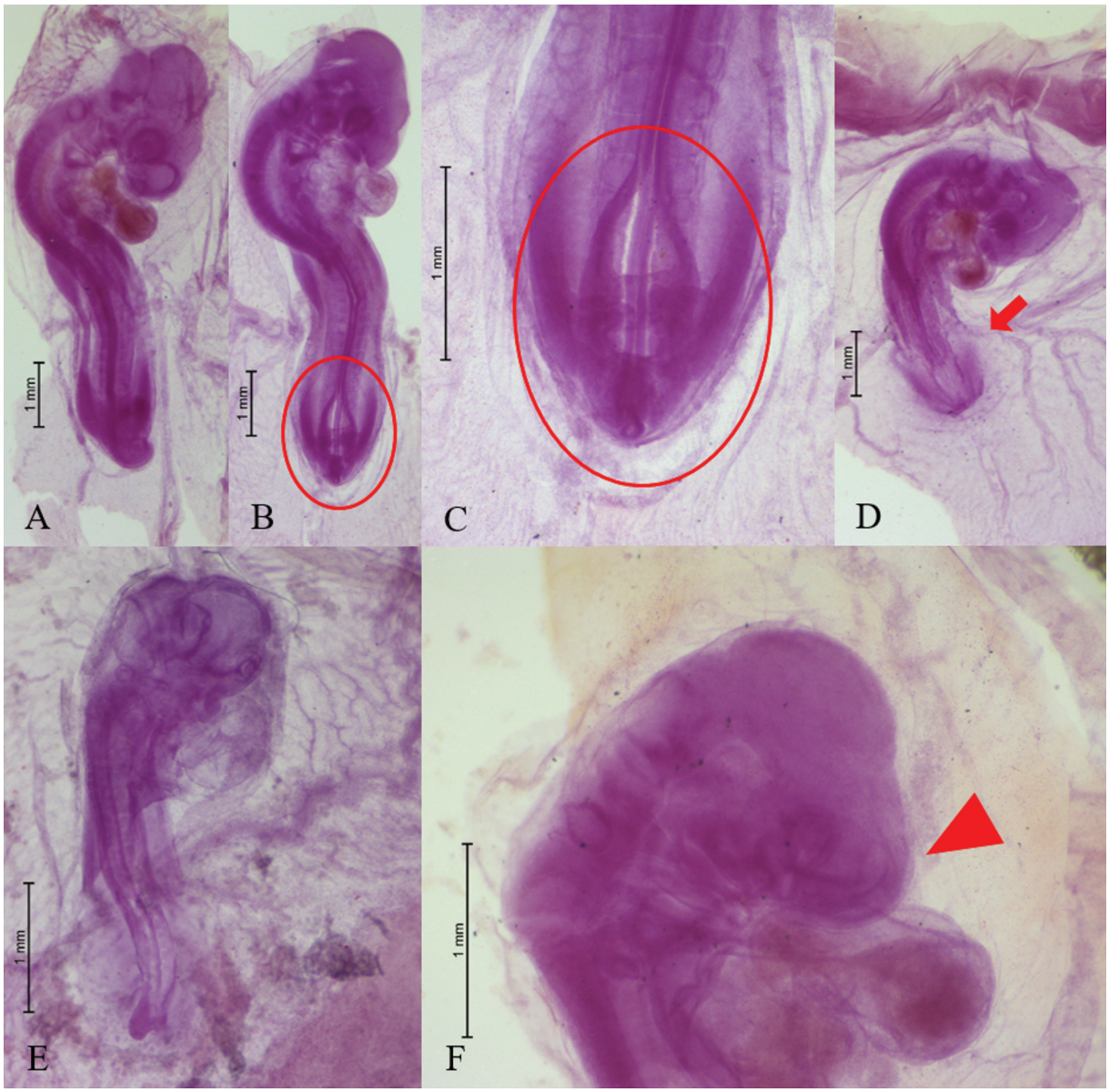

Figure 2. *G. gallus* embryos exposed to *G. lucidum* mycelial growth filtrates (MGF) through the air chamber and incubated for three days.

A: HH18 embryo with normal morphological traits; B: HH17 embryo presenting gastroschisis, shown in detail in C (circle); D: HH18 embryo with caudal atrophy (arrow); E: embryo in an undetermined stage of development, totally malformed; F: HH17 embryo showing failure in the telencephalon development (arrowhead).

congenital abnormalities have intrinsic and extrinsic causes and can even develop in normal environments (Gilbert and Barresi 2016; Carlson 2019). In consequence, errors are considered inherent to embryonic development.

Studies evaluating the toxicity and/or teratogenicity of fungal mycelial growth filtrates are insufficient. However, many studies report the effects of mycotoxins during embryonic development (Elsayed et al. 2019; Huang et al. 2019; Wu et al. 2019). Zahoor-ul-Hassan et al. (2012) concluded that chicks and chicken embryos exposed to ochratoxin A, mycotoxin produced by fungi of the genera *Aspergillus* and *Penicillium*, presented significant anatomorphological alterations, congenital abnormalities and altered biochemical parameters. Saleemi et al. (2015) found similar results in tests with aflatoxigenic fungal isolates, especially aflatoxin B_1, in chicken embryos. Authors observed toxic effects and prominent embryo mortality rates in the groups exposed to the highest concentrations

Table 4. Number of embryos per Hamburger-Hamilton embryonic stage and mean ranks (MR) per experimental group.

Experimental group	13	15	16	17	18	19	20	MR*
Negative control (CF)	-	1	2	2	9	6	-	51,1250
PD culture medium (CV)	-	-	2	9	5	3	1	41,8250
G. lucidum MGF (F01)	-	-	3	7	2	-	-	26,0417
Lignin-elicited *G. lucidum* MGF (F02)	1	-	1	6	5	3	1	44,2941
AS-elicited *G. lucidum* MGF (F03)	-	-	-	7	7	1	1	45,6563

* Mean ranks assigned by the Kruskal-Wallis test.

of aflatoxins (up to 100 ng/egg).

Regarding heart rate, there was a significant decrease when *G. lucidum* MGF (F01) and *G. lucidum* + lignin (F02) were applied. CV and F03 groups also showed a significant difference compared to the CF group, but without differences between themselves (Fig. 3). Average heart rate for the CF group remained at 157.8 bpm. The result is close to the average value of 150 bpm found by Akiyama et al. (1999), despite the difference regarding the methods, and the value of 153 bpm verified in embryos of 72 hours in the control group by Kmecick (2017). Ritchie et al. (2013) state that drugs that can induce periods of bradycardia can be potential teratogens for humans.

Through morphological analysis, it was possible to identify seven different Hamburger-Hamilton (HH) embryonic stages (HH13, HH15–HH20), predominantly stages HH17 and HH18 (Table 4). As the parameter "developmental stage" is a qualitative variable (not numerical), by the analysis using the Kruskal-Wallis test it was possible to verify a significant difference among the stages of development of F01 embryos when compared with embryos of CF, F02 and F03 groups, which did not present statistically significant differences among them. Mean number of ranks for the CV group was statistically equal to that of the other groups (Fig. 4).

This means that embryos exposed to *G. lucidum* MGF without elicitation were, at the time of collection, in younger stages of development than embryos from the other experimental groups. Statistically significant reduction in mean heart rate, observed in the F01 group (Fig. 3), may have limited cardiac output (Branum et al. 2013), which may have resulted in a delay in embryonic development. This factor, however, does not seem to have affected the other groups that also had a lower average heart rate, such as F02 and F03.

Studies involving hypothermia, reduced heart rate and delayed normal embryonic development corroborate this hypothesis. Burggren et al. (2016) consider temperature as a disruptive agent in the normal development process, since low temperatures can delay development (Tazawa

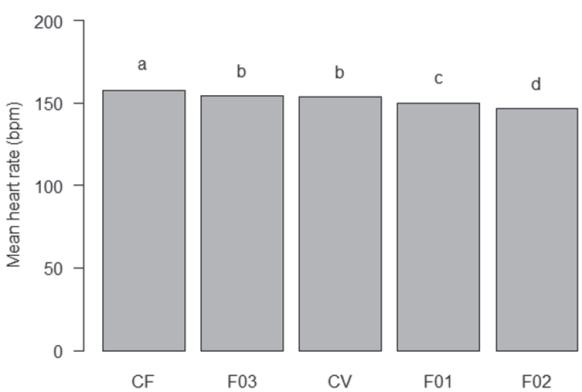

Figure 3. Mean heart rate (HR) of *G. gallus* embryos exposed to *G. lucidum* mycelial growth filtrates (MGF) through the air chamber and incubated for three days.

CF: negative control; CV: PD culture medium; F01: *G. lucidum* MGF; F02: lignin-elicited *G. lucidum* MGF; F03: AS-elicited *G. lucidum* MGF.
Means followed by different letters were considered statistically different from each other by Tukey's test, at 5% significance level.

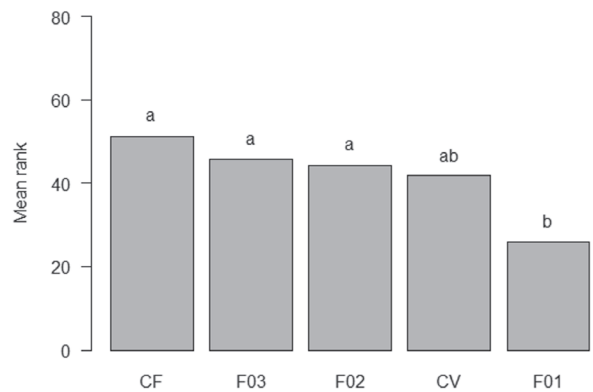

Figure 4. Comparison of the average number of ranks distributed by the Kruskal-Wallis test regarding Hamburger-Hamilton (HH) embryonic stages.

CF: negative control; CV: PD culture medium; F01: *G. lucidum* MGF; F02: lignin-elicited *G. lucidum* MGF; F03: AS-elicited *G. lucidum* MGF.
Means followed by different letters were considered statistically different from each other by the Kruskal-Wallis test, at 5% significance level.

1973) and growth (Peterka et al. 1996). In addition, Lee et al. (2011) observed that environmental hypothermia could reduce the normal heart rate of young chicken embryos (HH17 stage). Kockova et al. (2013) concluded that periods of bradycardia could lead to embryonic death by decreasing cardiac output, since the heart of embryos is still unable to adjust stroke volume according to variations in heart rate. Branum et al. (2013) could not observe a delay in the rate of development when exposing chicken embryos to a bradycardic drug – which decreased cardiac frequency and output. However, these authors were able to notice a 20% reduction in the growth rate, measured by the embryos' body mass.

Studies emphasizing the interference relationships of biocompounds on the stages of embryonic development are scant. Recently, in a test very similar to ours, Vismara (2019) did not observe statistically significant differences regarding the developmental stages of *G. gallus* embryos treated with essential oils of plant species. Arcain (2017) found a similar result, noticing no differences among control and treated groups, regarding stage of development, when exposing *G. gallus* embryos to a commercial synthetic fungicide.

Conclusion

We have concluded that *G. lucidum* filtrates showed fungicidal action on *E. diffusa in vitro* with a minimum inhibitory concentration of 5 mg/mL. Therefore, the MGF of *G. lucidum* shows potential to be used to control powdery mildew in soybean. New studies seeking to verify the *G. lucidum* MGF potential in other pathosystems of agricultural interest should be considered.

It was also possible to conclude that *G. lucidum* filtrates did not affect the embryonic development of *G. gallus*, proving to be non-toxic to this non-target organism. Despite this, significant differences were observed in the mean heart rate and stage of embryonic development, indicating a potential bradycardic effect of *G. lucidum* filtrates without elicitation. Our results corroborate the understanding that this model organism is ideal for embryotoxicity and teratogenicity studies, as pointed out by previous works. New tests are recommended to identify, isolate and characterize molecules present in the filtrates, so that the mechanisms of action on the embryonic development can be better understood.

Acknowledgements

The authors declare that there is no conflict of interest and thank the Federal University of Technology – Paraná, Campus Dois Vizinhos for providing reagents and facilities. This study was supported by Coordenação de Aperfeiçoamento de Pessoal de Nível Superior (Capes).

References

Ahmad MF (2020) *Ganoderma lucidum*: a rational pharmacological approach to surmount cancer. J Ethnopharmacol 260(113047).

Akiyama R, Mitsubayashi H, Tazawa H, Burggren WW (1999) Heart rate responses to altered ambient oxygen in early (days 3-9) chick embryos in the intact egg. J Comp Physiol - B Biochem Syst Environ Physiol 169(2):85-92.

American Veterinary Medical Association (2020) AVMA Guidelines for the Euthanasia of Animals: 2020 Edition. AVMA, Schaumburg.

Arcain BMS (2017) Efeito do Iprodiona (Rovral®) em *Gallus gallus*. Bachelor's Final Thesis. Universidade Federal da Integração Latino-Americana, Foz do Iguaçu, Brazil.

Arias-Londoño M, Zapata-Ocampo P, Mosquera-Arevalo Á, Sanchez-Torres J, Atehortua-Garcés L (2019) Antifungal protein determination for submerged cultures of the medicinal mushroom *Ganoderma lucidum* (Ganodermataceae) with activity over the phytopathogen fungus *Mycosphaerella fijiensis* (Mycosphaerellaceae). Actual Biológicas 41(111):53-64.

Atoji-Henrique K (2015) Crescimento micelial de *Ganoderma lucidum* em diferentes substratos e relação com concentração de β-glucanas, atividade antioxidante e efeitos sobre o desempenho de coelhos. PhD Thesis. Universidade Tecnológica Federal do Paraná, Pato Branco, Brazil.

Batra P, Sharma AK, Khajuria R (2013) Probing Lingzhi or Reishi medicinal mushroom *Ganoderma lucidum* (Higher Basidiomycetes): a bitter mushroom with amazing health benefits. Int J Med Mushrooms 15(2):127-143.

Bellairs R, Osmond M (2014) Atlas of chick development. 3rd ed. Academic Press, Oxford.

Branum SR, Yamada-Fisher M, Burggren W (2013) Reduced heart rate and cardiac output differentially affect angiogenesis, growth, and development in early chicken embryos (*Gallus domesticus*). Physiol Biochem Zool 86(3):370-382.

Burggren WW, Santin JF, Antich MR (2016) Cardio-respiratory development in bird embryos: new insights from a venerable animal model. Rev Bras Zootec 45(11):709-728.

Carlson BM (2019) Human Embryology and Developmental Biology. 6th Ed. Elsevier, St. Louis.

Çelik B, Özparlak H (2019) Determination of genotoxic and antigenotoxic effects of wild-grown Reishi mushroom (*Ganoderma lucidum*) using the hen's egg test for analysis of micronucleus induction. Biotech Histochem 94(8):628-636.

Ćilerdžić J, Stajić M, Vukojević J (2016a) Potential of submergedly cultivated mycelia of *Ganoderma* spp. as antioxidant and antimicrobial agents. Curr Pharm Biotechnol 17(3):275-282.

Ćilerdžić J, Kosanić M, Stajić M, Vukojević J, Ranković B (2016b) Species of genus *Ganoderma* (Agaricomycetes) fermentation broth: a novel antioxidant and antimicrobial agent. Int J Med Mushrooms 18(5):397-404.

Clinical and Laboratory Standards Institute (2002) Método de referência para testes de diluição em caldo para determinação da sensibilidade a terapia antifúngica de fungos filamentosos; norma aprovada. NCCLS, Wayne. (NCCLS granted translation permission to Agência Nacional de Vigilância Sanitária, Brazil).

Cruz MP da, Mazaro SM, Bruzamarello J, Vismara E de S, Ghedin ÁL, Possenti JC, Vítola FMD (2019) Bioactive compounds of *Ganoderma lucidum* activate the defense mechanisms of soybean plants and reduce the severity of powdery mildew. J Agric Sci 11(13):99-114.

Dulay RMR, Kalaw SP, Reyes RG, Alfonso NF, Eguchi F (2012) Teratogenic and toxic effects of Lingzhi or Reishi medicinal mushroom, *Ganoderma lucidum* (W.Curt.:Fr.) P. Karst. (Higher basidiomycetes), on zebrafish embryo as model. Int J Med Mushrooms 14(5):507-512.

Dunn M, Gaynor L (2020) Impact and control of powdery mildew on irrigated soybean varieties grown in Southeast Australia. Agronomy 10(4):514.

Elsayed MAE, Mohamed NE, Hatab MH, Elaroussi MA (2019) Oxidative stress of in-ovo ochratoxin a administered during chick embryonic development. Brazilian J Poult Sci 21(1):eRBCA-2019-0637.

Environmental Protection Agency (1996) Microbial Pesticide Test Guidelines: OPPTS 885.4000 Background for Nontarget Organism Testing of Microbial Pest Control Agents. EPA, Washington.

Gilbert SF, Barresi MJF (2016) Developmental Biology. 11th ed. Sinauer Associates, Sunderland.

Haas J, Baungratz A, Takahashi SE, Potrich M, Lozano ER, Mazaro SMM (2017) Toxicity assessment of insecticidal plants to chicken. Rev Bras Plantas Med 19(2):190-196.

Hamburger V, Hamilton HL (1951) A series of normal stages in the development of the chick embryo. J Morphol 88(1):49-92.

Heleno SA, Ferreira ICFR, Esteves AP, Ćirić A, Glamočlija J, Martins A, Soković M, Queiroz MJRP (2013) Antimicrobial and demelanizing activity of *Ganoderma lucidum* extract, p-hydroxybenzoic and cinnamic acids and their synthetic acetylated glucuronide methyl esters. Food Chem Toxicol 58:95-100.

Hosmer DW, Lemeshow S (2000) Applied Logistic Regression. 2nd ed. John Wiley & Sons, London.

Huang C, Wang F, Chan W (2019) Enniatin B1 exerts embryotoxic effects on mouse blastocysts and induces oxidative stress and immunotoxicity during embryo development. Environ Toxicol 34(1):48-59.

Jogaiah S, Kurjogi M, Abdelrahman M, Hanumanthappa N, Tran L-SP (2019) *Ganoderma applanatum*-mediated green synthesis of silver nanoparticles: structural characterization, and *in vitro* and *in vivo* biomedical and agrochemical properties. Arab J Chem 12(7):1108-1120.

Kamra A, Bhatt AB (2012) Evaluation of antimicrobial and antioxidant activity of *Ganoderma lucidum* extracts against human pathogenic bacteria. Int J Pharm Pharm Sci 4(2):359-362.

Keypour S, Riahi H, Moradali MF, Rafati H (2008) Investigation of the antibacterial activity of a chloroform extract of Ling Zhi or Reishi medicinal mushroom, *Ganoderma lucidum* (W. Curt.: Fr.) P. Karst. (Aphyllophoromycetideae), from Iran. Int J Med Mushrooms 10(4):345-349.

Kmecick M (2017) Avaliação dos efeitos do cádmio e ácido perfluorooctanóico nos estágios iniciais de desenvolvimento de embriões de ave (*Gallus gallus*). Master Thesis. Universidade Federal do Paraná, Curitiba, Brazil.

Kockova R, Svatunkova J, Novotny J, Hejnova L, Ostadal B, Sedmera D (2013) Heart rate changes mediate the embryotoxic effect of antiarrhythmic drugs in the chick embryo. Am J Physiol - Hear Circ Physiol 304(6):895-902.

Kruskal WH, Wallis WA (1952) Use of ranks in one-criterion variance analysis. J Am Stat Assoc 47(260):583-621.

Lakhanpal TN, Rana M (2005) Medicinal and nutraceutical genetic resources of mushrooms. Plant Genet Resour 3(2):288-303.

Lee S-S, Lee P-L, Chen C-F, Wang S-Y, Chen K-Y (2003) Antitumor Effects of polysaccharides of *Ganoderma lucidum* (Curt.:Fr.) P. Karst. (Ling Zhi, Reishi mushroom) (Aphyllophoromycetideae). Int J Med Mushrooms 5(1):1-16.

Lee SJ, Yeom E, Ha H, Nam KH (2011) Cardiac outflow and wall motion in hypothermic chick embryos. Microvasc Res 82(3):296-303.

Lim T-H, Kim M-S, Lee D-H, Lee Y-N, Park J-K, Youn H-N, Lee H-J, Yang S-Y, Cho Y-W, Lee J-B, Park S-Y, Choi I-S, Song C-S (2012) Use of bacteriophage for biological control of *Salmonella* Enteritidis infection in chicken. Res Vet Sci 93(3):1173-1178.

Lu J, He R, Sun P, Zhang F, Linhardt RJ, Zhang A (2020) Molecular mechanisms of bioactive polysaccharides from *Ganoderma lucidum* (Lingzhi), a review. Int J Biol Macromol 150:765-774.

Machado AA de S, Zarfl C, Rehse S, Kloas W (2017) Low-dose effects: nonmonotonic responses for the toxicity of a *Bacillus thuringiensis* biocide to *Daphnia magna*. Environ Sci Technol 51(3):1679-1686.

McLaughlin J, Marliac J-P, Verrette MJ, Mutchler MK, Fitzhugh OG (1963) The injection of chemicals into the yolk sac of fertile eggs prior to incubation as a toxicity test. Toxicol Appl Pharmacol 5(6):760-771.

Mendiburu F (2020) agricolae: Statistical Procedures for Agricultural Research. R package, version 1.3-3.
Ministério da Agricultura, Pecuária e Abastecimento (2012). Manual de Procedimentos para Registro de Agrotóxicos. MAPA, Brasília.
Mothana RAA, Jansen R, Jülich WD, Lindequist U (2000) Ganomycins A and B, new antimicrobial farnesyl hydroquinones from the basidiomycete *Ganoderma pfeifferi*. J Nat Prod 63(3):416-418.
Murthy HN, Lee E-J, Paek K-Y (2014) Production of secondary metabolites from cell and organ cultures: strategies and approaches for biomass improvement and metabolite accumulation. Plant Cell Tiss Organ Cult 118(1):1-16.
Nascimento PAM, Okamoto MKH, Bach EE, Wadt NSY (2015) Avaliação da toxicidade do extrato hidroetanólico do fungo *Ganoderma lucidum*. Rev Ciênc Farm Básica Apl 36(2, supl. 1):1.
Nelder JA, Wedderburn RWM (1972) Generalized linear models. J R Stat Soc Ser A 135(3):370-384.
Neuhäuser M (2011) Wilcoxon-Mann-Whitney test. In Lovric M, ed., International Encyclopedia of Statistical Science. Springer, Berlin, 1656-1658.
Ofodile LN, Uma NU, Kokubun T, Grayer RJ, Ogundipe OT, Simmonds MSJ (2005) Antimicrobial activity of some *Ganoderma* species from Nigeria. Phyther Res 19(4):310-313.
Organisation for Economic Co-operation and Development (2012) OECD Guidance to the Environmental Safety Evaluation of Microbial Biocontrol Agents. OECD, Paris.
Ortolani-Machado CF, Rios FS, Freitas PF, Okada MA, Rodrigues-Galdino AM, Maiolino CV, Tamada MH (2012) Métodos para a manipulação e o preparo de embriões e larvas. In Ribeiro CAO, Reis-Filho HS, Grötzner SR, org., Técnicas e métodos para utilização prática em microscopia. Santos, São Paulo, 237-294.
Özparlak H, ÇelİK B, Balta D (2018) *Ganoderma lucidum'un* Türkiye'deki yabani ve kültür formlarının tavuk embriyoları üzerindeki bazı etkilerinin karşılaştırılması. Mantar Derg 9(2):188-195.
Perez-Holguin G, Robles-Hernández L, González-Franco AC, Hernández-Huerta J (2017) Control *in vitro* de *Erwinia amylovora*, con extractos bioactivos de *Ganoderma lucidum*. Rev Mex Fitosanidad 1(1):1-7.
Pérez-Vega E, Trabanco N, Campa A, Ferreira JJ (2013) Genetic mapping of two genes conferring resistance to powdery mildew in common bean (*Phaseolus vulgaris* L.). Theor Appl Genet 126(6):1503-1512.
Perina FJ, Alves E, Pereira RB, Lucas GC, Labory CRG, Castro HA de (2013) Essential oils and whole milk in the control of soybean powdery mildew. Ciência Rural 43(11):1938-1944.
Peterka M, Peterková R, Likovský Z (1996) Teratogenic and lethal effects of long-term hyperthermia and hypothermia in the chick embryo. Reprod Toxicol 10(4):327-332.
R Core Team (2020) R: A language and environment for statistical computing. R Foundation for Statistical Computing, Vienna.
Rallis C (2007) Chickens get their place in the sun. Genome Biol 8(5):306.
Resende A, Souza PIDM DE, Souza JR DE, Blum LEB (2009) Ação do hipoclorito de sódio no controle do *Erysiphe diffusa* na soja. Rev Caatinga 22(4):53-59.
Ritchie HE, Ababneh DH, Oakes DJ, Power CA, Webster WS (2013) The teratogenic effect of dofetilide during rat limb development and association with drug-induced bradycardia and hypoxia in the embryo. Birth Defects Res Part B - Dev Reprod Toxicol 98(2):144-153.
Rosenbruch M. 1997. Zur Sensitivität des Embryos im bebrüteten Hühnerei. ALTEX 14(3):111-113.
RStudio Team (2020) RStudio: integrated development for R. RStudio, Boston.
Saleemi MK, Khan MZ, Khan A, Hassan ZU, Khan WA, Rafique S, Fatima Z, Sultan A (2015) Embryotoxic and histopathological investigations of in-ovo inoculation of aflatoxigenic fungal extracts in chicken embryos. Pak Vet J 35(4):403-408.
Schoenwolf GC (1999) The avian embryo: a model for descriptive and experimental embryology. In Moody SA, ed., Cell lineage and fate determination. Academic Press, San Diego, 429-436.
Singleton VL, Rossi JA (1965) Colorimetry of total phenolics with phosphomolybdic-phosphotungstic acid reagents. Am J Enol Vitic 16(3):144-158.
Smith SM, Flentke GR, Garic A (2012) Avian models in teratology and developmental toxicology. In Harris C, Hansen JM, ed., Developmental Toxicology: methods and protocols. Humana Press, Totowa, 85-103.
Summanen P, Wexler HM, Finegold SM (1992) Antimicrobial susceptibility testing of *Bilophila wadsworthia* by using triphenyltetrazolium chloride to facilitate endpoint determination. Antimicrob Agents Chemother 36(8):1658-1664.
Tazawa H (1973) Hypothermal effect on the gas exchange in chicken embryo. Respir Physiol 17(1):21-31.
Tukey JW (1949) Comparing individual means in the analysis of variance. Biometrics 5(2):99-114.
Vergara MN, Canto-Soler MV (2012) Rediscovering the chick embryo as a model to study retinal development. Neural Dev 7(1):1-19.
Vismara LS (2019) Essential oils to induce resistance in strawberries to gray mold, *Botrytis cinerea in vitro* and toxicological action. PhD Thesis. Universidade Tecnológica Federal do Paraná, Pato Branco, Brazil.
Wald A (1943) Tests of statistical hypotheses concerning several parameters when the number of observations is large. Trans Am Math Soc 54(3):426-482.

Wang H, Ng TB (2006) Ganodermin, an antifungal protein from fruiting bodies of the medicinal mushroom *Ganoderma lucidum*. Peptides 27(1):27-30.

Wu TS, Cheng YC, Chen PJ, Huang YT, Yu FY, Liu BH (2019) Exposure to aflatoxin B_1 interferes with locomotion and neural development in zebrafish embryos and larvae. Chemosphere 217:905-913.

Yang Y, Zhang H, Zuo J, Gong X, Yi F, Zhu W, Li L (2019) Advances in research on the active constituents and physiological effects of *Ganoderma lucidum*. Biomed Dermatology 3(6):1-17.

Yim E-C, Kim H-J, Kim S-J (2014) Acute toxicity assessment of camphor in biopesticides by using *Daphnia magna* and *Danio rerio*. Environ Health Toxicol 29:e2014008.

Zahoor-ul-Hassan, Khan MZ, Saleemi MK, Khan A, Javed I, Bhatti SA (2012) Toxico-pathological effects of *in ovo* inoculation of ochratoxin A (OTA) in chick embryos and subsequently in hatched chicks. Toxicol Pathol 40(1):33-39.

Zeileis A, Hothorn T (2002) Diagnostic checking in regression relationships. R News 2(3):7-10.

Acta Biologica Szegediensis

Volume 65(1):59-64, 2021
Acta Biologica Szegediensis
http://abs.bibl.u-szeged.hu/index.php/abs
DOI:10.14232/abs.2021.1.59-64

ARTICLE

Acaricidal activity of nishinda (*Vitex negundo*) leaf and garlic (*Allium sativum*) bulb extract against red spider mite, *Oligonychus coffeae* (Acari: Tetranychidae) in tea plantations of Darjeeling hill, West Bengal, India

Piu Banerjee[1], Arghya Laha[1], Indrani Samaddar[1], Himani Biswas[2], Debjani Sarkar[3], Sovan Roy[4], Goutam K. Saha[5], Sanjoy Podder[1]*

[1]Allergology and Applied Entomology Research Laboratory, Department of Zoology, University of Burdwan, Bardhaman-713104, West Bengal, India
[2]Department of Zoology, Krishnagar Government College, Krishnagar-741101, West Bengal, India
[3]Department of Zoology, APC Roy Government College, Siliguri-734010, West Bengal, India
[4]Department of Science and Technology and Biotechnology, Vigyan Chetana Bhavan, Kolkata-700064, West Bengal, India
[5]Department of Zoology, University of Calcutta, Kolkata-700019, West Bengal, India

ABSTRACT The red spider mite, *Oligonychus coffeae* (Nietner) serves as a serious threat to the Darjeeling tea plantations affecting the quality of the leaves. Various plant extracts are currently being researched as an alternative to the chemical pesticides to control the red spider mites. In the present study, the leaves of *Vitex negundo* L. and the bulb of *Allium sativum* L. were analyzed for their acaricidal activity on the larval, nymphal and adult stages of the mite. Both the extracts were found to have potent activity against red spider mites and may prove to be potential acaricides in future.
Acta Biol Szeged 65(1):59-64 (2021)

KEY WORDS
Darjeeling
garlic bulb extract
Nishinda
Oligonychus coffeae
tea

ARTICLE INFORMATION
Submitted
11 February 2021.
Accepted
24 July 2021.
***Corresponding author**
E-mail: skpzoo2@rediffmail.com

Introduction

Growing food and beverage crops in a sustainable way to obtain optimal yield and nutrition with sensible use of renewable resources while maintaining the biodiversity and soil fertility with least ecological disruption is a challenge for the farmers and associated stakeholders in the present decade. In this endeavor, cultivation of tea is no exception. In India, tea is grown in about 42.2-million-hectare land. Owing to the flavor and the quality, the tea originating from Darjeeling hills is highly preferred both in India and overseas.

More than one thousand arthropods have been recorded to feed on different parts of the tea plants (Chen and Chen 1989) all over the world. Among them, *Oligonychus coffeae* Nietner, the tea red spider mite, a major arthropod pest that attacks most cultivars in tea plantations of Darjeeling, India (Das 1965; Banerjee et al. 2020) played a significant role for causing damage to tea. The red spider mite increased within a short period of time in the tea plantations due to its high reproductive capacity (Das 1959a,1959b, 1960). Despite adopting several management strategies in the tea gardens of the Darjeeling hills, West Bengal, India, pest infestations are quite prevalent. Many of the tea gardens of Darjeeling hills have been using organic farming methods, with least use of the chemicals for regulation of the pests. Therefore, pest infestations increased leading to a decrease in the quality of tea produced (Bhujel 2016). This in turn leads to a decrease in export with a loss of millions of rupees in terms of revenue. Therefore, an enhanced management regime is required to combat the pest and pest related effects on the tealeaves.

Natural products from plants are an excellent source of pesticidal compounds, especially insecticides, as many plant species have evolved chemical protection from insects. Several classes of insecticides (e.g., the pyrethroids) are based on compounds from plants. During the last few years, during an increasingly intensive search by

many research groups all over the world, the plant family Lamiaceae and Amaryllidaceae were identified as two of the most promising sources with insect-control properties (Ho et al. 1996; Uritu et al. 2018). In particular, some members of the genera *Vitex* and *Allium* were found to be highly effective against insects and mites (Yathiraj and Jagadish 1999; Attia et al. 2012). Unfortunately, information regarding efficacy of these two plant extracts to control mites is very scarce from India. Therefore, the present work is designed to evaluate the efficacy of these two plant extracts to control tea red spider mite (*O. coffeae*).

Materials and methods

Rearing of red spider mite (O. coffeae)

Mites were collected from different tea fields of Darjeeling and a continuous stock culture of *O. coffeae* has been maintained in rearing tray throughout the period of experiment in an incubator at 25 ± 2 °C and 70-75% relative humidity (RH).

Preparation of plant extracts

Two types of plant materials have been used for extract preparation: 1) leaves of nishinda (*Vitex negundo* L); 2) bulb of garlic (*Allium sativum* L). The different concentrations ranging from 0.5 to 6.5 mg/ml (0.5, 1, 1.5, 2, 2.5, 3, 3.5, 4, 4.5, 5, 5.5, 6, and 6.5 mg/ml) was obtained by diluting stock in 20 ml distilled water. The procedures of extract preparation are as follows:

Nishinda leaf extract (NLE)

Healthy leaves were collected in zipper bags. These leaves were then washed with running water, dried for 5-6 days under shade and coarsely grounded. The powder derived from this process was subjected to extraction. 10 g of that powder were taken in a conical flask (250 mL), dipped in 100 ml methanol, and allowed to stand overnight for extraction. The material was then filtered through Whatman no.1 filter paper and kept in an open Petri dish for complete evaporation. The extraction procedure was repeated for three times with the residues remaining in the filter paper. After completion of the evaporation, the sticky greenish residue found on Petri dish was scrapped out using a scalpel and treated as stock material for preparation of different concentrations.

Garlic bulb extract (GBE)

For preparation of GBE, the protective layer of garlic cloves was peeled out and 10 g of garlic was weighed, rinsed and crushed in a mixer grinder. The homogenized garlic was then taken in a conical flask (250 ml), dipped in 100 ml methanol and allowed to stand overnight for extraction. The material was then filtered through Whatman no.1 filter paper in a beaker (250 ml) and kept in an open Petri dish for complete evaporation. The extraction procedure was repeated thrice with the residues remaining in the filter paper. After completion of the evaporation, a sticky white-yellowish residue was found on Petri dish and was scrapped out using scalpel. This was treated as stock material for preparation of different concentrations.

Laboratory bioassay for acaricidal activity test on larvae, nymphs and adults

In-vitro assay for control of mites were performed with different concentrations of plant extracts. All the assays were done in an incubator at 25 ± 2 °C and 70-75% RH. Tealeaf discs of 8 cm diameter were dipped into different concentrations of both NLE and GBE for five minutes and then kept under a ceiling fan for drying. These leaf discs were placed with its dorsal surface up over the wet cotton taken in a Petri dish. Fifty healthy mites were then released on each treated leaf disc. The assay was replicated ten times for each concentration. Water treated leaves were taken as control. The leaves were observed under stereo-binocular microscope at every 24 h and the number of mites that survived was counted, for seven days consecutively.

Table 1. Larvicidal effects of the nishinda (*V. negundo*) leaf extracts and garlic (*A. sativum*) bulb extract on the larva of *O. coffeae*, at the median lethal concentrations (mg/mL). * = P value significant.

	Nishinda (*V. negundo*) Median ± SD							Garlic (*A. sativum*) Median ± SD						
Hours	24	48	72	96	120	144	168	24	48	72	96	120	144	168
LC50-value	3.04±0.10	2.63±0.07	2.09±0.12	1.89±0.11	1.72±0.11	1.69±0.11	1.56±0.34	3.60±0.14	3.19±0.13	2.72±0.18	2.29±0.19	2.11±0.10	1.93±0.14	1.81±0.19
Slope	6.52±0.40	4.57±0.53	3.25±0.24	3.01±0.34	2.94±0.29	2.84 ±0.55	2.20±0.35	6.18±0.58	4.65±0.34	3.06±0.30	2.76±0.51	2.74±0.49	2.55±0.50	2.62±0.32
Intercept	-3.12±1.89	-1.95±0.22	-1.04±0.13	-0.82±0.11	-0.73±0.11	-0.49±0.32	-0.53±0.18	-3.57±0.32	-2.34±0.15	-1.29±0.14	-0.96±0.13	-0.80±0.58	-0.74±0.19	-0.70±0.19
R-value	0.99	0.99	0.91	0.88	0.78	0.87	0.83	0.97	0.98	0.95	0.91	0.89	0.88	0.91
P-value	<0.0001*	<0.0001*	0.0016*	0.008*	0.0446*	0.0482*	0.0481*	<0.0001*	<0.0001*	<0.0001*	0.0013*	0.0062*	0.0168*	0.026*
t-test	t=14.80, df=69, p<0.001*													

Table 2. Nymphicidal effects of the nishinda (*V. negundo*) leaf extracts and garlic (*A. sativum*) bulb extract on the larva of *O. coffeae*, at the median lethal concentrations (mg/mL). * = P value significant.

	Nishinda (*V. negundo*) Median ± SD							Garlic (*A. sativum*) Median ± SD						
Hours	24	48	72	96	120	144	168	24	48	72	96	120	144	168
LC50-value	3.73 ±0.40	3.29 ±0.06	2.86±0.09	2.56±0.16	2.10±0.22	2.23±0.47	1.60±0.23	4.14±0.09	3.69±0.10	2.92±0.11	2.37±0.20	2.05±0.12	1.81±0.14	1.33±0.12
Slope	8.28 ±0.55	6.47 ±0.64	4.47 ±0.79	2.83 ±0.28	2.55 ±0.18	1.77 ±0.46	1.79 ±0.34	8.82±0.74	6.06±0.60	4.50±0.46	3.11±0.27	2.60±0.21	2.23±0.26	2.00±0.20
Intercept	-4.71±0.65	-3.35±0.34	-2.03±0.36	-1.14 ±0.13	-0.81 ±0.11	-0.60 ±0.11	-0.35±0.10	-5.49±0.52	-3.43±0.33	-2.09±1.36	-1.15±0.12	-0.83±0.09	-0.51±0.10	-0.28±0.08
R-value	0.97	0.98	0.97	0.92	0.9	0.94	0.94	0.96	0.98	0.92	0.87	0.86	0.88	0.81
P-value	0.0005*	<0.0001*	0.0001*	0.0022*	0.0118*	0.0123*	0.0126*	0.0011*	<0.0001*	0.0004*	0.0019*	0.006*	0.007*	0.026*
t-test	t=0.71, df=69, p=0.48													

Statistical analysis

In the present study, the efficiency of NLE and GBE has been evaluated at different concentrations (0.5-6.5 mg/ml) for seven days at 24 h interval against larval, nymphal and adult red spider mite and the data obtained from experiments were subjected to probit analysis (Finney 1971) to estimate LC_{50} value. The correlation between concentration of pesticides and probit value was estimated by linear regression. Unpaired t-test has been done to compare the toxicity level between different pesticides used. P<0.05 was considered as significant. All the analysis was done using Prism Ver. 7 (Graph Pad Prism, San Diego, CA).

Results

LC_{50} of NLE and GBE for mite larva

Table 1. shows the LC_{50} values for the NLE and GBE on larva stage of mite for 24, 48, 72, 96, 120, 144 and 168 h of experiment. Results according to probit analysis reveals that the lethal concentration (LC_{50}) of NLE to mite larva for 24, 48, 72, 96, 120, 144 and 168 h of exposure are 3.04, 2.63, 2.09, 1.89, 1.72, 1.69 and 1.56 mg/mL and that for GBE are 3.60, 3.19, 2.72, 2.29, 2.11, 1.93 and 1.81 mg/ml, respectively. A gradual reduction in slope function corresponding to an increase in the exposure time from 24 to 168 h has been observed. Observations on the upper and lower confidence limits show a decreasing trend from 24 to 168 h. As NLE shows LC_{50} values which are significantly lower than GBE (t = 14.80, df = 69, p<0.001), this revealed that NLE is a more potent larvicide than GBE. Values of correlation coefficient (R) for each time interval demonstrate (Table 1) that there is a positive correlation between concentration of pesticides and mortality of larvae, which is statistically significant.

LC_{50} of NLE and GBE for mite nymph

The LC_{50} value for NLE and GBE on nymph stage of mite for 24, 48, 72, 96, 120, 144 and 168 h of experiment has been depicted in Table 2. Probit analysis explore that the LC_{50} values for NLE to *O. coffeae* (nymphs) were found to be 3.73, 3.29, 2.86, 2.56, 2.10, 2.23 and 1.60 mg/ml and for GBE the LC_{50} values are 4.14, 3.69, 2.92, 2.37, 2.05, 1.81 and 1.33 mg/ml for 24, 48, 72, 96, 120, 144 and 168 h, respectively. Initially, NLE seemed to be more potent but with increasing exposure, GBE had lower LC_{50} values. A progressive decline in slope function corresponding to an increment in the exposure time from 24 to 168 h has been found. As the exposure time is raised, the contact acaricidal activity increased. The upper and lower confidence limits revealed a diminishing trend from 24 to 168 h. Control with water shows no mortality of nymph. Correlation coefficient (R) value against each hour indicates (Table 2) that there is a significant positive correlation between

Table 3. Adulticidal effects of the nishinda (*V. negundo*) leaf extracts and garlic (*A. sativum*) bulb extract on the larva of *O. coffeae*, at the median lethal concentrations (mg/mL). * = P value significant.

	Nishinda (*V. negundo*) Median ± SD							Garlic (*A. sativum*) Median ± SD						
Hours	24	48	72	96	120	144	168	24	48	72	96	120	144	168
LC50-value	4.89±0.06	4.48±0.09	4.08±0.10	3.73±0.10	3.34±0.14	2.46 ±0.28	2.03±0.17	5.33±0.07	4.78±0.05	4.32±0.07	3.55±0.07	3.22±0.09	2.86±0.07	2.20±0.18
Slope	9.98 ±0.91	8.08 ±1.32	5.31 ±1.34	3.90 ±0.68	3.08±0.57	2.74±0.30	2.23±0.32	8.69±0.63	7.06±0.54	5.16±0.13	3.91±0.18	2.69±0.13	2.30±0.20	2.32±0.25
Intercept	-6.90±0.60	-5.23±0.87	-3.23±0.82	-2.26±0.35	-1.63±0.25	-1.03±0.05	-0.67±0.05	-6.26±0.42	-4.79±0.35	-3.28±0.07	-2.15±0.10	-1.36±0.06	-1.03±0.06	-0.77±0.06
R-value	0.99	0.97	0.94	0.96	0.96	0.86	0.85	0.99	0.98	0.96	0.9	0.9	0.89	0.8
P-value	<0.0001*	<0.0001*	<0.0001*	<0.0001*	<0.0001*	0.0022*	0.0069*	<0.0001*	<0.0001*	<0.0001*	0.0001*	0.0001*	0.0004*	0.0054*
t-test	t=4.76, df=69, p<0.001*													

concentration of pesticides and mortality of nymph.

LC_{50} of NLE and GBE for mite adult

Result according to probit analysis in Table 3 showed that mortality of *O. coffeae* adult was directly proportional to the time elapsed after treatment according to each enhancing concentration (mg/ml). LC_{50} values for NLE on adults are 4.89, 4.48, 4.08, 3.73, 3.34, 2.46 and 2.03 mg/ml and for GBE the LC_{50} values are 5.33, 4.78, 4.32, 3.55, 3.22, 2.86 and 2.20 mg/ml for 24, 48, 72, 96, 120, 144 and 168 h, respectively. Inclination value and upper-lower confidence limits also decreased continuously with increasing time. In case of control, mortality was absent with respect to NLE and GBE. LC_{50} values for NLE on adult is significantly lower than GBE ($t = 4.76$, $df = 69$, $p<0.001$), implying that NLE is more toxic to adult stage of mite than GBE. Correlation coefficient (R) value for both green pesticides (NLE and GBE) indicate that there exists a positive correlation between pesticides concentrations and mite mortality which is statistically significant and this is also evident that increase in exposure time period to pesticides concentrations influences on mortality of mite.

Discussion

Application of chemical pesticides for controlling mites in tealeaves has been greatly diminished with the increase in global awareness (Roy et al. 2008). Out of 2400 plant species having the potential to subdue harmful creatures, about 100 species are utilized for controlling mites (Yang et al. 2007). Different researchers extensively studied the acaricidal effects of the extracts of these plants. The currently reliable and reproducible leaf disc bioassay derived by imitating the unique feeding habits of mites was established after many trials and errors (Mitra et al. 2015). The present bioassay was done by using tea leaf pieces dipped in different concentrations of nishinda leaf extract (NLE) and garlic bulb extract (GBE) on *O. coffeae*.

Garlic, a vegetable bulb, (*A. sativum* L.) belonging to family Amaryllidaceae, is well known for its acaricidal features (Attia et al. 2012). It is now termed as pesticide with minimum risk, which may provide a safe and feasible alternative to synthetic pesticides. It is easily available and cost effective to farmers (Su and Mulla 1998; Panella et al. 2005; Isman et al. 2008; Akyazi et al. 2018). It is well known that acaricidal effects of plant extracts are interconnected with their chemical compositions (Isman et al. 2001; Singh et al. 2001). *A. sativum* contains approximately 33 sulfur compounds (alliin, allicin, ajoene, allylpropyl disulfide, diallyl trisulfide, S-allylcysteine, vinyldithiines, S-allylmercaptocystein, and others); minimum four times more sulphur than any other high-sulphur vegetables, inclusive of onions, broccoli, and cauliflower (Attia et al. 2012). It also consists of 17 amino acids (arginine and others), several enzymes (e.g., allinase, peroxidases, and myrosinase), and minerals (selenium, germanium, tellurium, and other trace minerals) (Newall et al. 1996; Omar and Wabel 2010). A large amount of organosulfur substances is responsible for toxic effects of *A. sativum* (Attia et al. 2011; Singh et al. 2001; Virtanen 1965; Roy et al. 2006; Mohammed 2013; Habashy et al. 2016; Wang et al. 2016). Binding of the garlic lectin to the glycosylated epithelial membrane of the insect gut is the predetermining factor for insecticidal activity, which has been revealed by the earlier reports (Bandyopadhyay et al. 2001). The present study showed that LC_{50} value was 5.33 mg/ml after 24 h of experiment against *O. coffeae* adult. LC_{50} values of GBE for nymphs and larva of red spider mite were observed to be 4.14 mg/ml and 3.60 mg/ml, respectively, after 24 h of treatment reveals that nymphicidal and larvicidal activity were more effective than adulticidal (5.33 mg/ml). The toxic effect of GBE was concentration and time dependent.

Five-leaved chaste tree nishinda (*V. negundo*) is a large aromatic shrubby plant belonging to family Lamiaceae, a willowy plant with a lofty grow in rainfed areas of West Bengal. *V. negundo* contains alkaloids, saponin and flavonoids revealed by TLC analysis (Khan et al. 2012). Better efficacy of *V. negundo* leaf extract on *T. urticae* has been reported by Yathiraj and Jagadish (1999). Aqueous leaf extracts (6%) of *V. negundo* showed 76% adult mortality of red spider mites, reported by Sugeetha and Srinivasa (1999), which strongly supports our present findings. We found that, the LC_{50} value of NLE for adult, nymph and larva stage of *O. coffeae* was 4.89, 3.73 and 3.04 mg/ml, respectively, at 24 h of experiment, which indicate NLE is more potent than GBE. The difference in the application methods may cause differences between efficiency of extracts. Higher activity of methanol leaf extracts from *V. negundo* at 1-6% concentration on III instar larvae of *Spodoptera litura* was recorded by Deepthy et al. (2010) which strongly corroborate our present findings.

Conclusion

Both NLE and GBE were found to possess significant acaricidal properties. Both the extracts were effective on the larva, nymph and adult stages of the red spider mite and when compared, NLE proved better among the two. NLE significantly had lower LC_{50} values than GBE on all the stages of mites with increasing time except the nymphal stage where, LC_{50} of both extracts were nearly equal. The study successfully underlines the acaricidal properties of both plants, but the experiments were done

in-vitro condition. To establish both compounds as potent acaricides in future, the study needs to be extended to the tea plantations in Darjeeling.

Acknowledgements

We are thankful to the Principal, Barasat Govt. College, Kolkata for providing institutional research infrastructure. Financial support for this work was provided by grants from Department of Science & Technology, Govt. of West Bengal [Sanction No.:1170(Sanc.)/ST/P/S&T/1G-4/2016, dated- 02.03.16] to Dr. Sanjoy Podder.

References

Akyazi R, Soysal M, Altunç EY, Lisle A, Hassan E, Akyol D (2018) Acaricidal and sublethal effects of tobacco leaf and garlic bulb extract and soft soap on *Tetranychus urticae* Koch (Acari: Trombidiformes: Tetranychidae). Syst Appl Acarol 23(10):2054-2069.

Attia S, Grissa KL, Mailleux AC, Lognay G, Euskin S, Mayoufi S, Hance T (2012) Effective concentrations of garlic distillate (*Allium sativum*) for the control of *Tetranychus urticae* (Tetranychidae). J Appl Entomol 136:302-312.

Bandyopadhyay S, Roy A, Das S (2001) Binding of garlic (*Allium sativum*) leaf lectin to the gut receptors of homopteran pests is correlated to its insecticidal activity. Plant Sci 161(5):1025-1033.

Banerjee P, Islam MM, Laha A, Biswas H, Saha, NC, Saha GK, Sarkar D, Bhattacharya S, Podder S (2020) Phytochemical analysis of mite-infested tea leaves of Darjeeling Hills, India. Phytochem Anal 31(3):277-286.

Bhujel A, Singh M, Choubey M, Singh M (2016) Pest and diseases management in Darjeeling tea. Int J Agric Sci Res 6(3):469-472.

Chen Z, Chen X (1989) An analysis of the world tea pest fauna. J Tea Sci 9(1):13-22.

Das GM (1959a) Bionomics of the tea red spider, *Oligonychus coffeae* (Nietner). Bull Entomol Res 50:265-274.

Das GM (1959b) Occurrence of red spider mite in relation to cultural practices in North- East India. Two and a Bud. 6(4):3-10.

Das GM (1960) Occurrence of red spider mite *Oligonychus coffeae*, (Nietner) on tea in North- East India in relation to pruning and defoliation. Bull Entomol Res 51:415-426.

Das GM (1965) Pest of Tea in North-East India and their Control. Tea Research Association, Tocklai, Assam, India.

Deepthy KB, Sheela MK, Jacob SS, Estelitta TJ (2010) Insecticidal and growth inhibitory action of *Vitex negundo* L. against Asian army worm, *Spodoptera litura* Fab. J Biopest 3(1):289-295.

Finney DJ (1971) Probit Analysis, 3rd ed. Cambridge University Press, Cambridge, UK.

Habashy MG, Al-Akhdar HH, Boraie DM, Ghareeb ZE (2016) Laboratory and semi-field evaluation of garlic aqueous extract as acaricide against two Tetranychid mites (Acari: Tetranychidae). J Plant Prot Path Mansoura Univ 7(10):623-628.

Ho SH, Koh L, Ma Y, Huang Y, Sim KY (1996) The oil of garlic, *Allium sativum* L. (Amaryllidaceae), as a potential grain protectant against *Tribolium castaneum* (Herbst) and *Sitophilus zeamais* Motsch. Postharvest Biol Technol 9:41-48.

Isman MB (2008) Botanical insecticides: for richer or poorer. Pest Manag Sci 64:8-11.

Isman MB, Wan AJ, Passreiter CM (2001) Insecticidal activity of essential oils to the tobacco cutworm *Spodoptera litura*. Fitoterapia 72:65-68.

Khan MA, Shah AH, Maqbol A, Khan N, Rahman ZU (2012) Miticidal activity of methanolic extract of *Vitex negundo-lam* against *Sarcoptes scabiei* in animals and man. J Anim Plant Sci 22(2 Suppl):102-107.

Mitra S, Gupta SK, Ghosh S (2015) Bio-efficacy of some green pesticides towards mortality and repellency against *Petrobia harti* Ewing (Acari: Tetranychidae) infesting medicinal weed, *Oxalis corniculata* L. (Oxalidaceae). Int J Appl Res 1(11):739-742.

Mohammed KS (2013) Antibacterial activity of *Allium Sativum* (Garlic) and identification of active compound by GC-MS analysis. Int J Pharm Bio Sci 4(4):1071-1076.

Newall CA, Anderson LA, Phillipson JD (1996) Herbal Medicines: A guide for health-care professionals. Vol IX. Pharmaceutical Press, London, UK.

Omar SH, Al-Wabel NA (2010) Organosulfur compounds and possible mechanism of garlic in cancer. Saudi Pharm J 18(1):51-58.

Panella NA, Dolan MC, Karcchesy JJ, Xiong Y, Peralta-Cruz J, Khasawneh MJ, Montenieri A, Maupin GO (2005) Use of novel compounds for pest control: insecticidal and acaricidal activity of essential oil components from heartwood of Alaska yellow cedar. J Med Entomol 42:352-358.

Roy A, Chakraborti D, Das S (2008) Effectiveness of garlic lectin on red spider mite of tea. J Plant Interact 3(3):157-162.

Roy J, Shakleya DM, Callery PS, Thomas JG (2006) Chemical constituents and antimicrobial activity of a traditional herbal medicine containing garlic and black cumin. Afr J Trad CAM 3(2):1-7.

Singh UP, Prithiviraj B, Sharma BK, Singh M, Ray AB (2001) Role of garlic (*Allium sativum* L.) in human and plant diseases. Indian J Exp Biol 39:310-322.

Su T, Mulla MS (1998) Ovicidal activity of neem products (azadirachtin) against *Culex tarsalis* and *Culex quinque-*

fasciatus (Diptera: Culcidae). J Am Mosq Control Assoc 14:204-209.

Sugeetha S, Srinivasa N (1999) Seasonal abundance of red spider mite, *Tetranychus macfarlanei* on okra varieties in Bangalore. J Acarol 15(1,2):10-14.

Uritu CM, Mihai CT, Stanciu GD, Dodi G, Alexa-Stratulat T, Luca A, Leon-Constantin MM, Stefanescu R, Bild V, Melnic S, Tamba BI (2018) Medicinal Plants of the Family Lamiaceae in Pain Therapy: A Review. Pain Res Manag 7801543.

Virtanen AI (1965) Studies on organic sulphur compounds and other labile substances in plants. Phytochemistry 4:207-228.

Wang X, Yang Y, Liu R, Zhou Z, Zhang M (2016) Identification of antioxidants in aged garlic extract by Gas Chromatography-Mass Spectrometry and Liquid Chromatography-Mass Spectrometry. Int J Food Prop 19:474-483.

Yang HZ, Li Q, Lei HD (2007) Research and application of botanical acaricides. Pesticide 46:81-85.

Yathiraj BR, Jagadish PS (1999) Plant extracts – future promising tools in the integrated management of spider mites, *Tetranychus urticae* (Acari: Tetranychidae). J Acarol 15(1-2):40-43.

Acta Biologica Szegediensis

Volume 65(1):65-73, 2021
Acta Biologica Szegediensis
http://abs.bibl.u-szeged.hu/index.php/abs
DOI:10.14232/abs.2021.1.65-73

ARTICLE

A purified lectin with larvicidal activity from a woodland mushroom, *Agaricus semotus* Fr.

Isaiah O. Adedoyin[1], Taiwo S. Adewole[2], Titilayo O. Agunbiade[3], Francis B. Adewoyin[4], Adenike Kuku[1],*

[1]Department of Biochemistry and Molecular Biology, Obafemi Awolowo University, Ile-Ife, Osun State, Nigeria.
[2]Department of Chemical Sciences, Kings University, Ode-Omu, Osun State, Nigeria.
[3]Department of Chemical Sciences, Oduduwa University, Ipetumodu, Osun State, Nigeria.
[4]Drug Research and Production Unit, Faculty of Pharmacy, Obafemi Awolowo University, Ile-Ife, Osun State, Nigeria.

ABSTRACT This study investigated the larvicidal activity on *Culex quinquefasciatus* of lectin purified from fresh fruiting bodies of woodland mushroom, *Agaricus semotus*. *A. semotus* lectin (ASL) was purified via ion-exchange chromatography on DEAE-cellulose A-25 and size exclusion chromatography on Sephadex G-100 matrix. Molecular weight (16.6 kDa) was estimated by sodium dodecyl sulfate polyacrylamide gel electrophoresis (SDS-PAGE). The effects of temperature, pH, metal chelation- and larvicidal activity of ASL were also investigated. The ASL indifferently agglutinated the erythrocytes of the human ABO blood system and was stable at acidic pH and below 50 °C whereas 66% of its activity was lost at 60 °C with complete inactivation at 70 °C. ASL is a metalloprotein requiring barium ion as chelation of metals by 50 mM EDTA rendered the lectin inactive, while the addition of $BaCl_2$, among other metal salts, restored the activity. ASL showed larvicidal activity against *C. quinquefasciatus* larvae after 24 h with a mortality of 5 and 95% at 5 and 25 mg/mL respectively, and LC_{50} of 13.80 mg/mL. This study concluded that purified *A. semotus* lectin showed impressive larvicidal activity, which could be exploited in its development as an insecticidal agent. **Acta Biol Szeged 65(1):65-73 (2021)**

KEY WORDS
Agaricus semotus
Culex quinquefasciatus
larvicidal activity
lectin

ARTICLE INFORMATION
Submitted
21 December 2020.
Accepted
17 February 2021.
***Corresponding author**
E-mail: adenikekuku@yahoo.com;
akuku@oauife.edu.ng

Introduction

Diseases transmitted by mosquitoes are one of the endemic health-related environmental menaces on the rise worldwide, which contribute to a high loss of life, especially in tropical countries with low income (Wilke et al. 2017; Fonseca et al. 2019). *Culex quinquefasciatus* Say, 1823 (*Culicidae*, southern house mosquito) is vastly distributed in subtropical regions of the world (Lopes et al. 2019). It is incursive, and belongs to the *Culex pipiens* species complex, which feed on mammalian and avian blood, *C. quinquefasciatus* is considered a medically significant species, because of their implicated roles in the transmission of zoonotic diseases including those caused by *Wuchereria bancrofti,* West Nile virus, and arbovirus (Fonseca et al. 2004; Lima-Camara et al. 2016).

Although majorly found in Africa, *C. quinquefasciatus* usually spread beyond their domiciled environment, posing a severe risk to public health (Farnesi et al. 2015; Cuthbert et al. 2020). As part of control measures to curb mosquito establishment and proliferation, the World Health Organization (WHO) introduced a manual on the management of these quintessential vectors (Takken and van den Berg 2019). Due to the advent of mosquito strains resistant to synthetic insecticides, together with potential environmental and health threats associated with these chemicals, alternative bio-control agents are being sought (Bellinato et al. 2016; Camaroti et al. 2017; Santos 2020).

The non-enzymatic lectins with unique sugar-binding characteristics are ubiquitous proteins capable of reversible discrete interaction with cell surface carbohydrate associated structures and involved in diverse biological and pathological functions (He et al. 2015; Muszyńska et al. 2018; Nascimento et al. 2020; Perduca et al. 2020). Aside from being a remarkable tool in blood group determination, lectins also perform defense-related functions (Silva et al. 2020). Although originally identified in plants and animals, exploration of fungal lectins is becoming popular because of their peculiar carbohydrate specificity coupled with potential application in biotechnology and biomedicine (Singh et al. 2010; Varrot et al. 2013; Hassan et al. 2015; Singh et al. 2015). Mushrooms have attracted numerous research activities due their diverse inherent bioactive constituents including lectins (Singh et al. 2010;

Largeteau et al. 2011).

Worldwide, *Agaricus* genus has over 300 members, which are distinguished by their unique spore coloration, among other structural features (Zhang et al. 2019). In this study a lectin was purified from the fresh fruiting bodies of woodland mushroom and its larvicidal activity was investigated towards *C. quinquefasciatus* to explore its potential in insect control.

Materials and Methods

Materials and chemicals

Glutaraldehyde, Folin reagent, ethylenediaminetetraacetic acid (EDTA), acrylamide, bovine serum albumin, sodium dodecyl sulfate (SDS), sugars, Coomassie Brilliant Blue R 250 and molecular weight protein markers (10-170 kDa) were purchased from Sigma-Aldrich (St Louis, Missouri, USA). Purchase of Sephadex G-100 and DEAE cellulose A-25 was from Pharmacia Fine Chemicals (Uppsala, Sweden). The quality of all reagents was research-quality.

A, B, O human blood groups were collected with informed consent from healthy subjects.

Collection of mushroom

Woodland mushroom (*A. semotus* Fries) was collected on farmland near the Department of Electrical and Electronics Engineering, Obafemi Awolowo University, Ile-Ife (South-West Nigeria). Identification was done at the Department of Microbiology (Mycology Laboratory), Obafemi Awolowo University, Ile-Ife, Nigeria.

A. semotus crude extract preparation

Approximately 16 g mushroom sample was homogenized and extracted using 0.025 M Phosphate Buffered Saline, pH 7.2 (1:5 w/v) and was stirred at 4 °C overnight. Resulting mixture was centrifuged at 4000 rpm for 15 min and filtered through cheesecloth to get the crude extract, which was stored at -20 °C until use.

Protein concentration assay

Assay method of Lowry et al. (1951) was employed in estimating protein concentration. Standard protein used was bovine serum albumin (1 mg/mL).

Hemagglutination and sugar specificity assays

Human A, B, and O blood groups were collected into lithium-heparin bottles. Erythrocytes were recovered from the centrifuged blood samples and fixed using glutaraldehyde (Bing et al. 1967). Hemagglutination assay and sugar specificity test was performed as described by Kuku and Eretan (2004) in a U-shaped 96-well microtiter plate. Tested sugars were D-mannitol, fructose, L-sorbose, galactose, D-mannose, D-glucosamine hydrochloride, N-acetyl-D-glucosamine, inulin, maltose, glycogen, D-lactose monohydrate, D-glucose monohydrate, and starch.

Purification of A. semotus lectin (ASL)

Ion exchange chromatography on DEAE cellulose A-25

Chromatography column (1.5 x 20 cm, Bio-Rad) packed with DEAE- cellulose A-25 matrix, and equilibrated with 10 mM Tris-HCl buffer, pH 7.3, was used to purify the crude protein extract (3 mL, ≈33 mg protein). Fractions (2 mL) were collected at 24 mL/h flow rate. Unadsorbed fractions were eluted with the equilibration buffer (10 mM Tris-HCl buffer, pH 7.3), while adsorbed fractions eluted with the same buffer containing 0.2 M NaCl. Fractions were monitored at 280 nm, and hemagglutinating activities were assayed. Active peak fractions (unadsorbed peak) were pooled, dialyzed (against 10 mM Tris-HCl buffer, pH 7.3, and distilled water) for 48 h, freeze-dried, and kept at -20 °C.

Size exclusion chromatography on Sephadex G-100

Five milliliters (≈ 30 mg protein) of the pooled DEAE active fractions (unadsorbed peak) was loaded on Sephadex G-100 column (2.5 x 20 cm, Bio-Rad) equilibrated with phosphate-buffered saline (0.02 M, pH 7.2), and fractions (4 mL) collected at 30 mL/h flow rate. Fractions were monitored at 280 nm, and hemagglutinating activity assayed. Active peak fractions were collected, dialyzed, freeze-dried, and kept frozen at -20 °C.

Physicochemical characterization of ASL

Denaturing gel electrophoresis (12.5% acrylamide gel, Tris-HCl system) was employed in the determination of ASL subunit molecular weight using standard marker proteins of 10-170 kDa range, as described by Laemmli

Table 1. Purification summary.

Fractions	Total protein (mg)	Total activity (HU)	Specific activity (HU/mg)	Yield (%)	Purification fold
Crude extract	5550	1024	0.184	100.0	1.00
Ion exchange chromatography (IEC-1)	585.90	512	0.873	50.0	4.74
Size exclusion chromatography (SEC-2)	101.8	128	1.257	12.5	6.83

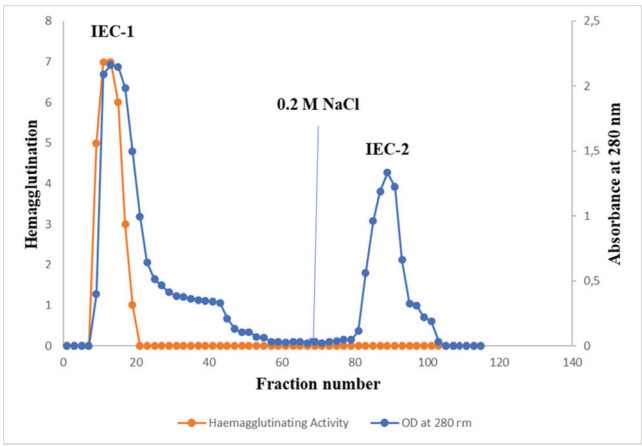

Figure 1. Ion exchange chromatography of *A. semotus* crude extract.

and Favre (1970).

Assay method of Sampaio et al. (1998) was employed in investigating temperature effect on ASL hemagglutinating activity. Aliquot of ASL (500 µL) was subjected to temperature variation (30-90 °C) for 60 min using a water bath (Model DK-420, Movel Scientific Instruments, Zhejiang, China). Incubated ASL was swiftly iced-cooled and activity was assayed. Activity of ASL was served as control at 25 °C.

The pH effect on ASL hemagglutinating activity was investigated by incubating lectin aliquots (500 µL) at 25 °C for 60 min with buffer solutions of pH 2-11 range (0.2 M citrate, pH 2-6; 0.2 M Tris-HCl, pH 7-8, and 0.2 M glycine-NaOH, pH 9-11). Control was ASL incubated in PBS, pH 7.2 and results presented as described by Nakagawa et al. (1996).

To investigate the divalent cation requirement of ASL, assay experiment of Wang et al. (1996) was employed. Aliquot of ASL was dialyzed for 24 h against 50 mM EDTA and hemagglutinating activity assayed. Thereafter, the demetallized lectin aliquots were incubated differently with $BaCl_2$, $HgCl_2$, $MgCl_2$, $SnCl_2$, and $CaCl_2$ (10 mM, 50 µL) for 2 h, and each time, assayed for hemagglutinating activity.

Larvicidal assay

C. quinquefasciatus larvae were cultured in an insectarium under regulated conditions of relative humidity 70 ± 10% and at 27 ± 2 °C with a 12-12 light-dark regime at the Drug Research and Production Unit (DRPU), Faculty of Pharmacy, Obafemi Awolowo University, Ile-Ife. Free adult mosquitoes were allowed to lay eggs in the habitats provided for them in the laboratory and egg rafts collected for hatching in glass and plastic bowls. To promote larva development and female fecundity, hatched mosquito larvae were fed daily with fish food *ad libitum*.

Larvicidal activity of ASL was investigated as described in our previous study (Johnny et al. 2016). Laboratory–reared fourth instar larvae of *C. quinquefasciatus* were exposed to varying concentrations (5-25 mg/mL) of ASL according to standard procedure (WHO 1981). Comprehensively, 20 larvae were introduced into plastic beakers (50 mL) for each concentration of ASL. Experimentations were done in triplicates at 27 ± 2 °C, with one control (distilled H_2O) set for each. Motionless larvae or those which settled at the bottom of test beakers with no sensitivity to involuntary stimulus or light, or after mild probing failed to move were considered dead. Percentage mortalities were recorded for each concentration after 24 h of the exposure period and obtained data statistically analyzed.

Statistical analysis

Experimental data were analyzed using StatPlus® 2006 (AnalystSoft, Canada) to find the lethal concentrations (LC_{50}) of larvae in 24 h by probit analysis with a reliability interval of 95% (Finney 1971; Islam et al. 2013).

Results

Purification, hemagglutinating activity, and sugar specificity of Agaricus semotus lectin (ASL)

Ion exchange and size exclusion chromatography purified ASL from *A. semotus* to homogeneity with yield and purification fold of 12.5% and 6.83, respectively (Table 1).

Two distinct peaks were obtained from the elution profile of *A. semotus* crude extract on DEAE cellulose A-25 column (Fig. 1), of which only the unadsorbed peak (IEC-1) exhibited hemagglutinating activity. Size exclusion chromatography of the DEAE-active peak (IEC-1) on Sephadex G-100 matrix also resulted in two protein peaks (Fig. 2), but only second peak (SEC-2) showed hemagglutinating activity, which constituted the homogeneous ASL used for further studies.

Hemagglutination assay showed that ASL indifferently agglutinated the erythrocytes of the human ABO blood group, and this activity was strongly inhibited by inulin among tested sugars (Table 2).

Physicochemical characterization of ASL

SDS-PAGE analysis of ASL revealed a distinct band with a relative molecular weight of 16.6 kDa (Fig. 3). ASL lost its activity at 70 °C (Fig. 4) and stable at acidic pH (Fig. 5).

Larvicidal study

The ASL treatment resulted the concentration-dependent mortality of *C. quinquefasciatus* larvae with the lowest mortality of 5% at 5 mg/mL and the highest mortality of

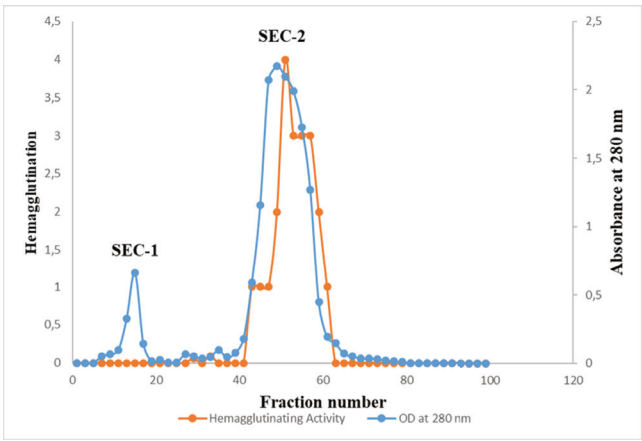

Figure 2. Size exclusion chromatography of the DEAE-Unadsorbed peak (IEC-1).

95% at 25 mg/mL concentration after 24 h (Table 3) with LC_{50} of 13.767 mg/mL (Fig. 6).

Table 2. Hapten inhibition test of ASL purified from *A. semotus.*

Sugar	Hemagglutination titre
Control	2^9
Fructose	2^7
L-Sorbose	2^7
Galactose	2^7
D- Mannose	2^7
D- Mannitol	2^9
D- Glucosamine-hydrochloride	2^9
D- Glucose monohydrate	2^8
N-acetyl-D-glucosamine	2^8
Inulin	2^2
Maltose	2^8
Glycogen	2^8
D-Lactose monohydrate	2^9
Starch	2^{12}

Experiments comprised ASL (100 µL) diluted serially in a 96-well microtitre plate. Equal volumes (50 µL) of respective sugar solutions (0.2 M) and 2% human blood group A erythrocytes suspension were introduced to the wells. Positive control contained no sugars, and negative control contained neither ASL nor sugars. Experiments were done in triplicates.

Discussion

Purification, hemagglutinating activity and sugar specificity of Agaricus semotus lectin (ASL)

Diverse chromatographic techniques are being used in the purification of mushroom lectins, however, recent studies have reported the effectiveness of ion-exchange and size exclusion chromatographic techniques as an alternative to highly preferred single-step affinity chromatography, which exploits sugar specificity of the lectin (Chandrasekaran et al. 2016; Wang et al. 2018; Panchak 2019). Elution profile of ASL on DEAE cellulose A-25 matrix reported in this study was similar to the chromatographic behavior of *A. arvensis* lectin (AAL) (Zhao et al. 2011).

A. semotus lectin (ASL) exhibited a non-specific agglutination towards the human ABO erythrocytes, characteristics mainly associated with an unique group of promiscuous lectins (panalectins), which have been identified mainly in plants, but rarely in mushrooms (Kuku et al. 2000; Akinyoola et al. 2016; Oladokun et al. 2019). However, lectins have been already identified and isolated within the genus *Agaricus*, there is not any previous report on the lectins of *A. semotus* (Kawagishi et al. 1988; Mikiashvili et al. 2006; Nakamura-Tsuruta et al. 2006; Zhang et al. 2019).

The hapten inhibition test to determine the sugar specificity of ASL showed that D-mannose, L-sorbose, galactose, and fructose slightly decreased the hemagglutinating activity, while inulin (a fructan) strongly inhibited the activity, although starch enhanced activity among the sugars tested (Table 2). Inhibition of the hemagglutinating activity of ASL by more than one simple and/or complex sugar reported in this study is not uncommon among mushroom lectins, especially within the genus *Agaricus*, as similar characteristics have been reported for lec-

Table 3. Larvicidal activity of ASL on *C. quinquefasciatus*.

S/N	Concentration (mg/mL)	Number of larvae	Recorded death	Mortality %
1	Control (distilled water)	20.00	0.00 ± 0.00	0.00 ± 0.00
2	5.00	20.00	1.00 ± 0.05	5.00 ± 0.12
3	10.00	20.00	5.00 ± 0.25	25.00 ± 0.31
4	15.00	20.00	8.00 ± 0.40	40.00 ± 0.11
5	20.00	20.00	15.00 ± 0.75	75.00 ± 0.25
6	25.00	20.00	19.00 ± 0.95	95.00 ± 0.11

Experiments were done in triplicates. Data were presented as mean ± SEM (standard error of mean).

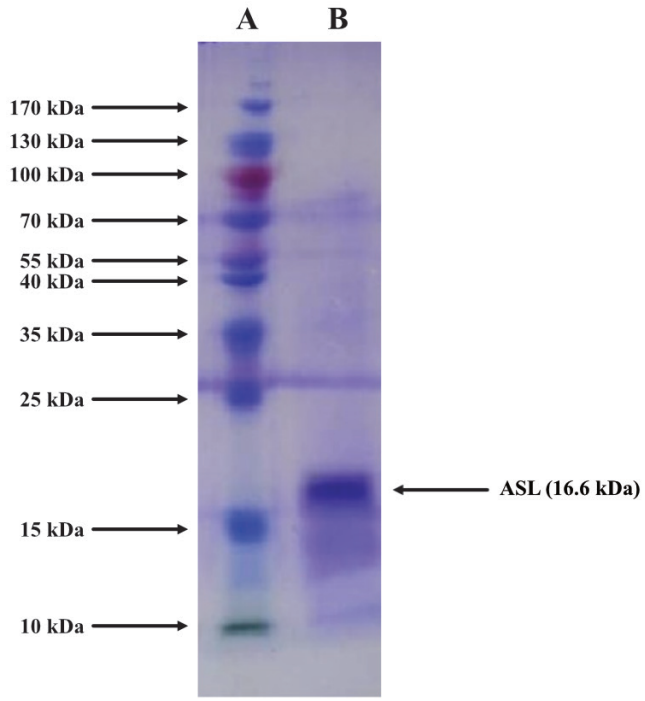

Figure 3. Electrophoretogram of SDS-PAGE of *A. semotus* lectin (ASL) and molecular weight markers (10-170 kDa). Lane A (Standard marker proteins), lane B (purified ASL).

tins isolated from *A. blazei*, *A. bisporus,* and *A. pilatianus* (Kawagishi et al. 1988; Nakamura-Tsuruta et al. 2006; Mikiashvili et al. 2006).

Inulin specificity obtained for ASL is similar to that of *A. arvensis* lectin (Zhao et al. 2011). Zhang et al. (2019) also reported inulin inhibition of *A. bitorquis* lectin suggesting a conserved inulin-binding specificity regarding isolated lectins from the genus *Agaricus*, which might be exploited in a structure-function relationship for practicable biotechnological application, especially through molecular docking. Other mushroom lectins reportedly inhibited by inulin include *Armillaria luteo-virens* lectin, *Pholiota adipose* lectin, and *Hericium erinaceum* lectin (Feng et al. 2006; Zhang et al. 2009; Li et al. 2010).

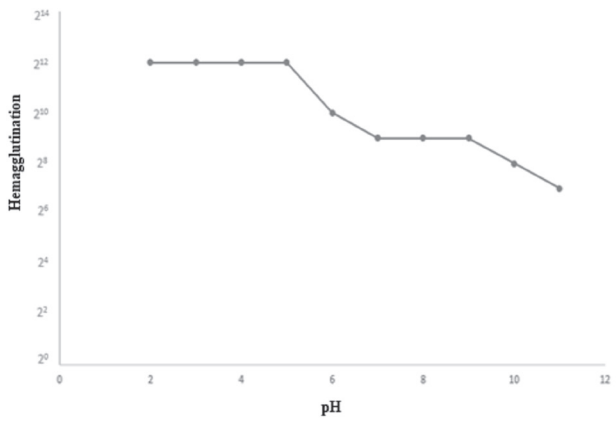

Figure 4. Effect of temperature on the hemagglutinating activity of ASL.

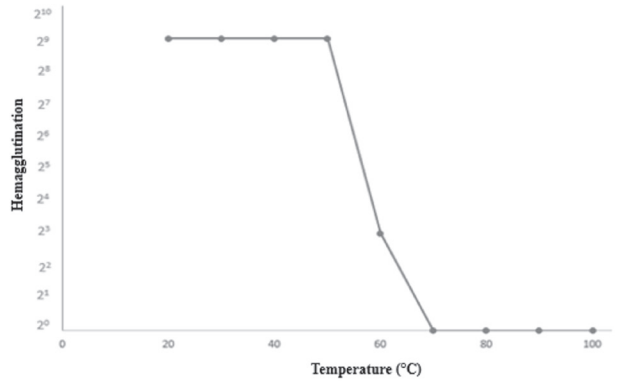

Figure 5. Effect of pH on the hemagglutinating activity of ASL.

Physicochemical characterization of ASL

Fungal lectins, especially those isolated from mushrooms exhibit profound variation in their physicochemical properties (Hassan et al. 2015; Singh et al. 2020). The molecular weight of ASL (16.6 kDa) is similar to the weight reported for *A. blazei* lectin (16 kDa) (Kawagishi et al. 1988). ASL maintained 100% activity up to 50 °C, however, lost 66% of the activity at 60 °C and completely inactivated at 70 °C (Figure 4). ASL is moderately thermostable, as mushroom lectins are reportedly usually stable at a moderate temperature with gradual loss of activity as the temperature increases (Alborés 2014; Wang et al.

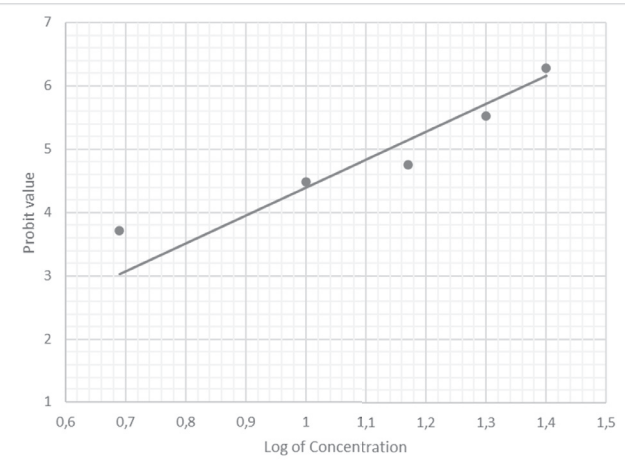

Figure 6. Probit graph for determination of LC_{50}.

2019). However, this result contradicts with the study of Zhao et al. (2011), who reported *A. arvensis* lectin was thermostable up to 90 °C. Several reports have shown that the thermostability of lectins differs, as lectins usually undergo unprecedented conformational changes under harsh temperatures, which might culminate in inactivation mostly owing to the destabilization of interactions necessary for their native conformation (Wang et al. 1996; Singh and Saxena 2013). ASL was stable at acidic pH with maximum activity within pH 2–5, with a 41% loss of activity within pH 7-9 and 50% loss at pH 11 (Fig. 5). Stability of ASL at acidic pH shown was similar to that reported for *Gymnopilus spectabilis* lectin (Alborés et al. 2014).

ASL was completely inactivated by 50 mM EDTA, however, when different metal salts were added to the assay medium, $BaCl_2$ restored 33% of the lectin activity suggesting ASL might be a metalloprotein. The result obtained for ASL contradicts the report on *A. arvensis* lectin (AAL), which was unaffected by divalent ions and enhanced by trivalent ions (Zhao et al. 2011).

Larvicidal study

Chemical method of insect control is one of the major mechanisms of mitigating diseases propagated by these organisms with long-term effects linked with insect resistance, together with detrimental effects on the ecosystem, and human health, paving way for exploration of safer and eco-friendly natural alternatives such as lectins (Gautam et al. 2013; Shaurub et al. 2015; Demok et al. 2019; Satoto et al. 2019; Kumar et al. 2020).

As a distinctive component of the innate defense system of their host, mushroom lectins have a unique ability to recognize diverse carbohydrate-associated structures that mediate most of their varying biological activities (Singh and Saxena 2013; Sabotič et al. 2016). Previous studies on entomotoxic lectins have suggested the fatality induced by these proteins usually involves multiple complementary mechanisms including induction of apoptosis and interaction with specific carbohydrates/glycan structures of vital enzymes, especially those engaged in metabolism and detoxification (de Oliveira et al. 2016; Napoleão et al. 2018). In fact, because of their multivalent assembly, fungal lectins can cross-link cell surface glycoconjugates or trigger distinct oligomerization of glycosylated signaling receptors, which may affect their turnover (Hamshou et al. 2012). Morphological damages of the gut initiated by excessive proteolysis due to specific binding to peritrophic matrixes or epithelial cells of target insects have also been connected to their insecticidal/larvicidal activity (Coelho et al. 2009). As reported by Coelho and co-workers, *Moringa oleifera* lectin increased lumen volume and disrupted the midgut epithelium of *Aedes aegypti* larvae and peritrophic membrane of *Anagasta kuehniella* larvae, ultimately resulting in gut cell death (Coelho et al. 2009; de Oliviera et al. 2017).

Entomotoxic lectins have also been reported to alter critical target insects' biological functions such as pupation, survival, larval development, and adult emergence (Kaur et al. 2009). *Dioscorea batatas* lectin was reported to alter the development of *Helicoverpa armigera* larvae by interacting strongly with vital intracellular structures (Ohizumi et al. 2009).

The entomotoxic lectins vary in physicochemical characteristics, and there are many potential targets because of their multivalent highly stereospecific binding with diverse arrays of insect glycan structures, however, differences in their spatial arrangement together with the proportion of carbohydrate recognition domain may expound the disparity in toxicity mechanisms elicited by these quintessential bioactive proteins (Fitches et al. 2012; Yang et al. 2014; Rani et al. 2017; Singh et al. 2020).

Conclusion

This study concluded that a lectin purified from *A. semotus* showed potent larvicidal activity against *C. quinquefasciatus,* which suggests its application as an alternative and eco-friendly larvicide/insecticide in the control of mosquitoes to mitigate mosquitoes-borne diseases and mortalities. However, a better comprehension of the action mechanism used by the lectin might help further research to investigate the possibilities of biotechnological applications of mushroom lectins in agriculture against phytophagous insects.

References

Akinyoola KA, Odekanyin OO, Kuku A, Sosan MB (2016) Anti-insect potential of a lectin from the tuber, *Dioscorea mangenotiana* towards *Eldana saccharina* (Lepidoptera: Pyralidae). J Agric Biotechnol Sustain Dev 8(3):16-26.

Alborés S, Mora P, Bustamante MJ, Cerdeiras MP, Fraguas LF (2014) Purification and applications of a lectin from the mushroom *Gymnopilus spectabilis*. Appl Microbiol Biotechnol 172:2081-2090.

Bellinato DF, Viana-Medeiros PF, Araújo SC, Martins AJ, Lima JBR Valle D (2016) Resistance status to the insecticides temephos, deltamethrin, and diflubenzuron in Brazilian *Aedes aegypti* populations. BioMed Res Int 8603263:1-12.

Bing DH, Weyand JGM, Stavitsky AB (1967) Hemagglutination with aldehyde-fixed erythrocytes for assay of antigens and antibodies. Proc Society Exp Biol Med

124(4):1166-1170.

Camaroti JRSL, Oliveira APS, Paiva PMG, Pontual EV, Napoleão TH (2017) Phytoinsecticides for controlling pests and mosquito vectors of diseases. In Green V, Ed., Biocontrol Agents: Types, Applications and Research Insights. Nova Science Publishers, New York, 147-188.

Chandrasekaran G, Lee YC, Park H, Wu Y, Shin HJ (2016) Antibacterial and antifungal activities of lectin extracted from fruiting bodies of the Korean cauliflower medicinal mushroom, *Sparassis latifolia* (Agaricomycetes). Int J Med Mush 18(4):291-299.

Coelho JS, Santos NDL, Napoleão TH, Gomes FS, Ferreira RS, Zingali RB, Coelho LCCB, Leite SP, Navarro DMAF, Paiva PMG (2009) Effect of *Moringa oleifera* lectin on development and mortality of *Aedes aegypti*. Chemosphere 77:934-938.

Cuthbert RN, Cunningham EM, Crane K, Dick JTA, Callaghan A, Coughlan NE (2020) In for the kill: novel biosecurity approaches for invasive and medically important mosquito species. Mang Biol Invasions 11(1):9-25.

de Oliveira APS, de Santana Silva LL, de Albuquerque Lima T, Pontual EV, de Lima Santos ND, Coelho LCBB, Navarro DMDAF, Zingali RB, Napoleão TH, Paiva PMG (2016) Biotechnological value of *Moringa oleifera* seed cake as source of insecticidal lectin against *Aedes aegypti*. Process Biochem 51(10):1683-1690.

de Oliveira CFR, de Moura MC, Napoleão TH, Paiva PMG, Coelho LCBB, Macedo MLR (2017) A chitin-binding lectin from *Moringa oleifera* seeds (WSMoL) impairs digestive physiology of the Mediterranean flour larvae, *Anagasta kuehniella*. P Biochem Physiol 142:67-76.

Demok S, Endersby-Harshman N, Vinit R, Timinao L, Robinson LJ, Susapu M, Makita L, Laman M, Hoffmann A, Karl S (2019) Insecticide resistance status of *Aedes aegypti* and *Aedes albopictus* mosquitoes in Papua New Guinea. Parasit Vec 12:333.

Farnesi LC, Menna-Barreto RFS, Martins AJ, Valle D, Rezense GL (2015) Physical features and chitin content of eggs from the mosquito vectors *Aedes aegypti*, *Anopheles aquasalis* and *Culex quinquifasciatus*: Connection with distinct levels of resistance to desiccation. J Ins Physiol 83:43-52.

Feng K, Liu QH, Ng TB, Wang HX (2006) Isolation and characterization of a novel lectin from the mushroom *Armillaria luteo-virens*. Biochem Biophys Res Commun 345:1573-1578.

Finney DJ (1971) Probit analysis. 3rd Ed., Cambridge University Press, New York.

Fitches EC, Pyati P, King GF, Gatehouse JA (2012) Fusion to snowdrop Lectin magnifies the oral activity of insecticidal v-Hexatoxin-Hv1a peptide by enabling its delivery to the central nervous system. PLoS One 7(6):e39389.

Fonseca DM, Keyghobadi N, Malcolm CA, Mehmet C, Schaffner F, Mogi M, Fleischer RC, Wilkerson RC (2004) Emerging vectors in the *Culex pipiens* complex. Sci 303(5663):1535-1538.

Fonseca V, Xavier J, de Oliveira T, de Filippis AMB, Acantara LCJ, Giovanetti M (2019) Mosquito-borne viral diseases: control and prevention in the genomics era. In Curr T Epidemiol Vector-Borne Dis IntechOpen.

Gautam K, Kumar P, Poonia S (2013) Larvicidal and GC – MS analysis of flavonoids of *Vitex negundo* and *Andrographis paniculata* against two vector mosquitoes *Anopheles stephensi* and *Aedes aegypti*. J Vec B Dis 50:171-178.

Hamshou M, van Damme EJ, Vandenborre G, Ghesquiere B, Trooskens G, Gevaert K, Smagghe G (2012) GalNAc/Gal-binding *Rhizoctonia solani* agglutinin has antiproliferative activity in *Drosophila melanogaster* S2 cells via MAPK and JAK/STAT signaling. PLoS ONE 7(4):e33680.

Hassan MAA, Rouf R, Tiralongo E, May TW, Tiralongo J (2015) Mushroom lectins: specificity, structure and bioactivity relevant to human disease. Int J Mol Sci 16(4):7802-7838.

He S, Shi J, Walid E, Zhang H, Ma Y, Xue SJ (2015) Reverse micellar extraction of lectin from black turtle bean (*Phaseolus vulgaris*): Optimisation of extraction conditions by response surface methodology. Food Chem 166:93-100.

Islam MS, Saiful M, Hossain M, Sikder M, Morshed M, Hossain M (2013) Acute toxicity of the mixtures of grease and engine wash oil on fish, *Pangasius sutchi* under laboratory condition. Int J Life Sci Biotech Pharm Res 2(1):306-317.

Johnny II, Kuku A, Odekanyin OO, Adesina SK (2016) A lectin with larvicidal potential from the fresh leaves of *Agelanthus brunneus* (Engl.) Van Tiegh Loranthaceae. J Pharm Res Int 13(3):1-9.

Kaur M, Singh K, Rup PJ, Kamboj SS, Singh J (2009) Anti-insect potential of lectins from *Arisaema species* towards *Bactrocera cucurbitae*. J Environ Biol 36:1263-1268.

Kawagishi H, Nomura A, Yumen T, Mizuno T, Hagiwara T, Nakamura T (1988) Isolation and properties of a lectin from the fruiting bodies of *Agaricus blazei*. C Res 183(1):150-154.

Kuku A, Eretan OB (2004) Purification and partial characterization of a lectin from the fresh leaves of *Kalanchoe crenata* (Andr.) Haw. BMB Rep 37(2):229-233.

Kuku A, Stoppini M, Cobianchi A, Minetti G, Balduini C, Aboderin A (2000) The complete primary structure of a mannose/glucose specific lectin from the seeds of *Dioclea reflexa* (Hook, F.). Nig J Biochem Mol Biol 15:115-119.

Kumar D, Kumar P, Singh H, Agrawal V (2020) Biocontrol of mosquito vectors through herbal-derived silver nanoparticles: prospects and challenges. E Sci Pol Res 27(21):25987-26024.

Laemmli UK, Favre M (1970) Maturation of the head of bacteriophage T4. I. DNA packaging events. J Mol Biol

80:575-599.
Largeteau ML, Llarena-Hernández RC, Regnault-Roger C, Savoie JM (2011) The medicinal *Agaricus* mushroom cultivated in Brazil: biology, cultivation and non-medicinal valorisation. Appl Microbiol Biotechnol 92(5):897-907.
Li YR, Zhang GQ, Ng, TB, Wang HX (2010) A novel lectin with antiproliferative and HIV-1 reverse transcriptase inhibitory activities from dried fruiting bodies of the monkey head mushroom *Hericium erinaceum*. BioMed Res Int 2010:716515.
Lima-Camara TN (2016) Emerging arboviruses and public health challenges in Brazil. Rev Saude Publica 50:36.
Lopes RP, Lima JPB, Martins AJ (2019) Insecticide resistance in *Culex quinquefasciatus* Say, 1823 in Brazil: a review. Parasites Vectors 12(1):591.
Lowry OH, Rosebrough NJ, Farr AL, Randall RJ (1951) Protein measurement with the Folin phenol reagent. J Biol Chem 193(1):265-275.
Mikiashvili NA, Elisashvili V, Wasser SP, Nevo E (2006) Comparative study of lectin activity of higher Basidiomycetes. Int J Med Mush 8(1):31-38.
Muszyńska B, Grzywacz-Kisielewska A, Kała K, Gdula-Argasińska J (2018) Anti-inflammatory properties of edible mushrooms: A review. Food Chem 243:373-381.
Nakagawa R, Yasokawa D, Ikeda T, Nagashima K (1996) Purification and characterization of two lectins from callus of *Helianthus tuberosus*. Biosci Biotechnol Biochem 60:259-262.
Nakamura-Tsuruta S, Kominami J, Kuno A, Hirabayashi J (2006) Evidence that *Agaricus bisporus* agglutinin (ABA) has dual sugar-binding specificity. Biochem Biophys Res Commun 347:215-220.
Napoleão TH, Albuquerque LP, Santos ND, Nova IC, Lima TA, Paiva PM, Pontual EV (2018) Insect mid gut structures and molecules as targets of plant-derived protease inhibitors and lectins. P Manag Sci 75(5):1212-1222.
Nascimento KS, Silva MTL, Oliveira MV, Lossio CF, Pinto-Junior VR, Osterne VJS, Cavada BS (2020) *Dalbergieae* lectins: A review of lectins from species of a primitive *Papilionoideae* (leguminous) tribe. Int J Biol Macromol 144:509-526.
Ohizumi Y, Gaidamashvili M, Ohwada S, Matsuda K, Kominami J, Nakamura-Tsuruta S, Hirabayashi J, Naganuma T, Ogawa T, Muramoto K (2009) Mannose-binding lectin from yam (*Dioscorea batatas*) tubers with insecticidal properties against *Helicoverpa armigera* (Lepidoptera: Noctuidae). J Agric Food Chem 57(7):2896-2902.
Oladokun BO, Omisore ON, Osukoya OA, Kuku A (2019) Anti-nociceptive and anti-inflammatory activities of *Tetracarpidium conophorum* seed lectin. Sci Afr 3:1-9.
Panchak LV (2019) Russulaceae family mushrooms lectins: Function, purification, structural features and possibilities of practical applications. Biotech Acta 12:29-38.
Perduca M, Destefanis L, Bovi M, Galliano M, Munari F, Assfalg M, Ferrari F, Monaco HL, Capaldi S (2020) Structure and properties of the oyster mushroom (*Pleurotus ostreatus*) lectin (POL). Glycobiology 30(8):550-562.
Rani S, Sharma V, Hada A, Bhattacharya RC, Koundal KR (2017) Fusion gene construct preparation with lectin and protease inhibitor genes against aphids and efficient genetic transformation of *Brassica juncea* using cotyledons explants. Acta Physiol Plant 39(5):115.
Sabotič J, Ohm RA, Künzler M (2016) Entomotoxic and nematotoxic lectins and protease inhibitors from fungal fruiting bodies. Appl Microbiol Biotechnol 100(1):91-111.
Sampaio LA, Tesser M, Pickersgill AR (1998) Temperature effects on sex differentiation of two South American atherinids, *Odontesthes argentinensis* and *Patagonina hatchery*. Environ Biol Fish 47:624-629.
Santos NDL, Napoleão TH, Benevides CA, Albuquerque LP, Pontual EV, Oliveira APS, Coelho LCBB, Navarro DMAF, Paiva PMG (2020) Effect of gamma irradiation of *Moringa oleifera* seed lectin on its larvicidal, ovicidal, and oviposition-stimulant activities against *Aedes aegypti*. S Afr J Bot 129:3-8.
Satoto TBT, Satrisno H, Lazuardi L, Diptyanusa A (2019) Insecticide resistance in *Aedes aegypti*: an impact from human urbanization? PLoS One 14(6):e0218079.
Shaurub EH, Abd El-Aziz NM (2015) Biochemical effects of lambda-cyhalothrin and lufenuron on *Culex pipiens* L (Diptera: Culicidae). Int J Mosq Res 2:122-126.
Silva AJ, Cavalcanti VLR, Porto ALF, Gama WA, Brandão-Costa, RMP, Bezerra RP (2020) The green microalgae *Tetradesmus obliquus* (*Scenedesmus acutus*) as lectin source in the recognition of ABO blood type: purification and characterization. J Appl Phycol 1-8.
Singh AP, Saxena KD (2013) Biological activity of purified *Momordica charantia* lectin. Chem Sci Trans 2:258-262.
Singh RS, Bhari R, Kaur HP (2010) Mushroom lectins: current status and future perspectives. Crit Rev Biotech 30(2):99-126.
Singh RS, Thakur SR, Bansal P (2015) Algal lectins as promising biomolecules for biomedical research. Crit Rev Microbiol 41:77-88.
Singh RS, Walia AK, Kennedy JF (2020) Mushroom lectins in biomedical research and development. Int J Biol Macromol 151:1340-1350.
Takken W, van den Berg H (2019) Manual on prevention of establishment and control of mosquitoes of public health importance in the WHO European Region. Copenhagen: World Health Organization.
Varrot A, Basheer SM, Imberty A (2013) Fungal lectins: structure, function and potential applications. Curr Opin Struct Biol 23(5):678-685.
Wang HX, Liu WK, Ng TB, Ooi VEC, Chang ST (1996) The immunomodulatory and antitumor activities of lectins

from the mushroom *Tricholoma mongolicum.* Immunopharmacol 31:205-211.

Wang Y, Wua B, Shaob J, Jiaa J, Tiana Y, Shua X, Rena X, Guana Y (2018) Extraction, purification and physicochemical properties of a novel lectin from *Laetiporus sulphureus* mushroom. LWT Food Sci Technol 91:151-159.

Wilke ABB, Medeiros-Sousa AR, Ceretti-Junior W, Marrelli MT (2017) Mosquito populations' dynamics associated with climate variations. Acta Trop 166:343-350.

WHO (1981) World Health Organizations. Instruction for determining the susceptibility or resistance of mosquito larvae to insect development inhibitors. (WHO/VBC/81.812). Geneva, 1-6.

Yang S, Pyati P, Fitches E, Gatehouse J (2014) A recombinant fusion protein containing a spider toxin specific for the insect voltage-gated sodium ion channel shows oral toxicity towards insects of different orders. Biochem Mol Biol 47(100):1-11.

Zhang GQ, Chen QJ, Hua J, Liu ZL, Sun Y, Xu X, Han P, Wang HX (2019) An inulin-specific lectin with anti-HIV-1 reverse transcriptase, antiproliferative, and mitogenic activities from the edible mushroom *Agaricus bitorquis*. Biomed Res Int 2019:1341370.

Zhang GQ, Sun J, Wang HX, NG TB (2009) A novel lectin with antiproliferative activity from the medicinal mushroom *Pholiota adipose*. Acta Biochim Pol 56:415-421.

Zhao JK, Zhao YC, Li SH, Wang HX, Ng TB (2011) Isolation and characterization of a novel thermostable lectin from the wild edible mushroom *Agaricus arvensis*. J Basic Microbiol 51(3):304-311.

Acta Biologica Szegediensis

Volume 65(1):75-84, 2021
Acta Biologica Szegediensis
http://abs.bibl.u-szeged.hu/index.php/abs

DOI:10.14232/abs.2021.1.75-84

ARTICLE

Perturbation of the mucosa-associated anaerobic gut microbiota in streptozotocin-induced diabetic rats

Roland Wirth[1,3], Nikolett Bódi[2], Zita Szalai[2], Lalitha Chandrakumar[2], Gergely Maróti[3], Kornél L Kovács[1,4], Zoltán Bagi[1], Diána Mezei[2], János Balázs[2], Mária Bagyánszki[2]*

[1]Department of Biotechnology, Faculty of Science and Informatics, University of Szeged, Szeged, H-6720, Hungary
[2]Department of Physiology, Anatomy and Neuroscience, Faculty of Science and Informatics, University of Szeged, Szeged, H-6720, Hungary
[3]Institute of Plant Biology, Biological Research Centre, Eötvös Loránd Research Network, Szeged, H-6720, Hungary
[4]Department of Oral Biology and Experimental Dental Research, Faculty of Dentistry, University of Szeged, Szeged, Hungary

ABSTRACT Our aim was to map the gut region-specific differences of the mucosa-associated microbiome distribution in a streptozotocin-induced diabetic rat model. Tissue samples from the duodenum, ileum and colon were collected 10 weeks after the onset of hyperglycaemia to analyse the mucosa-associated microbiota using next-generation DNA sequencing. Striking differences were observed in the mucosa-associated microbiota of the duodenum between diabetic and control rats. A significant invasion of the aerobic genus *Mycoplasma* was apparent in diabetes, and the abundance of the anaerobic phylum Firmicutes decreased massively. It is noteworthy that insulin treatment eliminated the *Mycoplasma* invasion in the duodenum and apparently restored the anaerobic environment in the mucosa. In the ileum the abundance of the phylum Firmicutes increased in the diabetic samples. Although the proportion of the phylum Proteobacteria decreased moderately, its composition changed significantly, and insulin treatment induced only minor alterations. In the diabetic samples of colon, the abundance of the phylum Firmicutes decreased slightly, the relative number of the bacteria in the phylum Bacteroidetes increased strongly as compared to the control values, and after insulin treatment this increase was more significant. Chronic hyperglycaemia has the most prominent effect on the mucosa-associated microbiota in the duodenum.
Acta Biol Szeged 65(1):75-84 (2021)

KEY WORDS
animal model
hyperglycaemia
mucosa-associated microbiota
next-generation DNA sequencing
type 1 diabetes

ARTICLE INFORMATION
Submitted
20 January 2021.
Accepted
04 April 2021.
***Corresponding author**
E-mail: bmarcsi@bio.u-szeged.hu

Introduction

Type 1 diabetes (T1D) is an autoimmune disease with a strong genetic basis, and it is obvious that several environmental factors contribute to the disease (Jerram and Leslie 2017; Kugelberg 2017). The gastrointestinal tract is colonized by microbiota, a large and complex microbial community, consist of mainly bacteria. Microbiota also includes commensal populations of fungi, viruses, archaea, and protists (de Oliveira et al. 2017; Flemer et al. 2017; Matijašić et al. 2020). The role of the gut microbiota in T1D ethology has been the subject of research over the last decade to clarify disease development and to determine preventive approaches (e.g., diet manipulation, probiotic administration) (de Oliveira et al. 2017; Marino et al. 2017; Mishra et al. 2019; Tanca et al. 2018; Tian et al. 2017; Wirth et al. 2014).

Studies corroborated that intestinal dysbiosis affects gut permeability via their metabolites and plays a role in T1D development, but there is no evidence for the specific role of intestinal microbiota in the development of autoimmunity to beta-cells and in tissue damage (de Oliveira et al. 2017; Knip and Honkanen 2017; Paun et al. 2017; Tian et al. 2017).

Investigations along the longitudinal axis of the gastrointestinal (GI) tract corroborated a high level of similarity between the rat model and humans in the oxygenation levels as well as in microbial diversity (Li et al. 2017). Oxygen levels in the air (≈21% = 145 mmHg = 19,331.7 Pa) drop dramatically to around 32 mmHg (4,266.3 Pa) in the rat and human duodenum and <3 mmHg (<400.0 Pa) in the colon (Albenberg et al. 2014). Due to the radial gradients the oxygenation landscape in the GI tract is inhomogeneous but with all practical measures it is considered an anaerobic environment inhabited by facultative and obligate anaerobic microbial communities. A correlation between the diminishing oxygen levels and

the characteristic anaerobic microbes exists along the GI tract (Albenberg et al. 2014; Wirth et al. 2014). Previous studies have indicated the involvement of perturbed microbiota in inflammatory bowel diseases (IBD), i.e. Crohn' disease and ulcerative colitis (Chermesh and Shamir 2009). Although there are numerous similarities between IBD and T1D, the microbial alterations caused by T1D in the mucosa have not been addressed before.

The host-microbiota interactions have been recognized as highly site-specific, and the local crosstalk determines intestinal function and physiology (Sommer and Backhed 2016). The overwhelming majority of the samples used to study microbial events in the gut were taken from colonic stools (Flemer et al. 2017; Hu et al. 2017; Marino et al. 2017; Paun et al. 2017; Qi et al. 2016) with the assumption that the microbiota of the colon represents the microbiota of the entire GI tract. Although the ease of sampling may justify the selection of this sampling site, numerous studies warned that the microbiome of the colon does not unequivocally represent the microbial activities in the upper GI regions. Our previous experiments investigated the possible correlation among the diabetes-related gut region-dependent nitrergic myenteric neuropathy, the altered mesenteric capillaries (Bodi et al. 2012; Izbeki et al. 2008) and the spatially restricted distribution of the lumen-associated microbiota (LAM) in the GI tract (Wirth et al. 2014). The regionally distinct alterations in the microbiome along the longitudinal axis of the GI tract correlated well with the regional manifestations of diabetes-related enteric neuropathy and mesenteric capillary damage (Wirth et al. 2014).

In this study, we investigated the composition of the mucosa-associated microbiome (MAM) along the gut in the same STZ-induced diabetic and insulin-treated diabetic rat model to search for a causal relationship between the prevalence of bacteria in the specific parts of the GI tract and region-specific myenteric nitrergic neuropathy. We noted that surprisingly a significant perturbation of the anaerobic microbial community took place in the T1D duodenum, which disappeared upon insulin treatment although insulin could not restore the healthy GI microbiome.

Materials and Methods

Animal model

The experiments were performed on male Wistar rats (Crl: WI BR; Toxi-Coop Zrt., weighing 210-260 g) with strict adherence to the National Institutes of Health (Bethesda, MD, USA) guidelines and the EU directive 2010/63/EU for the protection of animals used for scientific purposes. The study was approved by the National Scientific Ethical Committee on Animal Experimentation (National Competent Authority), with the license number XX./1487/2014. The rats were kept in the animal care facility of the Institute of Surgical Research of the University of Szeged in Type III plastic cages in a 12/12-h day/night cycle under standard air temperature and humidity conditions. Standard laboratory chow (Farmer-Mix Kft., Zsámbék, Hungary) and water were provided ad libitum.

The rats were divided randomly into three groups: STZ-induced diabetics (n = 3), insulin-treated diabetics (n = 4), and sex- and age-matched controls (n = 5). Hyperglycaemia was induced as described previously (Bodi et al. 2012; Izbeki et al. 2008). The animals were considered diabetic if the non-fasting blood glucose concentration was higher than 18 mM. From this time on one group of hyperglycaemic rats received a subcutaneous injection of insulin (Humulin M3; Eli Lilly Nederland, Utrecht) each morning (2 IU) and afternoon (2 IU). The non-fasting blood glucose concentration and the weight of each animal were measured weekly.

Tissue handling

Ten weeks after the onset of hyperglycaemia, the animals were sacrificed by cervical dislocation under chloral hydrate anaesthesia (375 mg/kg i. p.). The pancreas and gut segments of the control, STZ-induced diabetic and insulin-treated diabetic rats were dissected and rinsed in sterile distilled water (Milli-Q).

Immunohistochemical staining

For immunohistochemistry, paraffin-embedded pancreas sections were immunostained with insulin marker. Briefly, after blocking in PB containing 0.1% bovine serum albumin, 10% normal goat serum and 0.3% Triton X-100, the samples were incubated overnight with anti-insulin (mouse; Sigma-Aldrich, Budapest, Hungary; final dilution 1:100) primary antibody. After washing in PB, sections were incubated with anti-mouse Cy3 (Jackson Immuno Research Laboratories, Baltimore Pike, PA; final dilution 1:200) secondary antibody for 2 hours. All incubations were carried out at room temperature. Negative controls were performed by omitting the primary antibody, when no immunoreactivity was observed. Sections were mounted on slides in Fluoroshield™ with DAPI histology mounting medium (Sigma-Aldrich, Budapest, Hungary), observed and photographed with a Zeiss Imager Z.2 fluorescent microscope equipped with an Axiocam 506 mono camera.

DNA isolation and next-generation sequencing

Three-cm-long samples were taken from the duodenum (1 cm distal to the pylorus), the ileum (1 cm proximal to the ileocaecal junction), and the proximal colon and processed

Table 1. Weight and glycaemic characteristics of the three experimental groups of rats (means ± SEM).

	Weight (g)		Blood glucose level (mM)	
	initial	final	initial	final (average)
Controls (n = 5)	232.2 ± 7.29	486 ± 4.93 *	7.08 ± 0.22	6.3 ± 0.13
STZ-induced diabetics (n = 3)	235.3 ± 10.48	382.7 ± 3.53 *, °	6.6 ± 0.1	23.31 ± 0.53 *, °
Insulin-treated diabetics (n = 4)	251.5 ± 4.35	481.5 ± 13.4 *, +	6.65 ± 0.18	9.48± 0.14 *, °, +

*: Initial vs. final ($p < 0.0001$); °: control vs. diabetic group ($p < 0.0001$); +: diabetic vs. insulin-treated diabetic group ($p < 0.0001$). Statistical analysis was performed with one-way ANOVA and the Newman–Keuls test. Analyses were carried out with GraphPad Prism 6.0 (GraphPad Software, La Jolla, CA, the United States of America). A probability of $P < 0.05$ was set as the level of significance.

for metagenomic studies. For removing the intestinal contents, the dissected gut segments were washed thoroughly twice with a strong jet of sterile distilled water (2 x 10 ml, Milli-Q), and the 3-cm-long intestinal tissue samples were placed and shaken in 10 ml sterile distilled water (Milli-Q) in sterile Falcon tubes.

Three ml of supernatant was used for total-community DNA isolation. The extractions were carried out with the Macherey-Nagel Nucleospin Soil kit following the supplier's instructions (Macherey-Nagel: 740780.250, Germany, Düren). For efficient cell lysis, SL1 buffer, SLX Lysis Enhancer and deadbeat were used. The samples originating from the same animal group and the same gut segments were pooled. Shotgun metagenome sequencing was carried out following the recommendations of the Ion Torrent PGM sequencing platform (Life Technologies, Hungary, Budapest). The preparation of sample libraries was made by the Life Technologies IonXpress fragment plus library protocol (4471269). Samples were quantified by using the Ion device library quantitation kit (4468802) and Step One Real Time PCR (Applied Biosystems Hungary, Budapest). Ion OneTouch 2 and Ion OneTouch ES devices were used with the Ion PGM Template OT2 200 kit (4480974). Barcoding was made by the IonXpress barcode kit (4471250). Sequencing was performed using the Ion PGM Sequencing kit (4474004) on an Ion Torrent PGM 316Chip (Wirth et al. 2014). Quality values were determined for each nucleotide. The 100-200 nt individual reads were further analysed using the MG-RAST software package, which is a modified version of RAST (Rapid Annotations based on Subsystem Technology). The MG-RAST pipeline performs quality control, protein prediction, clustering and similarity-based annotation on nucleic acid sequence datasets. The MG-RAST server analyses against several reference datasets (protein and nucleic acid databases) (Meyer et al. 2008). The acceptable percentage of identity was set to >80%, the minimum alignment length was 50 nt and the e-value cut-off was <10-5. The generated matches of external databases were used to compute the derived data (Randle-Boggis et al. 2016; Wirth et al. 2014). Eukaryotic and unassigned data were disregarded during the distribution calculation of taxonomical abundance. Data are available under the „Microbiome of rat intestinal epithelium" project in MG-RAST.

Results

Characteristics of experimental animals

The general characteristics of the control, diabetic, and insulin-treated diabetic rats 10 weeks after the onset of hyperglycaemia are shown in Table 1. The diabetic rats had reduced body weight and an increased blood glucose concentration (23.31 ± 0.53 mM) as compared with the age- and sex-matched controls (6.30 ± 0.13 mM). The insulin-treated diabetic rats did not differ significantly from the control animals in this respect. Their average blood glucose concentration was significantly elevated (9.48 ± 0.14 mM), but it was closer to the control level.

Anti-insulin immunohistochemical staining showed smaller Langerhans islets and weaker insulin-immunostaining in the diabetic and insulin-treated diabetic animals than in the controls (Fig. 1).

The composition of the mucosal microbiome along the rat GI tract

Two sets of metagenomic data were evaluated in the present study. The distributions were determined at phylum, class and order levels (Fig. 2-4). Eukaryotic and unclassified data were disregarded. In this way, we present the distribution of abundances of the bacterial taxa longitudinally along the diabetic intestinal mucosa for the first time.

The mucosa-associated microbiome of the diabetic duodenum

Striking differences were observed in the composition of the anaerobic microbial community of the duodenum between the diabetic and the control rats. Within the domain Bacteria, the phylum Firmicutes (69%) predominated in the control duodenum. The majority of the Firmicutes were

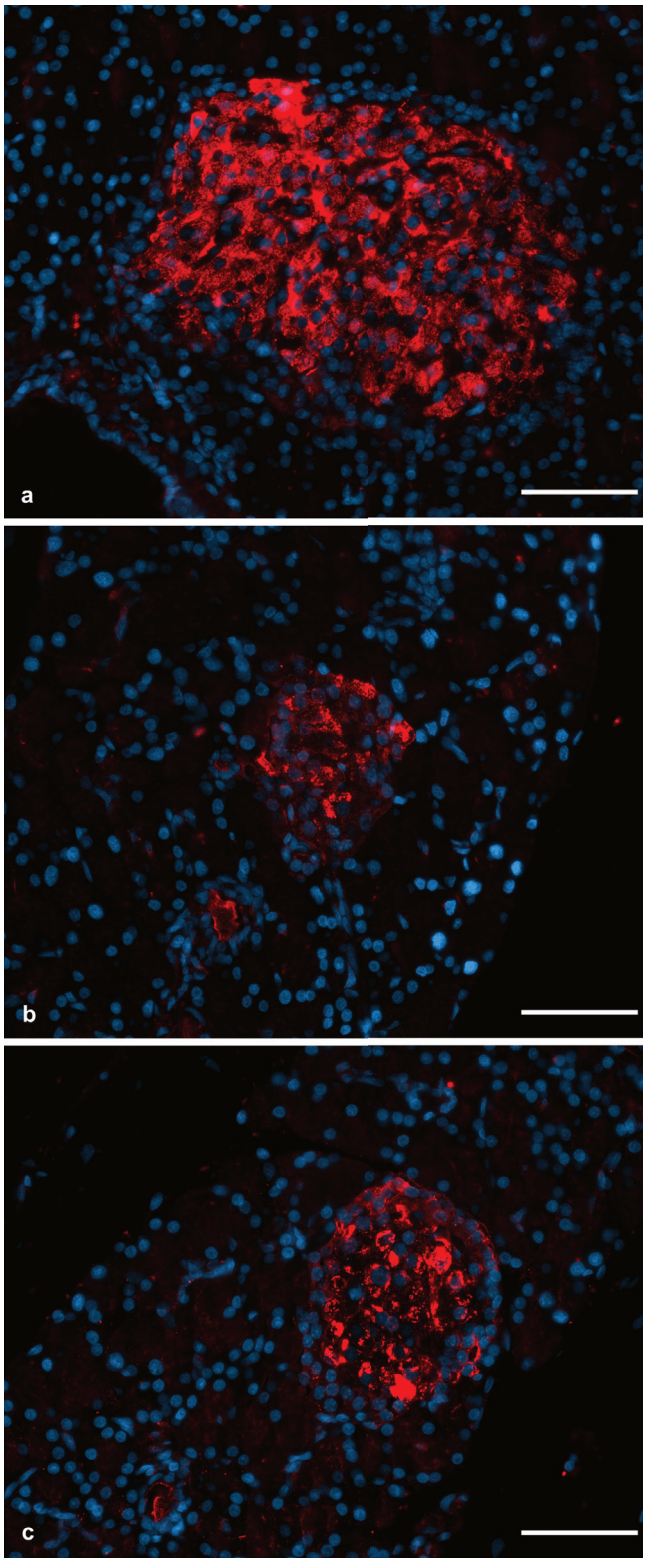

Figure 1. Insulin immunoreactivity in paraffin sections from control (a), diabetic (b) and insulin-treated diabetic (c) rat pancreas (red: insulin; blue: DAPI). Scale bar: 40 µm.

identified to the classes Clostridia (66%) and Bacilli (2%). A substantial invasion of the aerobic genus Mycoplasma of the phylum Tenericutes (not observed in the controls) was apparent in diabetes (14%), and the abundance of the phylum Firmicutes decreased massively (about 56% vs. 69% in controls). The class Bacilli, including the order Lactobacillales was not observed in the diabetic samples (Fig. 2).

The phylum Proteobacteria showed decreased abundance in diabetes as compared to the controls, and within this phylum a remarkable change was observed at the level of lower taxonomic units. The abundances of the classes Gammaproteobacteria and Betaproteobacteria decreased, whereas the class Deltaproteobacteria (not observed in the controls) appeared (2%).

From among the other phyla, the phylum Actinobacteria was appreciably represented both in the control (4%) and in the diabetic (3%) duodenum.

It is noteworthy that insulin treatment eliminated the Mycoplasma (1%) infiltration in the duodenum (Fig. 2). In other aspects, the diversity and distribution of prokaryotes in the insulin-treated diabetic rats did not differ markedly from the healthy controls. The majority of the domain Bacteria was identified in the phyla Firmicutes (65%) and Proteobacteria (~ 25%). The phylum Bacteroidetes (4%) was also represented in the insulin-treated duodenum. As in the control duodenum, the order Lactobacillales was also observed in the insulin-treated samples (3%).

The mucosa-associated microbiome of the diabetic ileum

The majority of the domain Bacteria belonged to the phyla Firmicutes (63%) and Proteobacteria (~25%) in the control ileum. The abundance of the phylum Firmicutes increased in the diabetic samples (68%) (Fig. 3).

Although the proportion of the phylum Proteobacteria decreased moderately (22%), its composition changed strikingly. The class Epsilonproteobacteria, including the order Campylobacterales was basically eradicated from the diabetic samples, whereas in the control it represented 10% of the Bacteria.

The diversity and distribution of prokaryotes in the insulin-treated diabetic rats did not differ markedly from the healthy controls (Fig. 3). The abundances of the predominant phyla Firmicutes and Proteobacteria were about 62% and 26%, respectively. The class Epsilonproteobacteria, including the order Campylobacterales (9%), was also detected in the insulin-treated samples.

The mucosa-associated microbiome of the diabetic colon

The phyla Firmicutes, Bacteroidetes and Proteobacteria still ruled over the microbial landscape, totaling about

Figure 2. Compositions of the control (a), diabetic (b) and insulin-treated diabetic (c) mucosa-associated microbiome in the duodenum at phylum, class and order levels. The abbreviated and color-coded taxa are indicated on the right side in taxonomic levels. A striking invasion of the genus *Mycoplasma* was apparent in diabetes and the representation of the phylum Firmicutes decreased massively. It is noteworthy that the insulin treatment eliminated the *Mycoplasma* invasion.

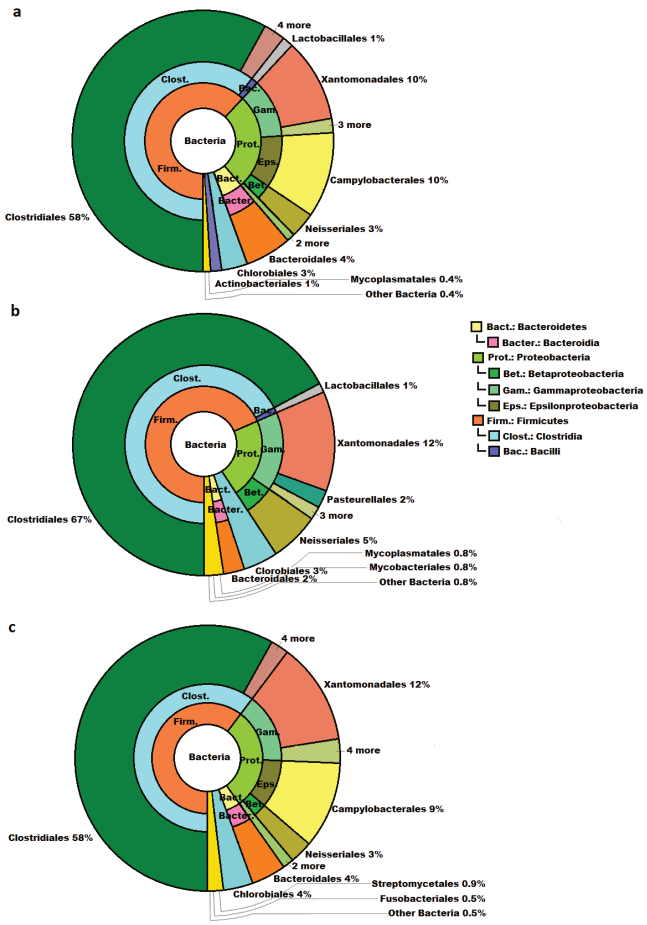

Figure 3. Compositions of the control (a), diabetic (b) and insulin-treated diabetic (c) mucosa-associated microbiome in the ileum at phylum, class and order levels. The abbreviated and color-coded taxa are indicated on the right side in taxonomic levels. In the domain Bacteria the phyla Firmicutes and Proteobacteria predominated. The composition of the phyla Proteobacteria changed strikingly. The class Epsilonproteobacteria was basically eradicated from the diabetic samples.

39%, 31% and 17% of the population in the control colon, respectively. In the diabetic samples the abundance of the phylum Firmicutes decreased slightly (~35%); the relative number of the bacteria belonging to the phylum Bacteroidetes increased strongly (44%) as compared to the control values (Fig. 4).

The abundance of the phylum Proteobacteria (6%) was almost three times lower in the diabetic colon relative to the control. Both Epsilonproteobacteria and Gammaproteobacteria showed decreased abundance in the diabetic colon, moreover the order Campylobacterales was almost eradicated (1% vs. 8% in the control).

The phyla Firmicutes (49%) and Bacteroidetes (26%) accounted for the overwhelming majority of bacteria present in this gut segment of insulin-treated rats (Fig. 4), followed by the Proteobacteria (19%).

The abundance of the phylum Firmicutes was notably higher (49%) in the insulin-treated samples as compared to the controls (39%). In this phylum the proportion of the unclassified Clostridiales showed a major increase relative to the controls (28% vs. 15% in the control).

The abundances of the classes Epsilonproteobacteria (~7%), Gammaproteobacteria (9%) and the order Campylobacterales (7%) were similar to the corresponding control data.

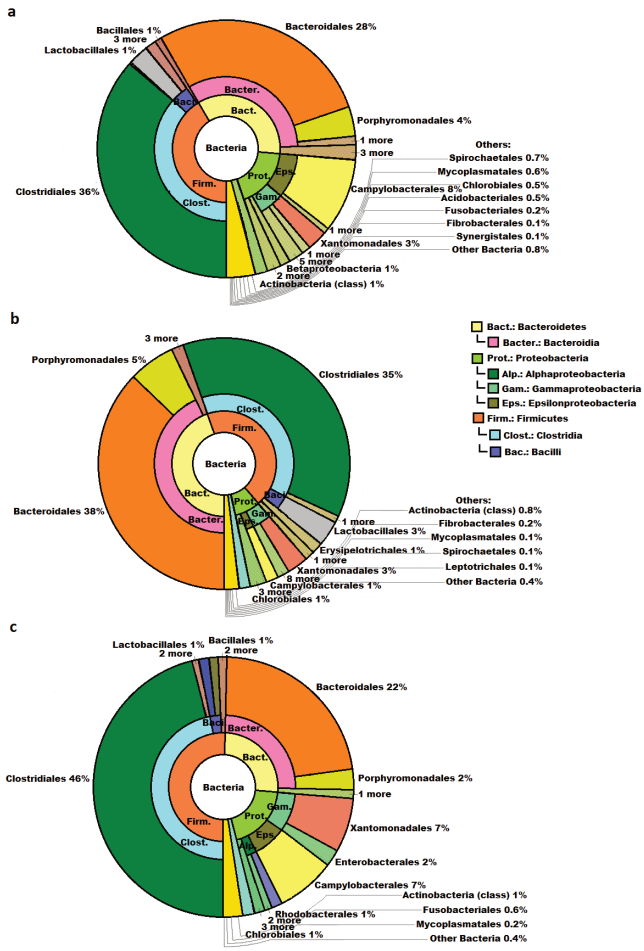

Figure 4. Compositions of the control (a), diabetic (b) and insulin-treated diabetic (c) mucosa-associated microbiome in the colon at phylum, class and order levels. The abbreviated and color-coded taxa are indicated on the right side in taxonomic levels. The domain Bacteria comprised the phyla Firmicutes, Bacteroidetes and Proteobacteria. The phylum Bacteroidetes increased, whereas the phylum Proteobacteria decreased in abundance in the diabetic colon. In the insulin-treated colon the abundance of the phylum Firmicutes was notably higher than in the controls.

Discussion

A growing number of evidences support site-specific host-microbiota interactions and local host-microbiota crosstalk determining intestinal functions and physiology (Bashir et al. 2016; Kelly et al. 2017; Sommer and Backhed 2016; Wang et al. 2010; Wirth et al. 2014). Our previous results (Wirth et al. 2014) showed strong correlation between the regionally distinct alterations of LAM in STZ-treated rats with the regional manifestations of diabetes-related enteric neuropathy and mesenteric capillary damage (Bodi et al. 2012; Izbeki et al. 2008). These data suggested that the myenteric neurons in a specific gut segment are not only targets of T1D, but a significant factor in the pathogenesis of autoimmune diabetes and enteric neuropathy initiated by the gut region-specific alteration of the LAM. The massive invasion of the Gram-negative *Klebsiella* in the ileum could be directly associated with the inflammation, and it could be a critical environmental trigger, initiating the pathological cascade from the epithelium to the enteric neurons, resulting altered neuro-immune interactions, enteric neuropathy and GI motility disorders. Members of the genus *Klebsiella* are known facultative anaerobe pathogenic bacteria (Li et al. 2017), which have not been implicated in T1D before, but can be a major causative agent in type 2 diabetes associated pyrogenic liver abscess (Lee et al. 2017). The lumen of the rat GI tract is an anaerobic environment (Li et al. 2017) where the facultative anaerobe *Klebsiella* may not be unprecedented but indicated an aerobic intrusion into the T1D microbiota.

While the LAM can only indirectly interact, MAM interacts both directly and indirectly with the host epithelium (Bajaj et al. 2012; Gevers et al. 2014; Van den Abbeele et al. 2011). It has been reported recently that the MAM but not the LAM of patients changed in various pathological states, like IBD or hepatic encephalopathy. These findings substantiate that mucosal host-microbiota interactions may be of importance (Sommer and Backhed 2016). Therefore, in this study our first goal was to explore the gut region-specific differences in the composition of the MAM, and secondly to determine the effect of chronic hyperglycaemia and immediate insulin treatment on the composition of MAM.

The results showed significant intestinal region-dependent differences in the composition of the MAM microbiota in the control rats. In the duodenum, the abundance of the phylum Firmicutes predominated, followed by the phylum Proteobacteria. In the ileum, besides these two phyla, Bacteroidetes also emerged, and in the colon samples, the abundance of this latter phylum further increased. Although the relative abundance of Firmicutes decreased along the GI tract, at the level of lower taxonomic units, characteristic signs of increasing microbial diversity and rearrangement of the microbiota were evident.

Our previous results showed that in STZ-induced diabetes the duodenum was the only gut segment in which a decrease in the number of nitrergic myenteric neurons was not accompanied by a decrease in the total number of neurons (Izbeki et al. 2008), and the limited diabetes-related structural alterations in the mesenteric capillaries were completely prevented by insulin treatment (Bodi et al. 2012). Interestingly, the effect of hyperglycaemia on the composition of MAM was the most prominent in the duodenum, where a massive invasion of

the phylum Tenericutes (including class Mollicutes, genus *Mycoplasma*) was observed. The presence of the aerobic *Mycoplasma* in the diabetic duodenum is unexpected. The oxygen availability has been thoroughly mapped along the GI tract of murine animals and humans (Albenberg et al. 2014; He et al. 1999; Zheng et al. 2015; Zweier et al. 2003). The various methods employed in these studies gave somewhat fluctuating oxygen levels due to both longitudinal and radial oxygen gradients (Zheng et al. 2015). *Mycoplasma* was not detected in the duodenal lumen of the T1D rats (Wirth et al. 2014). *Mycoplasma* can adhere to and to fuse with epithelial and immune cells (Rajilic-Stojanovic and de Vos 2014). In addition, the steep oxygen gradient from the anaerobic lumen towards the richly vascularized mucosa may explain the diabetes associated *Mycoplasma* attack. Although *Mycoplasma* infection has been reported in rare enteropathy (Roca-Lema et al. 2019), in IBD (Chen et al. 2001) and Crohn's disease (Roediger and Macfarlane 2002; Roediger 2004), it has not been implicated with diabetes related inflammations before (Sicard et al. 2017). A recent paper showed higher abundance of the phylum Tenericutes (class Mollicutes) in obese rats as compared to their lean counterparts. Some representatives of Mollicutes have been shown to import certain types of carbohydrates common in westernized diet for both mice and humans (e.g., glucose, fructose, and sucrose) and to metabolize these imported sugars to short-chain fatty acids, which could be readily absorbed by the host (Yan et al. 2016). Studies proved that the intestinal dendritic cells and macrophages are hyporesponsive to pathogen-associated molecular patterns (de Oliveira et al. 2017), but when epithelial barrier breakdown occurs, like in diabetes (Li and Atkinson 2015; Vaarala et al. 2008), the pattern recognition receptors, which are present in innate immune cells, recognize gut microbiota and trigger an inflammatory cascade, proinflammatory cytokine secretion, and the activation of adaptive immune responses. The number of intestinal immune cells is the lowest in the duodenum (Mowat and Agace 2014), which may augment the inflammation and prevent myenteric neuronal loss in this intestinal segment even in the presence of the pronounced reorganization of the mucosa-associated microbiota. It is perhaps of great importance that insulin treatment eliminated the genus *Mycoplasma* from the diabetic duodenum. This indicates that among other therapeutic functions of insulin, it helps to restore the healthy anaerobic microbial community in the GI tract.

In the ileum, where a significant decrease in the total number of myenteric neurons is accompanied by severe structural damage of the mesenteric capillaries in rats with STZ-induced diabetes (Bodi et al. 2012; Izbeki et al. 2008), the abundance of the phylum Proteobacteria decreased moderately, but its composition changed strikingly (Wirth et al. 2014). The class Epsilonproteobacteria, including the microaerophilic genera *Helicobacter* and *Wolinella* was basically eradicated from the diabetic samples, whereas in the controls this class represented 10% of the Bacteria.

We suppose that the high number and the diversity of immune cells in the ileum contribute to the chronic hyperglycaemia-related alterations in this gut segment. The resident microbiota regulates the development of specific subsets of lymphocytes in the gut. T helper type 17 (Th17) lymphocytes are essential in defence against bacterial infections and play roles in autoimmune disease development by producing pro-inflammatory cytokines. It was observed that the so called segmented filamentous bacteria (genetic relatives of the genus *Clostridium*), promote the generation of Th17 cells and the induction of regulatory T cells in the gut (de Oliveira et al. 2017).

Significant myenteric neuronal loss was observed earlier in the diabetic colon, which was completely prevented by insulin treatment (Izbeki et al. 2008). Unlike the ileum, the structural alterations of the microvessels remained unchanged in insulin-treated rats relative to their diabetic counterparts (Bodi et al. 2012). In the control samples the phyla Firmicutes, Bacteroidetes and Proteobacteria predominated. In the diabetic colon, the abundances of the phyla Firmicutes and Proteobacteria decreased, as described in other studies (Emani et al. 2015), whereas that of the phylum Bacteroidetes increased relative to the control rats.

The important role of gut microbiota dysbiosis was demonstrated in driving enteric neurodegeneration in mice colon via Toll-like receptor 4 exhibiting increased plasma lipopolysaccharide concentrations (Anitha et al. 2016; Reichardt et al. 2017).

Similarly to previous data (Galley et al. 2014; Van den Abbeele et al. 2011), our results show that the MAM differed substantially from LAM (Wirth et al. 2014). The duodenum presented the most prominent difference between the mucosa-associated and luminal microbiota. Although the abundance of the phylum Firmicutes was similar in the MAM and LAM, the proportions of Lactobacillales (LAM 31% vs. MAM 2%), Actinobacteria (LAM 21% vs. MAM 4 %) and Clostridia (LAM 20% vs. MAM 67%) were different.

In the ileum the differences were also significant (Lactobacillales LAM: 55% vs. MAM 0%, Clostridia LAM 1% vs. MAM 64%, Bacteroidetes LAM 0% vs. MAM 6%, Proteobacteria LAM 33% vs. MAM 23%), whereas the slightest difference was observed in the colon (Lactobacillales LAM 5% vs. MAM 1%, Clostridia LAM 33% vs. MAM 37%, Bacteroidetes LAM 40% vs. MAM 35%).

The effect of immediate insulin treatment on the

composition of MAM had a significant beneficial effect in all investigated gut segments, although, like the LAM, the normal gut flora was not totally restored.

Conclusions

In comparison to our earlier results on the LAM (Wirth et al. 2014) with the new data reported here on the MAM along the GI tract in the same STZ-induced rat model of T1D, we conclude that chronic hyperglycaemia has the most prominent effect on the LAM in the ileum, whereas in the case of MAM major changes were encountered in the duodenum. The facultative anaerobe *Klebsiella* invasion of the ileum in LAM (Wirth et al. 2014) and a similar assault by the aerobic *Mycoplasma* in the MAM indicate that local perturbation of the anaerobic environment and microbiota may play important role in the autoimmune inflammation related to T1D. This environmental factor has not been considered before and should be considered in understanding the ethology and treatment of T1D as well as similar gastrointestinal inflammatory diseases. The results presented here also confirmed two previous assumptions. First, the composition of the intestinal microbiota did not change significantly in diabetes in the colon, where the diversity of bacteria is the highest in the entire GI tract, but it changed seriously in the small intestine, which has received less attention so far in spite of the obvious diagnostic and therapeutic consequences. The variations due to the disturbed physiological status are more pronounced in the small intestine due to the lower diversity of the community. The hyperglycaemia-related alterations of microbiota were region-specific in the small intestine and were distinctly affected by insulin replacement. Second, the investigation of both the LAM and the MAM is necessary for exploring the details of the alteration of the gut microbiota in different pathological states, such as T1D. A particular attention should be paid to the oxygen gradients developing in the diseased GI tracts.

With the detailed characterization of both the LAM and MAM in the various parts of the GI tract, the intriguing question remains: how does the microbiota contribute to malnutrition in the duodenum, intestinal inflammation in the ileum and colon, and cancer in the colon? Future studies must reveal the details of the sensitive crosstalk and delicate interactions between the members of the complex microbial community and the host's epithelial barrier and immune system to combat diseases such as T1D.

Acknowledgments

This study has been supported in part by the Hungarian National Research, Development and Innovation Fund projects GINOP-2.2.1-15-2017-00081, GINOP-2.3.3-15-2016-00006 and GINOP-2.2.1-15-2017-00033, and the Hungarian NKFIH fund projects PD132145 (R.W), FK123899 (G.M.), and FK131789 (N.B.). This work was also supported by the János Bolyai Research Scholarship (for G.M., M.B. and N.B.) of the Hungarian Academy of Sciences and ÚNKP-20-5 - New National Excellence Program of the Ministry for Innovation and Technology from the source of the National Research, Development and Innovation Fund (N.B.).

References

Albenberg L, Esipova TV, Judge CP, Bittinger K, Chen J, Laughlin A, Grunberg S, Baldassano RN, Lewis JD, Li H, Thom SR, Bushman FD, Vinogradov SA, Wu GD (2014) Correlation between intraluminal oxygen gradient and radial partitioning of intestinal microbiota. Gastroenterology 147:1055-1063 e8.

Anitha M, Reichardt F, Tabatabavakili S, Nezami BG, Chassaing B, Mwangi S, Vijay-Kumar M, Gewirtz A, Srinivasan S (2016) Intestinal dysbiosis contributes to the delayed gastrointestinal transit in high-fat diet fed mice. Cell Mol Gastroenterol Hepatol 2:328-339.

Bajaj JS, Hylemon PB, Ridlon JM, Heuman DM, Daita K, White MB, Monteith P, Noble NA, Sikaroodi M, Gillevet PM (2012) Colonic mucosal microbiome differs from stool microbiome in cirrhosis and hepatic encephalopathy and is linked to cognition and inflammation. Am J Physiol Gastrointest Liver Physiol 303:G675-685.

Bashir M, Prietl B, Tauschmann M, Mautner SI, Kump PK, Treiber G, Wurm P, Gorkiewicz G, Hogenauer C, Pieber TR (2016) Effects of high doses of vitamin D3 on mucosa-associated gut microbiome vary between regions of the human gastrointestinal tract. Eur J Nutr 55:1479-1489.

Bodi N, Talapka P, Poles MZ, Hermesz E, Jancso Z, Katarova Z, Izbeki F, Wittmann T, Fekete E, Bagyanszki M (2012) Gut region-specific diabetic damage to the capillary endothelium adjacent to the myenteric plexus. Microcirculation 19:316-326.

Chen W, Li D, Paulus B, Wilson I, Chadwick VS (2001) High prevalence of Mycoplasma pneumoniae in intestinal mucosal biopsies from patients with inflammatory bowel disease and controls. Dig Dis Sci 46:2529-2535.

Chermesh I, Shamir R (2009) The role of microbiota in inflammatory bowel disease. Annales Nestlé 67:27-38.

de Oliveira GLV, Leite AZ, Higuchi BS, Gonzaga MI, Mari-

ano VS (2017) Intestinal dysbiosis and probiotic applications in autoimmune diseases. Immunology 152:1-12.

Emani R, Alam C, Pekkala S, Zafar S, Emani MR, Hanninen A (2015) Peritoneal cavity is a route for gut-derived microbial signals to promote autoimmunity in non-obese diabetic mice. Scand J Immunol 81:102-109.

Flemer B, Gaci N, Borrel G, Sanderson IR, Chaudhary PP, Tottey W, O'Toole PW, Brugere JF (2017) Fecal microbiota variation across the lifespan of the healthy laboratory rat. Gut Microbes 8:428-439.

Galley JD, Yu Z, Kumar P, Dowd SE, Lyte M, Bailey MT (2014) The structures of the colonic mucosa-associated and luminal microbial communities are distinct and differentially affected by a prolonged murine stressor. Gut Microbes 5:748-760.

Gevers D, Kugathasan S, Denson LA, Vazquez-Baeza Y, Van Treuren W, Ren B, Schwager E, Knights D, Song SJ, Yassour M, Morgan XC, Kostic AD, Luo C, Gonzalez A, McDonald D, Haberman Y, Walters T, Baker S, Rosh J, Stephens M, Heyman M, Markowitz J, Baldassano R, Griffiths A, Sylvester F, Mack D, Kim S, Crandall W, Hyams J, Huttenhower C, Knight R, Xavier RJ (2014) The treatment-naive microbiome in new-onset Crohn's disease. Cell Host Microbe 15:382-392.

He G, Shankar RA, Chzhan M, Samouilov A, Kuppusamy P, Zweier JL (1999) Noninvasive measurement of anatomic structure and intraluminal oxygenation in the gastrointestinal tract of living mice with spatial and spectral EPR imaging. Proc Natl Acad Sci U S A 96:4586-4591.

Hu Y, Wong FS, Wen L (2017) Antibiotics, gut microbiota, environment in early life and type 1 diabetes. Pharmacol Res 119:219-226.

Izbeki F, Wittman T, Rosztoczy A, Linke N, Bodi N, Fekete E, Bagyanszki M (2008) Immediate insulin treatment prevents gut motility alterations and loss of nitrergic neurons in the ileum and colon of rats with streptozotocin-induced diabetes. Diabetes Res Clin Pract 80:192-198.

Jerram ST, Leslie RD (2017) The genetic architecture of type 1 diabetes. Genes (Basel) 8(8):209.

Kelly J, Daly K, Moran AW, Ryan S, Bravo D, Shirazi-Beechey SP (2017) Composition and diversity of mucosa-associated microbiota along the entire length of the pig gastrointestinal tract; dietary influences. Environ Microbiol 19:1425-1438.

Knip M, Honkanen J (2017) Modulation of type 1 diabetes risk by the intestinal microbiome. Curr Diab Rep 17:105.

Kugelberg E (2017) Microbiota: Diet can protect against type 1 diabetes. Nat Rev Immunol 17:279.

Lee IR, Sng E, Lee KO, Molton JS, Chan M, Kalimuddin S, Izharuddin E, Lye DC, Archuleta S, Gan YH (2017) Comparison of diabetic and non-diabetic human leukocytic responses to different capsule types of *Klebsiella pneumoniae* responsible for causing pyogenic liver abscess. Front Cell Infect Microbiol 7:401.

Li D, Chen H, Mao B, Yang Q, Zhao J, Gu Z, Zhang H, Chen YQ, Chen W (2017) Microbial biogeography and core microbiota of the rat digestive tract. Sci Rep 8:45840.

Li X, Atkinson MA (2015) The role for gut permeability in the pathogenesis of type 1 diabetes - a solid or leaky concept? Pediatr Diabetes 16:485-492.

Marino E, Richards JL, McLeod KH, Stanley D, Yap YA, Knight J, McKenzie C, Kranich J, Oliveira AC, Rossello FJ, Krishnamurthy B, Nefzger CM, Macia L, Thorburn A, Baxter AG, Morahan G, Wong LH, Polo JM, Moore RJ, Lockett TJ, Clarke JM, Topping DL, Harrison LC, Mackay CR (2017) Gut microbial metabolites limit the frequency of autoimmune T cells and protect against type 1 diabetes. Nat Immunol 18:552-562.

Matijašić M, Meštrović T, Paljetak HC, Perić M,Barešić A, Verbanac D (2020) Gut Microbiota beyond Bacteria—Mycobiome, Virome, Archaeome, and Eukaryotic Parasites in IBD. Int J Mol Sci 21:2668.

Meyer F, Paarmann D, D'Souza M, Olson R, Glass EM, Kubal M, Paczian T, Rodriguez A, Stevens R, Wilke A, Wilkening J, Edwards RA (2008) The metagenomics RAST server - a public resource for the automatic phylogenetic and functional analysis of metagenomes. BMC Bioinformatics 9:386.

Mishra SP, Wang S, Nagpal R, Miller B, Singh R, Taraphder S, Yadav H (2019) Probiotics and prebiotics for the amelioration of type 1 diabetes: Present and future perspectives. Microorganisms 7(3):67.

Mowat AM, Agace WW (2014) Regional specialization within the intestinal immune system. Nat Rev Immunol 14:667-685.

Paun A, Yau C, Danska JS (2017) The influence of the microbiome on type 1 diabetes. J Immunol 198:590-595.

Qi CJ, Zhang Q, Yu M, Xu JP, Zheng J, Wang T, Xiao XH (2016) Imbalance of fecal microbiota at newly diagnosed type 1 diabetes in Chinese children. Chin Med J (Engl) 129:1298-1304.

Rajilic-Stojanovic M, de Vos WM (2014) The first 1000 cultured species of the human gastrointestinal microbiota. FEMS Microbiol Rev 38:996-1047.

Randle-Boggis RJ, Helgason T, Sapp M, Ashton PD (2016) Evaluating techniques for metagenome annotation using simulated sequence data. FEMS Microbiol Ecol 92: fiw095.

Reichardt F, Chassaing B, Nezami BG, Li G, Tabatabavakili S, Mwangi S, Uppal K, Liang B, Vijay-Kumar M, Jones D, Gewirtz AT, Srinivasan S (2017) Western diet induces colonic nitrergic myenteric neuropathy and dysmotility in mice via saturated fatty acid- and lipopolysaccharide-induced TLR4 signalling. J Physiol 595:1831-1846.

Roca-Lema D, Martinez-Iglesias O, Fernandez de Ana Portela C, Rodriguez-Blanco A, Valladares-Ayerbes M,

Diaz-Diaz A, Casas-Pais A, Prego C, Figueroa A (2019) In vitro anti-proliferative and anti-invasive effect of polysaccharide-rich extracts from *Trametes versicolor* and *Grifola frondosa* in Colon Cancer Cells. Int J Med Sci 16:231-240.

Roediger WE (2004) Intestinal mycoplasma in Crohn's disease. Novartis Found Symp 263:85-93; discussion 93-98, 211-218.

Roediger WE, Macfarlane GT (2002) A role for intestinal mycoplasmas in the aetiology of Crohn's disease? J Appl Microbiol 92:377-381.

Sicard JF, Le Bihan G, Vogeleer P, Jacques M, Harel J (2017) Interactions of intestinal bacteria with components of the intestinal mucus. Front Cell Infect Microbiol 7:387.

Sommer F, Backhed F (2016) Know your neighbor: Microbiota and host epithelial cells interact locally to control intestinal function and physiology. Bioessays 38:455-464.

Tanca A, Palomba A, Fraumene C, Manghina V, Silverman M, Uzzau S (2018) Clostridial butyrate biosynthesis enzymes are significantly depleted in the gut microbiota of nonobese diabetic mice. 3(5):e00492-18.

Tian J, Li M, Lian F, Tong X (2017) The hundred most-cited publications in microbiota of diabetes research: A bibliometric analysis. Medicine (Baltimore) 96:e7338.

Vaarala O, Atkinson MA, Neu J (2008) The "perfect storm" for type 1 diabetes: the complex interplay between intestinal microbiota, gut permeability, and mucosal immunity. Diabetes 57:2555-2562.

Van den Abbeele P, Van de Wiele T, Verstraete W, Possemiers S (2011) The host selects mucosal and luminal associations of coevolved gut microorganisms: a novel concept. FEMS Microbiol Rev 35:681-704.

Wang Y, Devkota S, Musch MW, Jabri B, Nagler C, Antonopoulos DA, Chervonsky A, Chang EB (2010) Regional mucosa-associated microbiota determine physiological expression of TLR2 and TLR4 in murine colon. PLoS One 5:e13607.

Wirth R, Bodi N, Maroti G, Bagyanszki M, Talapka P, Fekete E, Bagi Z, Kovacs KL (2014) Regionally distinct alterations in the composition of the gut microbiota in rats with streptozotocin-induced diabetes. PLoS One 9:e110440.

Yan X, Feng B, Li P, Tang Z, Wang L (2016) Microflora disturbance during progression of glucose intolerance and effect of sitagliptin: An animal study. J Diabetes Res 2016:2093171.

Zheng L, Kelly CJ, Colgan SP (2015) Physiologic hypoxia and oxygen homeostasis in the healthy intestine. A review in the theme: cellular responses to hypoxia. Am J Physiol Cell Physiol 309:C350-360.

Zweier JL, He G, Samouilov A, Kuppusamy P (2003) EPR spectroscopy and imaging of oxygen: applications to the gastrointestinal tract. Adv Exp Med Biol 530:123-31.

Acta Biologica Szegediensis

Volume 65(1):85-92, 2021
Acta Biologica Szegediensis
http://abs.bibl.u-szeged.hu/index.php/abs
DOI:10.14232/abs.2021.1.85-92

ARTICLE

Insights on carbapenem-resistant *Acinetobacter baumannii*: phenotypic characterization of relevant isolates

Matthew Gavino Donadu[1,2], Stefania Zanetti[1], Ádám László Nagy[3], Ibrahim Barrak[4], Mário Gajdács[5,6]*

[1]Department of Biomedical Sciences, University of Sassari, Sassari, Italy
[2]Department of Chemistry and Pharmacy, University of Sassari, Sassari, Italy
[3]Department of Prosthodontics, Faculty of Dentistry, University of Szeged, Szeged, Hungary
[4]Department of Periodontology, Faculty of Dentistry, University of Szeged, Szeged, Hungary
[5]Department of Pharmacodynamics and Biopharmacy, Faculty of Pharmacy, University of Szeged, Szeged, Hungary
[6]Institute of Medical Microbiology, Faculty of Medicine, Semmelweis University, Budapest, Hungary

ABSTRACT *Acinetobacter baumannii* (*A. baumannii*) is an important nosocomial pathogen, which may be a causative agent in a wide-range of human pathologies. Carbapenems are usually considered the last safe and effective choice of drugs for the treatment of Gram-negative infections. The emergence of carbapenem-resistant *A. baumannii* (CRAB) is a critical public health issue as they leave clinicians with limited therapeutic options. In this study, phenotypic methods were used to characterize sixty-two (n = 62) *A. baumannii* isolates, which were included based on their suspected non-susceptibility to meropenem. Minimum inhibitory concentrations (MICs) of meropenem, levofloxacin, gentamicin, sulfamethoxazole/trimethoprim, tigecycline were determined using E-tests, while colistin MICs were determined using broth microdilution. The isolates were subjected to the modified Hodge test (MHT), the modified carbapenem-inactivation method (mCIM) and the imipenem/EDTA combined disk test (CDT). Efflux pump overexpression was studied using agar plates containing phenylalanine-arginine β-naphthylamide (PAβN). Assessment of biofilm-formation was carried out using the crystal violet tube-adherence method. 64.5% of the strains showed meropenem MICs in the resistant range (>8 mg/L), resistance rates were similarly high to the other tested antibiotics. The MHT and mCIM assay were positive in 79.0% and 67.7% of cases, respectively; the presence of an MBL was suggested for 29.0% of isolates. Efflux-pump overexpression was seen in 12.9% of isolates. 54.8% of the isolates were characterized as strong biofilm-producers. Microbiology laboratories have an important role in differentiating the distinct mechanisms by which these pathogens develop the CRAB phenotype, as plasmid-borne carbapenemases are significant from the standpoint of public health microbiology.

Acta Biol Szeged 65(1):85-92 (2021)

KEY WORDS
Acinetobacter
antibiotic
biofilm
carbapenem
carbapenem-resistance
efflux pump
phenotypic assay

ARTICLE INFORMATION
Submitted
11 May 2021.
Accepted
28 July 2021.
***Corresponding author**
E-mail: mariopharma92@gmail.com

Introduction

The introduction of penicillin G, the first β-lactam antibiotic in the 1940s has been a hallmark in the history of medicine, as this drug (and the subsequent iterations of β-lactam antibiotics that later followed) allowed for the treatment of life-threatening infections, that were previously considered lethal (Lobanovska and Pilla 2017; Erdem et al. 2011). In addition, antibiotics have indirectly pawed the way for the development of many modern medical disciplines, including complex surgery, transplantation medicine, cancer chemotherapy, neonatology, and the treatment of sepsis (Gajdács 2019; van Duin and Paterson 2016). β-lactams are bactericidal drugs that include penicillin-derivatives, cephalosporins, carbapenems and monobactams; β-lactams are often preferred as first-choice agents in many clinical situations, due to their safety, tolerability, and overall clinical efficacy (Papp-Wallace et al. 2011; El-Gamal et al. 2017). Out of this antimicrobial group, carbapenems (namely imipenem, meropenem, ertapenem and doripenem) have some of the broadest spectrum of activity, being effective in the therapy of infections caused by a plethora of aerobic and anaerobic pathogens (Gajdács et al. 2020). The increasing emergence of antimicrobial resistance (AMR) in bacteria has become one of the most critical public health issues of the 21st century (Medina and Pieper 2016); many trans-national public health organizations have expressed their concerns over the worsening situation, including the European Centers

for Disease Prevention and Control (ECDC), estimating that drug-resistant bacteria are responsible for over 400 000 infections and 25 000 excess deaths annually in the EU alone (ECDC 2009). In a similar report the US Centers for Disease Control (CDC) has projected over two million multidrug-resistant (MDR) infections and 23 000 excess deaths per year (CDC 2020). The phenomenon of AMR may be characterized by two important hallmarks: a) disinterest of pharmaceutical companies towards the development of antimicrobial drugs (due to the lack of returning investments and difficulties in attaining marketing authorization) (Cannas et al. 2015; Chaves-López et al. 2018; Gajdács and Spengler 2019; Usai et al. 2019), and b) the inappropriate use of existing antimicrobials, including their prescription in inappropriate indications, their non-prescription sales (especially from informal healthcare-providers) and their use in self-medication by patients to relieve symptoms (Aslam et al. 2020; Gajdács et al. 2018; Grigoryan et al. 2019). The latter issue is especially critical, as the consumption of antibiotics have been directly linked to the emergence of increasing resistance rates (Johnson 2005; Olesen et al. 2018).

Non-fermenting Gram-negative bacteria (NFGNB) are a heterogenous group of aerobic microorganisms within the Proteobacteria phylum, characterized by the incapacity to ferment sugars (e.g., glucose, maltose) to generate energy for their vital cellular functions (Enoch et al. 2007). From a clinical perspective, the most relevant pathogens among NFGNB include species from the *Acinetobacter baumannii-calcoaceticus* (ABC) complex (consisting of *A. baumannii*, *A. calcoaceticus*, *A. nosocomilalis*, and *A. pitti*), *Pseudomonas aeruginosa*, *Burkholderia cepacia* complex (BCC) and *Stenotrophomonas maltophilia* (Enoch et al. 2007; Gajdács et al. 2019). Due to their adaptability to various ecological niches, NFGNB are often isolated from natural sources, such as aquatic environments, the soil and as plant pathogens (Chawla et al. 2013). *A. baumannii* is one of the most important nosocomial pathogens – possessing the ability to withstand harsh environmental conditions and to persist in healthcare facilities for months in a protective biofilm (often leading to inter- and intra-hospital outbreaks) – which may be a causative agent in a wide-range of pathologies, including respiratory tract infections, bacteraemia/sepsis, meningitis, surgical site and wound infections and urinary tract infections (Sarshar et al. 2021). In addition to being intrinsically resistant to several antibiotics, *A. baumannii* also has the propensity to acquire resistance-determinants against a wide range of antibiotic classes (Bonomo and Szabó 2006). The development of extensively drug resistant (XDR) or even pandrug-resistant (PDR) strains of *A. baumannii* severely limits the therapeutic options of clinicians, often forcing them to turn to antimicrobials with pronounced toxicity (Rangel et al. 2020); these infections are often characterized by high mortality rates (a recent meta-analysis has reported that 79.9% of *A. baumannii* causing hospital-associated pneumonia (HAP) or ventilation-associated pneumonia (VAP) was MDR, with an overall mortality rate of 42.6% (95% CI, 37.2-48.1%)) (Lim et al. 2019).

Carbapenems have been considered a safe and effective alternative in the therapy of *A. baumannii* infections; however, the rising incidence of carbapenem-resistant *A. baumannii* (CRAB) is a critical concern, which has been facilitated by the sharp increase in the use of carbapenem antibiotics (brought on by the high prevalence of extended-spectrum β-lactamase-producing (ESBL) *Enterobacteriaceae*) and the successful spread of several international clones (Codjoe and Donkor 2018; Frakking et al. 2013; Makharita et al. 2020; Matsui et al. 2018). As CRAB-associated infections often lead to therapeutic failure, clinical microbiology laboratories have pivotal roles in the detection of these isolates, both from a clinical and an infection control perspective (to limit their spread); although molecular techniques (polymerase chain reaction, whole-genome sequencing) are the gold standard in the characterization of suspected CRAB isolates, these techniques are expensive and not always readily attainable by routine laboratories (Bua et al. 2018).

The aim of our present laboratory-based study was to characterize a selection of carbapenem non-susceptible *A. baumannii* isolates using various phenotypic methods – which are available in most routine clinical microbiology laboratories – and to provide insights into the epidemiological features of these pathogens.

Materials and methods

Bacterial strains

A total of sixty-two (n = 62) *A. baumannii* isolates were included in this study, which were kindly provided by various Hungarian and Italian hospitals, originating from different clinical materials. Inclusion of these strains was based on the non-susceptibility criteria to meropenem (MER) used in routine clinical microbiology, defined by EUCAST (European Committee on Antimicrobial Susceptibility Testing) guidelines v.9.0 (MER disk diameter 23-21 mm: intermediate, <21 mm: resistant) (https://www.eucast.org/clinical_breakpoints/). Identification of the isolates was carried out based on classical phenotypic and biochemical panel-based methods (Leber 2016). All isolates included in the study were re-identified as *A. baumannii* before further assays. For shorter time periods (<1 month), the bacterial strains were maintained on blood agar with continuous passage. For longer periods, the strains were kept in a -80 °C freezer, in a 1:4 mixture of

Table 1. MIC values of meropenem and ancillary antibiotics on the tested bacterial strains.

	Resistant strains (n, %)	MIC range (mg/L)	MIC50 (mg/L)	MIC90 (mg/L)
Meropenem (MER)	40 (64.5%)	0.5-64	8	32
Levofloxacin (LEV)	42 (67.7%)	0.125-16	2	4
Sulfamethoxazole/trimethoprim (SXT)	33 (53.2%)	0.064-16	2	4
Gentamicin (GEN)	28 (45.2%)	0.5-64	2	16
Tigecycline (TIG)	28 (45.2%)	0.125-8	0.5	2
Colistin (COL)	0 (0%)	0.128-2	0.5	1

85% glycerol and liquid Luria-Bertani medium. During our experiments *A. baumannii* ATCC 19606 was used as a control strain.

Minimum inhibitory concentrations (MICs) of meropenem and ancillary antibiotics

MICs of MER, gentamicin (GEN), levofloxacin (LEV), sulfamethoxazole/trimethoprim (SXT) and tigecycline (TIG) were determined by E-tests (Liofilchem, Roseto degli Abruzzi, Italy) on Mueller-Hinton agar plates (Oxoid, Basingstoke, UK). MIC determination for colistin (COL) was carried out using the broth microdilution method in cation-adjusted Mueller-Hinton broth (MERLIN Diagnostika, Berlin, Germany). The interpretation of the results was based on the European Committee on Antimicrobial Susceptibility Testing (EUCAST) breakpoints v.9.0 (https://www.eucast.org/clinical_breakpoints/). In case of TIG, epidemiological cut-off values were used for interpretation (MIC≤0.5 mg/L as susceptible, MIC>0.5 mg/L as resistant) (Gajdács et al. 2020).

Phenotypic detection of carbapenemase and metallo-β-lactamase production

To establish carbapenemase-production in the isolates included in the study, the isolates were subjected to the modified Hodge test (MHT) and the modified carbapenem-inactivation method (mCIM), optimized for *A. baumannii*, as previously described (Chou et al. 2020; Pitout et al. 2008; Rao et al. 2019). In both assays, MER disks (10 μg; Oxoid, Basingstoke, UK) were utilized and *Escherichia coli* ATCC 25922 was used as an indicator organism.

Metallo-β-lactamase (MBL) production was tested using the imipenem/EDTA combined disk test (CDT), as described previously (Makharita et al. 2020). In preparation to this assay, imipenem/EDTA disks were prepared by adding 750 μg of a sterile 0.5 M EDTA solution to a 10 μg imipenem disk, then disks were dried in a 37 °C incubator. The assay was considered positive if the inhibition zone diameter (≥17 mm) of the imipenem/EDTA disk increased compared to the imipenem disk alone (Makharita et al. 2020).

Phenotypic detection of efflux pump overexpression

The effect of phenylalanine-arginine β-naphthylamide (PAβN; a compound with well-known efflux pump inhibitory activity) on the MICs of MER was detected using the agar dilution method described previously (Khalili et al. 2019). During the experiments, the concentration of PAβN was 40 μg/mL in the agar base. A two-fold decrease in MER MICs in the presence of PAβN, compared to the MIC values without the inhibitor, was considered as positivity for efflux pump overexpression (Khalili et al. 2019; Gajdács 2020).

Detection of biofilm-production by the tube-adherence method

Assessment of biofilm-formation was carried out in the tube-adherence method described previously (Dumaru et al. 2019; Behzadi et al. 2020). In short, glass tubes containing 1 mL of sterile trypticase soy broth (bioMérieux, Marcy-l'Étoile, France) were inoculated with 1 μL of the overnight culture of a respective bacterial strains. Respective tubes were then incubated statically for 24 h at 37 °C. Verification of planktonic growth was observed visually. After the incubation period, the supernatant was then discarded, the adhered cells were rinsed three times with phosphate buffer saline (PBS; Sigma-Aldrich; Budapest, Hungary) and the tubes were patted dry on a paper towel. The contents of the tubes were treated with a 1 mL solution of 0.1% crystal violet (CV; Sigma-Aldrich, Budapest, Hungary) to stain the adhered biomass; the tubes were incubated for 3 h at room temperature with the staining solution. The CV solution was then discarded, the tubes were again rinsed three times with PBS and finally, they were patted dry on a paper towel. Biofilm-formation was observed visually; based on the appearance of visible biofilm lining at the bottom and on wall of the glass tubes, the strains were classified as non-biofilm producers (-), weak biofilm producers (-/+) and strong biofilm producers (+) (Dumaru et al. 2019). All experiments were evaluated by two independent researchers.

Statistical analysis

Descriptive statistical analysis (including means and

percentages to characterize data) was performed using Microsoft Excel 2013 (Microsoft, Redmond, WA, USA).

Ethical considerations

The study was conducted in accordance with the Declaration of Helsinki and national and institutional ethical standards. Ethical approval for the study protocol was obtained from the Human Institutional and Regional Biomedical Research Ethics Committee, University of Szeged (registration number: 140/2021-SZTE [5019]).

Results

MICs of the tested antibiotics

The MICs of the tested antibiotics, including MIC_{50}, MIC_{90} values, MIC ranges and the percentage of resistant isolates are presented in Table 1. Among the tested ancillary antibiotics, the highest levels of resistance were observed for LEV (n = 42, 67.7%) and SXT (n = 33, 53.2%). All tested isolates were susceptible to COL, with MIC values ranging between 0.128 and 2 mg/L. Based on EUCAST breakpoints, n = 40 (64.5%) of isolates showed MICs above the resistance breakpoint for MER (8 mg/L), with MICs ranging between 0.5 and 64 mg/L.

Phenotypic detection of carbapenemase, MBL production and efflux pump overexpression

Phenotypic detection of carbapenemases was carried out via the use of the modified Hodge test (MHT) and the modified carbapenem-inactivation (mCIM) method. Overall, n = 49 (79.0%) and n = 42 (67.7%) of tested isolates were positive for phenotypic detection of carbapenemases in the MHT and mCIM assays, respectively. If we consider the results of the antibiotic susceptibility testing (MER MIC > 8 mg/L) as a reference in our study, the agreement between the results of the MIC determination and the results of the MHT and mCIM tests were 81.6% and 95.2%. MBL-production was observed in n = 18 (29.0%) using the imipenem/EDTA combined disk test (CDT). Efflux pump-overexpression (based on the PAβN screening agar) was detected in n = 8 (12.9%) of isolates. In the case of n = 3 isolates, efflux pump-overexpression and MHT/mCIM-positivity were detected simultaneously, which was associated with high MICs for MER. Interestingly, for n=3 isolates, high MER MICs were seen with no efflux pump overexpression and negative results in the MHT and mCIM tests.

Biofilm-production in the tested isolates

Out of the sixty-two (n = 62) isolates included in this study, over half (n = 34, 54.8%) was found to be a strong biofilm-producer (+); on the other hand, weak biofilm-producers (-/+) (n = 16; 25.1%) and non-biofilm-positive isolates (-) (n = 12; 20.1%) were seen in similar numbers.

Discussion

AMR is global public health concern, which warrants intersectoral attention, including the public, healthcare-professionals, and government leaders; worsening resistance rates threaten the administration of effective therapy in both humans and animals, in addition to hindering the attainment of Sustainable Development Goals (SDGs) (Gajdács et al. 2021; United Nations 2020). Carbapenems are broad-spectrum agents that are usually considered the last safe and effective choice of drugs for the treatment of MDR Gram-negative infections in many patient populations, especially for the empirical therapy of patients in severe conditions, e.g., in the intensive care unit (cf. fluoroquinolones and aminoglycosides may be contraindicated for many individuals) (Doi 2019). *A. baumannii* can rapidly colonize patients in nosocomial settings, which may be a source of future infections, especially in immunocompromised individuals (Mirzaei et al. 2020). Increased levels of carbapenem-consumption – both locally and globally – has led to the increased prevalence of CRAB (Behzadi and Behzadi 2011; Mózes et al. 2014); based on the data of the ECDC Surveillance Atlas of Infectious Diseases (https://atlas.ecdc.europa.eu/public/index.aspx), the ratio of CRAB isolates in 2014 Hungary and Italy were 64.5% and 89.9%, respectively; this ratio has decreased over a 5-year period (2019), being 51.0% and 79.2% in the same countries. However, the rates of combined resistance (i.e. resistance against fluoroquinolones, aminoglycosides and carbapenems) has increased substantially in Hungary between the 5-year period (2014: Hungary: 38.4%, Italy: 86.3%; 2019: Hungary: 45.6%, Italy: 76.5%). The significance of this was underlined when the World Organization published a list of priority pathogens consisting of MDR bacteria, in which CRAB was categorized as a critical pathogen with highest urgency for the development of novel antimicrobials and alternative antimicrobial treatment strategies (e.g., antimicrobial peptides, photodynamic therapy, phages) (Liu et al. 2020; Stájer et al. 2020; WHO 2017).

In our present study, a collection of *A. baumannii* isolates – suspected of being CRAB – were included and their characterization was carried out using various phenotypic assays. Among the isolates, 64.5% of the strains showed MER MICs in the resistant range, while apart from COL (which retained its susceptibility), resistance rates were similarly high to the other tested antibiotics. Phenotypic carbapenemase detection methods were positive in 79.0% (MHT) and 67.7% (mCIM) of cases, respectively, while the

presence of an MBL was suggested for 29.0% of isolates. Efflux-pump overexpression seemed to be less relevant in the CRAB phenotype, with 12.9% being positive in the plate-based *in vitro* assay. Lastly, over half (54.8%) of the isolates were characterized as strong biofilm-producers.

Carbapenem resistance in *A. baumannii* may be mediated by mutations affecting the penicillin-binding proteins (PBPs), mutations in the porin channels (reducing the transport of antibiotics into the periplasmic space) and over-expression of efflux pumps (e.g., AdeABC) (Makharita et al. 2020; Miljovic et al. 2016); however, the most well-characterized mechanism of resistance in these pathogens is the production of β-lactamase enzymes (carbapenemases), capable of hydrolyzing these last-resort drugs (Bonomo and Szabó 2006; Butler et al. 2019; Makharita et al. 2020). When it comes to *A. baumannii*, Ambler Class D (OXA-type) carbapenemases are the most relevant (Bonomo and Szabó 2006; Butler et al. 2019; Halat and Mourbareck 2020; Makharita et al. 2020); nevertheless, there have been increasing number of reports of resistance mediated by some Class A (KPC) and Class B (VIM, NDM) carbapenemases as well (Halat and Mourbareck 2020; Rodríguez et al. 2018). Most clinical *A. baumannii* isolates harbor a chromosomal blaOXA-51-like carbapenemase; however, presence of this enzyme will only lead to phenotypic carbapenem resistance in conjunction with other resistance determinants (Bonomo and Szabó 2006; Butler et al. 2019; Halat and Mourbareck 2020; Makharita et al. 2020). The carriage of plasmid-borne blaOXA-23-like and blaOXA-58-like carbapenemases is more relevant both for phenotypic resistance and for the potential dissemination in a given healthcare setting/region (Bonomo and Szabó 2006; Halat and Mourbareck 2020; Makharita et al. 2020). In many clinical isolates, the combination of the above-mentioned resistance mechanisms – in addition to the pharmacokinetic barrier provided by the protective biofilm *in vivo* – may result in high MIC values for carbapenems (Cunda et al. 2019; Halat and Mourbareck 2020). Microbiology laboratories have an important role in differentiating the distinct mechanisms by which these pathogens develop the CRAB phenotype, because – as opposed to isolates with chromosomal mutations – isolates carrying plasmid-borne carbapenemases have significance from the standpoint of public health microbiology (Makharita et al. 2020). While there have been renewed interest in the use of tetracycline-type drugs (i.e. tigecycline, eravacycline, omadacycline), in case of carbapenem-resistance, COL is often the only remaining therapeutic option (Butler et al. 2019; Qureshi et al. 2015); this drug is a polycationic peptide, which is given intravenously, leading to the disruption of the outer cell membrane in the relevant pathogens (i.e. displacing bivalent cations), and subsequent bacterial cell death. Nevertheless, COL has severe adverse events (nephrotoxicity, neurotoxicity) and disadvantageous pharmacokinetic properties, which may limit its usefulness in critically ill patients (Gajdács et al. 2020). In addition, the number reports on COL-resistance are increasingly common around the globe, both regarding the members of the *Enterobacteriaceae* family and for NFGNBs (Butler et al. 2019; Qureshi et al. 2015); for example, in the EuSCAPE Survey (European survey of carbapenemase-producing *Enterobacteriaceae*), COL resistance in carbapenem-resistant *E. coli* and *Klebsiella* spp. was 28.3% (Grundmann et al. 2016). On the other hand, surveillance studies in the US have shown that prevalence of CRAB strains ranged between 33%-58%, which has corresponded to a ~5% resistance to COL (Hidron et al. 2008; Queenan et al. 2012). The present epidemiological situation highlights the important role of antimicrobial resistance surveillance (both on a national and an international level) and stewardship interventions to preserve the efficacy of carbapenem antibiotics for future use.

Acknowledgements

M.G. was supported by the János Bolyai Research Scholarship (BO/00144/20/5) of the Hungarian Academy of Sciences. The research was supported by the ÚNKP-20-5-SZTE-330 New National Excellence Program of the Ministry for Innovation and Technology from the source of the National Research, Development and Innovation Fund. Support from Ministry of Human Capacities, Hungary grant 20391-3/2018/FEKUSTRAT is acknowledged. M.G. would also like to acknowledge the support of ESCMID's "30 under 30" Award.

References

Aslam A, Gajdács M, Zin CS, Ab RNS, Ahmed SI, Zafar MZ, Jamshed S (2020) Evidence of the practice of self-medication with antibiotics among the lay public in low- and middle-income countries: A scoping review. Antibiotics 9:e597.

Behzadi P, Behzadi E (2011) A study on apoptosis inducing effects of UVB irradiation in *Pseudomonas aeruginosa*. Roum Arch Microbiol Immunol 70:74-77.

Bua A, Usai D, Donadu M, Ospina DJ, Paparella A, Chavez-Lopez C, Serio A, Rossi C, Zanetti S, Molicotti P (2017) Antimicrobial activity of *Austroeupatorium inulaefolium* (H.B.K.) against intracellular and extracellular organisms. Nat Prod Res 32:2869-2871.

Bonomo RA, Szabó D (2006) Mechanisms of multidrug resistance in *Acinetobacter* species and *Pseudomonas ae-*

ruginosa. Clin Infect Dis 43:S49-S56.
Butler DA, Biagi M, Tan X, Qasmieh S, Bulman ZP, Wenzler E (2019) Multidrug resistant *Acinetobacter baumannii*: Resistance by any other name would still be hard to treat. Curr Infect Dis Rep 21:e46.
Cannas S, Usai D, Pinna A, Benvenuti S, Tardugno R, Donadu M, Zanetti S, Kaliamurthy J, Molicotti P (2015) Essential oils in ocular pathology: an experimental study. J Infect Dev Ctries 9:650-654.
CDC Antibiotic/Antimicrobial Resistance (AR/AMR) (2020) Available online: https://www.cdc.gov/drugresistance/biggest_threats.html (accessed on 9 May 2021).
Chawla K, Vishwanath S, Munim FC (2013) Nonfermenting gram-negative bacilli other than *Pseudomonas aeruginosa* and *Acinetobacter* spp. causing respiratory tract infections in a tertiary care center. J Glob Infect Dis 5:144-148.
Chaves-López C, Usai D, Donadu M, Serio A, González-Mina RT, Simeoni MC, Molicotti P, Zanetti S, Pinna A, Paparella A (2018) Potential of *Borojoa patinoi* Cuatrecasas water extract to inhibit nosocomial antibiotic resistant bacteria and cancer cell proliferation in vitro. Food Funct 9:2725-2734.
Chou CH, Lai YR, Chi CY, Ho MW, Chen CL, Liao WC, Ho CH, Chen YA, Chen CY, Lin YT, Lin CD, Lai CH (2020) Long-term surveillance of antibiotic prescriptions and the prevalence of antimicrobial resistance in non-fermenting gram-negative bacilli. Microorganisms 8:e397.
Codjoe FS, Donkor ES (2018) Carbapenem resistance: a review. Med Sci 6:e1.
Cunda P, Iribarnegaray V, Papa-Ezdra R, Bado I, González MJ, Zunino P, Vignoli R, Scavone P (2020) Characterization of the different stages of biofilm formation and antibiotic susceptibility in a clinical *Acinetobacter baumannii* strain. Microbial Drug Res 26:569-575.
Doi Y (2019) Treatment options for carbapenem-resistant gram-negative bacterial infections. Clin Infect Dis 69:S565-S575.
Dumaru R, Baral R, Shrestha LB (2019) Study of biofilm formation and antibiotic resistance pattern of gram-negative bacilli among the clinical isolates at BPKIHS, Dharan. BMC Res Notes 12:e38.
ECDC/EMEA joint technical report. The bacterial challenge: Time to react (2009) Available online: https://www.ecdc.europa.eu/en/publications-data/ecdcemea-joint-technical-report-bacterial-challenge-time-react (accessed on 9 May 2021).
El-Gamal MI, Brahim I, Hisham N, Aladdin R, Mohammed H, Bahaaeldin A (2017) Recent updates of carbapenem antibiotics. Eur J Med Chem 131:185–95.
Enoch DA, Birkett CI, Ludlam HA (2007) Non-fermentative gram-negative bacteria. Int J Antimicrob Agents 29:S33-S41.
Erdem H, Tetik A, Arun O, Besirbellioglu BA, Coskun O, Eyigun CP (2011) War and infection in the pre-antibiotic era: The third Ottoman army in 1915. Scand J Infect Dis 43:690-695.
Frakking FNJ, Rottier WC, Dorigo-Zetsma W, van Hattem JMA, van Hees BC, Klutymans JAWJN, Lutgens SPM, Prins JM, Thijsen SFT, Verbon A, Vlaminckx BJM, Stuart JWC, Hall MAL, Bonten MJM (2013) Appropriateness of empirical treatment and outcome in bacteremia caused by extended-spectrum-b-lactamase-producing bacteria. Antimicrob Agent Chemother 57:3092-3099.
Gajdács M (2019) [Excess mortality due to pandrug resistant bacteria: a survey of the literature]. Hung Health Prom J 60:29-34.
Gajdács M (2020) Carbapenem-resistant but cephalosporin-susceptible *Pseudomonas aeruginosa* in urinary tract infections: Opportunity for colistin sparing. Antibiotics 9:e153.
Gajdács M, Ábrók M, Lázár A, Jánvári L, Tóth Á, Terhes G, Burián K (2020) Detection of VIM, NDM and OXA-48 producing carbapenem resistant Enterobacterales among clinical isolates in Southern Hungary. Acta Microbiol Immunol Hung 67:209-215.
Gajdács M, Burián K, Terhes G (2019) Resistance levels and epidemiology of non-fermenting gram-negative bacteria in urinary tract infections of inpatients and outpatients (RENFUTI): A 10-year epidemiological snapshot. Antibiotics 8:e143.
Gajdács M, Paulik E, Szabó A (2018) [The opinion of community pharmacists related to antibiotic use and resistance]. Acta Pharm Hung 88:249-252.
Gajdács M, Spengler G (2019) The role of drug repurposing in the development of novel antimicrobial drugs: Non-antibiotic pharmacological agents as quorum sensing-inhibitors. Antibiotics 8:e270.
Gajdács M, Urbán E, Stájer A, Baráth Z (2021) Antimicrobial resistance in the context of the sustainable development goals: A brief review. Eur J Investig Health Psychol Educ 11:71-82.
Grigoryan L, Germanos G, Zoorob R, Juneja S, Raphael JL, Paasche-Orlow MK (2019) Use of antibiotics without a prescription in the U.S. population: A scoping review. Ann Int Med 171:257-263.
Grundmann H, Glasner C, Albiger B, Aanensen DM, Tomlinson TC, Andrasevic AT, Canton R, Carmeli Y, Friedrich AW, Giske CG, Glupczyski Y, Gniadowski M, Livermore DM, Nordman P, Poirel L, Rossolini GM, Seifert H, Vatopoulous A, Walsh T, Woodford N, Monnet D, European survey of carbapenemase-producing *Enterobacteriaceae* (EuSCAPE) working group (2017) Occurrence of carbapenemase-producing *Klebsiella pneumoniae* and *Escherichia coli* in the european survey of carbapenemase-producing *Enterobacteriaceae* (EuSCAPE): a prospective, multinational study. Lancet Infect Dis 17:153-163.

Halat DH, Moubareck CA (2020) The current burden of carbapenemases: Review of significant properties and dissemination among gram-negative bacteria. Antibiotics 9:e186.

Hidron AI, Edwards JR, Patel J, Horan TC, Sievert DM, Pollock DA, Fridkin SK, National Healthcare Safety Network Team, Participating National Healthcare Safety Network Facilities (2008) NHSN annual update: antimicrobial-resistant pathogens associated with healthcare-associated infections: annual summary of data reported to the National Healthcare Safety Network at the Centers for Disease Control and Prevention, 2006-2007. Infect Control Hosp Epidemiol 29:996-1011.

Johnson A (2005) Outpatient consumption of antibiotics is linked to antibiotic resistance in Europe: results from the European surveillance of antimicrobial consumption. Euro Surveill 10:e050224.5

Khalili Y, Yekani M, Goli HR, Memar MY (2019) Characterization of carbapenem-resistant but cephalosporin-susceptible *Pseudomonas aeruginosa*. Acta Microbiol Immunol Hung 66:529-540.

Leber AL (Ed.) (2016) Clinical Microbiology Procedures Handbook. 4th ed.; ASM Press, Washington, DC, USA; ISBN 978-1-55581-880-7.

Lim SMS, Abidin AZ, Liew SM, Roberts JA, Sime FB (2019) The global prevalence of multidrug-resistance among *Acinetobacter baumannii* causing hospital-acquired and ventilator-associated pneumonia and its associated mortality: A systematic review and meta-analysis. J Infect 79:593-600.

Liu W, Wu Z, Mao C, Guo G, Zeng Z, Fei Y, Wan S, Peng J, Wu J (2020) Antimicrobial peptide cec4 eradicates the bacteria of clinical carbapenem-resistant *Acinetobacter baumannii* biofilm. Front Microbiol 11:e1532.

Lobanovska M, Pilla G (2017) Penicillin's discovery and antibiotic resistance: Lessons for the future? Yale J Biol Med 90:135-145.

Makharita RR, El-Kholy I, Hetta HL, Abdelaziz MH, Hagagy FI, Ahmed AA, Algammal AM (2020) Antibiogram and genetic characterization of carbapenem-resistant gram-negative pathogens incriminated in healthcare-associated infections. Infect Drug Res 13:3991-4002.

Matsui M, Suzuki M, Suzuki M, Yatsuyanagi J, Watahiki M, Hiraki Y, Kawano F, Tsutsui A, Shibayama K, Suzuki S (2018) Distribution and molecular characterization of *Acinetobacter baumannii* international clone II lineage in Japan. Antimicrob Agents Chemother 62:e02190-17.

Medina E, Pieper DH (2016) Tackling threats and future problems of multidrug-resistant bacteria. Curr Top Microbiol Immunol 398:3-33.

Miljovic G, Pejakov L, Vujosevic D (2016) Antibiotic susceptibility of *Acinetobacter* species in intensive care unit in Montenegro. J Chemother 28:273-276.

Mirzaei B, Bazgir ZN, Goli HR, Iranpour F, Mohammadi F, Babei R (2020) Prevalence of multi-drug resistant (MDR) and extensively drug-resistant (XDR) phenotypes of *Pseudomonas aeruginosa* and *Acinetobacter baumannii* isolated in clinical samples from Northeast of Iran. BMC Res Notes 13:e380.

Mózes J, Ebrahimi F, Gorácz O, Miszti C, Kardos G (2014) Effect of carbapenem consumption patterns on the molecular epidemiology and carbapenem resistance of *Acinetobacter baumannii*. J Med Microbiol 63:1654-1662.

Olesen SW, Barnett ML, MacFadden DR, Brownstein JS, Hernández-Díaz S, Lipsitch M, Grad YH (2018) The distribution of antibiotic use and its association with antibiotic resistance. eLife 7:e39435.

Papp-Wallace KM, Endimiani A, Taracila MA, Bonomo RA (2011) Carbapenems: past, present, and future. Antimicrob Agent Chemother 55:4943-4960.

Pitout JD Revathi G, Chow BL, Kabera B, Kariuki S, Nordmann P, Poirel L (2008) Metallo-β-lactamase-producing *Pseudomonas aeruginosa* isolates in Tunisia. Clin Microbiol Infect 14:755-759.

Queenan AM, Pillar CM, Deane J, Sahm DF, Lynch AS, Flamm RK, Peterson J, Davies TA (2012) Multidrug resistance among *Acinetobacter* spp. in the USA and activity profile of key agents: results from CAPITAL Surveillance 2010. Diagn Microbiol Infect Dis 73:267-270.

Quoreshi ZA, Hittle LE, O'Hara JA, Rivera JI, Syed A, Shields RK, Pasculle AW, Ernst RK, Doi Y (2015) Colistin-resistant *Acinetobacter baumannii*: Beyond carbapenem resistance. Clin Infect Dis 60:1295-1303.

Rao MR, Chandrashaker P, Mahale RP, Shivappa SG, Gowda RS, Chitharagi VB (2019) Detection of carbapenemase production in *Enterobacteriaceae* and *Pseudomonas* species by carbapenemase Nordmann–Poirel test. J Lab Physicians 11:107-110.

Rangel K, Lechuga GC, Souza ALA, da Silva Carvalho JPR, Bos MHSV, De Simone SG (2020) Pan-drug resistant *Acinetobacter baumannii*, but not other strains, are Rresistant to the bee venom peptide melittin. Antibiotics 9:e178.

Rodríguez CH, Nastro M, Famiglietti A (2018) Carbapenemases in *Acinetobacter baumannii*. Review of their dissemination in Latin America. Rev Argent Microbiol 50:327-333.

Sarshar M, Behzadi P, Scribano D, Palamara AT, Ambrosi C (2021) *Acinetobacter baumannii*: An ancient commensal with weapons of a pathogen. Pathogens 10:e387.

Senobar Tahaei SA, Stájer A, Barrak I, Ostorházi E, Szabó D, Gajdács M (2021) Correlation between biofilm-formation and the antibiotic resistant phenotype in *Staphylococcus aureus* isolates: A laboratory-based study in Hungary and a review of the literature. Infect Drug Res 14:1155-1168.

Stájer A, Kajári S, Gajdács M, Musah-Eroje M, Baráth Z (2020) Utility of photodynamic therapy in dentistry:

Current concepts. Dent J 8:e43.
Usai D, Donadu M, Bua A, Molicotti P, Zanetti S, Piras S, Corona P, Ibba R, Carta A (2019) Enhancement of antimicrobial activity of pump inhibitors associating drugs. J Infect Dev Ctries 13:162-164.
UN SDG targets and indicators. Available online: https://sdg.humanrights.dk/en/goals-and-targets (accessed on 9 May 2021).
van Duin D, Paterson D (2016) Multidrug resistant bacteria in the community: Trends and lessons learned. Infect Dis Clin N Am 30:377-390.
WHO (2017) WHO publishes list of bacteria for which new antibiotics are urgently needed. Available online: https://www.who.int/news/item/27-02-2017-who-publishes-list-of-bacteria-for-which-new-antibiotics-are-urgently-needed (accessed on 9 May 2021).

Acta Biologica Szegediensis

Volume 65(1):93-103, 2021
Acta Biologica Szegediensis
http://abs.bibl.u-szeged.hu/index.php/abs

DOI:10.14232/abs.2021.1.93-103

ARTICLE

Understanding the nature and dynamics of *Mycobacterium ulcerans* cytochrome P450 monooxygenases (CYPs) – a bioinformatics approach

Saubashya Sur

Postgraduate Department of Botany, Life Sciences Block, Ramananda College, Bishnupur-722122, West Bengal, India

ABSTRACT Cytochrome P450 monooxygenases (CYPs or P450s) are catalytically versatile hemoproteins, associated with drug metabolism, substrate utilization and pathogenesis. *Mycobacterium ulcerans* is a human pathogen causing Buruli ulcer. The study intended to investigate frequency and diversity of CYPs from *M. ulcerans* strains, understand the pan-CYPome clustering patterns and interconnection of CYPs using bioinformatics tools. *M. ulcerans* strains demonstrated the presence of 261 CYPs categorized into 35 families and 38 subfamilies. CYP138, CYP140, CYP189 and CYP125 were the flourishing families. Around, 20 CYP families and 20 subfamilies were conserved. Flourishing and conserved CYP families/subfamilies were associated with lipid metabolism, substrate utilization etc. CYP140 had a role in pathogenesis. CYP279 was the least dominant family. CYP135, CYP183, CYP190, CYP271 and CYP276 were diagnostic markers for *M. ulcerans* subsp. *shinshuense* strain ATCC 33728 and *M. ulcerans* strain P7741. The pan-CYPome specified that *M. ulcerans* is evolving by gaining CYPs. CYP centric clustering revealed diversity and resemblances among *M. ulcerans* strains. More diverse nature of the *M. ulcerans* strain Harvey could be attributed to its larger size and geographical location. Co-occurrence network demonstrated mutual associations amongst substantial number of CYP families/subfamilies. This work provided comprehensive understanding of previously unexplored CYPs from *M. ulcerans*. **Acta Biol Szeged 65(1):93-103 (2021)**

KEY WORDS

clustering
CYP identification
cytochrome P450 monooxygenases
co-occurrence network
Mycobacterium ulcerans

ARTICLE INFORMATION

Submitted
10 March 2021.
Accepted
03 June 2021.
***Corresponding author**
E-mail: saubashya@gmail.com

Introduction

Hemoproteins like cytochrome P450 monooxygenases (CYPs) are universally present among all the living kingdoms (Kweon et al. 2020). The accessibility of large number of plants, animal and bacterial genomes in the public databases during last 20 years have resulted in the documentation of numerous cytochrome P450 monooxygenases. These hemo-thiolate enzymes first discovered in 1962, have been known to be vital for the evolution of different organisms (Nelson 2013). Phylogenetic studies on cytochrome P450 monooxygenases have highlighted that CYP51 is an ancient P450 which gave rise to the contemporary CYPs (Yoshida et al. 2000; Nelson 1999). CYP51 remained conserved across prokaryotes and eukaryotes (Parvez et al. 2016). Cytochrome P450 monooxygenases are associated with several biochemical reactions (Coon 2005) and form an indispensable part of an organism's primary and secondary metabolism (Parvez et al. 2016). Researches on the CYPs from bacteria have revealed their intricate structure function relationships (Parvez et al. 2016). Multiple lines of evidence have demonstrated the role of bacterial CYPs in drug metabolism and pathogenesis (Kweon et al. 2020; Furge and Guengerich 2006; Brezna et al. 2006). Bacterial CYPs are also known to be biotechnologically important (McLean et al. 2015).

Non-tuberculous mycobacteria dwell in varied environments and are responsible for nosocomial infections in immunocompromised and vulnerable persons (Ahmed et al. 2020). *Mycobacterium ulcerans* is a non-tuberculous mycobacterium responsible for a severe skin disease called Buruli ulcer (BU) (Ohtsuka et al. 2013). It has been a common infectious disease in Ivory Coast, Ghana, Benin, Democratic Republic of Congo and Uganda (van der Werf et al. 1999). However, a number of infections has been reported from aquatic environments in Japan (Luo et al. 2015), Australia (O' Brien et al. 2019), China, certain regions of Central and South America (Merritt et al. 2010). Anthropogenic activities have been one of the reasons behind the emergence *M. ulcerans* (Zingue et al. 2018). It initiates inflammation by attacking the skin, subcutaneous fat cells (Merritt et al. 2010) and secretes mycolactone toxin (Liu et al. 2019) during Buruli ulcer.

Table 1. Summary of the analysis of MU-7 dataset using CYPminer

Dataset	Total No. of CYPs	CYP categorization		Pan-CYPome				Principal CYP families	Principal CYP subfamilies
				Pan		Core			
		Family	Subfamily	Family	Subfamily	Family	Subfamily		
MU-7	261	35	38	35	38	20	20	CYP138	CYP164A3P
								CYP140	CYP140A
								CYP189	CYP125A6P
								CYP125	CYP138A

Consequently, a necrotizing and painless infection occur which damages the skin, tissues of upper and lower limbs as well as bones (de Souza et al. 2012). Delay in treatment often result in disabilities (Yotsu et al. 2015). Till date no vaccine is available, and surgery seems to be an option for treating Buruli ulcer (Tai et al. 2018). Combination of a couple of antibiotics along with surgery has also been successful (Yotsu et al. 2018). Still, none had been more effective compared to the other (Yotsu et al. 2018) and increased pathogenicity has been linked to stable evolution of *M. ulcerans* (Tai et al. 2018).

There have been limited studies on the bacterial CYPs (Parvez et al. 2016; Mthetwa et al. 2018; Senate et al. 2019; Lau et al. 2019; Khumalo et al. 2020) compared to eukaryotes (Parvez et al. 2016). Nevertheless, observations on the role of CYPs in bacterial pathogenesis (Kweon et al. 2020), use of CYP141 for diagnosis of *Mycobacterium tuberculosis* (Darban-Sarokhalil et al. 2011) and indispensability of CYP121 for the existence of tuberculosis pathogen (McLean et al. 2008) demonstrated its importance in infectious bacteria. An evolutionary analysis of CYPs from 60 mycobacterial species offered insights into their coverage, conservation and structural dynamics (Parvez et al. 2016). Others focused on genome level analysis, especially identification and classification of CYPs from some mycobacterial species along with eukaryotes (Kweon et al. 2020). Nevertheless, there is a dearth of work on CYPs from *M. ulcerans*. There is scarcity from the perspective of identification, classification and comparative analysis of the total CYP complement from *M. ulcerans*. Given the significance of *M. ulcerans* as an emerging pathogen with steady evolutionary rate (Tai et al. 2018), there is a need to recognize the nature and diversity of CYPs from the total CYP complement. Availability of the complete genomes of different strains of *M. ulcerans*, isolated from different geographical locations has unlocked the prospect of studying the whole CYP complement.

The objectives of this study were to a) identify and categorize the CYPs from *M. ulcerans* strains, b) investigate the nature of the pan-CYPome, c) survey CYP centric clustering patterns, d) understand interconnection of CYPs via co-occurrence network and e) examine the CYP cloud to recognize the frequency and diversity of CYPs. Given the wide-ranging functionalities of CYPs, this sort of investigation will generate significant insights into the characteristic features, patterns of dynamics and diversity of *M. ulcerans* CYPs. Furthermore, it will throw light on the nature of the physiology and lifestyle of *M. ulcerans.*

Materials and methods

Retrieval of sequences

Protein sequences from the genomes of 7 strains of human pathogenic *M. ulcerans* (publicly available as of 01/01/2021), viz., *M. ulcerans* strain SGL03 (Genome ID 1809.14), *M. ulcerans* strain S4018 (Genome ID 1809.16), latest annotated version of *M. ulcerans* strain P7741 (Genome ID 1809.18), *M. ulcerans* strain CSURQ0185 (Genome ID 1809.19), *M. ulcerans* strain Agy99 (Genome ID 362242.7) along with its plasmid, latest annotated version of *M. ulcerans* subsp. *shinshuense* strain ATCC 33728 (Genome ID 1124626.4) along with its plasmid and *M. ulcerans* strain Harvey (Genome ID 1299332.3) were retrieved from the PATRIC database version 3.6.8. This complete dataset comprising 7 strains of *M. ulcerans* will henceforth be referred to as MU-7.

Software and databases

A Python based software CYPminer (https://github.com/Okweon/CYPminer), clustering algorithm USEARCH (Edgar 2010) and RPSBLAST software (Marchler-Bauer et al. 2009) were downloaded. Additionally, P450 and RPS databases necessary for running CYPminer were also retrieved (https://github.com/Okweon/CYPminer).

Data pre-processing and orthologous clustering

Protein sequences from the MU-7 dataset were used as input for CYPminer. Next, USEARCH (Edgar 2010) was utilized by CYPminer for the purpose of clustering with a sequence identity cut-off of 55%. This was done to accomplish CYP specific evaluation. A FASTA file with representative protein sequences and an UCLUST

Table 2. Frequency data of CYPs at the family and sub family in *M. ulcerans* strains and plasmids from the MU-7 dataset

Organism with No. of coding sequences (CDS)	CYP frequency	
	Family	Subfamily
M. ulcerans strain SGL03 (PATRIC CDS=5611)	34	34
M. ulcerans strain S4018 (PATRIC CDS=5926)	36	36
M. ulcerans strain P7741 (PATRIC CDS=5894)	37	37
M. ulcerans strain CSURQ0185 (PATRIC CDS=5945)	34	34
M. ulcerans strain Agy99 (PATRIC CDS=5844)	38	38
M. ulcerans subsp. shinshuense strain ATCC 33728 (PATRIC CDS=5689)	37	37
M. ulcerans strain Harvey (PATRIC CDS=9118)	45	45

formatted file harboring cluster information was generated as output.

Identification and categorization of CYPs

In order to identify sequences with CYPs, CYPminer executed the RPSBLAST software by utilizing FASTA file of the representative protein sequences. Subsequently, these representative protein sequences were compared with the localized RPS database housing CYP domains. A cut-off was set at 0.00001. Next, the protein sequences containing conserved CYP domains were used for USEARCH BLAST against the localized P450 database (Kweon et al. 2020). Then, CYPminer categorized CYP proteins having ≥40% and ≥55% identity to corresponding P450 families and subfamilies, while those having <40% identity was designated as novel. This categorization was based on international nomenclature (Nebert et al. 1987).

Determination of pan-CYPome and clustering

Here, CYPminer utilized the UCLUST file housing cluster information and the result of CYP categorization for a number of Genome-CYP Matrix (GCM) analysis. Investigation of the pan-CYPome and clustering are integrated components of the GCM analysis. CYPminer yielded a pan-CYPome comprising of total complement of CYPs (Kweon et al. 2020) obtained from the studied strains of *M. ulcerans*. Moreover, it also yielded the core-CYPome. Additionally, hierarchically clustered heatmaps of CYP family and subfamilies were created by utilizing the python heatmap cluster library.

Determination of co-occurrence network and CYP cloud

The CYPminer workflow was subjected to GCM analysis for constructing the CYP co-occurrence network and CYP cloud. For this purpose, the Python pyvis and word cloud libraries were employed. While CYP co-occurrence network signified relationships between CYPs, CYP cloud examined CYP frequency. The former considered CYPs present within a genome to be related resulting in co-occurrence, while the latter generated a word cloud containing an impression of the rate of CYP incidence. The CYP co-occurrence networks were generated for both CYP families and subfamilies.

Results

Mycobacterium ulcerans CYPs and their categorization

Data mining of the MU-7 dataset using CYPminer revealed the occurrence of 261 CYPs (Table 1). These CYPs were categorized into 35 families and 38 subfamilies. There were no new families or subfamilies. Closer inspection of CYP families indicated that CYP138, CYP140, CYP189 and CYP125 were the principal ones having 19, 13, 13 and 12 members respectively. About 20 CYP families viz. CYP51, CYP105, CYP123-126, CYP130, CYP136-139, CYP142-143, CYP150, CYP164, CYP185, CYP189, CYP191, CYP226 and CYP278 were present among all the 7 strains of *M. ulcerans* indicating their conserved nature. In contrast, the CYP279 family was only present in *M. ulcerans* strain P7741. CYP families viz. CYP135, CYP147, CYP183, CYP190, CYP271 and CYP276 were only found in *M. ulcerans* subsp. *shinshuense* strain ATCC 33728 and *M. ulcerans* strain P7741. Likewise, CYP140A, CYP2164A3P, CYP125A6P and CYP138A were the principal subfamilies housing 13, 13, 12 and 12 members. About 20 CYP subfamilies viz. CYP51B, CYP105Q, CYP123-124A, CYP125A6, CYP126A, CYP130A, CYP136-138A, CYP139A3P, CYP142-143A, CYP150A, CYP164A3P, CYP185A, CYP189A, CYP191A, CYP226B and CYP278A were extant among all the 7 strains of *M. ulcerans*. While CYP138B occurred only in *M. ulcerans* subsp. *shinshuense* strain ATCC 33728, CYP279A was only found in *M. ulcerans* strain P7741. Moreover, CYP subfamilies viz. CYP135B, CYP147G, CYP183B, CYP190A, CYP271A and CYP276A were noticed only in *M. ulcerans* subsp. *shinshuense* strain ATCC 33728 and *M. ulcerans* strain P7741.

Table 1. showed the occurrence of 35 and 38 pan CYP families and subfamilies. Table 2. highlighted that *M. ul-*

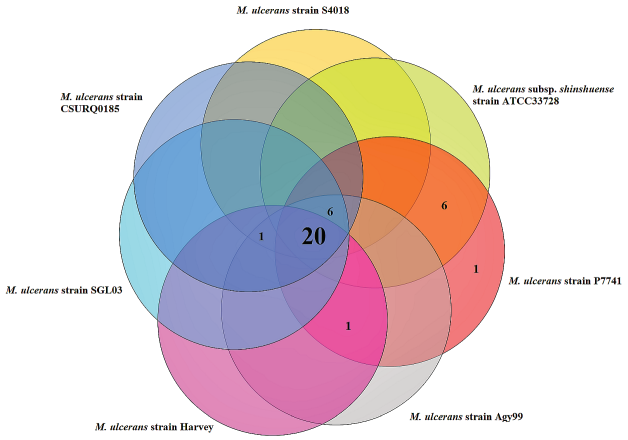

Figure 1. Pan-CYPome family profile from the MU-7 dataset. The Venn diagram intended to demonstrate the Pan and Core CYP families. Circles symbolized genomes and the overlapping regions signified CYP families shared by respective genomes. Numeral figures represented the number of CYP families found therein. The number of Core families (in the centre) in the Pan-CYPome were 20. The Pan-CYPome consisted of 35 families in total.

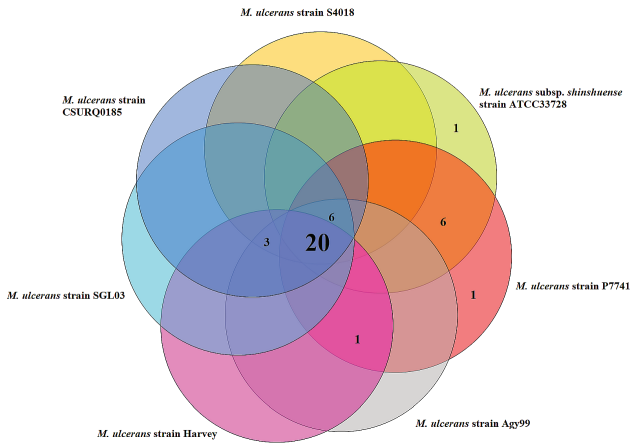

Figure 2. Pan-CYPome subfamily profile from the MU-7 dataset. The Venn diagram intended to demonstrate the Pan and Core CYP subfamilies. Circles symbolized genomes and the overlapping regions signified CYP subfamilies shared by respective genomes. Numeral figures represented the number of CYP subfamilies found therein. The number of Core subfamilies (in the centre) in the Pan-CYPome were 20. The Pan-CYPome consisted of 38 subfamilies in total.

cerans strain Harvey housed the highest number of CYPs (45 families and subfamilies) followed by *M. ulcerans* strain Agy99 (38 families and subfamilies). *M. ulcerans* strain SGL03 and *M. ulcerans* strain CSURQ0185 had the lowest CYP frequency (34 families and subfamilies each) amongst the 7 strains. The frequency of CYPs corresponded with the number of coding sequences in some of the strains.

Pan-CYPome of Mycobacterium ulcerans

Fig. 1. demonstrated the pan-CYPome family profile from MU-7 dataset. It highlighted the full complement of CYP families incorporating the studied strains of *M. ulcerans*. CYPMiner showed a total of 35 families in the pan-CYPome. This consisted of 20 core families that were common to all the seven strains. Thus, a sizeable proportion of the CYP families belong to the core. Six CYP families were shared among six strains. *M. ulcerans* subsp. *shinshuense* strain ATCC 33728 and *M. ulcerans* strain P7741 also shared 6 CYP families. The number of CYP family exclusively shared by five strains was 1. Three strains viz., *M. ulcerans* strain Harvey, *M. ulcerans* strain Agy99 and *M. ulcerans* strain P7741 too shared 1 CYP family. Additionally, the presence of one unique strain specific CYP family in *M. ulcerans* strain P7741 supported earlier observations.

Fig. 2. portrayed the pan-CYPome subfamily profile from MU-7, dataset signifying the full complement of CYP subfamilies. A total of 38 subfamilies were present in the pan-CYPome. A few parallels were noticed between the pan-CYPome family and subfamily profiles. The pan-CYPome subfamily profile comprised of a high share of 20 core CYP subfamilies present in all seven trains. Similar to the pan-CYPome family profile, six CYP subfamilies were also shared between six strains. *M. ulcerans* subsp. *shinshuense* strain ATCC 33728 and *M. ulcerans* strain P7741 too shared 6 CYP subfamilies. Three CYP subfamilies were exclusively shared by five strains. *M. ulcerans* strain Harvey, *M. ulcerans* strain Agy99 and *M. ulcerans* strain P7741 too shared 1 CYP subfamily. Unique strain specific subfamilies were observed only in *M. ulcerans* subsp. *shinshuense* strain ATCC 33728 and *M. ulcerans* strain P7741 respectively.

CYP centric clustering analysis

Fig. 3. portrayed the CYP centric family heatmap cluster with dendrograms. It was observed that the 7 *M. ulcerans* genomes were grouped into two major clusters consisting of smaller clusters. It was noticed from Fig. 3 that *M. ulcerans* subsp. *shinshuense* strain ATCC 33728 and *M. ulcerans* strain P7741 had a comparable CYP family profile and were distinctly clustered together at some distance from the rest. This was the first major cluster. In this cluster, the frequency of 19 CYP families like CYP51, CYP105, CYP124-126, CYP130, CYP136-137, CYP139, CYP142, CYP147, CYP183, CYP185, CYP189-190, CYP226, CYP271, CYP276 and CYP278 was 1 in both the organisms. Similarly, the frequency of CYP135 and CYP150 were 2 in both. Furthermore, the frequency of CYP144 were 0 in both the organisms. The frequency of other CYP families varied between these microorganisms.

Others viz. *M. ulcerans* strain Harvey, *M. ulcerans* strain

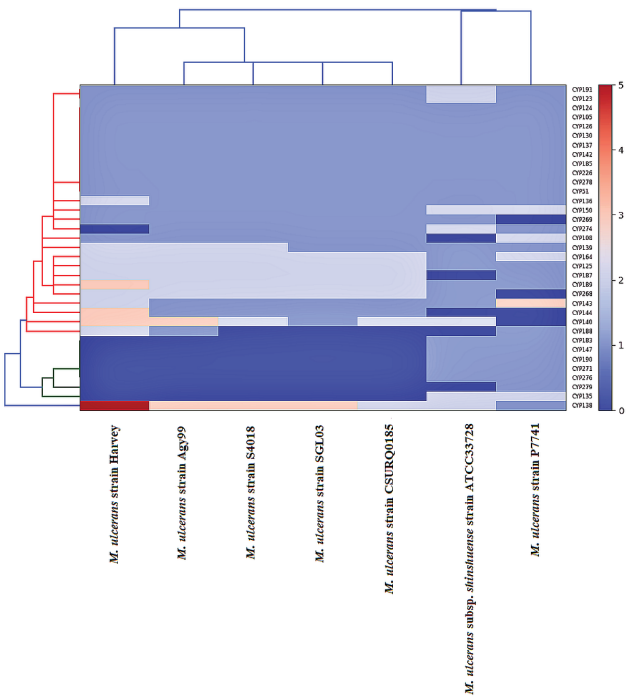

Figure 3. CYP centric family heat map cluster from *M. ulcerans*. Right side of the vertical axis denoted the frequency of incidence of individual CYP families while left side denoted relationship among CYP subfamilies. Lower side of the horizontal axis represented the studied strains of *M. ulcerans*. Upper side of the horizontal axis represented the CYP centric phylogenetic clusters. Colours in the scale of 0-5 indicated frequency.

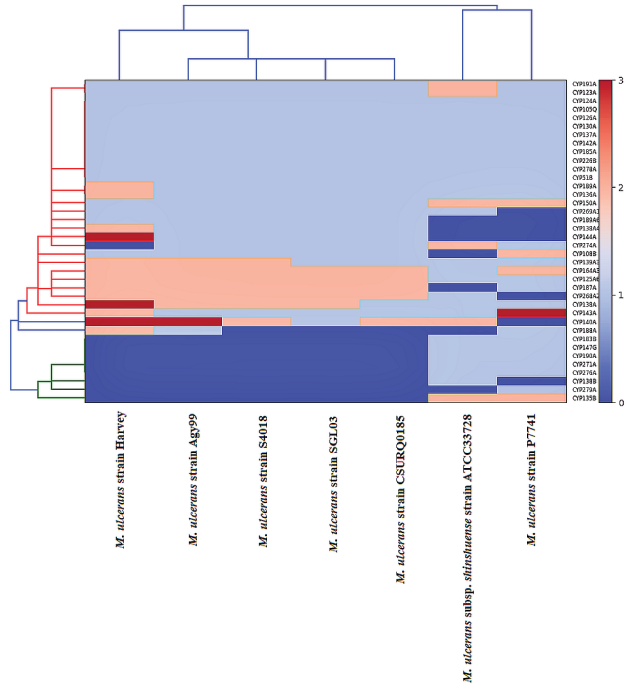

Figure 4. CYP centric subfamily heat map cluster from *M. ulcerans*. Right side of the vertical axis denote the frequency of incidence of individual CYP subfamilies and left side relationships among CYP subfamilies. Lower side of the horizontal axis represented the studied strains of *M. ulcerans*. Upper side of the horizontal axis represented CYP centric phylogenetic clusters. Colours in the scale of 0-3 indicated frequency.

CSURQ0185, *M. ulcerans* strain SGL03, *M. ulcerans* strain S4018 and *M. ulcerans* strain Agy99, formed the second major cluster. They were divided into smaller clusters which were close to each other. A closer investigation of these 5 genomes revealed that, *M. ulcerans* strain S4018, *M. ulcerans* strain Agy99, *M. ulcerans* strain SGL03 and *M. ulcerans* strain CSURQ0185 were assembled together owing to some resemblances in the CYP family profile. However, *M. ulcerans* strain Harvey showed some variations regarding frequencies of CYP136, CYP138, CYP140, CYP143-144, CYP188-189 and CYP274. As far as the parallels are concerned, the frequency of CYP135, CYP147, CYP183, CYP190, CYP271, CYP276 and CYP279 were 0 in all these 5 genomes. Likewise, the frequency of CYP125, CYP164, CYP187 and CYP268 were 2 in these. A frequency of 1 was observed in 14 CYP families viz. CYP51, CYP105, CYP123-124, CYP126, CYP130, CYP137, CYP142, CYP150, CYP185, CYP191, CYP226, CYP269 and CYP278 within these 5 genomes. Overall, all 7 genomes showed resemblance in having a frequency of 1 for 10 CYP families viz. CYP51, CYP105, CYP124, CYP126, CYP130, CYP137, CYP142, CYP185, CYP226 and CYP278.

The CYP centric subfamily heatmap cluster with dendrograms (Fig. 4) which showed some similarity with the pattern visible in the family heatmap. Here too the 7 *M. ulcerans* genomes were grouped into two main clusters. Fig. 4. demonstrated that *M. ulcerans* subsp. *shinshuense* strain ATCC 33728 and *M. ulcerans* strain P7741 had good degree of similarity in the CYP subfamily profile. They were grouped together forming one of the two major clusters at a distance from others. In this cluster, the frequency of 20 CYP subfamilies viz. CYP51B, CYP105Q, CYP124A, CYP125A6P, CYP126A, CYP130A, CYP136-138A, CYP139A3P, CYP142A, CYP147G, CYP183B, CYP185A, CYP189-190A, CYP226B, CYP271A, CYP274A, CYP276A and CYP278A were 1 in both. Likewise, the frequency was 2 for CYP135B and CYP150A. Additionally, the frequency of CYP138A4P, CYP144A and CYP189A6P was 0 in both. *M. ulcerans* subsp. *shinshuense* strain ATCC 33728 and *M. ulcerans* strain P7741 showed differences in rest of the subfamilies.

M. ulcerans strain Harvey, *M. ulcerans* strain Agy99, *M. ulcerans* strain S4018, *M. ulcerans* strain SGL03 and *M. ulcerans* strain CSURQ0185 shaped the second major

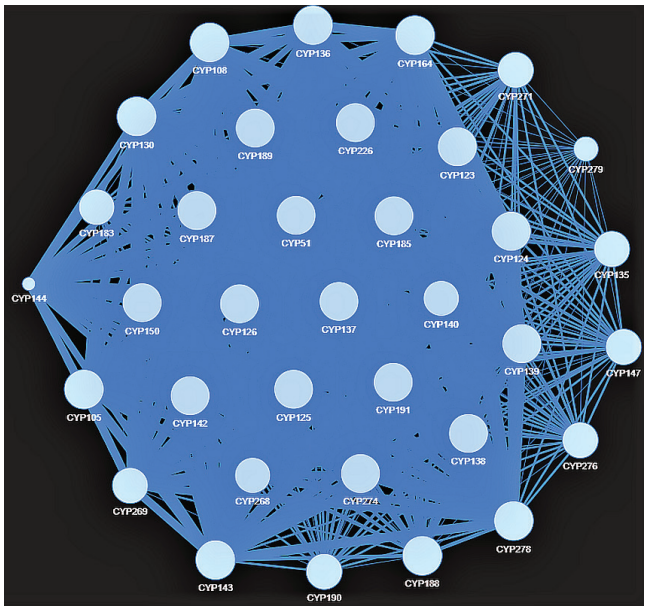

Figure 5. CYP family co-occurrence network from MU-7 dataset.

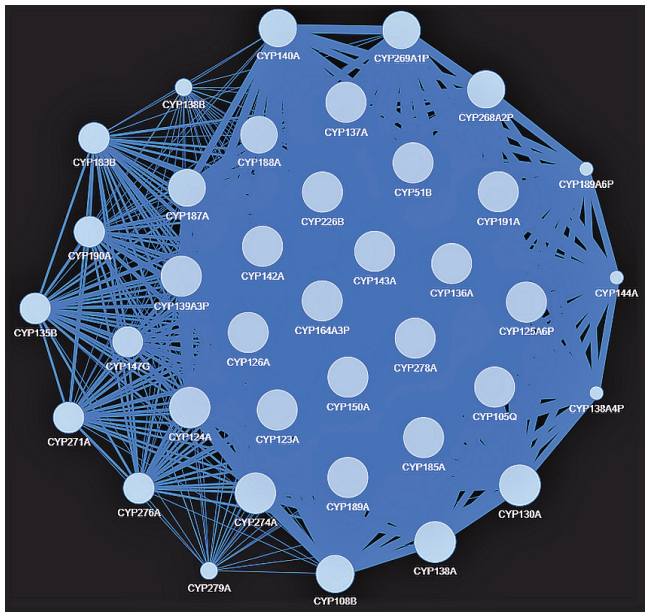

Figure 6. CYP subfamily co-occurrence network from MU-7 dataset.

cluster. It was grouped into smaller clusters. Analysis of these 5 genomes revealed that, *M. ulcerans* strain Agy99, *M. ulcerans* strain S4018, *M. ulcerans* strain SGL03 and *M. ulcerans* strain CSURQ0185 were clustered together due to some similarities in the frequency of CYP subfamilies. *M. ulcerans* strain Harvey differed from other 4 genomes within the second major cluster in the frequency of 8 CYP subfamilies viz. CYP36A, CYP138A, CYP138A4P, CYP143-144A, CYP188-189A and CYP274A. As far as similarities are concerned, it was noticed that the frequency of CYP135B, CYP138B, CYP147G, CYP183B, CYP190A, CYP271A CYP276A and CYP279A were 0 in all the 5 genomes within this cluster. Additionally, a frequency of 1 was detected in 16 CYP subfamilies viz. CYP51B, CYP105Q, CYP108B, CYP123-124A, CYP126A, CYP130A, CYP137A, CYP142A, CYP150A, CYP185A, CYP189A6P, CYP191A, CYP226B, CYP269A1P and CYP278A in each of these genomes. Furthermore, each of them had a frequency of 2 in 4 CYP subfamilies viz. CYP125A6P, CYP164A3P, CYP187A and CYP268A2P. Examination of the 7 genomes from two major clusters revealed similarity in 10 CYP subfamilies. These subfamilies viz., CYP51B, CYP105Q, CYP124A, CYP126A, CYP130A, CYP137A, CYP142A, CYP185A, CYP226B and CYP278A had a frequency of 1.

CYP co-occurrence network in Mycobacterium ulcerans

Figs. 5 and 6 portrayed the CYP family and subfamily co-occurrence networks from the MU-7 dataset. Based on their corresponding occurrence in *M. ulcerans* genomes, the mutual connectivity of the identified CYPs were demonstrated by these co-occurrence networks. It was observed from Fig. 5. that a considerable number CYP families formed big nodes and were strongly clustered together. They had a high connection degree (greater number of edges connected to the nodes) with thick width. The degree of the nodes was reflected in the size. These included the principal CYP families, CYP138, CYP140, CYP189, CYP125, conserved CYP51 (Parvez et al. 2016) in addition to a host of others. On the other hand, less dominant CYP families viz. CYP135, CYP147, CYP183, CYP190, CYP271, CYP276 and CYP279 showed reduced compactness in the connection with thin width. The co-occurrence network of the CYP subfamilies (Fig. 6) also displayed a condensed cluster of a number of CYP subfamilies with big nodes, thick width and high connection degree. This cluster housed key CYP subfamilies viz. CYP125A6P, CYP164A3P, conserved CYP51B as well as others. However, the least dominant subfamilies displayed reduced compactness, connectivity and thin width. These included CYP135B, CYP138B, CYP183B, CYP190A, CYP271A, CYP276A and CYP279A.

CYP cloud of Mycobacterium ulcerans

Fig. 7(a-b) graphically represented the CYP cloud displaying CYP frequency at the family and subfamily level from the MU-7 dataset. The principal families and subfamilies depicted in bigger font have been highlighted earlier (Table 1). Moderate and least dominant families and subfamilies were displayed in medium and smaller fonts respectively. A deeper probe revealed that *M. ulcerans* strain Harvey had the highest concentration of the principal CYP families

CYP138, CYP140 and CYP189 with a copy number of 5, 3 and 3. A copy number of 2 was observed in CYP125 and CYP268 for *M. ulcerans* strain Harvey, *M. ulcerans* strain CSURQ0185, *M. ulcerans* strain SGL03, *M. ulcerans* strain S4018 and *M. ulcerans* strain Agy99. CYP279 was the least dominant family having a solitary copy number in *M. ulcerans* strain P7741. Other less dominant families, CYP147, CYP183, CYP190, CYP271 and CYP276 with a frequency of 1 were present only in *M. ulcerans* subsp. *shinshuense* strain ATCC 33728 and *M. ulcerans* strain P7741.

M. ulcerans strain Harvey and *M. ulcerans* strain Agy99 had a copy number of 3 in the principal subfamilies, CYP140A and CYP138A. Other principal subfamilies, CYP125A6P and CYP164A3P had a copy number of 2 in *M. ulcerans* strain Harvey, *M. ulcerans* strain CSURQ0185, *M. ulcerans* strain SGL03, *M. ulcerans* strain S4018, *M. ulcerans* strain Agy99 and *M. ulcerans* strain P7741. The least dominant subfamilies, CYP138B and CYP279A with solitary counts were detected in *M. ulcerans* subsp. *shinshuense* strain ATCC 33728 and *M. ulcerans* strain P7741. Additionally, other less dominant subfamilies, CYP183B, CYP190A, CYP271A and CYP276A with an incidence of 1 were found in *M. ulcerans* subsp. *shinshuense* strain ATCC 33728 and *M. ulcerans* strain P7741.

Discussion

In this work, cytochrome P450 monooxygenases (CYPs) were identified and categorized from various *M. ulcerans* strains. Using this information, a number of downstream investigations at the family and subfamily level concerning the pan-CYPome, CYP centric clustering, interrelationship networks, frequency and variations of CYPs were carried out. The results were mutually supportive. The outcome of these analyses had underlined several important characteristics of *M. ulcerans* CYPs that could pave the way for further studies.

M. ulcerans is a human pathogen. Examination of individual *M. ulcerans* strains revealed that they had low concentration (ranging from 34-45) of CYP families. The outcome agrees with the fact that mycobacterial human pathogens tend to possess lower CYPs owing to their adaptation to human pathogenic lifestyle where they must survive by fighting the host's immunity and exploit carbon sources (Parvez et al. 2016; Senate et al. 2019). *M. ulcerans* strains showed difference between them regarding the number of CYP families and subfamilies. This had something to do with the size of the genomes, especially in *M. ulcerans* strain Harvey. Here greater number of coding sequences corresponded to increased CYPs while smaller number coding sequences in *M. ulcerans* strain SGL03 resulted in lower CYPs. This is in line with the observations from other mycobacterial species (Parvez et al. 2016). Again, *M. ulcerans* strain Harvey was isolated in USA (https://patricbrc.org/view/Taxonomy/2#view_tab=genomes&filter=and(keyword(Mycobacterium),keyword(ulcerans)) and its' difference from other strains regarding number of CYPs, clustering of families and subfamilies in the CYP heatmaps (Figs. 3-4) may be attributed to geographical location. Previous works have specified the role of geographical location in variation among bacterial strains (Sen et al. 2008; Sur et al. 2008).

The incidence of comparatively higher number of members in CYP families, CYP138, CYP140, CYP189 and CYP125 designated that they were flourishing. This phenomenon has also been reported in other organisms (Syed et al. 2014; Parvez et al. 2016). These flourishing families played a crucial part in *M. ulcerans* physiology. CYP138, CYP140, CYP189 and CYP125 are known to be associated with heme binding (https://www.uniprot.org/uniprot/P9WPM3), mycolactone synthesis (Mve-Obiang et al. 2005), monooxygenase activity (Parvez et al. 2016) and steroid hydroxylation (Mc Lean et al. 2009). Given

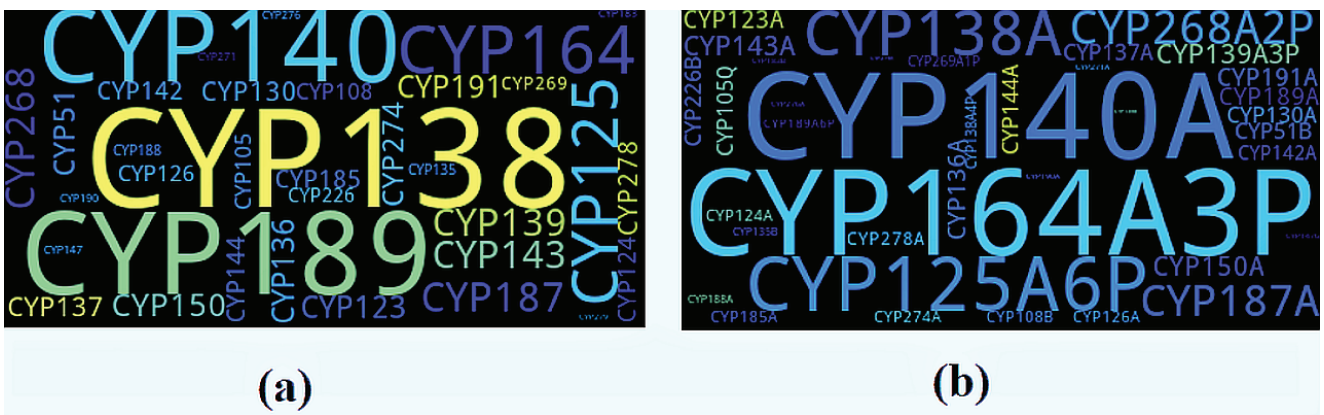

Figure 7. CYP clouds of the (a) family and (b) subfamily from MU-7 dataset.

that *M. ulcerans* secrete mycolactone toxin during Buruli ulcer, the dominance of CYP140 point to its influence on the disease. This is strengthened by its presence in almost all the *M. ulcerans* strains. Occurrence of 20 CYP families among all the 7 *M. ulcerans* strains, portrayed that they were conserved within these strains and suggested their importance. A number of them like CYP51, CYP105, CYP124, CYP125, CYP142, CYP150, CYP185 function in lipid metabolism, steroid metabolism (Kelly and Kelly 2013), diterpenoid oxidation (Moody and Loveridge 2014), steroids, fatty acid hydroxylation (Johnston et al. 2009; Johnston et al. 2010; Mc Lean et al. 2009) and polycyclic aromatic hydrocarbon hydroxylation (Brezna et al. 2006). Earlier works have specified that these families assisted *Mycobacterium* in assimilating host compounds (Senate et al. 2019). Presence of CYP279 family only in *M. ulcerans* strain P7741 indicated that this can act as a diagnostic marker for this strain. Nevertheless, incidence of CYP135, CYP147, CYP183, CYP190, CYP271 and CYP276 only in *M. ulcerans* subsp. *shinshuense* strain ATCC 33728 and *M. ulcerans* strain P7741 revealed that these families may be improved diagnostic markers than CYP279 owing to occurrence in two strains. Their existence stated their importance in these *M. ulcerans* strains. Most of the least dominant CYP families limited to few *M. ulcerans* strains were orphans (Parvez et al. 2016). This is line with earlier observations on P450s from other mycobacteria (Parvez et al. 2016). The outcome from CYP subfamilies were consistent with that of the families. Analysis of the CYP families and subfamilies from *M. ulcerans* indicated that they were designed for utilization of lipids.

The pan-CYPome family and subfamily profile from *M. ulcerans* indicated accumulation of new CYPs with each newly added genome, and the ability to continuously extent their total set of CYPs. It is probable that by acquisition of CYPs and diversification, *M. ulcerans* is evolving. This may have consequences in terms of the diversity and lifestyle of *M. ulcerans* strains. Considerable proportion of core CYP families and subfamilies in the pan-CYPome, is probably an outcome of a number of strains, family and subfamily-specific CYPs, reflecting the dynamics of *M. ulcerans*. Analysis of the core CYP families and subfamilies provided clues on the role of common CYPs essential for the lifestyle of *M. ulcerans*. As mentioned earlier most of them are flourishing and are involved in lipid, steroid metabolism, heme binding etc. These are vital for the survival of the species.

CYP centric clustering pattern of the families and subfamilies revealed that despite isolation from different geographical locations, *M. ulcerans* subsp. *shinshuense* strain ATCC 33728 (isolated from Japan) and *M. ulcerans* strain P7741 (isolated from French Guyana) (https://www.patricbrc.org/view/GenomeList/?and(keyword(Mycobacterium),keyword(ulcerans))#view_tab=genomes), were grouped together in the first major cluster owing to similarities in the CYP frequency of 22 families and 25 subfamilies. The CYP centric clustering pattern in the second major cluster indicated that, *M. ulcerans* strain Harvey (isolated from USA), *M. ulcerans* Agy99 (isolated from Ghana), *M. ulcerans* strain S4018 (isolated from Benin), *M. ulcerans* strain SGL03 (isolated from Democratic Republic of Congo) and *M. ulcerans* strain CSURQ0185 (isolated from Ivory Coast) (https://www.patricbrc.org/view/GenomeList/?and(keyword(Mycobacterium),keyword(ulcerans))#view_tab=genomes), had resemblances in the CYP frequency of 25 families and 28 subfamilies. While the four African strains showed some parallels with each other, *M. ulcerans* strain Harvey (isolated from USA) differed from these in the CYP frequency of 8 families and subfamilies. Interestingly, this included the flourishing CYP families and subfamilies like CYP140, CYP138, CYP138A respectively. This difference exhibited by *M. ulcerans* strain Harvey was due to higher number of CYPs in the families and subfamilies compared to others. It is possible that higher number offered advantage for better adaptation to the host's environment and needs to be corroborated by future studies. Again, occurrence of 10 CYP families and subfamilies with a frequency of 1 among seven *M. ulcerans* strains highlighted the resemblances among them.

Findings from CYP family and subfamily co-occurrence network were in agreement with their frequencies. Sizeable number of CYP families including CYP138, CYP140, CYP189, CYP125 with big nodes, robust clustering, high connection degree and thick width were indicative of their high frequency and co-occurrence in *M. ulcerans* genomes. Again, strong clustering of majority of CYP families specified their mutual associations regarding CYP dynamics in *M. ulcerans* genomes. In contrast, low connection degree and thin width of CYP135, CYP147, CYP183, CYP190, CYP271, CYP276 and CYP279 signified less frequency and dissociation. The result of CYP subfamily co-occurrence network were supportive of the CYP family counterpart.

The observations from CYP family and subfamily clouds were in line with their frequency and variation in *M. ulcerans* strains. The incidence of high copy number of the flourishing families (CYP138, CYP140, CYP189, CYP125, CYP268) and subfamilies (CYP141A, CYP138A, CYP125A6P, CYP164A3P) indicated that they played a vital role in the metabolism and lifestyle of *M. ulcerans* strain Harvey, *M. ulcerans* strain CSURQ0185, *M. ulcerans* strain SGL03, *M. ulcerans* strain S4018 and *M. ulcerans* Agy99. Comparatively higher concentration of these in *M. ulcerans* strain Harvey indicated that this strain showed variation from the rest. This further strengthened the

hypothesis that comparatively larger genome manifested by higher number of coding sequences (CDS), and different geographical location of *M. ulcerans* strain Harvey may be the reason behind such variation.

Conclusions

This study using CYPminer pipeline provided relative understandings of CYPs from *Mycobacterium ulcerans* strains at the genome level. An attempt was made to get a picture of the CYPs from *M. ulcerans* strains since they are known to be involved in myriad metabolic processes. A total of 261 CYPs were identified. While some families and subfamilies flourished others had solitary presence. Several them were conserved across strains. A substantial number of them had strong mutually supportive relationships. Low number of CYP families coupled with the role of flourishing, conserved families and subfamilies in mycolactone synthesis, steroid hydroxylation, lipid metabolism, etc. indicated their physiological role in the lifestyle of *M. ulcerans*. The *M. ulcerans* strains showed difference and similarities between them in the context of incidence, frequency, copy number and clustering of CYP families and subfamilies. The outcome of this work enhanced our knowledge regarding the CYP dynamics in *M. ulcerans*. Future work should focus on exploring the role of *M. ulcerans* CYPs in secondary metabolite synthesis followed by assessment of their biosynthetic gene clusters since they may hold potential for the biopharmaceutical industry.

Acknowledgements

The author acknowledges the support of Ramananda College, India. The author thanks anonymous reviewers for their constructive comments.

References

Ahmed I, Tiberi S, Farooqi J, Jabeen K, Yeboah-Manu D, Migliori GB, Hasan R (2020) Non-tuberculous mycobacterial infections-A neglected and emerging problem. IJID 92S:S46-S50.

Brezna B, Kweon O, Stingley RL, Freeman JP, Khan AA, Polek B, Jones RC, Cerniglia CE (2006) Molecular characterization of cytochrome P450 genes in the polycyclic aromatic hydrocarbon degrading *Mycobacterium vanbaalenii* PYR-1. Appl Microbiol Biotechnol 71:522-532.

Coon MJ (2005) Cytochrome P450: nature's most versatile biological catalyst. Annu Rev Pharmacol Toxicol 45:1-25.

Darban-Sarokhalil D, Fooladi AA, Bameri Z, Nasiri MJ, Feizabadi MM (2011) Cytochrome CYP141: A new target for direct detection of *Mycobacterium tuberculosis* from clinical specimens. Acta Microbiol Immunol Hung 58:211-217.

de Souza DK, Quaye C, Mosi L, Addo P, Boakye D (2012) A quick and cost effective method for the diagnosis of *Mycobacterium ulcerans* infection. BMC Infect Dis 12:8.

Edgar RC (2010) Search and clustering orders of magnitude faster than BLAST. Bioinformatics. 26:2460-2461.

Furge LL, Guengerich FP (2006) Cytochrome P450 enzymes in drug metabolism and chemical toxicology: an introduction. Biochem Mol Biol Educ 34:66-74.

Johnston JB, Kells PM, Podust LM, Ortiz de Montellano PR (2009) Biochemical and structural characterization of CYP124: a methyl-branched lipid ω-hydroxylase from *Mycobacterium tuberculosis*. Proc Natl Acad Sci USA 106:20687-20692.

Johnston JB, Ouellet H, Ortiz de Montellano PR (2010) Functional redundancy of steroid C-26-monooxygenase activity in *Mycobacterium tuberculosis* revealed by biochemical and genetic analyses. J Biol Chem 285:36352-36360.

Kelly SL, Kelly DE (2013) Microbial cytochrome P450: Biodiversity and biotechnology, where do cytochrome P450 come from, what do they do and what can they do for us? Phil Trans R Soc B Biol Sci 368:20120476.

Khumalo JM, Nzuza N, Padayachee T, Chen W, Yu JH, Nelson DR, Syed K (2020) Comprehensive analyses of cytochrome P450 monooxygenases and secondary metabolite biosynthetic gene clusters in cyanobacteria. Int J Mol Sci 21:656.

Kweon K, Kim SJ, Kim JH, Nho SW, Bae D, Chon J, Hart M, Baek DH, Kim YC, Wang W, Kim SK, Sutherland JB, Cerniglia CE (2020) CYPminer: an automated cytochrome P450 identification, classification, and data analysis tool for genome data sets across kingdoms. BMC Bioinformatics 21:160.

Lau CKI, Feyereisen R, Nelson DR, Bell SG (2019) Analysis and preliminary characterisation of the cytochrome P450 monooxygenases from *Frankia* sp. EuI1c (*Frankia inefficax* sp.). Arch Biochem Biophys 669:11-21.

Liu Y, Gao Y, Liu J, Tan Y, Liu Z, Chhotaray C, Jiang H, Lu Z, Chiwala G, Wang S, Makafe G, Islam MM, Hameed HMA, Cai X, Wang C, Li X, Tan S, Zhang T (2019) The compound TB47 is highly bactericidal against *Mycobacterium ulcerans* in a Buruli ulcer mouse model. Nat Commun 10:524.

Luo Y, Degang Y, Ohtsuka M, Ishido Y, Ishii N, Suzuki K (2015) Detection of *Mycobacterium ulcerans* subsp. *shinshuense* DNA from a water channel in familial Buruli ulcer cases in Japan. Future Microbiol 10:461-469.

Marchler-Bauer A, Anderson JB, Chitsaz F, Derbyshire MK, DeWeese-Scott C, Fong JH, Geer LY, Geer RC, Gonzales

NR, Gwadz M, He S, Hurwitz DI, Jackson JD, Ke Z, Lanczycki CJ, Liebert CA, Liu C, Lu F, Lu S, Marchler GH, Mullokandov M, Song JS, Tasneem A, Thanki N, Yamashita RA, Zhang D, Zhang N, Bryant SH (2009) CDD: specific functional annotation with the conserved domain database. Nucleic Acids Res 37:D205-210.

McLean KJ, Carroll P, Lewis DG, Dunford AJ, Seward HE, Neeli R, Cheesman NR, Marsollier L, Douglas P, Smith WE, Rosenkrands I, Cole ST, Leys D, Parish T, Munro AW (2008) Characterization of active site structure in CYP121. A cytochrome P450 essential for viability of *Mycobacterium tuberculosis* H37Rv. J Biol Chem 283:33406-33416.

McLean KJ, Lafite P, Levy C, Cheesman MR, Mast N, Pikuleva IA, Leys D, Munro AW (2009) The structure of *Mycobacterium tuberculosis* CYP125: molecular basis for cholesterol binding in a P450 needed for host infection. J Biol Chem 284:35524-35533.

McLean KJ, Leys D, Munro AW (2015) Microbial cytochrome P450s. In Oritz de Montellano PR, Ed., Cytochrome P450: Structure, Mechanism, and Biochemistry. 4th Edn. Springer International Publishing, 261-407.

Merritt RW, Walker ED, Small PLC, Johnson PDR, Benbow ME, Boakye DE (2010) Ecology and transmission of Buruli ulcer disease: a systematic review. PLoS Negl Trop Dis 4:e911.

Moody SC, Loveridge EJ (2014) CYP105-diverse structures, functions and roles in an intriguing family of enzymes in *Streptomyces*. J Appl Microbiol 117:1549-1563.

Mve-Obiang A, Lee RE, Umstot ES, Trott KA, Grammer TC, Parker JM, Ranger BS, Grainger R, Mahrous EA, Small PLC (2005) A newly discovered mycobacterial pathogen isolated from laboratory colonies of *Xenopus* species with lethal infections produces a novel form of mycolactone, the *Mycobacterium ulcerans* macrolide toxin. Infect Immun 73:3307-3312.

Mthetwa BC, Chen W, Ngwenya ML, Kappo AP, Syed PR, Kapoormath R, Yu JH, Nelson DR, Syed K (2018) Comparative analyses of cytochrome P450s and those associated with secondary metabolism in *Bacillus* species. Int J Mol Sci 19:3623.

Nebert DW, Adesnik M, Coon MJ, Estabrook RW, Gonzalez FJ, Guengerich FP, Gunsalus IC, Johnson EF, Kemper B, Levin W, Phillips IR, Sato R, Waterman MR (1987) The P450 gene superfamily: recommended nomenclature. DNA 6:1-11.

Nelson DR (1999) Cytochrome P450 and the individuality of species. Arch Biochem Biophys 369:1-10.

Nelson DR (2013) A world of cytochrome P450s. Phil Trans R Soc B Biol Sci 368:20120430.

O'Brien DP, Murrie A, Meggesey P, Priestley J, Rajcoomar A, Athan E (2019) Spontaneous healing of *Mycobacterium ulcerans* disease in Australian patients. PLoS Negl Trop Dis 13:e0007178.

Ohtsuka M, Kikuchi N, Yamamoto T, Suzutani T, Nakanaga K, Suzuki K, Ishii N (2013) Buruli ulcer caused by *Mycobacterium ulcerans* subsp *shinshuense*: a rare case of familial concurrent occurrence and detection of insertion sequence 2404 in Japan. JAMA Dermatol 150:64-67.

Parvez M, Qhanya L, Mthakathi N, Kgoseimang IKR, Bamal HD, Pagadala NK, Xie T, Yang H, Chen H, Theron CW, Monyaki R, Raslemane SC, Salawe V, Mongale BL, Matowane RG, Abdalla SMH, Booi WI, van Wyk M, Olivier D, Boucher CE, Nelsen DR, Tuszynski JA, Blackburn JM, Yu JH, Mashele SS, Chen W, Syed K (2016) Molecular evolutionary dynamics of cytochrome P450 monooxygenases across kingdoms: Special focus on mycobacterial P450s. Sci Rep 6:33099.

Sen A, Sur S, Bothra AK, Benson DR, Normand P, Tisa LS (2008) The implication of life style on codon usage patterns and predicted highly expressed genes for three *Frankia* genomes. Antonie van Leeuwenhoek 93:335-346.

Senate LM, Tjatji MP, Pillay K, Chen W, Zondo NM, Syed PR, Mnguni FC, Chiliza ZE, Bamal HD, Karpoormath R, Khoza T, Mashele SS, Blackburn JM, Yu JH, Nelson DR, Syed K (2019) Similarities, variations, and evolution of cytochrome P450s in *Streptomyces* versus *Mycobacterium*. Sci Rep 9:3962.

Sur S, Bothra AK, Bajwa M, Tisa LS, Sen A (2008) *In silico* analysis of *Chlorobium* genomes divulge insights into the lifestyle of the bacteria. Res J Microbiol 3:600-613.

Syed K, Shale K, Pagadala NS, Tuszynski J (2014) Systematic identification and evolutionary analysis of catalytically versatile cytochrome P450 monooxygenase families enriched in model basidiomycete fungi. PLoS ONE 9:e86683.

Tai AYC, Athan E, Friedman ND, Hughes A, Walton A, O'Brien DP (2018) Increased severity and spread of *Mycobacterium ulcerans*, Southeastern Australia. Emerg Infect Dis 24:58-64.

van der Werf TS, van der Graaf WT, Tappero JW, Asiedu K (1999) *Mycobacterium ulcerans* infection. Lancet 354:1013-1018.

Yoshida M, Nakanaga K, Ogura Y, Toyoda A, Ooka T, Kazumi Y, Mitarai S, Ishii N, Hayashi T, Hoshino Y (2016) Complete genome sequence of *Mycobacterium ulcerans* subsp. *shinshuense*. Genome Announc 4:e01050-16.

Yoshida Y, Aoyama Y, Noshiro M, Gotoh O (2000) Sterol 14-demethylase P450 (CYP51) provides a breakthrough for the discussion on the evolution of cytochrome P450 gene superfamily. Biochem Biophys Res Commun 273:799-804.

Yotsu RR, Murase C, Sugawara M, Suzuki K, Nakanaga K, Ishii N, Asiedu K (2015) Revisiting Buruli ulcer. J Dermatol 42:1033-1041.

Zingue D, Bouam A, Tian RBD, Drancourt M (2018) Bu-

ruli ulcer, a prototype for ecosystem-related infection, caused by *Mycobacterium ulcerans*. Clin Microbiol Rev 31:e00045-17.

Acta Biologica Szegediensis

Volume 65(1):105-112, 2021
Acta Biologica Szegediensis
http://abs.bibl.u-szeged.hu/index.php/abs

DOI:10.14232/abs.2021.1.105-112

ARTICLE

Insights on carbapenem-resistant *Pseudomonas aeruginosa*: phenotypic characterization of relevant isolates

Mário Gajdács[1,2]*, Krisztina Kárpáti[3], Anette Stájer[4], Stefania Zanetti[5], Matthew Gavino Donadu[5,6]

[1] Department of Pharmacodynamics and Biopharmacy, Faculty of Pharmacy, University of Szeged, Szeged, Hungary
[2] Institute of Medical Microbiology, Faculty of Medicine, Semmelweis University, Budapest, Hungary
[3] Department of Orthodontics and Pediatric Dentistry, Faculty of Dentistry, University of Szeged, Szeged, Hungary
[4] Department of Periodontology, Faculty of Dentistry, University of Szeged, Szeged, Hungary
[5] Department of Biomedical Sciences, University of Sassari, Sassari, Italy
[6] Department of Chemistry and Pharmacy, University of Sassari, Sassari, Italy

ABSTRACT *Pseudomonas aeruginosa* (*P. aeruginosa*) is ubiquitous in nature, and may be a causative agent in severe, life-threatening infections. In >60% of cases, β-lactam antibiotics are used in the therapy of *P. aeruginosa* infections, therefore the emergence of carbapenem-resistant *P. aeruginosa* (CRPA) is a significant clinical concern. In this study, phenotypic methods were used to characterize fifty-four (n = 54) *P. aeruginosa* isolates, which were included based on their suspected non-susceptibility to meropenem. Minimum inhibitory concentrations (MICs) of meropenem, ceftazidime, cefepime, ciprofloxacin, gentamicin, were determined using E-tests, while colistin MICs were determined using broth microdilution. The isolates were subjected to the modified Hodge test (MHT), the modified carbapenem-inactivation method (mCIM) and the imipenem/EDTA combined disk test (CDT). AmpC and efflux pump overexpression was studied using agar plates containing cloxacillin and phenylalanine-arginine β-naphthylamide (PAβN), respectively. Assessment of biofilm-formation was carried out using the crystal violet tube-adherence method. 38.9% of the strains showed meropenem MICs in the resistant range (>8 mg/L). Efflux-pump overexpression and AmpC-hyperproduction was seen in 44.4% and 35.2% of isolates, respectively. 88.8% of the isolates were characterized as strong biofilm-producers. On the other hand, the presence of carbapenemases was suspected in a minority (16.7%) of tested isolates. As safe and effective therapeutic options in carbapenem-resistant Gram-negative infections are severely limited, characterization of these isolates using phenotypic and molecular-based methods is important to provide insights into the epidemiological features of these pathogens.
Acta Biol Szeged 65(1):105-112 (2021)

KEY WORDS
antibiotic
biofilm
carbapenem
carbapenem-resistance
efflux pump
phenotypic assay
Pseudomonas

ARTICLE INFORMATION
Submitted
11 May 2021.
Accepted
28 July 2021.
***Corresponding author**
E-mail: mariopharma92@gmail.com

Introduction

Pseudomonas aeruginosa (*P. aeruginosa*) is a non-fastidious, motile, oxidase-positive non-fermenting Gram-negative bacterial pathogen (belonging to the rRNA group I. among non-fermenters, based on the genomic classification of Palleroni) (Palleroni 1993; Palleroni 2010). *P. aeruginosa* is ubiquitous in nature (in soil, on plants, and in aquatic environments, in addition to being transmitted by birds and smaller mammals as reservoirs) and it is also frequently found in healthcare-associated environments (e.g., persisting in water taps and other inanimate surfaces, irrigation fluids, respiratory tubes, surgical theaters and on medical equipment, spreading via aerosol-formation) as a colonizer on patients (8-20% of infections are preceded by colonization of the relevant anatomical regions) (Blanc et al. 2007; Gumey et al. 2020; Hall et al. 2016). This pathogen may be a causative agent in severe, life-threatening infections (especially in immunocompromised individuals or in patients treated in intensive care units), including pneumonia (Szabó et al. 2005), bacteremia/sepsis (Behzadi et al. 2021), skin and soft tissue infections associated with burns and surgeries (Maenni et al. 2017), otitis externa, keratitis (Cannas et al. 2015) and urinary tract infections (Gajdács et al. 2020). In addition, *P. aeruginosa* may be an important colonizer in the airways of patients with cystic fibrosis and chronic obstructive pulmonary disease (COPD), leading to acute exacerbations and decreased quality of life (Clark et al. 2015; Shariff and Beri 2017).

P. aeruginosa is characterized by having a large (5.5-

7 Mb) genome a with pronounced genomic plasticity, including many regulatory genes, affecting motility, efflux proteins, metabolic pathways and the expression of virulence factors and antibiotic resistance determinants (Algammal et al. 2020; Behzadi and Behzadi 2011; Behzadi et al. 2021). The heterogeneity of the *P. aeruginosa* genome may be further increased through horizontal gene transfer, by the introduction of various mobile genetic elements (Suenaga et al. 2017). A plethora of virulence-determinants have been described in *P. aeruginosa*, including secreted virulence factors such as pigments, exotoxins, proteases and other enzymes (e.g., lipases, alkaline protease, elastase A, DNase), secretion systems (type I-VI) and an exopolysaccharide biofilm; in addition, bacterial cell wall-associated structural components, including lipopolysaccharide (LPS), flagella (for swarming, swimming, and twitching motility), pili, adhesins and lectins (Barrak et al. 2020; Behzadi et al. 2021; Hogardt and Heesemann 2013; Jain et al. 2012).

In the era of multidrug resistant (MDR) pathogens, the therapy of *P. aeruginosa* infections is becoming increasingly difficult (Bassetti et al. 2018; Füzi et al. 2017). To start with, this pathogen is intrinsically resistant to aminopenicillin/β-lactamase-inhibitor combinations, I–II. generation cephalosporins and orally administered III. generation cephalosporins, rifampin, tetracycline, chloramphenicol, trimethoprim-sulfamethoxazole and macrolides (Bassetti et al. 2018; Bonomo and Szabó 2006). Thus, the therapy of pseudomonad infections heavily relies on a select group of antibiotics, including III. and IV. generation parenterally administered cephalosporins, carbapenems, fluoroquinolones, aminoglycosides and colistin. Nevertheless, in >60% of cases, β-lactam antibiotics are used in the therapy of *P. aeruginosa* infections, therefore resistance against these agents (especially carbapenems) is a significant clinical concern (Algammal et al. 2020; Bassetti et al. 2018; Behzadi et al. 2021). The emergence of carbapenem-resistant *P. aeruginosa* (CRPA) may occur through a combination of resistance mechanisms, including decreased membrane permeability and porin loss (e.g., OprD, OprF porin mutants), overexpression of efflux pumps (MexAB-OprM and MexCD-OprJ), changes in penicillin-binding proteins (PBPs) and the production of either chromosomally-encoded or plasmid-mediated β-lactamase enzymes (carbapenemases) capable of hydrolyzing these drugs (Hassuna et al. 2020; Mirzaei et al. 2020). While in some non-fermenters possess chromosomally-mediated β-lactamases are the norm (e.g., L1 and L2 metallo-β-lactamases in *Stenotrophomonas malthophilia*), carbapenemases encoded on mobile genetic present a serious public health issue, as they are capable of widespread dissemination (Gajdács and Urbán 2019; Poole 2011); additionally, these genetic elements often include a wide range of other resistance determinants. The accumulation of intrinsic and plasmid-mediated resistance in *P. aeruginosa* may lead to the emergence of MDR, extensively-drug resistant (XDR) and pandrug-resistant (PDR) isolates (Gajdács 2019; Ranjan et al. 2020).

The characterization of carbapenem-resistant Gram-negative isolates using phenotypic and molecular-based methods is important to provide insights into the epidemiological features of these pathogens, both locally and internationally (Eszik et al. 2016; Mirzaei et al. 2020; Nordmann and Poirel 2019). The aim of our present laboratory-based study was to characterize a selection of carbapenem non-susceptible *P. aeruginosa* isolates using various phenotypic methods.

Materials and methods

Bacterial strains

A total of fifty-four (n = 54) *P. aeruginosa* isolates were included in this study, which were kindly provided by various Hungarian and Italian hospitals, originating from different clinical materials. Inclusion of these strains was based on the non-susceptibility criteria to meropenem (MER) used in routine clinical microbiology, defined by EUCAST (European Committee on Antimicrobial Susceptibility Testing) guidelines v.9.0 (meropenem disk diameter 23-18 mm: intermediate, <19 mm: resistant) (https://www.eucast.org/clinical_breakpoints/). Identification of the isolates was carried out based on classical phenotypic and biochemical panel-based methods (Leber 2016). All isolates included in the study were re-identified as *P. aeruginosa* before further assays. For shorter time periods (<1 month), the bacterial strains were maintained on blood agar with continuous passage. For longer periods, the strains were kept in a -80 °C freezer, in a 1:4 mixture of 85% glycerol and liquid Luria-Bertani medium. During our experiments *P. aeruginosa* ATCC 27853 was used as a control strain.

Minimum inhibitory concentrations (MICs) of meropenem and ancillary antibiotics

MICs of MER, ceftazidime (CEF), cefepime (CFP), gentamicin (GEN) and ciprofloxacin (CIP) were determined by E-tests (Liofilchem, Roseto degli Abruzzi, Italy) on Mueller-Hinton agar plates (Oxoid, Basingstoke, UK). MIC determination for colistin (COL) was carried out using the broth microdilution method in cation-adjusted Mueller-Hinton broth (MERLIN Diagnostika, Berlin, Germany) (Gajdács et al. 2020). The interpretation of the results was based on the European Committee on Antimicrobial Susceptibility Testing (EUCAST) breakpoints v.9.0 (https://www.eucast.org/clinical_breakpoints/).

Phenotypic detection of AmpC overexpression

Overexpression of AmpC β-lactamase enzymes was detected by an agar plate method, where the agar base was supplemented with cloxacillin (250 μg/mL), as cloxacillin inhibits the effects of AmpC β-lactamases (Khalili et al. 2019). A two-fold decrease in CEF MICs in the presence of cloxacillin, compared to MICs without cloxacillin, was considered as positivity for AmpC overexpression (Akhi et al. 2018).

Phenotypic detection of carbapenemase and metallo-β-lactamase (MBL) production

To establish carbapenemase-production in the isolates included in the study, the isolates were subjected to the modified Hodge test (MHT) and the modified carbapenem-inactivation method (mCIM), optimized for *P. aeruginosa*, as previously described (Chou et al. 2020; Pitout et al. 2008; Rao et al. 2019). In both assays, MER disks (10 μg; Oxoid, Basingstoke, UK) were utilized and *Escherichia coli* ATCC 25922 was used as an indicator organism.

Metallo-β-lactamase (MBL) production was tested using the imipenem/EDTA combined disk test (CDT), as described previously (Makharita et al. 2020). In preparation to this assay, imipenem/EDTA disks were prepared by adding 750 μg of a sterile 0.5 M EDTA solution to a 10 μg imipenem disk, then disks were dried in a 37 °C incubator. The assay was considered positive if the inhibition zone diameter (≥17 mm) of the imipenem/EDTA disk increased compared to the imipenem disk alone (Makharita et al. 2020).

Phenotypic detection of efflux pump overexpression

The effect of phenylalanine-arginine β-naphthylamide (PAβN; a compound with well-known efflux pump inhibitory activity) on the MICs of MER was detected using the agar dilution method described previously (Khalili et al. 2019). During the experiments, the concentration of PAβN was 40 μg/mL in the agar base. A two-fold decrease in MER MICs in the presence of PAβN, compared to the MIC values without the inhibitor, was considered as positivity for efflux pump overexpression (Khalili et al. 2019; Gajdács 2020).

Detection of biofilm-production by the tube-adherence method

Assessment of biofilm-formation was carried out in the tube-adherence method described previously (Dumaru et al. 2019; Senobar Tahaei et al. 2021). In short, glass tubes containing 1 mL of sterile trypticase soy broth (bioMérieux, Marcy-l'Étoile, France) were inoculated with 1 μL of the overnight culture of a respective bacterial strains. Respective tubes were then incubated statically for 24 h at 37 °C. Verification of planktonic growth was observed visually. After the incubation period, the supernatant was then discarded, the adhered cells were rinsed three times with phosphate buffer saline (PBS; Sigma-Aldrich; Budapest, Hungary) and the tubes were patted dry on a paper towel. The contents of the tubes were treated with a 1 mL solution of 0.1% crystal violet (CV; Sigma-Aldrich; Budapest, Hungary) to stain the adhered biomass; the tubes were incubated for 3 h at room temperature with the staining solution. The CV solution was then discarded, and the tubes were again rinsed three times with PBS and the tubes were patted dry on a paper towel. Biofilm-formation was observed visually; based on the appearance of visible biofilm lining at the bottom and on wall of the glass tubes, the strains were classified as non-biofilm producers (-), weak biofilm producers (-/+) and strong biofilm producers (+) (Dumaru et al. 2019). All experiments were evaluated by two independent researchers.

Statistical analysis

Descriptive statistical analysis (including means and percentages to characterize data) was performed using Microsoft Excel 2013 (Microsoft Corp.; Redmond, WA, USA).

Ethical considerations

The study was conducted in accordance with the Declaration of Helsinki and national and institutional ethical standards. Ethical approval for the study protocol was obtained from the Human Institutional and Regional Biomedical Research Ethics Committee, University of Szeged (registration number: 140/2021-SZTE [5019]).

Results

MICs of the tested antibiotics, phenotypic detection of AmpC overexpression

The MICs of the tested antibiotics, including MIC_{50}, MIC_{90} values, MIC ranges and the percentage of resistant isolates are presented in Table 1. The highest levels of resistance were observed for CIP (n = 42, 77.8%), followed by CEF (n = 36, 66.7%) and CFP (n = 33, 61.1%). All tested isolates were susceptible to COL, with MIC values ranging between 0.064 and 2 mg/L. Based on EUCAST breakpoints, n = 21 (38.9%) of isolates showed MICs above the resistance breakpoint for MER (8 mg/L), with MICs ranging between 0.5 and 64 mg/L. Among the tested *P. aeruginosa* isolates, overexpressions of AmpC-enzymes were observed in n = 19 (35.2%), where a two-fold decrease in the CEF MICs was seen in the presence of cloxacillin.

Table 1. MIC values of meropenem and ancillary antibiotics on the tested bacterial strains.

	Resistant strains (n, %)	MIC range (mg/L)	MIC50 (mg/L)	MIC90 (mg/L)
Meropenem (MER)	21 (38.9%)	0.5-64	4	16
Ceftazidime (CEF)	36 (66.7%)	0.5-256	8	64
Cefepime (CFP)	33 (61.1%)	0.5-256	8	64
Gentamicin (GEN)	28 (51.9%)	0.25-128	2	16
Ciprofloxacin (CIP)	42 (77.8%)	0.128-16	1	4
Colistin (COL)	0 (0%)	0.064-2	0.128	0.5

Phenotypic detection of carbapenemase, MBL production and efflux pump overexpression

To detect the presence of carbapenemases, two distinct phenotypic methods were utilized: n = 11 (20.4%) isolates presented with positive results in the modified Hodge test (MHT), while this number was n = 9 (16.7%) during the modified carbapenem-inactivation (mCIM) test. If we consider the results of the antibiotic susceptibility testing (MER MIC > 8 mg/L) as a reference in our study, the agreement between the results of the MIC determination and the results of the MHT and mCIM tests were 52.3% and 42.9%, respectively. MBL-production was noted in n = 3 (5.6%) of isolates, using the imipenem/EDTA combined disk test (CDT). Efflux pump-overexpression (based on the PAβN screening agar) was detected in n = 24 (44.4%) of isolates. In the case of n = 3 isolates, efflux pump-overexpression and MHT/mCIM-positivity were detected, while for n = 2 isolates, AmpC-hyperproduction and MHT/mCIM-positivity was seen; for n=6 isolates, high MER MICs were seen with efflux pump-overexpression and AmpC-hyperproduction and negative MHT/mCIM tests.

Biofilm production in the tested isolates

Majority (n = 48, 88.8%) of the tested isolates were strong (+) biofilm producers in the CV tube-based assay, while n = 4 (7.4%) were weak biofilm producers (-/+) and two (3.7%) did not form biofilm (-).

Discussion

Antimicrobial resistance has emerged as a significant public health issue in the 21st century, mainly stemming from the imprudent use of these agents in both community-based and inpatient settings, which has exacerbated the prevalence of resistant bacterial isolates (Aslam et al. 2020; Gajdács et al. 2018; Hemlata and Tiwari 2017); it has been suggested that infections caused by MDR bacteria may be one of the major causes of mortality by 2050 (Gajdács et al. 2021; Shallcross et al. 2015). Drug-resistant *P. aeruginosa* is a significant nosocomial pathogen with the potential to cause serious, difficult-to-treat infections (Kadri et al. 2018). For this reason, it is unsurprising that *P. aeruginosa* has been included among the so-called „ESKAPE" pathogens (designated by the Infectious Diseases Society of America; IDSA), listing the MDR bacteria that are of particular concern for healthcare (Pachori et al. 2016; Rice 2008). From a clinical standpoint, infections caused by CRPA present an important therapeutic problem, as even with the introduction of some novel antimicrobials (e.g., β-lactam-β-lactamase combinations, neoglycosides), there are limited number of safe and effective therapeutic alternatives remaining (Hu et al. 2019). Based on the data of the US Centers for Disease Control (CDC), the prevalence of CRPA was around ~12%, corresponding to ~51 000 nosocomial infections per year (Nordmann and Poirel 2019); while based on the data of the European Antimicrobial Resistance Surveillance Network (EARS-Net) for 2017, the population-weighted mean prevalence of CRPA in invasive isolates was 17.4% (lowest in Iceland [0%], highest in Romania 63.4%]) (ECDC 2019).

Carbapenem resistance in *Pseudomonas* more commonly occurs due to alternations in the membrane permeability (i.e. porin deficiency) and the overexpression of efflux pumps, while the production of carbapenemases is observed less frequently, especially when compared to the members of *Enterobacteriaceae* and *Acinetobacter* spp. (Nordmann and Poirel 2019). Initially, metallo-β-lactamases were characteristic for *Pseudomonas* spp.; in fact, both IMP (active-on-imipenem) and VIM-type (Verona intergon-encoded MBL) enzymes were first described in pseudomonads (Lauretti et al. 1999; Watanabe et al. 1991). Since then, the presence of many other carbapenemases (including the *Klebsiella pneumoniae* carbapenemase [KPC], and the New Delhi metallo-beta-lactamase [NDM]) were reported in CRPA isolates (Halat and Moubareck 2020; Nordmann and Poirel 2019). In our present study, a collection of *P. aeruginosa* isolates – suspected of being CRPA – were included and their characterization was carried out using various phenotypic assays. Among the isolates, 38.9% of the strains showed MER MICs in the resistant range, while apart from COL (which showed 100% susceptibility), resistance rates were high (>50%) against the other tested antibiotics as well. Similarly to

other reports in the literature, carbapenemase-detection methods were positive in a lower number of isolates, i.e. 20.4% for MHT and 16.7% for mCIM, whereas the presence MBL was suggested in only 5.6%, respectively. On the other hand, the prevalence of efflux pump overexpression was seen in a much higher rate, in 44.4% of isolates. Another common characteristic of clinical *P. aeruginosa* isolates is the production of a protective biofilm, which was verified *in vitro* in 88.8% of our isolates.

Between 2003 and 2005, the first outbreaks and the spread of MBL-producing *Pseudomonas* sp. was reported in Hungary, corresponding to two distinct groups of isolates based on serotyping (O11 and O12, respectively) with the carriage of VIM-4 (Libisch et al. 2006). Most of these isolates originated from either urine or tracheal aspirate samples and most of them had high MICs corresponding to imipenem (>256 mg/L) and MER (>32 mg/L) (Libisch et al. 2006). The first detection of a PER-1 and VIM-2-producing *P. aeruginosa* isolate was reported in 2008, which was associated with a Hungarian patient who was initially hospitalized in Egypt (Szabó et al. 2008); in this clinical case, three distinct *P. aeruginosa* strains were detected, one resistant to antipseudomonal cephalosporins (with MICs>256 mg/L), one resistant to imipenem only (MIC>32 mg/L) and one presenting with high-level resistance against imipenem (MIC>256 mg/L) and MER (MIC>32 mg/L) (Szabó et al. 2008). In an effort to provide the most effective therapy for patients affected by invasive *P. aeruginosa* infections, a Monte Carlo simulation was performed using the susceptibility data from Hungarian *P. aeruginosa* isolates: the results suggest that due to the worsening rates of resistance, as increasing doses, frequencies or infusion times, in addition to combination antimicrobial therapy may be relevant in the empiric therapy of *P. aeruginosa* in Hungary (Ludwig et al. 2006). Based on the surveillance data of the Hungarian National Public Health Centre, bloodstream infections were among the more common nosocomial infections caused by *P. aeruginosa* in recent years (Epi-Net 2021). A study group in Hungary has published the occurrence of MDR *P. aeruginosa* found in environmental sites contaminated by hydrocarbons between the period of 2002-2007; carbapenem-resistance was noted in 33% of isolates (Kaszab et al. 2010). The same study group has also recently reported ceftriaxone and imipenem resistance in 25.0% of tested environmental *P. aeruginosa* isolates; in addition, five out of the 44 isolates originating from sources as groundwater, soil or compost showed close genetic relatedness to clinically relevant pulse-field types based on pulse-field gel electrophoresis (PFGE) (Kaszab et al. 2019). In a laboratory-based study, n = 250 carbapenem-resistant *P. aeruginosa* were surveyed for their susceptibilities against ceftazidime-avibactam (C/A) and ceftolozane–tazobactam (C/T), in addition to a phenotypic-genotypic study for carbapenemase-production: prevalence of resistance to C/A and C/T was 33.6% and 32.4%, respectively; isolates producing positive CIM-tests were VIM (80%) or NDM (11%) producers (O'Neall et al. 2020). This study has concluded that in case of a negative CIM-test for a relevant carbapenem non-susceptible *P. aeruginosa* isolate, either C/A or C/T may be an effective therapeutic choice (O'Neall et al. 2020). A study involving n = 57 carbapenem-resistant, but cephalosporin susceptible (Car-R/Ceph-S) *P. aeruginosa* isolates originating from urinary tract infections has highlighted the role of efflux pump overexpression and overproduction of AmpC β-lactamases in the development of the carbapenem-resistant phenotype; the study has also highlighted that – although rare – these isolates may constitute a viable target for colistin-sparing strategies (Gajdács 2020). A similar study was performed in Turkey, where n=243 isolates were assessed by phenotypic and molecular methods: in this report, carbapenemase-producing isolates were not detected, while overexpression of MexAB-OprM (60.9%) and MexXY-OprM (68.8%) efflux pumps and decreased permeability due to OprD-related porin deficiency (68.8%) were the principal mechanisms of resistance (Khalili et al. 2019).

Due to the disadvantageous developments in antibiotic resistance trends globally (and the increasing prevalence of CRPA), it has been suggested that alternative antimicrobial therapeutic strategies should be explored more extensively (Hauser et al. 2016; Usai et al. 2019). These strategies may include physico-chemical modalities, such as sonobactericide (ultrasound), lasers and the use of photosensitizers for photodynamic therapy (Lattwein et al. 2020; Stájer et al. 2020); in contrast, novel pharmacological modalities include bacteriophages, probiotics, antimicrobial peptides, antibodies and antivirulence compounds, many of which were already included in some human clinical trials (Ghosh et al. 2019; Kumar et al. 2021). Compounds of natural origin have long been proposed as a potential source of novel antimicrobials for the treatment of drug resistant infections (either as monotherapy or as adjuvant), including MDR *Pseudomonas* (Ding et al. 2021; Amorese et al. 2018). These may include extracts of various plant materials, new bioactive compounds or phytopharmaceuticals and essential oils (Le NT et al. 2020); these compounds are often characterized by good safety and tolerability *in vivo*, in addition to having established indications in ethnopharmacology/traditional medicine (Le et al. 2020; Mazzarello et al. 2020). It may be assumed that – in addition to novel antibiotics – the introduction of such alternative treatments to the clinical practice may have a pronounced role in the treatment of difficult-to-treat infections in the 21st century.

Acknowledgements

M.G. was supported by the János Bolyai Research Scholarship (BO/00144/20/5) of the Hungarian Academy of Sciences. The research was supported by the ÚNKP-20-5-SZTE-330 New National Excellence Program of the Ministry for Innovation and Technology from the source of the National Research, Development and Innovation Fund. Support from Ministry of Human Capacities, Hungary grant 20391-3/2018/FEKUSTRAT is acknowledged. M.G. would also like to acknowledge the support of ESCMID's "30 under 30" Award.

References

Akhi MT, Khalili Y, Ghotaslou R, Yousefi S, Kafil HS, Naghili B, Sheikhalizadeh V (2018) Evaluation of carbapenem resistance mechanisms and its association with *Pseudomonas aeruginosa* infection in the Nortwest of Iran. Microb Drug Res 24:126-135.

Algammal AM, Mabrok M, Sivaramasamy E, Youssef FM, Atwa MH, El-Kholy AW, Hetta HF, Hozzein WN (2020) Emerging MDR-*Pseudomonas aeruginosa* in fish commonly harbor oprL and toxA virulence genes and bla-TEM, blaCTX-M, and tetA antibiotic-resistance genes. Sci Rep 10:e15961.

Aslam A, Gajdács M, Zin CS, Ab RNS, Ahmed SI, Zafar MZ, Jamshed S (2020) Evidence of the practice of self-medication with antibiotics among the lay public in low- and middle-income countries: A scoping review. Antibiotics 9:e597.

Barrak I, Baráth Z, Tián T, Venkei A, Gajdács M, Urbán E, Stájer A (2021) Effects of different decontaminating solutions used for the treatment of peri-implantitis on the growth of *Porphyromonas gingivalis*-an in vitro study. Acta Microbiol Immunol Hung 68:40-47.

Bassetti M, Vena A, Croxatto A, Righi E, Guery B (2018) How to manage *Pseudomonas aeruginosa* infections. Drugs Context 7:e212527.

Behzadi P, Baráth Z, Gajdács M (2021) It's not easy being green: A narrative review on the microbiology, virulence and therapeutic prospects of multidrug-resistant *Pseudomonas aeruginosa*. Antibiotics 10:e42.

Behzadi P, Behzadi E (2011) A study on apoptosis inducing effects of UVB irradiation in *Pseudomonas aeruginosa*. Roum Arch Microbiol Immunol 70:74-77.

Blanc DS, Francioli P, Zanetti G (2007) Molecular epidemiology of *Pseudomonas aeruginosa* in the intensive care units—A review. Open Microbiol J 1:8–11.

Bonomo RA, Szabó D (2006) Mechanisms of multidrug resistance in *Acinetobacter* species and *Pseudomonas aeruginosa*. Clin Infect Dis 43:S49-S56.

Cannas S, Usai D, Pinna A, Benvenuti S, Tardugno R, Donadu M, Zanetti S, Kaliamurthy J, Molicotti P (2015) Essential oils in ocular pathology: an experimental study. J Infect Dev Ctries 9:650-654.

Chou CH, Lai YR, Chi CY, Ho MW, Chen CL, Liao WC, Ho CH, Chen YA, Chen CY, Lin YT, Lin CD, Lai CH (2020) Long-term surveillance of antibiotic prescriptions and the prevalence of antimicrobial resistance in non-fermenting gram-negative bacilli. Microorganisms 8:e397.

Clark ST, Caballero JD, Cheang M, Coburn B, Wang PW, Donaldson SL, Zhang Y, Liu M, Keshavjee S, Yau YCW, Waters VJ, Tullis DE, Guttman DS, Hwang DM (2015) Phenotypic diversity within a *Pseudomonas aeruginosa* population infecting an adult with cystic fibrosis. Sci Rep 5:e10932.

Ding J, Gao X, Gui H, Ding X, Lu Y, An S, Liu Q (2021) Proteomic analysis of proteins associated with inhibition of *Pseudomonas aeruginosa* resistance to imipenem mediated by the chinese herbal medicine qi gui yin. Microb Drug Resist 27:462-470.

Amorese V, Donadu M, Usai D, Sanna A, Milia F, Pisanu F, Molicotti P, Zanetti S, Doria C (2018) *In vitro* activity of essential oils against *Pseudomonas aeruginosa* isolated from infected hip implants. J Infect Dev Ctries 11:996-1001.

Le NT, Donadu MG, Ho DV, Doan TQ, Le AT, Raal A, Usai D, Sanna G, Marchetti M, Usai M, Diaz N, Rappelli P, Zanetti S, Cappuccinelli P, Nguyen HT (2020) Biological activities of essential oil extracted from leaves of *Atalantia sessiflora* Guillaumin in Vietnam. J Infect Dev Ctries 9:1054-1064.

Dumaru R, Baral R, Shrestha LB (2019) Study of biofilm formation and antibiotic resistance pattern of gram-negative bacilli among the clinical isolates at BPKIHS, Dharan. BMC Res Notes 12:e38.

European centre for disease prevention and control. Surveillance of antimicrobial resistance in Europe - Annual report of the european antimicrobial resistance surveillance network (EARS-Net) 2017. Stockholm: ECDC; 2018. Available from: https://ecdc.europa.eu/sites/portal/files/documents/AMR-surveillance-EARS-Net-2017.pdf

Eszik I, Lantos I, Önder K, Somogyvári F, Burián K, Endrész V, Virók DP (2016) High dynamic range detection of *Chlamydia trachomatis* growth by direct quantitative PCR of the infected cells. J Microbiol Meth 120:15-22.

Epi-Net (2021) Carbapenem-resistant *Pseudomonas aeruginosa* in Hungary. Available online: https://epi-net.eu/outbreaks/700/700/ (Accessed on 10th of May 2021)

Füzi M, Szabó D, Csercsik R (2017) Double-serine fluoroquinolone resistance mutations advance major international clones and lineages of various multi-drug resistant bacteria. Front Microbiol 8:e2261.

Gajdács M (2020) Carbapenem-resistant but cephalosporin-susceptible *Pseudomonas aeruginosa* in urinary tract in-

fections: Opportunity for colistin sparing. Antibiotics 9:e153.

Gajdács M (2019) [Excess mortality due to pandrug resistant bacteria: a survey of the literature]. Hung Health Prom J 60:29-34.

Gajdács M, Paulik E, Szabó A (2018) [The opinion of community pharmacists related to antibiotic use and resistance]. Acta Pharm Hung 88:249-252.

Gajdács M, Urbán E (2019) Prevalence and antibiotic resistance of *Stenotrophomonas maltophilia* in respiratory tract samples: A 10-year epidemiological snapshot. Health Serv Manag Epidemiol 6:e2333392819870774.

Gajdács M, Ábrók M, Lázár A, Jánvári L, Tóth Á, Terhes G, Burián K (2020) Detection of VIM, NDM and OXA-48 producing carbapenem resistant Enterobacterales among clinical isolates in Southern Hungary. Acta Microbiol Immunol Hung 67: 209-215.

Gajdács M, Bátori Z, Ábrók M, Lázár A, Burián K (2020) Characterization of resistance in gram-negative urinary isolates using existing and novel indicators of clinical relevance: A 10-year data analysis. Life 10:e16.

Gajdács M, Urbán E, Stájer A, Baráth Z (2021) Antimicrobial resistance in the context of the sustainable development goals: A brief review. Eur J Investig Health Psychol Educ 11:71-82.

Ghosh C, Sarkar P, Issa R, Haldar J (2019) Alternatives to conventional antibiotics in the era of antimicrobial resistance. Trends Microbiol 27:323-338.

Gumey J, Pradier L, Griffin JS, Gougat-Barbera C, Chan BK, Turner PE, Kaltz O, Hochberg ME (2020) Phage steering of antibiotic-resistance evolution in the bacterial pathogen, *Pseudomonas aeruginosa*. Evol Med Pub Health 1:148–157.

Halat DH, Moubareck CA (2020) The current burden of carbapenemases: Review of significant properties and dissemination among gram-negative bacteria. Antibiotics 9:e186.

Hall S, McDermott C, Anoopkumar-Dukie S, McFarland AJ, Forbes A, Perkis AV, Davey AK, Chess-Williams R, Kiefel MJ, Arora D, Grant D, Grant GD (2016) Cellular effects of pyocyanin, a secreted virulence factor of *Pseudomonas aeruginosa*. Toxins 8:236.

Hassuna NA, Darwish MK, Sayed M, Ibrahem RA (2020) Molecular epidemiology and mechanisms of high-level resistance to meropenem and imipenem in *Pseudomonas aeruginosa*. Infect Drug Res 13:285–293.

Hauser AR, Mecsas J, Moir DT (2016) Beyond antibiotics: New therapeutic approaches for bacterial infections. Clin Infect Dis 63:89-95.

Hemlata ATJ, Tiwari A (2017) The ever changing face of antibiotic resistance: Prevailing problems and preventive measures. Curr Drug Metab 18:69-77.

Hogardt M, Heesemann J (2013) Microevolution of *Pseudomonas aeruginosa* to a chronic pathogen of the cystic fibrosis lung. Curr Top Microbiol Immunol 358:91-118.

Hu YY, Cao JM, Yang Q, Chen S, Lv HY, Zhou HW, Wu Z, Zhang R (2019) Risk factors for carbapenem-resistant *Pseudomonas aeruginosa*, Zhejiang province, China. Emerg Infect Dis 25:1861-1867.

Jain R, Behrens AJ, Kaever V, Kazmierczak BI (2012) Type IV pilus assembly in *Pseudomonas aeruginosa* over a broad range of cyclic di-GMP concentrations. J Bacteriol 194:4285-4294.

Kadri SS, Adjemian J, Lai YL, Spaulding AB, Ricotta E, Prevots DR, Powers JH III (2018) Difficult-to-treat resistance in gram-negative bacteremia at 173 US hospitals: Retrospective cohort analysis of prevalence, predictors, and outcome of resistance to all first-line agents. Clin Infect Dis 67:1803-1814.

Kaszab E, Radó J, Kriszt B, Pászti J, Lesinszki V, Szabó Á, Tóth G, Khaledi A, Szoboszlay S (2019) Groundwater, soil and compost, as possible sources of virulent and antibiotic-resistant *Pseudomonas aeruginosa*. Int J Environ Health Res https://doi.org/10.1080/09603123.2019.1691719

Kaszab E, Kriszt B, Atzél B, Szabó G, Szabó I, Harkai P, Szoboszlay S (2010) The occurrence of multidrug-resistant *Pseudomonas aeruginosa* on hydrocarbon-contaminated Sites. Microb Ecol 59:37-45.

Khalili Y, Yekani M, Goli HR, Memar MY (2019) Characterization of carbapenem-resistant but cephalosporin-susceptible *Pseudomonas aeruginosa*. Acta Microbiol Immunol Hung 66:529-540.

Kumar M, Sarma DK, Shubram S, Kumawat M, Verma V, Nina PB, Devraj JP, Kumar S, Singh B, Tiwari RR (2021) Futuristic non-antibiotic therapies to combat antibiotic resistance: A review. Front Microbiol 12:e609459.

Lattwein KR, Shekhar H, Kouijzer JJP, van Wamel WJB, Hollan KC, Kooiman K (2020) Sonobactericide: An emerging treatment strategy for bacterial infections. Ultrasound Med Biol 46:193-215.

Lauretti L, Riccio ML, Mazzariol A, Cornaglia G, Amicosante G, Fontana R, Rossolini GM (1999) Cloning and characterization of blaVIM, a new integron-borne metallo-beta-lactamase gene from a *Pseudomonas aeruginosa* clinical isolate. Antimicrob Agents Chemother 43:1584-1590.

Le NT, Ho DV, Doan TQ, Le AT, Raal A, Usai D, Madeddu S, Marchetti M, Usai M, Rappelli P, Diaz N, Zanetti S, Nguyen HT, Cappuccinelli P, Donadu M (2020) *In vitro* Antimicrobial Activity of Essential Oil Extracted from Leaves of *Leoheo domatiophorus* Chaowasku, D.T. Ngo and H.T. Le in Vietnam. Plants 9:e453.

Leber AL (Ed.) (2016) Clinical Microbiology Procedures Handbook, 4th ed., ASM Press, Washington, DC, USA.

Libisch B, Muzslay M, Gacs M, Minárovics J, Knausz M,

Watine J, Ternák G, Kenéz É, Kustos I, Rókusz L, Széles K, Balogh B, Füzi M (2006) Molecular epidemiology of VIM-4 metallo-β-lactamase-producing *Pseudomonas* sp. isolates in Hungary. Antimicrob Agents Chemother 50:4220-4223.

Ludwig E, Konkoly-Thege M, Kuti JL, Nicolau DP (2006) Optimising antibiotic dosing regimens based on pharmacodynamic target attainment against *Pseudomonas aeruginosa* collected in Hungarian hospitals. Int J Antimicrob Agents 28:433-438.

Maenni M, Bour M, Chatre P, Madec JY, Plésiat P, Jeannot K (2017) Resistance of animal strains of *Pseudomonas aeruginosa* to carbapenems. Front Microbiol 8:e1841.

Makharita RR, El-Kholy I, Hetta HL, Abdelaziz MH, Hagagy FI, Ahmed AA, Algammal AM (2020) Antibiogram and genetic characterization of carbapenem-resistant gram-negative pathogens incriminated in healthcare-associated infections. Infect Drug Res 13:3991-4002.

Mazzarello V, Gavini E, Rassu G, Donadu MG, Usai D, Piu G, Pomponi V, Sucato F, Zanetti S, Montesu MA (2020) Clinical assessment of new topical cream containing two essential oils combined with tretinoin in the treatment of acne. Clin Cosmet Investig Dermatol 13:233-239.

Mirzaei B, Bazgir ZN, Goli HR, Iranpour F, Mohammadi F, Babei R (2020) Prevalence of multi-drug resistant (MDR) and extensively drug-resistant (XDR) phenotypes of *Pseudomonas aeruginosa* and *Acinetobacter baumannii* isolated in clinical samples from Northeast of Iran. BMC Res Notes 13:e380.

Nordmann P, Poirel L (2019) Epidemiology and diagnostics of carbapenem resistance in gram-negative bacteria. Clin Infect Dis 69:S521-S528.

O'Neall D, Juhász E, Tóth Á, Urbán E, Szabó J, Melegh S, Katona K, Kristóf K (2020) Ceftazidime–avibactam and ceftolozane–tazobactam susceptibility of multidrug resistant *Pseudomonas aeruginosa* strains in Hungary. Acta Microbiol Immunol Hung 67:61-65.

Pachori P, Gothalwal R, Gandhi P (2016) Emergence of antibiotic resistance *Pseudomonas aeruginosa* in intensive care unit; A critical review. Genes Dis 6:e109.

Palleroni NJ (1993) *Pseudomonas* classification. A new case history in the taxonomy of gram-negative bacteria. Antonie Van Leeuwenhoek 64:231-351.

Palleroni NJ (2010) The *Pseudomonas* story. Environ Microbiol 12:1377–1383.

Pitout JD Revathi G, Chow BL, Kabera B, Kariuki S, Nordmann P, Poirel L (2008) Metallo-β-lactamase-producing *Pseudomonas aeruginosa* isolates in Tunisia. Clin Microbiol Infect 14:755-759.

Poole K (2011) *Pseudomonas aeruginosa*: Resistance to the max. Front Microbiol 2:e65.

Ranjan VK, Mukherjee S, Thakur S, Gupta K, Chakraborty R (2020) Pandrug-resistant *Pseudomonas* spp. expresses New Delhi metallo-β-lactamase-1 and consumes ampicillin as sole carbon source. Clin Microbiol Infect 27:472.e1-472.e5.

Rao MR, Chandrashaker P, Mahale RP, Shivappa SG, Gowda RS, Chitharagi VB (2019) Detection of carbapenemase production in *Enterobacteriaceae* and *Pseudomonas* species by carbapenemase Nordmann–Poirel test. J Lab Physicians 11:107-110.

Rice LB (2008) Federal funding for the study of antimicrobial resistance in nosocomial pathogens: No ESKAPE. J Infect Dis 197:1097-1081.

Senobar Tahaei SA, Stájer A, Barrak I, Ostorházi E, Szabó D, Gajdács M (2021) Correlation between biofilm-formation and the antibiotic resistant phenotype in *Staphylococcus aureus* isolates: A laboratory-based study in Hungary and a review of the literature. Infect Drug Res 14:1155-1168.

Shallcross LJ, Howard SJ, Fowler T, Davies SC (2015) Tackling the threat of antimicrobial resistance: From policy to sustainable action. Philos Trans R Soc Lond B Biol Sci 370:e20140082.

Shariff AM, Beri K (2017) Exacerbation of bronchiectasis by *Pseudomonas monteilii*: A case report. BMC Infect Dis 17:e511.

Stájer A, Kajári S, Gajdács M, Musah-Eroje M, Baráth Z (2020) Utility of photodynamic therapy in dentistry: Current concepts. Dent J 8:e43.

Suenaga H, Fujihara H, Kimura N, Hirose J, Watanabe T, Futagami T, Goto M, Shimodaira J, Furukawa K (2017) Insights into the genomic plasticity of *Pseudomonas putida* KF715, a strain with unique biphenyl-utilizing activity and genome instability properties. Environ Microbiol Rep 9:589-598.

Szabó D, Szentandrássy J, Juhász Z, Katona K, Nagy K, Rókusz L (2008) Imported PER-1 producing *Pseudomonas aeruginosa*, PER-1 producing *Acinetobacter baumanii* and VIM-2-producing *Pseudomonas aeruginosa* strains in Hungary. Ann Clin Microbiol Antimicrob 7:e12.

Szabó D, Silveria F, Fujitani S, Paterson DL (2005) Mechanisms of resistance of bacteria causing ventilator-associated pneumonia. Clin Chest Med 26:75-79.

Usai D, Donadu M, Bua A, Molicotti P, Zanetti S, Piras S, Corona P, Ibba R, Carta A (2019) Enhancement of antimicrobial activity of pump inhibitors associating drugs. J Infect Dev Ctries 13:162-164.

Watanabe M, Iyobe S, Inoue M, Mitsuhashi S (1991) Transferable imipenem resistance in *Pseudomonas aeruginosa*. Antimicrob Agents Chemother 35:147-151

Acta Biologica Szegediensis

Volume 65(1):113-117, 2021
Acta Biologica Szegediensis
http://abs.bibl.u-szeged.hu/index.php/abs

DOI:10.14232/abs.2021.1.113-117

ARTICLE

The effect of type II toxin-antitoxin systems on methicillin-resistant *Staphylococcus aureus* persister cell formation and antibiotic tolerance

Mandana Hosseini[1], Jamileh Nowroozi[1], Nour Amirmozafari[2]*

[1]Department of Microbiology, Tehran North Branch, Islamic Azad University, Tehran, Iran
[2]Department of Microbiology, School of Medicine, Iran University of Medical Sciences, Tehran, Iran

ABSTRACT Persister cells are defined as a subpopulation of bacteria in a dormant state with the ability to reduce bacterial metabolism and they are involved in antibiotic tolerance. Toxin-antitoxin (TA) systems have been previously suggested as important players in persistence. Therefore, this study aimed to study the involvement of TA systems in persister cell formation in methicillin-resistant *Staphylococcus aureus* following antibiotic exposure. Using TADB and RASTA database, two type II TA systems including MazF/MazE and RelE/RelB were predicted in *S. aureus*. The presence of these TA genes was determined in 5 methicillin-resistant *S. aureus* isolates and the standard strain S. aureus subsp. aureus N315 using PCR method. To induce persistence, isolates were exposed to lethal doses of ciprofloxacin and the expression of the studied TA system genes was measured after 5 h using Real-Time PCR. According to our results, all the studied isolates harbored the TA system genes. *S. aureus* was highly capable of persister cell formation following exposure to sub-MIC of ciprofloxacin and RT-qPCR showed a significant increase in the expression of the MazEF and RelBE loci, indicating their potential role in antibiotic tolerance. Considering the importance of antibiotic tolerance, further studies on persister cell formation and TA systems involved in this phenomenon are required to efficiently target these systems.

KEY WORDS
methicillin resistance
persister cells
real-time PCR
Staphylococcus aureus
TA systems

ARTICLE INFORMATION
Submitted
13 June 2021.
Accepted
1 July 2021.
***Corresponding author**
E-mail: amirmozafari@iums.ac.ir

Introduction

Persisters are defined as a subpopulation of bacterial cells in a non-growing state characterized by a transient phenotype state (Abbasi et al. 2015). Persister cells can survive lethal doses of antibiotics, and this tolerance, contrary to resistance, is not associated with genetic inheritance (Narimisa et al. 2020). As evidenced, these subpopulations of bacteria show biphasic killing curves following exposure to high doses of antibiotics, while many other bacteria are rapidly killed. These population of bacteria are clinically important as they contribute to antibiotic tolerance and thereby leading to chronic infections and treatment failure (Fisher et al. 2017). Persister cell formation has been attributed to many mechanism, the most studied one being the toxin-antitoxin (TA) systems (Page et al. 2016). TA systems are defined as small genetic loci widely distributed among bacterial genomes. These systems are comprised of a stable toxin and its cognate labile antitoxin coded on a single operon. (Guglielmini et al. 2011). To date, six classes of these TA systems have been identified based on the mechanism of activity and the nature of TA components, with type II being the most studied type. Type II TA systems are comprised of protein toxins and antitoxins and have been repeatedly reported as players of bacterial stress responses (Goeders et al. 2014). Upon stress, the antitoxin is degraded by cellular proteases such as Lon or Clp protease, and the liberated toxin component interferes with vital cellular processes such as translation, cell-wall synthesis and replication, which subsequently affect bacterial growth and lead to the emergence of persisters (Coussens et al. 2016).

Persister cell formation has been demonstrated in almost all bacterial pathogens, one of them being *Staphylococcus aureus* (Chang et al. 2020). *S. aureus* is considered as one of the major antibiotic-resistant pathogens and a public health concern (Rajabi et al. 2020). Resistance to penicillin in this bacterium was reported early after the discovery of penicillin. Even after the development of other antibiotics such as methicillin, emergence and worldwide outbreaks of methicillin-resistant *S. aureus* was reported, becoming a threat to global health (Mwangi et al. 2007). Reportedly, these isolates are also resistant to other classes of antibiotics, such as vancomycin. Apart from resistance, persisters can lead to chronic infections

Table 1. Predicted toxin-antitoxin systems in this study.

TA Type	Toxin	Antitoxin	Classification (family/domain)	Location on *S. aureus* N315
2	SA1873	SAS067	*MazEF*/RHH-*MazF*	2121172..2121701
2	SA2195	SA2196	*relBE*/PHD-RelE	2466001..2466518

and treatment failure, thereby doubling the burden of these bacterial species (Singh et al. 2017). Therefore, it is crucial to study these subpopulations of bacteria and the related mechanisms. For this purpose, this study aimed the evaluation of persister cell formation in MRSA isolates following exposure to different antibiotics and investigation of the expression levels of type II TA systems in these bacteria.

Materials and methods

Bacterial strains and growth conditions

In this study, *S. aureus* subsp. *aureus* N315 and 5 clinical MRSA isolates were used. Isolates were previously collected from burn wounds and taxonomical classification was carried out by using biochemical and molecular tests. Bacterial strains were stored in Brain Heart Infusion (BHI) broth (Merck, Darmstadt, Germany) containing 20% glycerol at -80 °C.

Determination of the Minimum Inhibitory Concentration (MIC)

MIC of ciprofloxacin (Sigma Aldrich, Germany) against *S. aureus* subsp. *aureus* N315 and MRSA isolates was determined by the broth microdilution assay using 96 U-shaped well plates (Singh et al. 2017). For this purpose, 100 µL of Mueller-Hinton broth (Oxoid, UK) was added to each well of the plate, and 100 µL of ciprofloxacin solution was added to the first well and serially diluted. Finally, 100 µL of the overnight culture containing ~3×10^8 bacterial cells were added to each well. For MIC determination, the plate was incubated at 37 °C for 24 h and bacterial growth was recorded. MIC values for ciprofloxacin was measured independently in triplicates.

Persister formation

To induce persister cells in the studied isolates, bacterial cultures in the exponential phase were exposed to high doses of ciprofloxacin. For quantification of the persister cells, a single colony of MRSA isolates or *S. aureus* subsp. *aureus* N315 was inoculated into 5ml BHI broth (Merck, Darmstadt, Germany) for 24 h. Then, bacterial subculture was diluted 1:100 and incubated at 37 °C on a shaker at 200 rpm to obtain an optical density of 0.4 at 600 nm. To draw bacterial killing curves, bacterial cultures in the exponential phase were exposed to 10-fold MIC concentration of ciprofloxacin, and cultures were grown at 37 °C (220 rpm) for 3.5 h. After centrifugation at 1400 rpm for 5 min, bacterial cultures were washed with PBS twice and after supernatant removal, fresh BHI broth was added and centrifuged at 220 rpm at 37 °C. After ciprofloxacin stress, bacterial cells were washed twice by 0.85% sterile PBS for ciprofloxacin removal and after serial dilutions of bacterial culture, bacterial cells were inoculated onto BHI agar for CFU determination. Bacterial culture without ciprofloxacin exposure was selected as the control.

Identification of TA system genes and their detection by polymerase chain reaction (PCR)

Prediction of TA systems in *S. aureus* subsp. *aureus* N315 was carried out by using RASTA-bacteria and TADB2.0

Table 2. Primers used in this study.

TA System	Sequence (5' - 3')		Annealing temperature (°C)	Amplicon size (bp)
gyrB	F	AGGTCTTGGAGAAATGAATG	62	113
	R	CAAATGTTTGGTCCGCTT		
SA1873 (T)	F	AAGGGGGAGTCAGACCTGTA	58	91
	R	ATCCTACCAGTTATTGCCGC		
SAS067 (AT)	F	TCAAAATAGAAGTCATAGCTTAGAACA	57	157
	R	TCATTCATTCGTTGAATTAGAAGAT		
SA2195 (T)	F	ATTACGTTTTCGCCTCAAGC	59	154
	R	TCAGATTCGATTTTAACTTTTCAGG		
SA2196 (AT)	F	CGCTCGACAGAATTTAAAGG	58	152
	R	TTGGGTTCTGTTGGAGGTAAA		

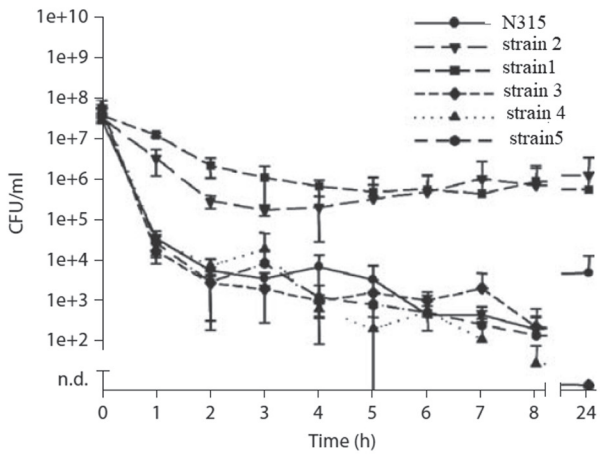

Figure 1. Time-dependent killing curve of the studied strains at exponential growth following exposure to 5 µg/ml of ciprofloxacin.

database (Sevin et al. 2007, Xie et al. 2018). Two TA loci including *mazEF* and *relBE* were predicted (Table 1). To investigate the presence of these TA systems in our studied isolates, we performed PCR assay using specific primers targeting these loci designed by Oligo 7 and Primer 3 (Table 2). For this purpose, total DNA of bacterial isolates was extracted using boiling method as previously described (Junior et al. 2016). A total final volume of 25 µL of PCR reaction consisted of 12.5 µL MasterMix (Amplicon, USA), 2 µL of each primer (forward and reverse with the concentration of 10 pmol), 2 µL of template bacterial DNA, and 6.5 µL sterile distilled water. Thermal cycling program consisted of initial denaturation for 5 min at 94 °C, followed by 30 cycles of denaturation for 1 min at 94 °C, annealing (based on Table 2) for 30 s, extension for 1 min at 72 °C, and final extension for 5 min at 72 °C. PCR amplicons were then analyzed by electrophoresis on 1.5% agarose gel.

Relative RT-qPCR

Total RNA was extracted from 1 ml of the studied bacterial cultures in the exponential phase after 5 h of treatment with 100-fold MICs concentrations of ciprofloxacin. Total RNA of *S. aureus* that was not exposed to ciprofloxacin was also extracted as the control, using high pure RNA isolation kit (Roche, Germany) according to the protocols provided by the manufacturer. For removing DNA contamination, DNaseI treatment was carried out (Thermo Scientific, USA) according to the protocol. To assess RNA quality, NanoDrop spectrophotometer (Thermo Scientific, USA) and gel electrophoresis analysis were used. For cDNA synthesis, cDNA Synthesis Kit (Thermo Scientific, USA) was used. Primers used for real-time PCR was the same used for our PCR assay (Table 2). Quantitative reverse transcription-PCR (RT-qPCR) was carried out in triplicates for each sample using a Rotor-Gene thermal cycler (Corbett Life Sciences, Sydney, Australia) with SYBR Green method (Ampliqon Co, Denmark). Total 20 µL amplification reaction contained 2 µL of cDNA, 10 µL SYBR Green master mix, 7 µL nuclease-free water, and 0.8 µL of each forward and reverse primer. PCR reaction was as follows: an initial denaturation at 95 °C for 1 min, followed by 40 cycles at 95 °C for 20 s, annealing temperature (Table 2) for 25 s, and 72 °C for 20 s. *gyrB* was used as an internal control for normalization of the expression levels. The delta-delta Ct method was used for quantification of the relative fold changes in expression levels (Livak et al. 2001).

Statistical analysis

To assess significant differences in gene expression levels, T-Test and Mann-Whitney test were used. All data analyses and drawings were carried out with GraphPad Prism 8 (GraphPad Software).

Results

Persister cell formation assays

The MIC of ciprofloxacin was 0.5 µg/ml. To study the ability of persister cell formation, we treated the studied bacterial cultures in the exponential phase with 10-fold MIC Concentration of ciprofloxacin (5 µg/ml) and observed a rapid reduction in bacterial CFU values. This reduction rate varied from 94% for strain 1 to 99% for *S. aureus* subsp. *aureus* N315 after 5 h. Relatively constant CFU rate after 5 h up to 24 h was indicative of the presence of persister cells in response to ciprofloxacin exposure (Fig. 1).

Presence of TA system genes and their relative expression following antibiotic exposure

According to the results of PCR assay, all the studied strains harbored both *mazEF* and *relBE* TA loci. The expression levels of *mazF* and *relE* genes increased in isolates exposed to ciprofloxacin (p-value < 0.05). Also, *mazF* expression showed a higher increase compared to *relE* expression (Fig. 2).

Discussion

S. aureus isolates, and especially methicillin resistant *S. aureus* (MRSA), are considered as major pathogens that are responsible for nosocomial and community-acquired infections with high mortality rate, especially

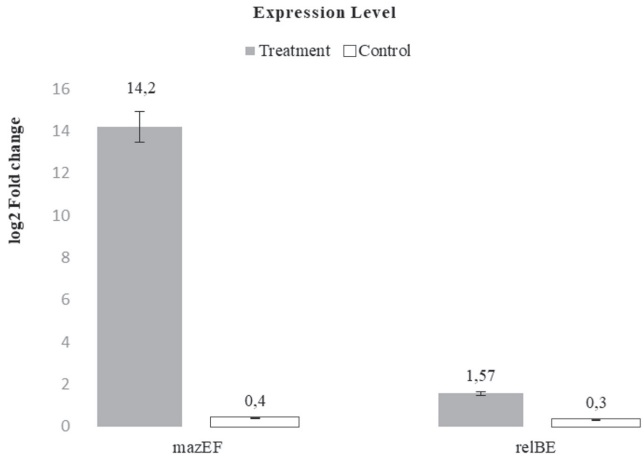

Figure 2. Expression levels of *mazF* and *relE* genes in the treatment and control groups.

in wound burn patients (Lee et al. 2018; Lakhundi et al. 2018). The major concern about infections caused by *S. aureus* is treatment failure of MRSA infections, leading to increased mortality rate and treatment costs (Turner et al. 2019; Gajdács 2019). Several studies have indicated the involvement of TA systems in bacterial persister cell formation following exposure to antibiotic stresses. Therefore, these systems could be potentially important for combating antibiotic tolerance in pathogenic bacteria (Wood 2016; Holden et al. 2018).

The effect of TA systems on persister cell formation was initially identified by Harris Moyed in 1983. He indicated that two mutations in *hipA* could increase the rate of persister cell formation for 10000 fold (Moyed et al. 1983). Following this notion, the effect of TA system toxins in persister cell formation was investigated by gene deletion or overexpression. Vázquez et al. indicated that the overexpression of *relE* and *mazF* could increase antibiotic tolerance and persister cell formation in *E. coli* strains (Vázquez-Laslop et al. 2006). Interestingly, a synergism has been indicated between protein toxins of TA systems and antibiotics. For instance, toxin component of the CcdA/CcdB and ParE/ParD systems are involved in inhibiting DNA amplification by affecting DNA gyrase, which is also a target for quinolones. Also, RelE/RelB and Phd/Doc systems affect ribosomal $tRNA^{fmet}$, thereby disrupting protein synthesis. Similarly, antibiotics including macrolides and clindamycin target the 50S subunit of bacterial ribosome, thereby inhibiting protein biosynthesis. Considering the overlap between TA system toxin and antibiotics as well as their role in programmed cell death, novel antimicrobial agents can be developed with the ability to disrupt the balance between toxins and their cognate antitoxins. Also, considering the role of TA systems in antibiotic tolerance, biofilm formation, and pathogenicity, these systems can be suitable targets to combat pathogenic bacteria. As an illustration, it has been previously shown that mutation in *hipBA* TA system of *E. coli* modulates persister cell formation (Butt et al. 2014).

According to RT-qPCR results, *mazF* and *relE* expression increased for 35.3- and 5.24-fold, respectively, compared to the control group, indicating their possible role in persister cell formation (p-value < 0.05). Several previous studies have indicated the involvement of MazF toxin in bacterial stress responses. MazEF system is generally one of the most studied TA systems in bacteria. For instance, in a study on *E. coli*, Engelberg-Kulka et al (2005) showed that this system is in fact a chromosomally encoded conserved loci with mRNA endonuclease activity that initiates programmed cell death in response to stress conditions, and finally retains a subpopulation of bacteria that can survive the harsh conditions (Engelberg-Kulka et al. 2005). Also, in another study on *Listeria monocytogenes* in 2018, Kalani et al. indicated that MazF toxin is activated in heat stress and therefore, it can contribute to bacterial survival (Kalani et al. 2018). In another study on *L. monocytogenes*, it was demonstrated that MazEF was activated during antibiotic stress, and is essential for bacterial survival (Curtis et al. 2017).

RelBE is another TA system in *E. coli* that has been extensively studied. This system is involved in bacterial response to amino acid deprivation and leads to the inhibition of translation. In a study conducted by Coskun et al. (2018), it was reported that TA system genes were encoded in the genome of *Pseudomonas aeruginosa* and *S. aureus* and all MRSA isolates (n=78) harbored *relBE* and *higBA* TA loci (Coskun 2018), which was in agreement to our study.

In a study by Butt and co-workers, it was shown that the exposure of *Burkholderia pseudomallei* to ciprofloxacin could increase HicA toxin levels and subsequently led to persister cell formation (Butt et al. 2014). Other studies have indicated that bactericidal antibiotics such as kanamycin have the ability to inhibit TA systems in *E. coli*. These TA systems included MazE/MazF, RelB/RelE, MqsR/MqsA, and BigB/BigA (Hu et al. 2010). In another study on the expression of TA system genes in *E. coli*, following exposure to kanamycin and ampicillin, all the mentioned TAs systems were inhibited, indicating that cell death following treatment with bactericidal antibiotics could be associated with many TA systems (Lee and Lee 2016).

References

Abbasi K, Tajbakhsh E (2015) Prevalence of Shiga toxin

genes and intimin genes in uropathogenic *Escherichia coli*. J Coast Life Med 3:791-796.

Butt A, Higman V, Williams C, Crump M, Hemsley C, Harmer N, Titball R (2014) The HicA toxin from *Burkholderia pseudomallei* has a role in persister cell formation. Biochem J 459:333-344.

Chang J, Lee R, Lee W (2020) A pursuit of *Staphylococcus aureus* continues: a role of persister cells. Arch Pharm Res 1-9.

Coskun U (2018) Effect of mazEF, higBA and relBE toxin-antitoxin systems on antibiotic resistance in *Pseudomonas aeruginosa* and *Staphylococcus* isolates. Malawi Med J 30:67-72.

Coussens N, Daines D, (2016) Wake me when it's over–bacterial toxin–antitoxin proteins and induced dormancy. Exp Biol Med 241:1332-1342.

Curtis T, Takeuchi I, Gram L, Knudsen G (2017) The influence of the toxin/antitoxin mazEF on growth and survival of *Listeria monocytogenes* under stress. Toxins 9:31.

Engelberg-Kulka H, Hazan R, Amitai S (2005) mazEF: a chromosomal toxin-antitoxin module that triggers programmed cell death in bacteria. J Cell Sci 118:4327-4332.

Fisher R, Gollan B, Helaine S (2017) Persistent bacterial infections and persister cells. Nat Rev Microbiol 15(8):453-464.

Gajdács M (2019) The continuing threat of methicillin-resistant *Staphylococcus aureus*. Antibiotics 8(2):52.

Goeders N, Van Melderen L (2014) Toxin-antitoxin systems as multilevel interaction systems. Toxins 6:304-324.

Guglielmini J, Van Melderen L (2011) Bacterial toxin-antitoxin systems: Translation inhibitors everywhere. Mob Genet Elements 1:283-306.

Holden D, Errington J (2018) Type II toxin-antitoxin systems and persister cells. MBio 9(5):e01574-18.

Hu MX, Zhang X, Li EL, Feng Y-J (2010) Recent advancements in toxin and antitoxin systems involved in bacterial programmed cell death. Int J Microbiol 2010:781430.

Junior J, Tamanini R, Soares B, de Oliveira A, de Godoi Silva F, da Silva F, Augusto N, Beloti V (2016) Efficiency of boiling and four other methods for genomic DNA extraction of deteriorating spore-forming bacteria from milk. Semin Cienc Agrar 37:3069-3078.

Kalani B, Irajian G, Lotfollahi L, Abdollahzadeh E, Razavi S (2018) Putative type II toxin-antitoxin systems in *Listeria monocytogenes* isolated from clinical, food, and animal samples in Iran. Microb Pathog 122:19-24.

Lakhundi S, Zhang K (2018) Methicillin-resistant *Staphylococcus aureus*: molecular characterization, evolution, and epidemiology. Clin Microbiol Rev 31(4):e00020-18.

Lee AS, de Lencastre H, Garau J, Kluytmans J, Malhotra-Kumar S, Peschel A, Harbarth S (2018) Methicillin-resistant *Staphylococcus aureus*. Nat Rev Dis Primers 4:1-23.

Lee K, Lee B (2016) Structure, biology, and therapeutic application of toxin–antitoxin systems in pathogenic bacteria. Toxins 8:305.

Livak K, Schmittgen T (2001) Analysis of relative gene expression data using real-time quantitative PCR and the 2−ΔΔCT method. Methods 25:402-408.

Moyed H, S. Bertrand K (1983) hipA, a newly recognized gene of *Escherichia coli* K-12 that affects frequency of persistence after inhibition of murein synthesis. J Bacteriol 155:768-775.

Mwangi M, Wu, Zhou Y, Sieradzki K, de Lencastre H, Richardson P, Bruce D, Rubin E, Myers E, Siggia E (2007) Tracking the in vivo evolution of multidrug resistance in *Staphylococcus aureus* by whole-genome sequencing. PNAS 104:9451-9456.

Narimisa N, Kalani B. S, Amraei F, Mohammadzadeh R, Mirkalantari S, Razavi S, Jazi F (2020) Type II toxin/antitoxin system genes expression in persister cells of *Klebsiella pneumoniae*. Rev Med Microbiol 31(4):215-220.

Page R, Peti W (2016) Toxin-antitoxin systems in bacterial growth arrest and persistence. Nat Chem Biol 12:208-214.

Rajabi S, Shivaee A, Khosravi A, Eshaghi M, Shahbazi S, Hosseini F (2020) Evaluation of multidrug efflux pump expression in clinical isolates of *Staphylococcus aureus*. Gene Rep 18:100537.

Sevin E, Barloy-Hubler F (2007) RASTA-Bacteria: a web-based tool for identifying toxin-antitoxin loci in prokaryotes. Genome Biol 8:R155.

Singh M, Matsuo M, Sasaki T, Morimoto Y, Hishinuma T, Hiramatsu K (2017) In vitro tolerance of drug-naive *Staphylococcus aureus* strain FDA209P to vancomycin. Antimicrob Agents Chemother 61(2):e01154-16.

Turner N, Sharma-Kuinkel B, Maskarinec S, Eichenberger E, Shah P, Carugati M, Holland T, Fowler G (2019) Methicillin-resistant *Staphylococcus aureus*: an overview of basic and clinical research. Nat Rev Microbiol 17:203-218.

Vázquez-Laslop N, Lee H, Neyfakh A (2006) Increased persistence in *Escherichia coli* caused by controlled expression of toxins or other unrelated proteins. J Bacteriol 188:3494-3497.

Wood T (2016) Combatting bacterial persister cells. Biotechnol Bioeng 113:476-483.

Xie Y, Wei Y, Shen Y, Li X, Zhou H, Tai C, Deng Z, Ou H (2018) TADB 2.0: an updated database of bacterial type II toxin–antitoxin loci. Nucleic Acids Res 46:D749-D753.

Acta Biologica Szegediensis

Volume 65(1):119-132, 2021
Acta Biologica Szegediensis
http://abs.bibl.u-szeged.hu/index.php/abs
DOI:10.14232/abs.2021.1.119-132

Abstracts of the Annual Conference of Doctoral School of Biology, University of Szeged – 2021.

The role of alternative histone usage in differentiated cell and tissue functions

Andrea Ábrahám

[1]Department of Biochemistry and Molecular Biology, Faculty of Science and Informatics, University of Szeged, Szeged, Hungary
[2]Institute of Biochemistry, Biological Research Centre, Szeged, Hungary
[3]Doctoral School of Biology, Faculty of Science and Informatics, University of Szeged, Szeged, Hungary

Histones play an essential role in the function of both dividing and post-mitotic cells through the regulation of chromatin related processes, such as replication, repair and gene expression. Any defect that affects the amount or structure of histone proteins can lead to cell death or to failures in division. Although several degenerative diseases and cancer types have been associated with histone dysfunctions, there are still many open questions about histone functions. In the focus of our interest is the role of replication indepent (RI) histones.

The *His4r* is the gene of an alternative form of the core histone *H4* in *Drosophila*. The gene is located outside the canonical histone cluster, it is present in the genome in one copy as typical alternative histones are, transcribed independently to the time of DNA replication, and has a regular eukaryotic gene structure. Unlike canonical histones, *His4r* contains an intron and the mRNA transcribed from it is polyadenylated. Nonetheless, the amino acid sequence of His4r protein is identical to that of the canonical H4, what poses the intriguing question that what could be the functional role of His4r.

In order to make possible distinquishing His4r from its identical canonical H4 counterpart we have created a transgenic *Drosophila* line in which the *His4r* gene is modified to produce His4r with a 3xFlag tag. Using this *Drosophila* line we analysed His4r expression in different tissues at several stages of fly development, and found that the ubiquitous expression of His4r becomes cell type-specific during neuronal development. Based on promoter analysis of *His4r*, and expression data from experiments of our own and others, we hypothesize that His4r may play a role in neuronal differentiation and environmental stress responses. To confirm this theory, we performed ChIP-seq experiment and found that His4r indeed showed an increased amount at inducible genes and genes controling neuronal differentiation. This genomic distribution raises the possibility that His4r may also play a role in the development of transcriptional memory. Experiments to verify this assumption are in progress.

Supervisors: Imre Boros, László Henn
e-mail: abrahama@brc.hu

Agricultural recycling of spent mushroom compost following microbiological processing

Henrietta Allaga

[1]Department of Microbiology, Faculty of Science and Informatics, University of Szeged, Szeged, Hungary
[2]Doctoral School of Biology, Faculty of Science and Informatics, University of Szeged, Szeged, Hungary

Besides spawn and mushroom compost, casing material with proper quality is also an important requisite of economical production of champignons (*Agaricus bisporus*). In mushroom growing houses, the compost colonized by the mushroom mycelia is covered by the casing material, the role of which is primarily to ensure the conditions for fruiting body formation and provide high water content. The nutrient-rich mushroom compost has low water retaining capacity, which is compensated by the casing material. The depletion of peat mines in Hungary and other European countries, as well as the environmental problems arising from peat mining lead to an emerging need for the development of alternative solutions for the production of high-quality casing materials. Due to its high fiber, as well as P, K, and N content, harvested mushroom compost may serve as an excellent raw material for the development of casing materials. The recycling of spent mushroom compost has been attempted in some cases by vermicomposting, and its microbiological re-composting might also be a possible alternative. The purpose of our work was the selection and characterization of fungal and bacterial strains that could be used for the controlled transformation of spent mushroom compost, thus recycling it as casing material.

A total of 32 bacterial and 23 fungal strains were isolated from samples deriving from experimental re-composting process

Volume 65(1):119-132, 2021
Acta Biologica Szegediensis
http://abs.bibl.u-szeged.hu/index.php/abs

DOI:10.14232/abs.2021.1.119-132

of spent mushroom compost. Species identification of the bacterial isolates, performed by sequence analysis of a fragment of the *gyrA* gene amplified by the gyrA-F and gyrA-R primers revealed *Bacillus subtilis* (3), *B. licheniformis* (8) and *B. safenesis* (1), *Bacillus* sp. (1). The *Lysinibacillus fusiformis* (2), *L. macroides* (3), *Lysinibacillus* sp. (1), *Ochrobactrum anthropi* (1), *Alcaligenes faecalis* (1), *Lactococcus lactis* (1), *Lactobacillus paraplantarum* (1), *Microbacterium* sp. (1) strains performed by EUB primers (Eub 341-F and Eub 1060-R). while fungi were identified by ITS 1-4 (internal transcribed spacer) region as *Mortierella wolfii* (6), *Mucor circinelloides* (4), *Fusarium solani* (1), *Geotrichum candidum* (4), *Geotrichum* sp. (1), *Lichtheimia ramosa* (1), *Penicillium griseofulvum* (1), *Trichosporon asahii* (1), *Rhodotorula mucilaginosa* (1) and *Trichoderma harzianum* species complex (1). *Aureobasidium pullulans* (3) strains were previously isolated and deposited in a strain collection. The *Bacillus* and *Aureobasidium* strains were subjected to ecophysiological characterization and extracellular enzyme activity assays as well as seed germination experiments. The examined *B. subtilis*, *B. licheniformis* and *A. pullulans* strains were found to produce high lipase, protease and cellulase activities. The spent mushroom compost is being tested for use as casing layer in mushroom cultivation, as well as a plant growth medium. The application of the re-composted spent mushroom compost as casing resulted in 509 g white button mushroom crop, while the maximum mushroom yield using peat was 402 g in a potted cultivation experiment. Based on our results we conclude that the re-composted spent mushroom compost may be a suitable raw material for the production of casing layer for mushroom cultivation, at it may even contribute to increasing mushroom yield.

Supervisors: Dr. László Kredics, Dr. Lóránt Hatvani
e-mail address: henrietta.allaga@gmail.com

Sigma-1 receptor agonist Fluvoxamine engages anti-inflammatory actions and decrease oxidative stress in TNBS-induced experimental colitis

Nikoletta Almási

[1]Department of Physiology, Anatomy and Neuroscience, Faculty of Science and Informatics, University of Szeged, Szeged, Hungary
[2]Doctoral School of Biology, Faculty of Science and Informatics, University of Szeged, Szeged, Hungary

Inflammatory bowel disease (IBD) is a serious health issue of the gastrointestinal tract, which is manifested mainly in prolonged gut inflammation and an imbalance between free radicals and antioxidants. Considering the autoimmune nature of the disease complete recovery is still not possible, however several treatment options exist to alleviate its symptoms. Sigma-1 receptor (σ1R) is originally described by Martin et al. as an opioid receptor. Now it is suggested based on ligand binding affinity measurements that σ1R seems to possess a unique receptor class. σ1R is located in the mitochondria-associated endoplasmic reticulum membrane and it is responsible for Ca^{2+} homeostasis. Furthermore, it seems that the activation of the receptor has anti-inflammatory and antioxidant properties.

Therefore, our study aimed to investigate the effects of the activation of σ1R in 2,4,6-trinitrobenzene sulfonic acid (TNBS)-induced experimental colitis. To this end, a single intracolonic (i.c.) TNBS administration was used in Wistar-Harlan rats to induce inflammation in the colon. Then to clarify the effects of σ1R activation in this inflammatory condition, i.c. administered fluvoxamine (FLV) was used as a σ1R agonist and BD1063 as an antagonist. A combination of the two ligands was also administered as a co-treatment for further clarification. Our radioligand binding studies with [^{3}H](+)-pentazocine ligand clearly showed the existence of the receptor in the colon and FLV treatment significantly increased the maximum binding capacity of σ1R compared to TNBS. Furthermore, FLV significantly reduced the colonic damage which effect was abolished by the co-treatment with BD1063 antagonist. Additionally, σ1R agonist FLV alleviated pro-inflammatory markers, such as myeloperoxidase (MPO) activity and interleukin-6 (IL-6), which effects were abolished by the administration of BD1063 antagonist. Furthermore, FLV was shown to decrease pro-oxidant factors, such as 3-nitrotyrosine (3-NT), and significantly increased glutathione (GSH) and peroxiredoxin-1 (PRDX-1) antioxidants. Taken together, the activation of σ1R through FLV administration seems to be a promising therapeutic approach against experimental IBD.

Supervisor: Krisztina Kupai
E-mail: almasi.niki91@gmail.com

Volume 65(1):119-132, 2021
Acta Biologica Szegediensis
http://abs.bibl.u-szeged.hu/index.php/abs

DOI:10.14232/abs.2021.1.119-132

Microtubule organizing centers contain testis-specific γ-TuRC proteins in spermatids of *Drosophila melanogaster*

Elham Alzyoud

[1]Department of Genetics, Faculty of Science and Informatics, University of Szeged, Szeged, Hungary
[2]Doctoral School of Biology, Faculty of Science and Informatics, University of Szeged, Szeged, Hungary

Centrosomes are the most studied Microtubule-Organizing Center (MTOC) in animal cells, they consist of a pair of centrioles surrounded by an amorphous pericentriolar material. Gamma Tubulin Ring Complex (γ-TuRC) is known as the main player for microtubules nucleation in MTOC. Proteins involved in the formation and the development of MTOC in *Drosophila* are conserved among eukaryotes. Mutations of many of MTOC proteins are known to cause diseases in human. γ-TuRC was studied in many *Drosophila* tissues but not in late spermatogenesis. Since later stages of *Drosophila* spermatogenesis are controlled mainly by testis-specific proteins, MTOC formation and cellular remodelling is an open question. Our aim was to study the γ-TuRC distribution and function during late stages of *Drosophila* spermatogenesis. γ-tubulin exists in two complexes in *Drosophila*: γ-tubulin Small complex (γ-TuSC) and γ-TuRC. γ-TuSC is smaller composed of two γ-tubulin and two Grip proteins: Grip84 and Grip91, while γ-TuRC composed of multiple γ-TuSC in addition of three or four γ-TuRC binding proteins: Grip128, Grip163, Grip75 and Grip71. We conducted phylogenetic analysis for the γ-TuRC component proteins, and we identified three testis-specific γ-TuRC proteins. γ-TuSC represented by t-Grip84 and t-Grip91 a paralogue of Grip84 and Grip91 respectively, the third one is t-Grip128 a paralogue of Grip128. This suggests the existence of testis-specific γ-TuRC (t-γ-TuRC). We analyzed the phenotype of the mutants of t-γ-TuRC genes. We found that t-Grip84 mutant is male sterile, t-Grip91 mutant is male semi-sterile and t-Grip128 mutant fertility is normal. We made transgenic lines and checked the localization of the tagged version of t-γ-TuRC proteins. They localize to the centriole adjunct after meiosis, and also to the nuclear tip during nuclear elongation and transfer to the surface of the mitochondria during cyst elongation. We analyzed the interactions of the t-γ-TuRC proteins biochemically and proved binding to γ-tubulin and Mzt1 and also the complex members to each other. Our results provided the first proof of the existence and essentiality of t-γ-TuRC, which can lead us to understand better the molecular composition of the different MTOCs during the late stages of spermatogenesis.

Supervisor: Dr. Rita Sinka
E-mail: alzyoud.elham@stud.u-szeged.hu

Exploring the potential of genetically modified bacteriophages against multidrug resistant (MDR), highly pathogenic bacterial species

Gábor Apjok

[1]Synthetic and Systems Biology Unit, Institute of Biochemistry, BRC, Szeged, Hungary
[2]Doctoral School of Biology, Faculty of Science and Informatics, University of Szeged, Szeged, Hungary

The rapid spread of antibiotic resistant pathogenic bacteria represents an ever-growing challenge around the globe. It is expected to become the leading cause of deaths in the near future. Fortunately, there are many promising alternatives under excessive development. One such direction is the application of bacteriophages (phages). Phages are bacterial viruses and are prime candidates as therapeutic agents. My main focus is to develop techniques to genetically modify phages to extend their contribution in the fight against MDR bacteria.

Both the direct, and indirect applicability of phages are addressed in my research. In the latter case, we developed a method to rapidly construct hybrid bacteriophage particles to serve as effective DNA delivery agents. These particles were then used to deliver metagenomic libraries into pathogenic species to mimic horizontal gene transfer, the main driving force behind the spread of antibiotic resistance. The novelty of this approach is the successful involvement of clinically relevant pathogenic species into such investigations. Our method can therefore shed light on previously unknown factors that shape the spread of antibiotic resistance. The next step is to extend the direct therapeutic applicability of bacteriophages using genome engineering techniques. The primary aim is the creation of phage cocktails consisting diverse sets of synthetic bacteriophages with enhanced features for clinical applications. To achieve this goal, we will build artificial phages using viral parts that are nec-

Volume 65(1):119-132, 2021
Acta Biologica Szegediensis
http://abs.bibl.u-szeged.hu/index.php/abs

DOI:10.14232/abs.2021.1.119-132

essary for their propagation and has therapeutic benefits. Our first step is to seek bacteriophages with therapeutic potential. To this end we isolated phages from hospital sewage targeting a set of MDR pathogenic strains. We have discovered dozens of novel phages, many of which we have sequenced and characterized, revealing therapeutically useful components that can be used to construct synthetic phages. Lastly, we are going to apply targeted mutagenesis using our own technique to further optimize the features of synthetic phages. The end goal of this research is to put the generated phage cocktails into practice.

Supervisors: Dr. Csaba Pál, Dr. Bálint Kintses
Email: agabor723@gmail.com

Mapping of symbiotic peptides of *Amorpha fruticosa*

Benedikta Balla

[1]Institute of Plant Biology, Biological Research Center, Szeged, Hungary
[2]Doctoral School of Biology, Faculty of Science and Informatics, University of Szeged, Szeged, Hungary

Nitrogen is a vital element for the development of living organisms thus plants, which can be introduced into the soil with artificial or natural fertilizers, the efficiency of this method is unsatisfactory and quite polluting. An obvious alternative would be the atmospheric nitrogen, but this cannot be utilized directly by plants due to its strong triple bond, it is converted by the diazotrophic bacteria into a form that can be taken up by plants. This includes the genus paraphyletic group of *Rhizobium bacteria*; whose members form a unique symbiotic organ with plants from Fabaceae family: the nodule.

A. fruticosa is also a species of the Fabaceae family. It moved from North America to Europe, where it spread rapidly. In Hungary, one of the typical shrub plants on the riverbanks of the Tisza, the intoxicating scent of bright purple flowers is one of the favourites of honeybees. At the beginning of our work, we collected wild plants and soil samples from its root zone, and then the plants were later grown under laboratory conditions. The symbiotic bacterium was re-isolated from wild-type nodules by excavation. The recovery and maintenance of the unknown organism proved to be a particularly difficult task, as only a negligible amount of information can be found in the literature. Due to the described and more detailed knowledge, we considered it very important to create the most accurate picture possible. Transmission and scanning electron microscopy sections as well as light and confocal microscopic images, demonstrated the nodule specific transformation of symbiotic bacteria to bacteroids, suggesting that this plant also expresses nodule-specific cysteine rich peptides like *Medicago truncatula* and its analogs, the NCR-like peptides. The intranodular conversion of nitrogen-fixing bacteroids, has evolved at least five times independently during evolution, but in case of *A. fruticosa* is perhaps the oldest or sixth form of choice, so the symbiosis chosen by us can play a key role in getting to know the process more extensively.

The efficiency of nitrogen fixation was confirmed by acetylene reduction experiments and compared to alfalfa in the absence of a reference. In general, the efficiency of 10-20-day old nodules is the highest. Knowing the 16S rRNA sequence, the symbiotic bacterium *Mesorhizobium amorpha* was probable.

Compounds produced by *A. fruticosa*, which are promising molecules for the treatment of diabetes, or their ability to improve soil through nitrogen fixation, reveal that this invasive, aggressive, and indestructible weed has untapped potential.

Supervisor: Attila Kereszt
E-mail: benedikta.balla@gmail.com

The effect of acute adenosine treatment on the blood-brain barrier tightness

Lilla Barna

[1]Institute of Biophysics, Biological Research Centre, Szeged, Hungary
[2]Doctoral School of Biology, Faculty of Science and Informatics, University of Szeged, Szeged, Hungary

Sleep restriction increases blood-brain barrier (BBB) permeability in mice to fluorescein, that is completely restored after 24 hours of sleep recovery. Adenosine, a potent somnogenic molecule, is accumulated during sleep loss and may regulate BBB permeability. The blockade of A2A adenosine receptors reverted the BBB dysfunction induced by sleep restriction in rats. Our

DOI:10.14232/abs.2021.1.119-132

aim was to investigate the presence of adenosine receptors in the cells of the BBB and the effect of acute adenosine treatment on BBB culture models and on BBB permeability in rats.

The mRNA expression of A1, A2A, A2B and A3 adenosine receptors were examined by qPCR. The kinetics of cell response was followed by real-time impedance measurement (RTCA-SP, Agilent). Primary rat brain endothelial cells in monoculture, in co-culture with glial cells, or with brain pericytes and glial cells were treated with adenosine, the A2A receptor agonist NECA and antagonist SCH-58261. The integrity of the barrier was tested by electrical resistance (TEER) measurements across the culture model of the BBB and permeability measurements performed both on cultures and in Wistar rats.

We verified that rat brain endothelial cells expressed mRNA for A2A and A2B receptors, but not for A1 and A3 receptors. Rat brain pericytes expressed A1, A2A and A2B, while astroglial cells expressed all four types of receptors. We demonstrated statistically significant increase in impedance values in both adenosine and NECA treatment groups in the first 2 hours, and no damage of brain endothelial cells was observed until 24 hours. Adenosine treatment from the luminal side of brain endothelial cells tightened the barrier and decreased the fluorescein permeability in monoculture and co-culture BBB models. Correspondingly, in Wistar rats treated with intracardiac adenosine injection BBB permeability was decreased for fluorescein and albumin. Adenosine treatment on the abluminal side increased the permeability in the triple co-culture model containing pericytes but not in monoculture and co-culture with glial cells. Adenosine given to the cerebrospinal fluid also increased BBB permeability. A2A receptor antagonist inhibited the effects of adenosine and NECA in culture and animal models.

We demonstrated the presence of adenosine receptors on cultured brain endothelial cells, pericytes and astroglial cells. Acute adenosine treatment from the luminal side acting directly on brain endothelial cells tightened the barrier in BBB culture models and in rats, which was blocked by an inhibitor of adenosine A2 receptors. We also revealed that brain pericytes may mediate the barrier opening effect of acute adenosine treatment from the abluminal side.

Supervisors: Dr. Mária Deli, Dr. András Harazin
E-mail: barna.lilla@brc.hu

Surfactin production profiling of different *Bacillus* strains isolated from vegetable rhizospheres

Attila Bartal

[1]Department of Microbiology, Faculty of Science and Informatics, University of Szeged, Szeged, Hungary
[2]Doctoral School of Biology, Faculty of Science and Informatics, University of Szeged, Szeged, Hungary

Surfactins are cyclic lipopeptides consisting of a β-hydroxy fatty acid and a peptide ring of seven amino acids linked together by a lactone bridge, forming the cyclic structure of the peptide chain. They possess a high variability in their fatty acid chain lengths and amino acid sequences, bearing numerous variants and isoforms. These compounds are produced mainly by *Bacillus* species and possess numerous biological effects such as antibacterial, antifungal and antiviral activities. Different *Bacillus* species and strains produce distinct variants of surfactins in various ratios, thus affecting the biological and environmental characteristics of the varying ferment broths. Owing to their surface effect, the research of surfactins in therapeutical, environmental and agricultural applications is also a subject of increasing interest.

For their surfactin production profiling, several *Bacillus* strains isolated from vegetable rhizospheres were identified by GC-FID technique. Then a fast and easily evaluable HPLC-HESI-MS method was developed using SIM/SRM mode to achieve the simultaneous quantitative and qualitative characterizations of the extracted ferment broths. Altogether the production profiles of 25 different *Bacillus* species and strains isolated from vegetable rhizospheres were acquired based on the developed methods. More than half of the examined *Bacillus* strains produced surfactins and the MS^2 spectra analyses of their sodiated precursor ions revealed a total of 29 surfactin variants and homologues. Certain surfactins were occurred with extremely high number of peaks with different retention times, suggesting the large numbers of variations in the branching of their fatty acid chains. Results supported the conclusions of our former studies stating that the appearance of previously rarely encountered group of surfactins with methyl esterified aspartic acid in their fifth amino acid position may be encountered in considerable numbers and the fatty acid chain lengths to vary between 12 and 18 carbon atoms.

Supervisor: Dr. András Szekeres
E-mail: bartaloszi@gmail.com

Volume 65(1):119-132, 2021
Acta Biologica Szegediensis
http://abs.bibl.u-szeged.hu/index.php/abs

DOI:10.14232/abs.2021.1.119-132

Detection, elimination and damaging effect of singlet oxygen in the photosynthetic apparatus of plants and unicellular microalgae

Faiza Bashir

[1]Institute of Plant Biology, Biological Research Centre, Szeged, Hungary
[2]Doctoral School of Biology, Faculty of Science and Informatics, University of Szeged, Szeged, Hungary

Singlet oxygen ($^1O_2$) is a highly reactive oxygen species and is produced in photosynthetic organisms under high light stress. $^1O_2$ is involved in the process of photoinhibition; however, the exact mechanism of action of $^1O_2$ is still unclear, and this is due to the lack of suitable methods to detect singlet oxygen intracellularly. The damaging effects of $^1O_2$ are also debated, and the main question of this debate is whether $^1O_2$ can directly damage the Photosystem II (PSII) complex or it can inhibit only the protein synthesis dependent repair of PSII.

Our aim was the detection of singlet oxygen, characterization of its role in photodamage of PSII and its elimination to prevent its damaging effects. $^1O_2$ was detected by various methods; electron paramagnetic resonance, fluorescence probing by Singlet Oxygen Sensor Green (SOSG), and oxygen uptake due to chemical trapping in vitro and in isolated thylakoids. Protoplasts were prepared to investigate the intracellularly produced $^1O_2$ by using intracellular $^1O_2$ labeling dye SOSG, as these fluorophores are impermeable to intact cells due to the presence of a cell wall. Our data demonstrated for the first time that SOSG is penetrated to the protoplasts of *Symbiodinium* sp., and therefore protoplasts are amenable to investigate singlet oxygen signaling in *Symbiodinium* sp. To eliminate the $^1O_2$, proline was found to be a quencher of singlet oxygen in vitro via a physical mechanism with a bimolecular quenching. To study the damaging effects of $^1O_2$, we employed a multiwell plate-based screening method combined with chlorophyll fluorescence imaging to characterize the effect of externally produced $^1O_2$ on the photosynthetic activity of isolated thylakoid membranes and intact *Chlorella sorokiniana* cells. The results show that the externally produced $^1O_2$ by the photosensitization reactions of rose bengal damages Photosystem II both in isolated thylakoid membranes and in intact cells in a concentration-dependent manner, indicating that $^1O_2$ plays a significant role in photodamage of Photosystem II.

Supervisors: Imre Vass, Szabo Milan
E-mail: scholar.faiza@gmail.com

Involvement of polyamine metabolism in plant developmental and stress responses

Péter Benkő

[1]Department of Plant Biology, Faculty of Science and Informatics, University of Szeged, Szeged, Hungary
[2]Doctoral School of Biology, Faculty of Science and Informatics, University of Szeged, Szeged, Hungary

Homeostasis of reactive oxygen species (ROS) is controlled by low molecular weight compounds, such as polyamines (PAs). Polyamine oxidases (PAO) participate in the regulation of PA homeostasis, mediating their oxidation/ back-conversion. Products of PAO-mediated enzymatic action include H_2O_2. Studies involving overexpression or downregulation of PAO indicate that H_2O_2 derived from PA catabolism is important in stress responses. Evidence also suggests that, parallel with ROS, production of reactive nitrogen species (RNS) and particularly nitric oxide (NO) also occurs during developmental processes and exposure of plants to different abiotic stresses. Considering the function of PA, PAO and NO in plant developmental and stress responses, and peroxisomal localization of certain PAO and peroxisomal accumulation of NO, regulatory role of PA metabolism, mainly the role of PAO, on NO generation was speculated. To monitor the effect of PAOs during abiotic stress responses and developmental processes *Arabidopsis thaliana* different mutant lines was used. During salt stress ROS production was increased in S-AtPAO3 plants. Interestingly, inhibition of NADPH oxidase resulted a decrease in ROS production of S-AtPAO3 roots. NO production was also affected by PA catabolism however not AtPAO3 but AtPAO2 was involved in this process. Involvement of AtPAO2 in heat stress responses was also investigated through the regulation of NO production by NR. Based on these results a possible cross talk between peroxisomal PAOs, NADPH oxidases, ROS and NO in salt and heat stress responses of *Arabidopsis* could be supposed.

To study the involvement of PA metabolism in pollen germination and pollen tube elongation in vitro pollen germination technique was used. Putrescine had a somewhat positive effect on pollen tube emergence, but negatively regulated its further elongation; spermidine enhanced both processes, while spermine had negative effect on pollen germination but did not in-

DOI:10.14232/abs.2021.1.119-132

fluenced pollen tube growth. Our data indicated that PAs regulate pollen germination primarily via regulating the ROS level, while tube elongation primarily influencing the NO level. Our results further supported the involvement of PAs in the regulation of pollen germination and elongation affecting ROS and/or NO levels in a polyamine- and cellular-region-specific way.

Supervisors: Prof. Dr. Attila Fehér; Katalin Pichererné Gémes Dr.
Email: benkopeter@hotmail.com

Role of jasmonic acid in chitosan-induced plant defence responses

Zalán Czékus

[1]Department of Plant Biology, Faculty of Science and Informatics, University of Szeged, Szeged, Hungary
[2]Doctoral School of Biology, Faculty of Science and Informatics, University of Szeged, Szeged, Hungary

The efficiency of plant defence reactions against pathogens is highly dependent on environmental factors, such as the availability of light. Among microbe-associated molecular patterns (MAMPs) one of the most-commonly-used is the fungal cell wall derivative chitosan (CHT) which is able to effectively induce plant defence responses. Plant hormones, especially jasmonic acid (JA) plays a crucial role in the regulation of these processes. However, the role of JA in the CHT-induced defence responses has not been clarified yet.

Therefore, the aim of our work was to examine the JA- and light-dependence of the CHT-induced defence responses by using JA-insensitive (*jai-1*) tomato plants which were kept in the light or under darkness after elicitor treatments. Moreover, our work also focuses on the development of systemic responses in the distal leaves from the treated ones which is also less studied. Stomatal closure is one of the first defence responses activated upon biotic stress stimuli. We found, that CHT induced significant stomatal closure in both genotypes locally as well as systemically, however it was inhibited in the absence of light. Production of superoxide radical was elevated upon CHT treatment in both wild type and *jai-1* plants locally and systemically, however, it was not observable in the dark. Significant change nor in hydrogen peroxide neither nitric oxide production was observable. CHT treatment significantly elevated the relative transcript level of *SlDEF9* locally in the leaves of wild type plants which was more significant under darkness but it was not induced in the *jai-1* mutants. Expression of the ethylene response gene *SlERF1* was significantly decreased after CHT treatment Interestingly, the relative transcript accumulation of *SlPR1* was also induced by CHT only in the wild type plants both locally and systemically. Our results suggest a potential fine-tuning role of JA in the CHT-induced defence responses which are also under light-dependent regulation.

This work was supported by the UNKP-20-3-SZTE-512 New National Excellence Program of the Ministry of Human Capacities and by the grant from the National Research, Development and Innovation Office of Hungary – NKFIH (NKFIH FK 124871).

Supervisor: Péter Poór, Attila Ördög
E-mail: czekus.z@bio.u-szeged.hu

Molecular investigation of DNA transposons as therapeutic gene delivery devices

Andrea Bakné Drubi

[1]Laboratory of Cancer Genome Research, Institute of Genetics, BRC Szeged
[2]Doctoral School of Biology, Faculty of Science and Informatics, University of Szeged, Szeged, Hungary

Gene therapy procedures offer tremendous promise for many serious diseases for which effective conventional therapy is not available. Initially, viral vectors were used for gene therapy to deliver the desired genetic information into the cell. DNA transposon systems have emerged as new players on the palette and *Sleeping Beauty* (SB) and *piggyBac* (PB) DNA transposons have since been used in clinical trials.

Our research is aimed at assessing the risk factors of these new gene therapeutic devices. For comparison, we treated the mouse model of the human Tyrosinemia type I disease with liver-targeted gene delivery using both the SB100 and the hyperPB systems, and then vector insertion sites were identified from the treated livers. To this end, we developed a novel next-generation

Volume 65(1):119-132, 2021
Acta Biologica Szegediensis
http://abs.bibl.u-szeged.hu/index.php/abs

DOI:10.14232/abs.2021.1.119-132

sequencing procedure that allows us to locate large number of integration sites and explore hitherto unknown features of the operation of the systems. With our next-generation sequencing method, we could observe the so-called hot regions, where a significant amount of vector integrations is clustered. We have studied these hot regions further, having explored some of the chromatin-level factors contributing to their formation. The hot regions are important for the safety of gene therapy protocols, because the given gene delivery vectors integrate into them with high frequency. Therefore, we examined the genomic positions of the SB and PB hot regions to assess whether they could pose a risk of carcinogenesis when disturbed by vector integrations. In addition, specific qPCR and RT-qPCR assays were used to better characterize the process of DNA transposon-mediated gene delivery. We identified the average therapeutic gene dose in the affected organs and determined the kinetics of transposase expression and transposon excision product accumulation. These measurements helped us to reveal another hitherto unrecognized risk factor of DNA transposon-mediated therapeutic gene delivery. Using a variety of molecular biological methods, we have assessed the consequences and risk factors of the application of hyperactive SB and PB transposon systems for gene therapy. In the light of our results, we can make safety-enhancing recommendations for the development of clinical gene delivery protocols. Our conclusions will be applicable to other transposon-based gene therapy protocols.

Supervisor: Lajos Mátés
E-mail: drubi.andrea@gmail.com

Investigating the effects of deubiquitinases on mutant Huntingtin induced pathology

Anita Farkas

[1]Department of Biochemistry and Molecular Biology, Faculty of Science and Informatics, University of Szeged, Szeged, Hungary
[2]Doctoral School of Biology, Faculty of Science and Informatics, University of Szeged, Szeged, Hungary

Huntington's disease (HD) is a dominantly inherited neurodegenerative disorder associated with the gradual degeneration of neurons. The disease is caused by the expansion of a CAG repeat in the *huntingtin* gene, which leads to the production of mutant Huntingtin (mHtt) protein that due to misfolding can easily form aggregates. The degradation of misfolded proteins is performed by the ubiquitin-proteosome system (UPS). In HD proteosomes and ubiquitins are sequestered to aggregates and the UPS is unable to fulfill its function. mHtt is polyubiquitinated but it is not degraded efficiently that eventually might lead to depletion of the free monoubiquitin pool. The removal of ubiquitin from proteins is performed by deubiquitinase enzymes (DUBs), which also play an important role in the maturation of monoubiquitin (mUb), and in the regulation of the half-life and activity of proteins.

Therefore, we investigated the effect of DUBs on the pathomechanism of HD. We performed a comprehensive genetic screen using 39 DUB mutant strains to study their effect on viability, longevity, motor activity, and neurodegeneration in a *Drosophila* model of HD (HD flies). We identified *CG4603,* a gene encoding an OTU family DUB, that ameliorated HD phenotypes if overexpressed. Analyzing mUb levels we found that while the level of mUb decreased with age in HD flies, it did not change with age in HD flies overexpressing CG4603. We examined the effect of CG4603 on mHtt aggregation, however, we found no difference in the number, size, and size distribution of aggregates compared to control animals. As CG4603 is involved in UPR processes we analyzed the expression of endoplasmic reticulum (ER) stress genes *Hsc70-3* and *fic*. Hsc70-3 is the major ER chaperone whose activation is regulated by another ER stress protein, named fic. The expression of *Hsc70-3* and *fic* genes appears to be reduced due to overexpression of *CG4603.* Our results show that CG4603 influences the ER stress response and may have an effect on maintaining the free monoubiquitin pool. To facilitate the study of the role of CG4603 in the pathogenesis of HD we cloned *CG4603*, *Hsc-70-3* and *fic* genes with FLAG-tag.

Supervisor: László Bodai
e-mail: bioanita88@gmail.com

Volume 65(1):119-132, 2021
Acta Biologica Szegediensis
http://abs.bibl.u-szeged.hu/index.php/abs

DOI:10.14232/abs.2021.1.119-132

Fatty acid components of Armillaria species

Huynh Thu

[1]Department of Microbiology, Faculty of Science and Informatics, University of Szeged, Szeged, Hungary
[2]Doctoral School of Biology, Faculty of Science and Informatics, University of Szeged, Szeged, Hungary

Fatty acids are important cellular components that are highly variable in fungi. The fatty acid composition could help to clarify the taxonomy of the plant pathogen *Armillaria* species. Furthermore, this could be useful as a diagnostic tool in the protection of our forests. This study investigated the fatty acid components extracted from *Armillaria* species. *Armillaria* species are plant-pathogenic fungi causing white rot, a severe destructive disease, on a wide range of hosts. *Armillaria* root disease has negatively impacted the health of trees and the whole forest productivity.

The Sherlock Chromatographic Analysis System (CAS) have been applied to identify and quantify the fatty acid components in *Armillaria* genus. *Armillaria* genus there are approximately 400 species form these *A. mellea*, *A. cepistipes*, *A. ostoyae*, and *A. gallica* were selected in our study. For the optimization of the culture condition, the strains were cultured in various medium during 30 days. After that, the mycelia were collected, lyophilized and the fatty acids were extracted and derivatized under various conditions to form fatty acid methyl esters (FAMEs). The final FAME extracts were run via gas chromatography controlled by CAS.

It could be concluded that culturing in potato-dextrose broth at 25^{0}C during for 30 days was the optimized condition of *Armillaria*-growth. The extraction-choosing process was followed the MIDI instruction started with 10 mg of lyophilized mycelia and 30 minutes of saponification. The analyzed results showed that the *Armillaria* species shared similar fatty acid profiles with minor differences. The 18:2 w6c shared 55-65% of fatty acid components is the largest composition. The 16:0 ranges from 17% to 19% of fatty acid components. The 12:0 is around 4% in *A. mellea* and *A. ostoyae*, and 8% in *A. cepistipes* and *A. gallica*, respectively. Other fatty acids were identified with trace.

Supervisor: Dr. Szekeres András, Dr. Sipos György
E-mail: huynh_thu@hcmut.edu.vn

Role of survival factor genes in the pathogenicity processes of *Mucor circinelloides*

Olivér Jáger

[1]Department of Microbiology, Faculty of Science and Informatics, University of Szeged, Szeged, Hungary
[2]Doctoral School of Biology, Faculty of Science and Informatics, University of Szeged, Szeged, Hungary

Mucor circinelloides is a filamentous fungus belonging to the order Mucorales. Several members of this fungal group may cause frequently fatal invasive infections called as mucormycoses.

Survival factor protein (SVF) plays a crucial role in the protection of cells from oxidative and other stresses (e.g. cold stress) in *Saccharomyces cerevisiae*. Furthermore, this protein participates in the sphingolipid biosynthesis of the cell membrane. Sphingolipid signalling performs an important role in the control of various crucial cellular processes. Transcriptomic studies showed the upregulation of the encoding genes in several human pathogenic fungi during the host-pathogen interactions. However, the function and regulation of the SVF protein and the encoding gene(s) are still quite unknown in mucormycosis-causing fungi.

In the *Mucor circinelloides* genome, two hypothetical *svf* genes were identified and named as *Svf1* and *Svf2*. We have studied the expression of the genes after culturing the fungus under different conditions by real-time quantitative reverse transcription PCR. Using the CRISPR/Cas9 technique, single gene disruption mutants were constructed for each gene and we have started the characterization of the resulting strains. Macromorphology and sensitivity to different stressor chemicals (e.g., acetate, H_2O_2, Congo red and Calcofluor white) were tested. Mutants showed altered characteristics compared to the original strain suggesting that the cellular integrity may be damaged in the mutants. Pathogenicity of the mutants was also examined in alternative *Drosophila melanogaster* model and a decreased virulence was detected. Moreover, we studied the pathogenicity in *Galleria mellonella* model too and we could observe increasing virulence. We also carried out susceptibility test of our strains against various antifungal drugs (e.g. different azoles, amphotericin B). Next to these investigations we studied the differences of carotene volume after various (e.g. H_2O_2, posaconazole, TritonX-100, SDS, calcofluor white, Congo red) treatments.

Supervisors: Tamás Papp, Gábor Nagy E-mail: jager.oliver.biology@gmail.com

Volume 65(1):119-132, 2021
Acta Biologica Szegediensis
http://abs.bibl.u-szeged.hu/index.php/abs

DOI:10.14232/abs.2021.1.119-132

Lipid-protein interaction in photosynthetic membranes

Kovács Terézia

[1]Department of Plant Biology, Faculty of Science and Informatics, University of Szeged, Szeged, Hungary
[2]Doctoral School of Biology, Faculty of Science and Informatics, University of Szeged, Szeged, Hungary

Cold stress is one of the major limiting environmental factor of plant growth. Overwintering plants have high plasticity at multiple points during their life cycle to adapt cooling of ambient temperature from seed germination. Cold acclimation in the vegetative stage is the main object of our research. Because of their longer growing period winter cereals out-yield the spring counterparts by 30-40%. The cold acclimation process is controlled apart from cold temperature, by the circadian clock, day length. It also depends on both the intensity and the spectral composition of light. The changes in the lipid membrane composition are important part of cols acclimation process. However, lipidome of plants has been recently studied extensively to elucidate the cold acclimation process mainly on the model plant *Arabidopsis*, and only scarcely in cereals such as winter barley. Moreover, to elucidate the possible lipid background of the light quality induced pre-hardening the process according to our best knowledge has not been studied, yet. Based on our results the white light + decreased red: far-red light ratio (WL+FR) and white light enridged blue light affected both (WL+BL) the lipid content and quality in the leaves of barley (*Hordeum vulgare* ssp. vulgare 'Nure') plants. Applying electrospray ionization triple quadrupole mass spectrometry, we can determine how the membrane lipid classes are quantitatively and qualitatively altering under different temperature and light conditions. We have seen a remarkable change at the HexCer, Lyso PC, MGDG, and MGDG/DGDG. Those are increased as a result of WL+FR and WL+BL treatment. PC/PE decreased in the leaf samples with lowering the temperature from 15 to 5°C in WL+FR but increased at WT+BL. The expression of MGD2, DGD, NC, LLO2, LOC, and AD3 genes increased significantly as a function of WL+FR at 15 °C after 1 day. We suggest that the light quality-induced freezing tolerance should be considered as an important part of the pre-hardening phase. In summary, the lipidome changes induced by cold acclimation and light regime well correlate with the freezing tolerance.

Supervisors: László Kovács, Gábor Galiba
E-mail: terezia.kovacs90@gmail.com

Morphological and molecular studies of diabetes-related intestinal dysfunction in the myenteric ganglia and their microenvironment of streptozotocin-induced diabetic rats

Diána Mezei

[1]Department of Physiology, Anatomy and Neuroscience, Faculty of Science and Informatics, University of Szeged, Szeged, Hungary
[2]Doctoral School of Biology, Faculty of Science and Informatics, University of Szeged, Szeged, Hungary

In type 1 diabetes (T1D), thickened endothelial basement membrane (BM) of mesenteric capillaries has been described. Our first aim was to study the thickness of BM surrounding myenteric ganglia in different gut segments in a T1D rat model. Our second aim was to quantify the expression of matrix metalloproteinase-9 (MMP9) and tissue inhibitor of metalloproteinase 1 (TIMP1), which are essential in the breakdown of extracellular matrix molecules. Gastrointestinal (GI) symptoms are common in diabetic patients; therefore, we have studied the proportion of serotonin-immunoreactive (5-HT-IR) neurons, which are crucial in the regulation of GI motility.

Samples were taken from the duodenum, ileum and colon of diabetic, insulin-treated diabetic and control rats ten weeks after the onset of streptozotocin-induced hyperglycaemia. The thickness of BM was measured by electron microscopic morphometry. Expressional changes of MMP9 and TIMP1 were evaluated by post-embedding immunohistochemistry in the myenteric ganglia, capillary endothelium and intestinal smooth muscle. Myenteric whole-mount preparations were immunostained with anti-5-HT and pan-neuronal anti-HuCD markers.

In diabetic rats, the BM surrounding the myenteric ganglia was significantly thicker in the ileum, but it remained unchanged in the duodenum compared to controls. In the diabetics, the MMP9 expression and the MMP9/TIMP1 ratio decreased significantly in the myenteric ganglia of ileum, but not in the duodenum compared to controls. In the ileal endothelium and smooth muscle, the expression of MMP9 was also lower in diabetic rats. Immediate insulin treatment had region-specific effects on diabetic alterations. The proportion of myenteric 5-HT-IR neurons enhanced in T1D in a region-specific manner. The im-

DOI:10.14232/abs.2021.1.119-132

mediate insulin replacement prevents the hyperglycaemia-induced higher amount of 5-HT-IR neurons and restores that to the control level in each investigated gut segments.

These hyperglycaemia-related alterations may play an important role in the development of GI symptoms in T1D.

Supervisor: Mária Bagyánszki
E-mail: mezeidiana810@gmail.com

Analysis of structure and catalytic mechanism of type VI sulfide:quinone oxidoreductase enzymes

Nikolett Miklovics

[1]Department of Biotechnology, Faculty of Science and Informatics, University of Szeged, Szeged, Hungary
[2]Doctoral School of Biology, Faculty of Science and Informatics, University of Szeged, Szeged, Hungary

Although sulfide is toxic at and above certain concentrations, it plays various important physiological roles in microorganisms and higher eukaryotes as electron donor, energy source and signal molecule. Sulfide:quinone oxidoreductases (Sqr) are ancient membrane-bound flavoproteins catalyzing sulfide oxidation coupled to quinone reduction. Based on phylogenetic analysis, Sqr enzymes are classified into six groups (type I-VI). *Thiocapsa roseopersicina* is a photosynthetic, purple sulfur bacterium which possesses a type VI Sqr enzyme (SqrF). Catalytic properties of the purified recombinant SqrF differed from other characterized Sqrs indicating a distinct catalytic mechanism in type VI Sqr enzymes. In our former studies, based on the biochemical analysis of the cysteine mutant enzymes, a model of sulfide oxidation mechanism of SqrF was suggested.

The aims of our studies were the identification and characterization of additional functional amino acids in the active centre of SqrF participating in the quinone binding and catalysis of the quinone reduction phase of the catalytic process. Based on sequence and structural alignments, Val331, Ile333 and Phe366 residues seemed to be involved in the formation of the quinone substrate binding pocket in the *T. roseopersicina* SqrF enzyme. These residues were replaced by site-directed mutagenesis and the mutant SqrF variants were biochemically characterized. Moreover, *in silico* approaches were applied for modeling the enzyme-substrate interactions. The experimental results revealed that all these amino acids play a role in the interaction between the protein and quinone molecules. Hydrophobic stacking interaction between the redox head group of quinone and the benzene ring of Phe366 residue is the most crucial component in the proper binding of the electron acceptor in the active site. Further site-directed mutagenesis experiments of a highly conserved amino acid, Glu163 located in the active centre near the FAD cofactor demonstrated that this residue has an essential role in the catalysis of sulfide oxidation. In the presented work, novel amino acids involved in the complex redox process catalysed by the SqrF enzyme have been identified. According to these results, our catalytic model established for SqrF enzymes was further improved.

Supervisor: Gábor, Rákhely; András Tóth
E-mail: mmiklovicsnnikolett@gmail.com

Characterization of potential agricultural bioeffector *Trichoderma* strains isolated from soils in the Hungary-Serbia cross border region

Viktor Dávid Nagy

[1]Department of Microbiology, Faculty of Science and Informatics, University of Szeged, Szeged, Hungary
[2]Doctoral School of Biology, Faculty of Science and Informatics, University of Szeged, Szeged, Hungary

Certain *Trichoderma* strains are commonly used as agricultural agents due to their beneficial effects to both plants and soil. In general, the consortia have one or two strains of these filamentous fungi and they usually play biocontrol and plant residue degrading roles. Several harmful *Trichoderma* species were also described. Some of them produce toxins, cause diseases in mushroom cultivation or could be opportunistic human pathogens. Therefore the selection of agricultural bioeffector strains should be performed with great care.

Our goal was to isolate, identify and characterize *Trichoderma* strains potentially applicable for agricultural purposes. We

Volume 65(1):119-132, 2021
Acta Biologica Szegediensis
http://abs.bibl.u-szeged.hu/index.php/abs

DOI:10.14232/abs.2021.1.119-132

isolated 48 *Trichoderma* strains from various agricultural soils in the Hungary-Serbia cross border region. The isolated strains were identified based on sequence analysis of a fragment of the translation elongation factor 1α (*tef1α*) gene. The identification is also important to exclude strains that belong to potentially harmful *Trichoderma* species such as *Trichoderma brevicompactum*, *T. longibrachiatum* or *T. aggressivum*. Cellulolytic enzyme activities was also measured. Based on the molecular identification and enzyme activity tests, 10 strains were selected. The 10 selected strains underwent a series of examinations to determine their pH and temperature optima and their tolerance to heavy metals and low water activity. The resistance to several fungicides was also tested to investigate the possibilities of combined application with antifungal agents. Biocontrol indices (BCI) were also examined in parallel with chitin degrading enzyme activity tests. Both experiments are good indicators of biocontrol abilities against filamentous fungal plant pathogens. We did not find strong correlations between the BCI values and the chitin degrading enzyme activities of the tested strains, although most of the strains showed promising antagonistic abilities against fungal plant pathogens. Plant growth promotion was also tested in greenhouse experiments on maize and alfalfa. Certain strains showed slight plant growth promotion in greenhouse experiments on maize and alfalfa seedlings, although the measured parameters were not significantly different from those of the untreated control.

Supervisors: Dr. László Kredics, Dr. Palanisamy Manikandan
E-mail: viktor.david.nagy@gmail.com

Predicting the spread of antibiotic resistance genes using functional metagenomic screens in pathogenic bacteria

Mónika Számel

[1]Translational Microbiology Unit, Department of Biochemistry, Biological Research Centre, Szeged
[2]Doctoral School of Biology, Faculty of Science and Informatics, University of Szeged, Szeged, Hungary

Horizontal gene transfer plays an important role in the development of multidrug resistance. In the present antibiotic resistant crisis, besides examining genomic mutations, it would be highly important to consider this evolutionary process in drug development.

Functional metagenomic screens has the potential to identify antibiotic resistance genes (ARGs) in different environments that are potential candidates for horizontal gene transfer. These screens, however, are usually performed in a single non-pathogenic host, therefore being insufficient to reveal the whole resistome of an environment and lacking clinical relevance. My work aimed to extend functional selections to non-model pathogenic bacteria to capture the resistome of three different environments. I constructed small-insert metagenomic libraries from microbial DNA of the human gut, contaminated soil samples and from the genomic DNA of 73 pathogenic bacteria isolated from hospitals. I introduced and expressed these libraries in the model organism *Escherichia coli* and in three pathogens: *Shigella sonnei*, *Klebsiella pneumoniae* and *Salmonella enterica*. I performed selection experiments in the presence of 6 newly developed antibiotics in comparison with their 7 older counterparts of the same antibiotic class. Overall, in the screens I identified 86 known ARGs, out of which only 50% is coming from the screens in *E. coli*, showing the need for multi-host selections. I also found that the majority of ARGs identified in all four hosts are known to be horizontally transferred in nature according to literature databases. This shows the predictive force of the screens. Moreover, according to my results, some resistance gene classes seem to be specific to certain hosts. Finally, as the number of already known resistance genes is not lower for new antibiotics compared to old ones, my work highlights the need for a more thorough resistance testing pipeline.

In sum, I showed that by the application of multi-host functional metagenomics we can gain a better coverage of the environmental resistomes and aid antibiotic development.

Supervisor: Bálint Kintses, Csaba Pál
E-mail: szamel.monika@brc.hu

Volume 65(1):119-132, 2021
Acta Biologica Szegediensis
http://abs.bibl.u-szeged.hu/index.php/abs

DOI:10.14232/abs.2021.1.119-132

Mesr4: a novel positive regulator of germline differentiation

Alexandra Brigitta Szarka-Kovács

[1]Institute of Genetic, Biological Research Centre, Szeged, Hungary
[2]Doctoral School of Biology, Faculty of Science and Informatics, University of Szeged, Szeged, Hungary

Adult stem cells divide continuously. One of the daughter cells remains in stem cell state and the other starts to differentiate. The main question of stem cell biology is how these cells know if they have to remain in stem cell state or they have to start their differentiation program. To investigate this fundamental biological phenomenon, the *Drosophila* ovary provides a perfect model system. The ovarian germline stem cells (GSCs) reside in a special microenvironment called stem cell niche. In the niche, the GSCs are surrounded by somatic cells secreting the Dpp signalling molecule which inhibits the expression of the main differentiation gene *bag of marbles* (*bam*) in the GSCs. After the division of the GSCs, one of the daughter cells is displaced from the niche, the negative Dpp signal cannot reach it, and becomes a pre-cystoblast (pre-CB). At this stage, initiation of bam expression promotes the differentiation into a cystoblast (CB). While the negative regulation of GSC differentiation is very well known, the positive factors are barely known.

Previous observations suggested that the nuclear protein, MesR4 is required for GSC differentiation. Cell biological analysis of the MesR4 depleted ovaries revealed that Mesr4 is required for the last step of pre-CB to CB transition in a cell autonomous manner. By a series of epistasis experiments and transcriptional analysis, we demonstrated that MesR4 positively regulates the transcription of bam. The Mesr4 protein contains eight C2H2 type zinc finger domains, a plant homeodomain finger, a nuclear localisation signal and an AAA-ATPase domain. We showed that the plant homeodomain finger and the AAA-ATPase domain are dispensable for the proper of Mesr4 function in the ovary suggesting that the DNA binding activity of the C2H2 type zinc fingers is essential for *bam* regulation. Based on our results, we propose the hypothesis that MesR4 directly binds the regulatory regions of the *bam* gene and act as a transcriptional activator. Our results indicate, that the lack the inhibitory Dpp signal is not sufficient, but an additional positive signal is required to complete the differentiation program in the GSCs.

Supervisor: Ferenc Jankovics
E-mail: szarka.brigitta@brc.hu

Complex examination of bacterial strains with plant growth-promoting and biocontrol potential

Anuar R. Zhumakayev

[1]Department of Microbiology, Faculty of Science and Informatics, University of Szeged, Szeged, Hungary
[2]Doctoral School of Biology, Faculty of Science and Informatics, University of Szeged, Szeged, Hungary

The application of plant growth-promoting bacteria (PGPB) and biocontrol agents in agricultural systems are promising strategies for the sustainable enhancement crop productivity. However, the effectiveness of PGPB *in vivo* is often limited by adverse environmental conditions like salinity or drought, as well as and the presence of xenobiotics, such as heavy metals or pesticides. Our work aimed the isolation of PGPB and their complex characterisation including tolerance to different abiotic stress factors.

Thirty strains were isolated from an agricultural soil sample previously exposed to the herbicide glyphosate on solid minimal medium amended with glyphosate as the sole carbon and nitrogen source (1 mg/ml). Ten strains showing the highest growth rate and different colony morphology were selected for the further studies. Based on the sequence analysis of fragments of the 16S rRNA and *rpoB* genes 7 strains were identified as *Pseudomonas resinovorans*, 2 as *Ensifer adhaerens*, and a single isolate as *Ochrobactrum anthropi,* which was excluded from the further assays due to its opportunistic human pathogenic nature. Among the 9 remaining strains, *E. adhaerens* SZMC 25856 and *P. resinovorans* SZMC 25875 could enhance root and total length of tomato seedlings significantly ($p<0.05$). Eight isolates showed remarkable siderophore-producing potential (12.66-36.44%), and 5 strains were able to synthesize the phytohormone indole-3-acetic acid (0.19-0.81 μg/ml). All strains tolerated Al, Cu, Fe, Mn, and Pb ions at 0.1 mM, and 14 different pesticides at 25 μg/ml concentration. They resisted also salinity (6.3-12.5 g/l NaCl) and drought (125 g/l polyethylene glycol 6000), and preferred pH 7.00-7.96. All *P. resinovorans* isolates could antagonize *Agrobacterium tumefaciens* and *A. vitis* (updated scientific name *Allorhizobium vitis*), the pathogens of grape, cherry, and walnut.

Our findings propose the possibility of applying the isolated strains, particularly *E. adhaerens* SZMC 25856 and *P. resinovorans*

Volume 65(1):119-132, 2021
Acta Biologica Szegediensis
http://abs.bibl.u-szeged.hu/index.php/abs

DOI:10.14232/abs.2021.1.119-132

SZMC 25875 as plant growth-promoting and biocontrol purposes even under adverse environmental conditions.

The work was supported by the Hungary-Serbia IPA Cross-border Co-operation Programme (PLANTSVITA; HUSRB/1602/41/0031) and the Stipendium Hungaricum Scholarship.

Supervisors: Csaba Vágvölgyi, Lóránt Hatvani
E-mail: anuar_zhumakaev@mail.ru

A simple *E. coli* system for studying sequence-specific DNA binding of proteins

Nikolett Zsibrita

[1]Institute of Biochemistry, Biological Research Centre, Szeged, Hungary
[2]Doctoral School of Biology, Faculty of Science and Informatics, University of Szeged, Szeged, Hungary

Sequence-specific DNA-protein interactions play essential roles in many biological processes. During characterization of DNA binding proteins, it is often important to test whether the protein can bind to a particular DNA sequence, and to determine how alterations in the protein or in the DNA affect the binding strength or specificity. The drawback of the available methods is that they either require purified proteins or protein fusions. We have developed a simple *in vivo* technique, which can detect binding of a protein to its target site without the requirement of creating protein fusions. The method called I-Block assay detects inhibition of the *E. coli lacI* gene transcription by the tested protein bound to its target site inserted next to the *lacI* promoter. The method was tested with two zinc finger proteins, with the λ phage repressor and with CRISPR-dCas9, but is expected to be generally applicable to all sequence-specific DNA binding proteins for which the target site is known (*Nucleic Acids Res.* 2020, 18;48(5):e28).

The I-Block assay uses β-galactosidase activity as readout and can, in its current form, process reactions involving the protein of interest and one or a few potential target sequences. Our current work aims to develop a high throughput version of the I-Block assay, which can select from a complex sequence library the best binding target sequence for a protein, or the best binding protein variant for a target sequence. To this end we first tested whether β-galactosidase production can be used as a selective phenotype on agar plates containing the non-inducing β-galactosidase substrate phenyl-β-D-galactopyranoside (P-gal) as the only carbon source. Unfortunately, the growth difference between the β-galactosidase producing and non-producing colonies was not large enough to reliably identify binding-positive clones. We now work on an alternative approach, in which the β-galactosidase gene is replaced by an antibiotic resistance gene allowing binding positive clones to be selected by virtue of their acquired antibiotic resistance.

Supervisor: Antal Kiss
E-mail: zsibrita.nikolett@brc.hu